FORSCHUNGSZENTRUM
ROSSENDORF e.V.

FZR-78

INSTITUTE OF NUCLEAR AND HADRONIC PHYSICS

BRD

Annual Report 1994

Annual Report 1994

Institute of Nuclear and Hadronic Physics

Editors:	F.	Dönau
	H.	Prade
Editorial staff:	W.	Enghardt
	K.	Möller
	J.	Mösner
	G.	Winter
	R.	Wünsch

Cover Picture

The front cover displays the inner part of the reaction chamber of the 4π-spectrometer FOBOS in Dubna. The target is spherically surrounded by pentagon- and hexagon-shaped position-sensitive double-grid avalanche counters (DGAC) in a distance of 50 cm. In one case, the DGAC is removed and the supporting grid structure of the subsequent Bragg ionization chamber is visible.

FZR-78
February 1995

Forschungszentrum Rossendorf e.V.
Postfach 51 01 19 · D-01314 Dresden
Bundesrepublik Deutschland

Telefon (0351) 591 3270
Telefax (0351) 591 3700
E-Mail prade@fz-rossendorf.de

Preface

The present third Annual Report of the Institute of Nuclear and Hadronic Physics (IKH) of the Research Center Rossendorf Inc. (FZR) summarizes the research activities, the results obtained and the progress achieved in 1994.

As in the previous years the major research activities at the IKH focussed at structure studies of the atomic nucleus and its constituents, the hadrons, as well as at the investigation of the behaviour of the nucleonic system in nucleus-nucleus collisions. Our research work is characterized by the participation in national and international collaborations and by the use of external accelerators and facilities at GSI Darmstadt, Research Center KFA Jülich, JINR Dubna, University of Cologne and TH Darmstadt.

The experimental groups of the IKH substantially took part in the completion of the corresponding experimental set-ups, i.e. the 4π-Detector at SIS/GSI, the Time-of-Fligth (TOF) Spectrometer and the 0°-Facility at COSY/Jülich, the Fragment Spectrometer FOBOS at the cyclotron U-400M in Dubna, and CLUSTER-Detectors for the γ-Detector Array EUROBALL at the Cologne Tandem accelerator and S-DALINAC/Darmstadt.

Using the possibilities of the modern IKH detector laboratory built up in the last years important contributions to these detector systems have been provided. Furthermore, first experiments have been performed with early implementations of the TOF and FOBOS spectrometers in Jülich and Dubna, respectively, as well as with the Phase II set-up of the 4π-Detector at GSI.

The theoretical investigations performed in 1994 dealt with the study of nuclear and subnuclear degrees of freedom, high-spin phenomena and the dynamics of open quantum systems.

In the field of applied research the use of Positron Emission Tomography (PET) for monitoring the radiation therapy with light heavy ions as planned at SIS/GSI has been the major topic in the IKH. For this purpose a new Positron Emission Tomograph consisting of two large BGO detector arrays has been constructed and testet in Rossendorf.

The results of our research, achieved in the last year, are presented in numerous publications in international journals, conference contributions and talks documented in this report.

In addition to these scientific activities considerable effort has been undertaken to write a proposal for a future own accelerator basis at the Research Center Rossendorf. An internal project study for a 250 MeV superconducting electron linac has been finished by the end of 1994 in close collaboration with the scientific departments "Experimental Facilities and Information Technology" as well as "New Accelerators"of the FZR and with the support of several institutions in Germany and abroad.

In this connection the traditional Holzhau - Meeting on nuclear physics organized in April 1994 proved to be a milestone for elaborating the scientific case of this project named ELBE (**E**lectron **L**inac with hight **B**rightness and low **E**mittance). The main topic of the meeting was devoted to physics with electron beams and it brought together many outstanding experts in this field.

Two further meetings succesfully organized by the IKH in 1994 belong to the highlights in the last year:

The "1994 Meeting for Nuclear and Particle Physics" (140 participants) was held in October in Pirna and continued the tradition of the German medium energy meetings organized every other year. In September the 5-th Symposium of the ALADIN Collaboration took place in Rathen near Dresden.

All scientific activities of the IKH have benefited from the general support of many institutions. First of all, we gratefully acknowledge the close and fruitful collaboration with our partner institutes in Germany and abroad. This cooperation has been and remains of vital importance for our institute.

Specific projects were financially supported by the Federal Ministry for Research and Technology (BMFT), the German Research Community (DFG), the State Ministry for Science and Art of Saxony (SMWK), the KFA Jülich and the GSI Darmstadt. We express our gratitude to all these institutions as well as to the Executive Board of the Research Center Rossendorf for its permanent help and the promotion of nuclear and hadronic physics in Rossendorf.

Harald Prade

CONTENTS

I Results of Research and Development

Explanation of special symbols:

Numerous research projects were funded by the Federal Ministry for Research and Technology (BMFT), the German Research Community (DFG), the GSI Darmstadt and the KFA Jülich, several were sponsored within the scientific technological cooperation between Germany and Russia or Poland. The support of theses institutions is indicated by using the letters "B", "D", "G", "K", "W", respectively, after the title of the corresponding contributions.

1 Theoretical Nuclear Physics

Determination of Radial Flow Energies from Energy Spectra of Intermediate Mass Fragments [B]

B. HEIDE [1] AND H.W. BARZ [1]

The analysis of the flow pattern of heavy-ion collisions by means of Boltzmann-type transport models reveals that the nucleonic flow is very sensitive to the impact parameter. For collisions of gold on gold at 150 A·MeV we have found a spherically symmetrical flow only for impact parameters up to 2 fm with a flow energy of about 12 MeV per nucleon. At larger impact parameters the flow becomes very asymmetric and the matters flows preferentially in and opposite to the beam direction.

In experiments [1,2] kinetic energy spectra are used to extract the flow energy since the kinetic energy of a fragment is proportional to its mass number. The flow energies obtained exceed our theoretical value by about 6 MeV. We traced this difference back to several reasons. On one hand the kinetic energy is increased by the additional Coulomb repulsion after break-up and by the recoil which the fragments obtain due to evaporation processes. While the first effect is proportional to the fragment mass and amounts to about 3 MeV per nucleon, the latter has a weak mass dependence and should not influence essentially the extracted value. On the other hand a proper impact parameter selection is very important. The matter has a considerable translational motion for non-central events. In fig. 1 the observed kinetic spectra for two different centrality criteria are shown in comparison with calculations which simulate these selection criteria by choosing impact parametrs of $b < 2$ fm and $b < 3$ fm, respectively. For both selections the average kinetic energies differ by about 3 MeV per nucleon and the calculations are compatible with a smaller flow for very central collisions.

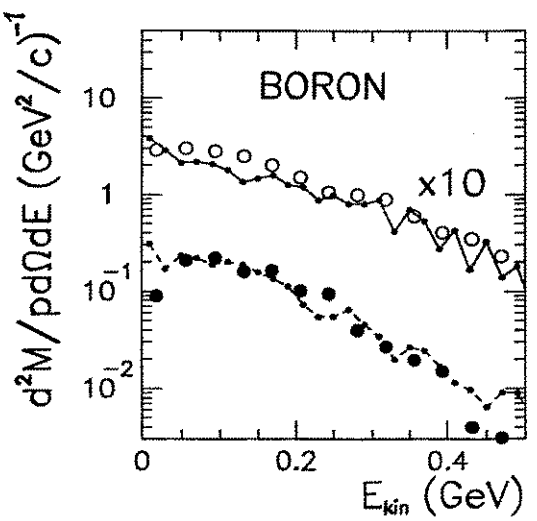

Fig. 1 *Calculated energy spectra for boron isotopes in the angular range from 25° to 45° in the centre-of-mass system (lines) compared to data for a moderate (circles) [1] and high (full circles) [2] centrality.*

[1] *Institut für Theoretische Physik, TU Dresden and Institut für Kern- und Hadronenphysik, FZ Rossendorf*

References

[1] W. Reisdorf, Proc. Int. Workshop XXII on Gross Properties of Nuclei and Nuclear Excitations, Hirschegg, Jan. 1994, eds. H.Feldmeier and W. Nörenberg, p.39

[2] S.C. Jeong et al., Phys. Rev. Lett. **72** (1994) 3468

Flow Pattern in Collisions of Gold on Gold[B]

H.W. BARZ [1] AND B. HEIDE [1]

Collective phenomena in heavy ion collisions are sensitive to the equation of state of nuclear matter. In recent experiments [1] colliding Au on Au with bombarding energies up to 400 MeV per nucleon, a large amount of radial flow was detected. BUU analyses [2] of gold on gold reactions have shown that for impact parameters up to 2 fm the flow ellipsoid is nearly spherical and becomes with increasing impact parameter strongly elongated. We simulate this behaviour by the following ansatz for the distribution w as a function of the position $\vec{r}$ and the velocity $\vec{v}$ of a fragment with mass number A in the forward and backward hemisphere, respectively:

$$w(\vec{r},\vec{v}) \propto F(\vec{r})\ \mathrm{e}^{-\frac{Am_N^2}{2}\sum_1^3 \Lambda_i[v_i - \frac{B_i}{m_N}(r_i - R_i) - \frac{g_i}{m_N}]^2}, \qquad (1)$$

where m_N is the nucleon mass. The coordinate system is oriented along the principal axes of the flow tensor, $\vec{R}$ denotes the centre-of-gravity of the forward or backward part of the matter which move with momenta $\vec{g}$ per nucleon in or oppositely to the main flow direction ($g_i \sim \delta_{i3}$), respectively, while the B_i describes the expanding flow directed from the centre. The components denote the motion in-plane (i=1), out-of-plane (i=2) and in the direction of the flow angle (i=3). In the special case $g_3 = B_3 \cdot R_3$ the backward and forward distributions form a continuous velocity field of a single source. The parameters $m_N\Lambda_i = 1/T_i$ measure the random motion of the fragments around the flow velocity, thus, T_i might be interpreted as temperatures. Using a cylindrical positional distribution F, the BUU calculations allow us to fit the parameters in eq. (1) to the nucleonic velocity field. The resulting flow energies are shown in fig. 1. For impact parameters up to 4 fm the collision pattern represent an asymmetrically expanding single source. For larger impact parameters we have found $g_3 > B_3 \cdot R_3$, thus, projectile and target remnants with small radial flow begin to separate from each other. This explains the differences between correlation functions measured [1] in central and semi-central collisions.

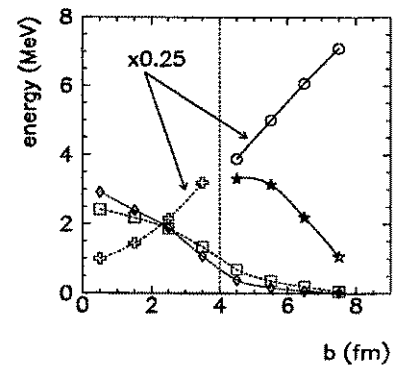

Fig.1. *Flow energies: radial flow along the flow axis (crosses), in-plane (diamonds), out-of-plane (squares). For impact parameters larger 4 fm the flow along the flow axis is split into a translational (circles) and an expansional part (stars).*

[1] *Institut für Theoretische Physik, TU Dresden and Institut für Kern- und Hadronenphysik, FZ Rossendorf*

References

[1] B. Kämpfer et al. (FOPI-Collaboration), Phys. Rev. **C48** (1993) R955;
Proc. Int. XXII Workshop on Gross Properties, Hirschegg, Jan. 1994,
Edt. H. Feldmeier and W. Nörenberg, p.113

[2] B. Heide and H.W. Barz, Phys. Lett. **B337** (1994) 53; Erratum **B340** (1994) 267

Molecular Dynamics Applied to Fragment Production in Heavy Ion Collisions[B]

H.W BARZ[1], D. IDIER[2], J. BONDORF[2], B. HEIDE[1] AND I.N. MISHUSTIN[2]

On the basis of the Boltzmann-Übling-Uhlenbeck approach using the algorithm of pseudo-particles [1] a molecular dynamical model has been developed replacing the pseudo-particles with real nucleons. The nucleons are described as wave packets $g_\Delta(r)$ with a width of Δ in position space. Using the zero-range Skyrme force we derive an effective Hamitonian which governs the motion of the nucleons in the mean field:

$$H = \sum_i [\frac{\boldsymbol{p}_i^2}{2m_N} + \frac{3}{4}t_0 n(\boldsymbol{r}_i) + \frac{3}{4}t_3 n(\boldsymbol{r}_i)^{1+\gamma}] + \frac{1}{2}\sum_{ij}[t_{12}(\boldsymbol{p}_i - \boldsymbol{p}_j)^2 + t'_{12}(r_{ij}^2 - 6\Delta^2)]g_{2\Delta}(r_{ij}), \quad (1)$$

where $\boldsymbol{r}_i$, $\boldsymbol{p}_i$ and $n(\boldsymbol{r})$ denote positions, momenta and density of the nucleons. The Skyrme parameters t_0, t_3, t_{12}, t'_{12} and γ determine the mean field including a repulsive momentum dependent force. In addition we consider nucleon-nucleon collisions using an in-medium cross-section of 30 mb and the Pauli blocking is taken into account.
Using a soft equation of state, $\gamma = 1/6$, the model has been applied to the collision of gold on gold at a bombarding energy of 150 MeV per nucleon. After a reaction time of 150 fm/c the nucleon distribution has been analysed to find clusters defined as an ensemble of particles with an inter-nuclear distance less than 3 fm. Central collisons with impact parameters up to 3.5 fm have been selected. In fig. 1 the resulting spectra are compared with experiment. The increase of the mean kinetic energy as a function of the fragment mass reveals the presence of a considerable radial flow of nuclear matter. Further investigations are in progress.

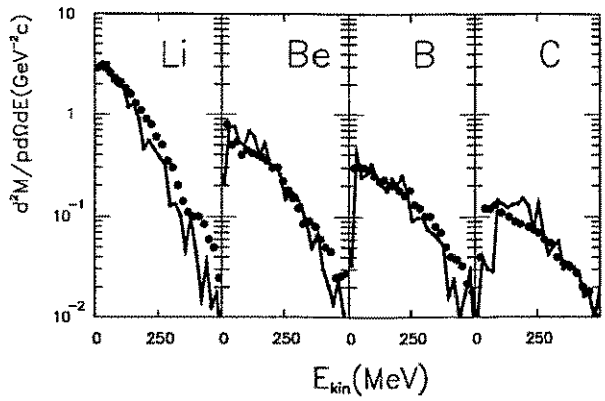

Fig. 1 *Calculated energy spectra (lines) of intermediate mass fragments measured between 25 and 45 degrees in the cm-system for the reaction of gold on gold at a bombarding energy of 150 MeV per nucleon compared with experiment (full circles) [2].*

[1] *Institut für Theoretische Physik, TU Dresden and Institut für Kern- und Hadronenphysik, FZR*
[2] *The Niels Bohr Institute, Copenhagen, Denmark*

References

[1] D. Idier, M. Farine, B. Remaud and F. Sebille, Ann. Phys. Fr. **19** (1994) 159
[2] W. Reisdorf, Proc. Int. XXII Workshop on Gross Properties, Hirschegg, Jan. 1994, Edt. H.Feldmeier and W. Nörenberg, p. 93

Kaon Polarization in Nuclear Matter[B]

E.E. KOLOMEITSEV, D.N. VOSKRESENSKY[1], B. KÄMPFER[2]

In the framework of a phenomenological approach we consider kaon excitations in nuclear matter. The kaon polarization operator is calculated by taking into account [1]: (*i*) the regular part in an expansion of the chiral Lagrangian with parameters fitted to the KN scattering data, (*ii*) the hyperon (Λ, Σ) nucleon-hole loops, which produce the pole terms in the polarization operator, (*iii*) the interaction of kaons with pions, which are softened in dense nuclear matter, (*iv*) some off-shell KN-interaction that we try to restore with Adler's consistency condition.

Fig. 1 shows the spectrum $\omega(k)$ of charged kaons for symmetric nuclear matter at density $\rho = \rho_o$ (i.e., saturation density, solid lines) and $\rho = 4\rho_o$ (dashed lines). Branches 1, 2 and Σ correspond to the K^- quasi-particles. The upper branch $\omega_1(k)$ transforms into the vacuum one at $\rho \to 0$. The Σ branch and the low-lying branch $\omega_2(k)$ consist mainly of the mixed states of Σ particles and proton- and neutron-holes and of the mixed states of Λ particles and proton-holes, respectively. Branch 3 becomes the branch of K^+ mesons after changing $\omega \to -\omega$, $k \to -k$. The Σ branch is very weakly occupied by the real kaons because of the small coupling constant, whereas the low-lying branch $\omega_2(k)$ is markedly occupied in rather wide interval of momenta. Fig. 1 shows also that the Σ branch does not practically change with increasing density. The origin of the low-lying branch in the spectrum of the K^- mesons is the Λ–proton coupling. With growing proton density the second branch is modified more strongly: at some density a minimum with $k = k_0 > 0$ appears, then the minimum value $\omega_c = \omega_2(k_o)$ decreases and equals zero at some value $\rho = \rho_c^-$ (in proton matter $\rho_c^- \simeq 4\rho_o$ for $\Sigma_{KN} = 1.4 m_\pi$, where Σ_{KN} is the usual KN sigma-term).

To investigate a possibility of kaon condensation in dense nuclear matter we calculate the energy of a system of neutrons, protons and condensed K^- mesons. We find that at $\rho \geq \rho_c^-$ an isotopic phase transition becomes energetically favorable. Thus, neutron star matter may consist of proton matter with p-wave K^- condensate at $\rho > \rho_c^-$. This phase transition is of a first order and occurs via some fluctuation mechanism when the proton enriched fluctuation in the neutron star matter with the overcritical density and size begins to grow due to the $n \to p + K^-$ reactions on its surface.

Exploiting isospin symmetry one can obtain the polarization operator of $\bar{K}^0$ mesons from the K^- polarization operator. More details can be found in [1].

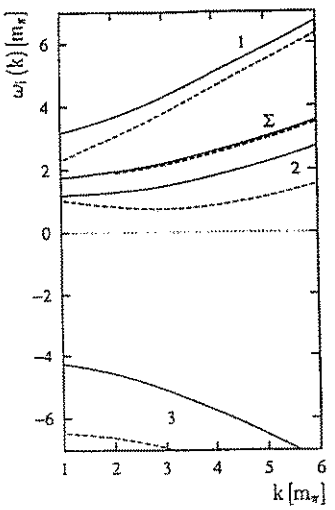

Fig. 1 *Spectrum of charged kaons in isospin-symmetric nuclear matter.*

[2] *GSI, Darmstadt*

[1] *Institut für Theoretische Physik, TU Dresden and Institut für Kern- und Hadronenphysik, FZR*

References

[1] E.E. Kolomeitsev, D.N. Voskresensky, B. Kämpfer, FZR-34 (1994)

Neutral ρ Meson Properties in an Isospin-Asymmetric Pion Medium[B]

T.I. GULAMOV[1], A.I. TITOV[1], B. KÄMPFER[2]

We calculate the ρ meson self-energy in a pion medium at finite temperature T and charge chemical potential μ_Q which is responsible for the difference of π^+ and π^- densities in matter. The calculation is performed within the functional integral representation for the partition function in order g_ρ^2. Our starting point is an effective Lagrangian which describes a system of charged pions and neutral vector ρ mesons

$$\mathcal{L} = \frac{1}{2}(D^\nu\phi)^* D_\nu\phi - \frac{1}{2}m_\pi^2\phi\phi^* - \frac{1}{4}\rho_{\mu\nu}\rho^{\mu\nu} + \frac{1}{2}m_\rho^2\rho^2, \tag{1}$$

where ϕ is the complex charged pion field, ρ stands for the vector field with the strength $\rho_{\mu\nu} = \partial_\mu\rho_\nu - \partial_\nu\rho_\mu$, and $D_\nu = \partial_\nu - ig_\rho\rho_\nu$ is the covariant derivative; μ, ν are Lorentz indices.

We find that the in-medium ρ mass m_ρ^* and width γ_ρ^* increase with the chemical potential μ_Q. At large values of $\mu_Q \sim m_\pi$ and temperatures $T > 100$ MeV these increases become substantial. It might be realized in charge fluctuations of the pion gas produced in the central region in relativistic heavy-ion collisions. The predicted effect is small for the mean value of μ_Q, which is expected from the proton-neutron asymmetry in intermediate energy heavy-ion collisions. In this region of μ_Q the found dependence is smaller than the temperature effect of Gale and Kapusta [1]. Some results of the involved calculations [2] are displayed in figs. 1 and 2.

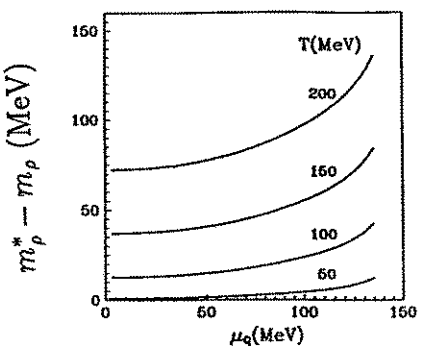

Fig. 1 *The difference $m_\rho^* - m_\rho$ as function of μ_Q at several temperatures.*

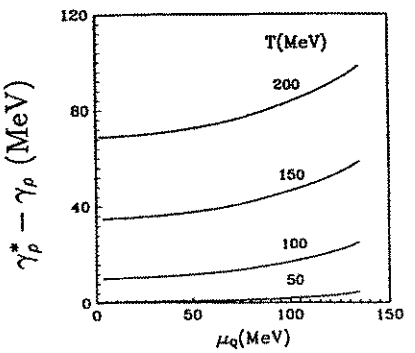

Fig. 2 *The difference $\gamma_\rho^* - \gamma_\rho$ as function of μ_Q at several temperatures.*

[1] *Bogoljubov Institut für Theoretische Physik, JINR Dubna, Russland*

[2] *Institut für Theoretische Physik, TU Dresden and Institut für Kern- und Hadronenphysik, FZR*

References

[1] C. Gale, J.I. Kapusta, Phys. Rev. **C35** (1987) 2107

[2] T.I. Gulamov, A.I. Titov, B. Kämpfer, FZR-66 (1994)

The Strange Quark-Gluon Plasma[B]

B. KÄMPFER[1], O. P. PAVLENKO[2], A. PESHIER, G. SOFF[3]

Many phenomenological models of the quark-gluon plasma rely on the popular bag model parametrizations: the u,d quarks and gluons are taken as massless particles, and a positive vacuum energy density is included to accomplish the phase transition to confined hadron matter. The available pure SU(3) gauge theory lattice data show, however, a behavior which cannot be described by the bag model. Instead, effective thermal gluon masses [1]

$$m^2(T) = \gamma\, g^2(T+T_s)\,T^2, \quad g^2(T) = \frac{16\pi^2}{11-\frac{2}{3}N_f}\,\frac{1}{\ln\left(\frac{T}{T_c}\right)^2} \tag{1}$$

account for the lattice data when employing an ideal quasi-particle gas expression for the pressure [2]. The parameter γ turns out to be approximately the same as predicted in high-temperature QCD calculations. T_s represents a phenomenological regularization. Only the physical transverse gluon modes are to be included.

We extend here such an effective model to include also quarks as thermal quasi-particles. While the current quark masses of the u,d flavors can be neglected, the treatment of the s quarks is not obvious. High-temperature QCD self-energy calculations suggest effective masses according to $m_s = \sqrt{m_{s,0}^2 + m^2(T)}$. In this case the strange current mass appears to be negligible; the partial pressures, energy densities and particle densities of u,d and s quarks are nearly the same, and the strange quarks give a significant contribution to the total energy density (see Fig. 1). One might also utilize an ansatz $m_s = m_{s,0} + m(T)$ for the effective masses. In such a case the strangeness contributions are about 20% of the u,d contributions. Such contributions are anyway important for the phase diagram with strangeness [3].

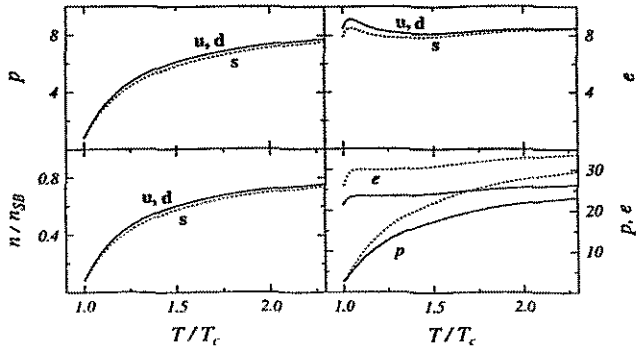

Fig. 1 *The partial pressures (left upper panel, in units of $T^4\frac{\pi^2}{90}$), the partial energy densities (right upper panel, in units of $T^4\frac{\pi^2}{30}$), the partial particle densities (left lower panel, in units of the Stephan Boltzmann values), and the total energy density and pressure (right lower panel, full {dotted} lines: 2 {3} flavor plasma).*

[1] *Institut für Theoretische Physik, TU Dresden and Institut für Kern- und Hadronenphysik, FZR*
[2] *Institute for Theoretical Physics, Kiev, Ukraine*
[3] *Institut für Theoretische Physik, TU Dresden*

References

[1] B. Kämpfer, O.P. Pavlenko, Nucl. Phys. **A566** (1994) 351c
[2] A. Peshier, B. Kämpfer, O. P. Pavlenko, G. Soff, Proc. of the Workshop on "Hot and dense hadron matter", Divonne (France), July 1994, (eds.) H.H. Gutbrod, J. Rafelski, Plenum Press (1995)
[3] B. Kämpfer, B. Lukacs, G. Paal, Cosmic phase transitions, Teubner Verlag, Stuttgart (1994)

Transverse Momentum Distribution of Hard Dileptons from a Quark-Gluon Plasma with Thermal Parton Masses[B]

A. PESHIER, B. KÄMPFER[1], O. P. PAVLENKO[2], G. SOFF[3]

In a recent paper [1] the possible patterns of the transverse momentum distribution of such penetrating probes as hard dileptons from pre-equilibrium parton matter has been analyzed. Strong transverse momentum dependences have been found. This is to be contrasted with the prediction that the transverse dilepton spectrum from an ideal quark-gluon plasma shows a flat distribution, i.e., a scaling property. However, in-medium effects give the partons effective thermal masses [2,3] which also cause scaling violations [1].
Here we report results within our model of thermal parton masses for the dilepton emission from a quark-gluon plasma. The analysis shows the presence of a kinematical threshold in the emission rate caused by the finite thermal masses. E.g., at a given transverse dilepton mass $M_T = (M^2 + Q_T^2)^{1/2}$ the minimum invariant mass M is given by twice the quark mass in case of the dominating quark fusion processes $q\bar{q} \to l\bar{l}$; therefore at large transverse dilepton momentum Q_T the rate has to approach zero due to kinematics. If the thermal quark mass is large enough it might also lead to a violation of the M_T scaling. To quantify these effects we calculate the transverse dilepton spectrum for our temperature dependent quark masses, scale-invariant longitudinal expansion, Boltzmann approximation of the distribution functions, and the temperature determined by the Bjorken equation (the thermal history is calculated self consistently with the equation of state which includes the finite thermal parton masses).
A calculated dimuon spectrum is displayed in Fig. 1. The main conclusion is that the value of the threshold at larger Q_T is mainly related to the effective quark masses at temperature being near T_c and appears to be almost independent of the initial state of the plasma. Such a universal threshold behavior of the dilepton Q_T spectra can be useful for the experimental verification of high effective parton masses in the quark-gluon plasma.

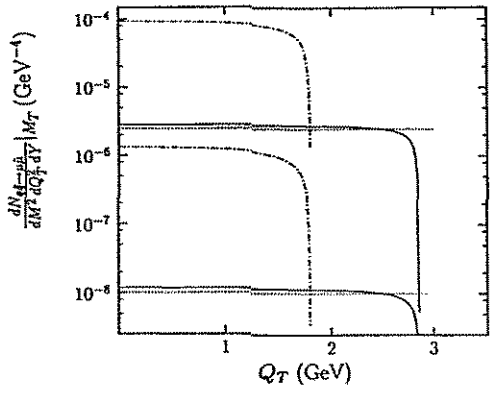

Fig. 1 *The dilepton yield at fixed transverse pair masses $M_T = 2, 3$ GeV (dot-dashed, full lines) as function of the transverse momentum Q_T. The upper (lower) curve uses the initial temperature $T_0 = 400$ (250) MeV. The dotted lines are for $m_q = 0$ GeV and bag model cooling in case of $M_T = 3$ GeV. For details consult [2,3].*

[1] *Institut für Theoretische Physik, TU Dresden and Institut für Kern- und Hadronenphysik, FZR*
[2] *Institute for Theoretical Physics, Kiev, Ukraine*
[3] *Institut für Theoretische Physik, TU Dresden*

References

[1] B. Kämpfer, O.P. Pavlenko, Phys. Rev. **C49** (1994) 2616
[2] A. Peshier, B. Kämpfer, O. P. Pavlenko, G. Soff, Phys. Lett. **B337** (1994) 235
[3] A. Peshier, Diploma Thesis, TU Dresden (1994), unpublished

Dielectron Production Cross Sections in pp and pd Reactions at 1 - 5 GeV[B]

A.I. TITOV[1], B. KÄMPFER[2], E.L. BRATKOVSKAYA[1]

The previous calculations of dielectron production cross sections in pp and pd reactions at 1 - 5 GeV [1] have been refined [2]. We use throughout the vector dominance model for all hadron-hadron-photon vertices. Dynamical suppression mechanisms (e.g., mass dependent Δ production rates, and correct energy dependence of the two-body T matrix) bring the elementary rate near to experimental data and previous estimates which do not use vector dominance. The Δ, η Dalitz decays and bremsstrahlung appear as dominant source of dielectrons. Bremsstrahlung is dealt with by an improved soft photon approximation which also applies to the pp collisions. Relying on a realistic deuteron wave function we also estimate the energy dependence of the ratio of dielectron yields in pp to pd reactions and find qualitative agreement with new experimental results.
In fig. 1 the invariant mass spectra are displayed. The experimental filter is taken into account. One observes a quite satisfactory description of the experimental data. A closer inspection of the ratio $\frac{d\sigma^{pd}}{dM} / \frac{d\sigma^{pp}}{dM}$, however, shows some discrepancies around 1 GeV proton energy. The theory seems here still to be hampered by uncertainties. It is just the range where dedicated heavy-ion experiments at GSI Darmstadt with the HADES detector can search for in-medium modifications of hadrons via the dielectron signals. Therefore, a more detailed study of the elementary cross sections is necessary.

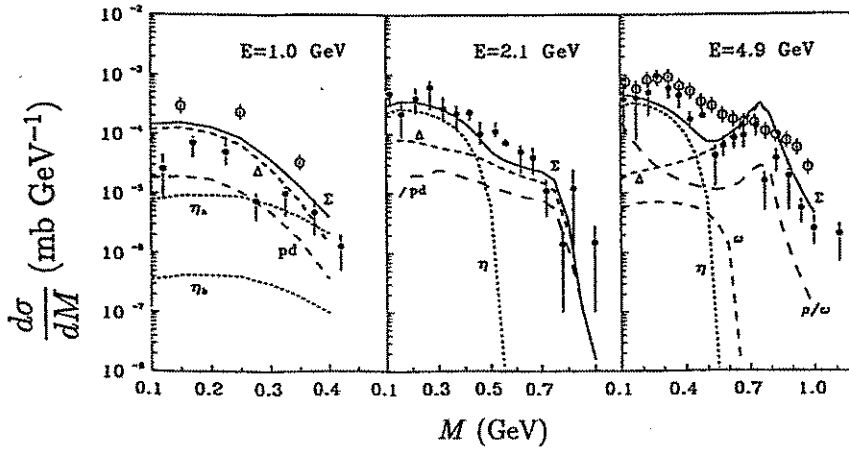

Fig. 1 *Dielectron invariant mass spectra for the pN collision at various energies (with DLS filter; pd labels bremsstrahlung, η, Δ, ω denote the corresponding Dalitz decay contributions, ρ/ω is the direct rho and omega decay, Σ is the sum of all contributions). Experimental data (heavy dots) are from $p\,^9Be$ collisions scaled by $A^{-2/3}$. Open circles at 1 GeV represent the product of calculated dielectron yields in pp collisions times the ratio of pd to pp dielectron production cross section. Open circles at 4.9 GeV are newer experimental data (see [2] for details).*

[1] *Bogoliubov Laboratory of Theoretical Physics, JINR Dubna, Russia*
[2] *Institut für Theoretische Physik, TU Dresden und Institut für Kern- und Hadronenphysik, FZR*

References

[1] B. Kämpfer, A.I. Titov, E.L. Bratkovskaya, Phys. Lett. **B301** (1993) 123
[2] A.I. Titov, B. Kämpfer, E.L. Bratkovskaya, FZR-34 (1994), Phys. Rev. **C51** (1995)

Flavor Evolution in a Parton Gas[B]

B. KÄMPFER[1], O. P. PAVLENKO[2]

Parton cascade models for ultrarelativistic heavy-ion collisions confirm Shuryaks hot glue scenario: at rather early stages there is a (nearly thermalized) hot gluon gas with a few quarks immersed. Even the gluon component might not be in chemical equilibrium but still undersaturated. To follow the evolution towards chemical equilibrium one can formulate rate equations [1] which include gluon multiplication $gg \to ggg$, gluon fusion processes $gg \to q\bar{q}$, $gg \to s\bar{s}$, flavor transmutation $q\bar{q} \to s\bar{s}$, and cross channels.
Such rate equations for the density evolution can be formulated as

$$\hat{n}_g = \frac{1}{2}\bar{\sigma}_{gg\to ggg}\, n_g^2\,(1-\lambda_g) - \bar{\sigma}_{gg\to q\bar{q}}\,(n_g^2 - n_q^2\, b) - \bar{\sigma}_{gg\to s\bar{s}}\,(n_g^2 - n_s^2\,\tilde{b}), \tag{1}$$

$$\hat{n}_q = \frac{1}{2}\bar{\sigma}_{gg\to q\bar{q}}\,(n_g^2 - n_q^2\, b) - \frac{1}{2}\bar{\sigma}_{q\bar{q}\to s\bar{s}}\,(n_q^2 - n_s^2\, c), \tag{2}$$

$$\hat{n}_s = \frac{1}{2}\bar{\sigma}_{gg\to s\bar{s}}\,(n_g^2 - n_s^2\,\tilde{b}) + \frac{1}{2}\bar{\sigma}_{q\bar{q}\to s\bar{s}}\,(n_q^2 - n_s^2\, c), \tag{3}$$

where $b \equiv \frac{\tilde{n}_g^2}{\tilde{n}_q^2}$, $\tilde{b} \equiv \frac{\tilde{n}_g^2}{\tilde{n}_s^2}$, $c \equiv \frac{\tilde{n}_q^2}{\tilde{n}_s^2}$ ($\tilde{n}...$ are the saturation densities) and $\lambda_g = n_g/\tilde{n}_g$ denotes the gluon fugacity. "$\hat{n}...$" means the comoving derivative. $\bar{\sigma}...$ stand for the thermally velocity-averaged elementary QCD cross sections. We solve these rate equations by taking into account the boost-invariant longitudinal expansion and the transverse expansion in the approximation of global relativistic hydrodynamics [2].
Since the corresponding cross sections are matter of debate, and also higher-order process might significantly contribute, we employ in one set (I) of calculations the cross sections of ref. [1], and in another set (II) we multiply the cross sections by a factor of 10. The results [3] are displayed in Fig. 1 for initial conditions as elucidated by parton cascade (HIJING) simulations [1] and estimated more qualitatively by Shuryak (for details see [2]). Given the range of uncertainties one observes that either all fugacities remain far below saturation (I) or the chemical equilibrium is very quickly achieved (II), even for the strange quarks. Despite these quite different flavor evolution scenarios we have shown [2] that such direct probes of the plasma evolution as the high-energy photons are rather insensitive. However, their absolute normalization depend quadratically on the initial particle densities.

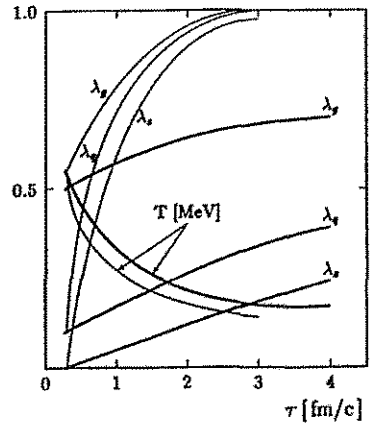

Fig. 1 *The evolution of the temperature T (in GeV) and the fugacities for the two scenarios (I/II - full/dashed lines) described in text.*

[1] *Institut für Theoretische Physik, TU Dresden und Institut für Kern- und Hadronenphysik, FZR*
[2] *Institute for Theoretical Physics, Kiev, Ukraine*

References

[1] T. Biro et al., Phys. Rev. **48** (1993) 1275
[2] B. Kämpfer, O.P. Pavlenko. Z. Phys. **C62** (1994) 491
[3] B. Kämpfer, O.P. Pavlenko, A. Peshier, G. Soff, in Proc. Strangeness'95, American Physics Institute (1995)

Rapidity Dependence of Thermal Dileptons Resulting from Hadronizing Quark-Gluon Matter with Finite Baryon Charge[B]

B. KÄMPFER[1], O.P. PAVLENKO[2], M.I. GORENSTEIN[2], A. PESHIER, G. SOFF[3]

The influence of the baryon charge on the rapidity distribution of dileptons produced in ultrarelativistic heavy-ion collisions is studied. We utilize realistic rapidity distributions of secondary particles (i.e., pions and baryons) expected for RHIC energies [1], which are extracted from RQMD simulations. As useful approximation we employ a frozen motion model with scaling invariant expansion of the hadronizing quark-gluon plasma. A more complete evolution scenario is envisaged. In our previous studies [2] we found important effects of transverse expansion as well as chemical and thermal relaxations.

We find a considerable suppression of the dilepton production yield at large rapidities due to the finite baryon density (see Fig. 1). There is an involved interplay of the initial entropy distribution, temperature, baryon chemical potential and initial time of evolution τ_0. The temperature is the dominating quantity, while the dilepton yield depends logarithmically on the baryon potential. We vary τ_0; the other parameters of the initial distributions are kept fix.

The comparison of our thermal dilepton rate with the Drell-Yan contribution is displayed in Fig. 2. Under such conditions the yield of pairs with invariant mass $M \sim 2$ GeV from the deconfined matter dominates over the hadron phase and a possible mixed stage. The best chances for identifying thermal dileptons are clearly around midrapidity.

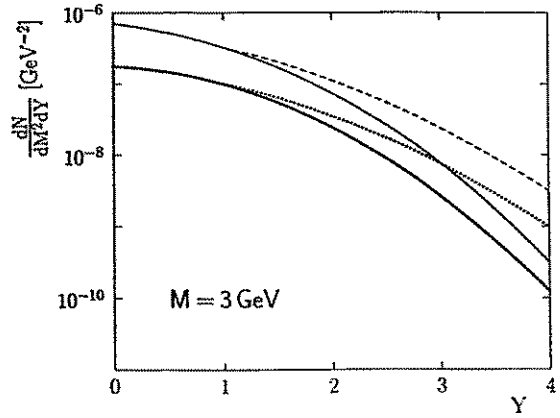

Fig. 1 *A comparison of our rapidity distribution of dileptons $dN_{l\bar{l}}/dM^2\,dY$ with the case of neglecting baryons (heavy full/thin lines - yield for $\tau_0 = 1./0.5$ fm·c^{-1}; dotted/dashed lines - yield for $\tau_0 = 1./0.5$ fm·c^{-1} and neglecting the baryon chemical potential).*

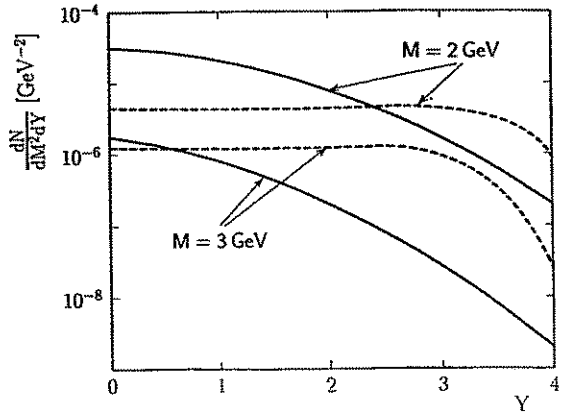

Fig. 2 *Rapidity distribution of the yield $dN_{l\bar{l}}/dM^2\,dY$ for $M = 2$ and 3 GeV (full lines). The initial conditions are fixed by $\tau_0 = 0.25$ fm/c (cf. [1] for more details). The dashed lines depict the Drell-Yan background for central Au + Au collisions at $\sqrt{s} = 200$ GeV.*

[1] *Institut für Theoretische Physik, TU Dresden and Institut für Kern- und Hadronenphysik, FZR*

[2] *Institut für Theoretische Physik, Kiev, Ukraine*

[3] *Institut für Theoretische Physik, TU Dresden*

References

[1] B. Kämpfer, O.P. Pavlenko, M.I. Gorenstein, A. Peshier, G. Soff, FZR-50 (1994)

[2] B. Kämpfer, O.P. Pavlenko, Phys. Lett. **B289** (1992) 127
B. Kämpfer, P. Koch, O.P. Pavlenko, Phys. Rev. **C49** (1994) 1132

A Calculation of the Tensor Analyzing Power T_{20} in Deuteron Break-up Reactions within the Bethe-Salpeter Formalism[B]

L.P. KAPTARI[1], A.YU. UMNIKOV[1,2], F.C. KHANNA[2], B. KÄMPFER[3]

Deuteron break-up reactions $A(D,p)X$ at medium and high energies are thought to serve as source of information on the high momentum components of the deuteron wave function. In the impulse approximation the differential cross section is proportional to the deuteron single-nucleon momentum density. This gives hope for the possibility of a direct extraction of the deuteron wave function from the experiment. Numerous experimental data have confirmed the impulse approximation picture for small internal momenta of nucleons in the deuteron, while a reasonable description of the data at higher momenta requires the incorporation of relativistic effects. It has been shown that even a minimal relativization procedure of the non-relativistic wave function is sufficient to describe fairly well the data in the kinematical region measured so far, except for a relatively broad shoulder around $p' \approx 0.3$ GeV/c (p' is the momentum of the final proton in the deuteron rest frame). Some unconventional processes have been considered as small corrections to the impulse approximation in attempts to explain this shoulder in the cross section. The success of such a simple but descriptive interpretation of the data has allowed one to discuss different aspects of the deuteron structure in these experiments.

In parallel, in the same experiments one measures the polarization characteristics of the deuteron, such as the tensor analyzing power T_{20} and the polarization transfer κ. These quantities are more sensitive to the reaction mechanism and to the internal structure of the colliding particles and give more detailed information. The first data on polarization phenomena has shown a discrepancy with theoretical predictions based on Bonn or Paris light-cone wave functions. The main disappointing moment here is that, while the theoretical calculation predicts a change of the sign of T_{20}, the experimentally deduced values seem to remain negative in the whole interval of the measured momenta. Very recent, preliminary data has confirmed that T_{20} is still negative, up to $p' \sim 0.5$ GeV/c. In this case an interpretation of the data in terms of a direct extraction of the deuteron wave function becomes doubtful. Even the very notion of an experimental deuteron wave function has to put into question. This challenge stimulated investigations of other mechanisms of interaction and possible manifestations of non-nucleonic degrees of freedom in the deuteron. All these additional contributions have been investigated as corrections to minimal relativization, and conclusions about the role of other mechanisms have been drawn relative to these results. Apart from the interests in other mechanisms, the investigation of relativistic effects in different approaches is still of a great importance.

We would like to emphasize that the contributions of other (unconventional) mechanisms may be discussed only after a consistent relativistic calculation of the main process. Nowadays the most complete relativistic investigation of one-nucleon exchange diagrams has been performed for backward elastic pD scattering by solving numerically the Bethe-Salpeter (BS) equation with a realistic interaction. Several authors studied the relativistic effects in the deuteron by considering the $D \to NN$ vertex within different approximations of the exact BS equation and applying it to electromagnetic and hadron elastic scattering of the deuteron. Up to now a consistent relativistic calculation for the deuteron break-up reactions and polarization phenomena in these processes is still lacking.

In a recent paper [1] we presented a relativistic analysis of the deuteron tensor analyzing power T_{20} (see Fig. 1) and the cross section in forward break-up reactions. A fully covariant expression for both the cross section and T_{20} is obtained within the Bethe-Salpeter formalism. Results of numerical calculations, utilizing the recently obtained numerical solution of the BS equation with a realistic interaction, are compared with the available experimental data and with several theoretical approaches, such as nonrelativistic and light cone calculations. It turns out that all these approaches still do not correctly describe the experimental data at $p' > 0.3$ GeV/c (see Fig. 1).

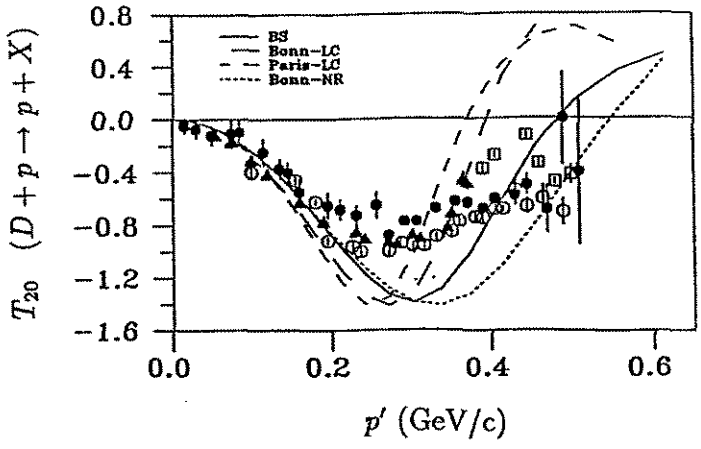

Fig. 1 *The differential deuteron tensor analyzing power as function of p' (solid line - our relativistic calculation [1] within the Bethe-Salpeter formalism, dotted line - non-relativistic calculation with the Bonn deuteron wave function, long-dashed (short-dashed) line - results of a minimal relativization within the light cone dynamics of the Bonn (Paris) wave functions; experimental data: triangles [2], open circles - [3], open squares - [3] (elastic backward pD-scattering), close circles - [4] ($^{12}C(D,p)X$ reactions).*

[1] *Bogoliubov Laboratory of Theoretical Physics, JINR Dubna, Russia*
[2] *Theoretical Physics Institute, University of Alberta, Edmonton, and TRIUMF, Vancouver, Canada*
[3] *Institut für Theoretische Physik, TU Dresden and Institut für Kern- und Hadronenphysik, FZR*

References

[1] L.P. Kaptari, A.Yu. Umnikov, F.C.Khanna, B. Kämpfer, FZR-64 (1994)
[2] C.F. Perdrisat et al., Phys. Rev. Lett. **59** (1987) 2840;
V. Punjabi et al., Phys. Rev. **C39** (1989) 608;
E. Cheung et al., Phys. Lett. **B 284** (1992) 210;
C.F. Perdrisat and V. Punjabi, Phys. Rev. **C42** (1990) 1899.
[3] L.S. Azhgirey et al., in *Proceedings of the XIV Few Body Conference, (ed.) F.Gross* 26-31 May, 1994, p. 18, Williamsburg, USA; Ibid. p. 22; V. Punjabi et al., ibid, p. 161
[4] V.G. Ableev et al., Nucl. Phys.**A 393** (1983) 491; JETP Lett. **47** (1988) 649; Few Body Systems **8** (1990) 137; JINR Rap. Comm. **1**[54] (1992) 108

Reproduction of Observables in the Bosonized NJL Model by a Reference Profil[B]

R. WÜNSCH, K. GOEKE[1], TH. MEISSNER[2]

We introduced a reference profile [1] which approximates the self-consistent meson field of the chiral quark-loop soliton obtained after bosonizing the Nambu & Jona-Lasinio model for the two light flavors [2]. The reference profile is independent of the regularization parameter and has a simple analytic shape. It interpolates smoothly between the exact asymptotic behavior of the meson profile at small and large separations, which can be determined analytically. Using the reference profile one avoids a self-consistent determination in a Hartree procedure, which is rather time-consuming. In this sense the reference profile is comparable with the Woods-Saxon potential modeling the average field of a nucleus.

We tested this approximation by evaluating expectation values of several observables. Soliton energies including partial contributions, mean-squared radii, axial-vector coupling strength, magnetic moments, and spurious center-of-mass and rotational energy as well were calculated using both the reference and the self-consistent profiles. In the physically relevant quark-mass region ($350\,\mathrm{MeV} \lesssim M \lesssim 500\,\mathrm{MeV}$) the deviations do not exceed 5 percent. Fig. 1 illustrates the deviations.

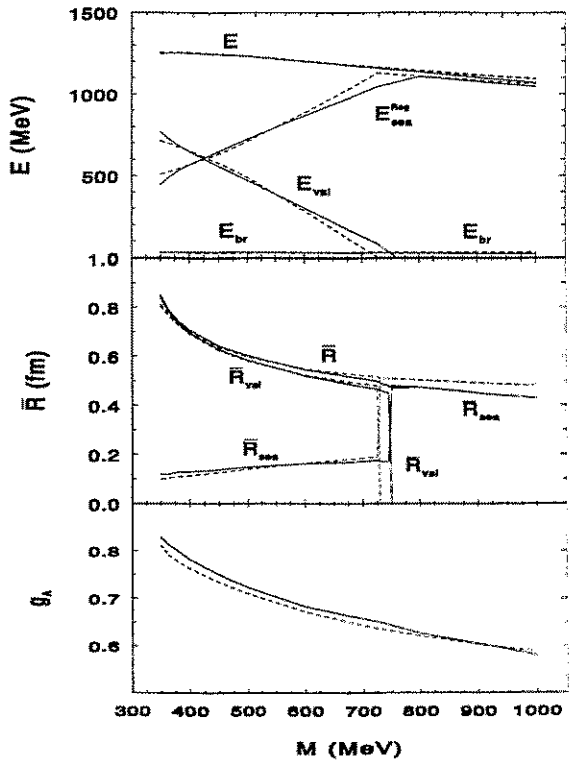

Fig. 1 *Nucleon observables [1,3] as a function of the constituent quark mass M calculated with self-consistently determined profiles (full lines) in comparison to the reference profile with R=0.42 fm (broken lines)*

Upper part: Total energy E, valence energy E_{val}, regularized sea energy E^{Reg}_{sea} and meson energy E_{br}.

Central part: Baryon mean square radius $\bar{R}$ and its valence and sea contributions.

Lower part: Proton axial-vector coupling constant g_A.

[1] *Institut für Theoretische Physik II, Ruhr-Universität Bochum*

[2] *Department of Physics and Astronomy, University of South Carolina*

References

[1] R. Wünsch, K. Goeke, Th. Meissner, *Z. Phys.* **A348** (1994) 111

[2] H. Reinhard, R. Wünsch, *Phys. Lett.* **B215** (1988) 577;
Th. Meissner, F. Grümmer, K. Goeke, *Phys. Lett.* **B227** (1989) 296

[3] R. Wünsch, **FZR 93-18**; *nucl-th*/9311017

Center-of-Mass and Isospin Corrected Observables of the NJL Hedgehog Soliton[B]

M. Schleif[1], R. Wünsch and Th. Meissner[2]

We studied [1] the effect of center-of-mass motion and isospin corrections on hedgehog meson fields and baryonic observables of a chiral quark-loop soliton derived from a two-flavor Nambu & Jona-Lasinio lagrangian. Fig. 1 shows the energy corrections resulting from translational and rotational zero modes, and from an additional collective rotation (cranking) of the soliton, which was introduced in order to adjust the isospin to the value of the nucleon or the Δ isobar, respectively. Minimizing an energy functional corrected by zero-mode and cranking energies we obtained corrected meson field and calculated mesonic and baryonic observables. The procedure corresponds to a 'variation after projection' on the semiclassical level.

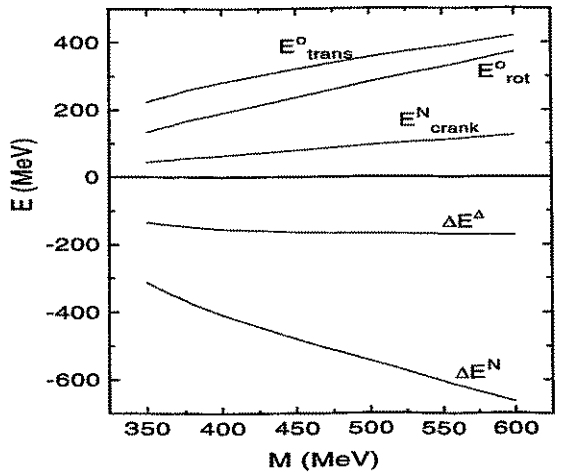

Fig. 1 *Spurious center-of-mass (E^o_{trans}), rotational (E^o_{rot}), cranking energies (E^N_{crank}) for the nucleon, and total energy corrections $\Delta E^{N,\Delta} = -E^o_{trans} - E^o_{rot} + E^{N,\Delta}_{crank}$ in dependence on the constituent quark mass M. The Δ cranking energy E^Δ_{crank} is 5 times larger than E^N_{crank}.*

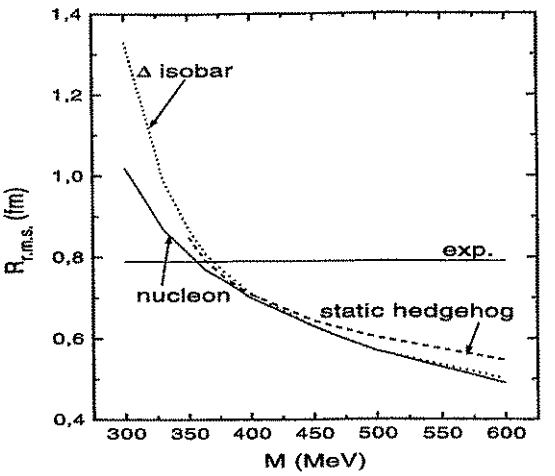

Fig. 2 *Baryonic root-mean-squared radius ($R_{r.m.s.}$) of the uncorrected static hedgehog field in comparison with radii calculated with corrected meson fields in dependence on the constituent quark mass M.*

Despite the considerable size of the energy corrections (fig. 1), in comparison to the static hedgehog energy of about 1300 MeV, expectation values are affected only moderately. In the physically relevant region of constituent quark masses (M$\approx$400 MeV), expectation values are modified by not more than 10 percent. Fig. 2 illustrates the influence of the corrections on the baryonic isoscalar root-mean-squared radius.

[1] *Institut für Kern- und Hadronenphysik, FZR* and *Institut für Theoretische Physik, TU Dresden*

[2] *Department of Physics and Astronomy, University of South Carolina*

References

[1] M. Schleif and R. Wünsch, **FZR – 55** (1994); *nucl-th/9409011*

Chiral Restoration and EOS for Nuclear Matter in the SU(2) Nambu & Jona–Lasinio (NJL) Model[B]

M. SCHLEIF[1] AND R. WÜNSCH

We have started to investigate the properties of a NJL hedgehog soliton [1] which is embedded in a medium of strongly interacting matter (quark gas). In a first step we studied the properties of the medium itself in dependence on temperature T and density ϱ. The medium is described by an effective lagrangian with a self-consistently determined σ field, which breaks chiral symmetry. The strength of the σ field is proportional to the expectation value $\langle\bar{q}q\rangle$ of quark-antiquark pairs (condensate). Quarks move in this medium with an effective mass $M^*(T,\varrho)$ (constituent quark mass) which is mainly determined by the strength of the σ field (dynamical mass).

Condensate and constituent mass decrease with increasing T and ϱ (Fig. 1). Above certain values of T and ϱ, M^* reduces to the current quark mass and chiral symmetry is (almost) restored. This transition can be described by a critical temperature T_c and a critical density ϱ_c defined as those values where $M^*(T,\varrho)$ reaches half its maximum value $M \equiv M^*(T{=}0,\varrho{=}0)$ [2]. From fig. 1 we get $T_c\,(\varrho{=}0) \approx 180\,\mathrm{MeV}$ and $\varrho_c\,(T{=}0) \approx 0.25\,\mathrm{fm}^{-3}$ for $M{=}350\,\mathrm{MeV}$.

Fig. 2 shows the equation of state $p(T,\varrho)$, which results from the effective NJL Lagrangian for $M{=}350\,\mathrm{MeV}$. A minimum is found at $T \approx 0$ and $\varrho \approx 2\varrho_o$, where ϱ_o is the normal nuclear matter density. A modified SU(2) NJL model incorporating the scale anomaly of QCD by introducing an additional dilaton field, which is identified with the gluon condensate, gives similar results [3].

In a next step we shall add a single hedgehog solitons to the medium and study its properties in dependence on T and ϱ.

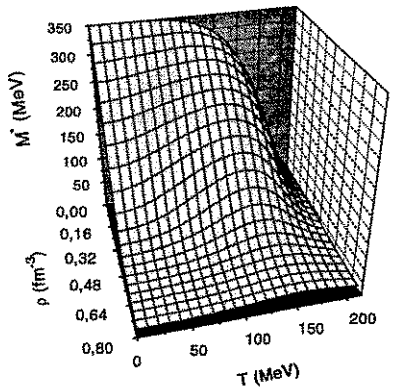

Fig. 1 *Constituent quark mass M^* in dependence on the baryon density ϱ and temperature T for a finite quark current mass.*

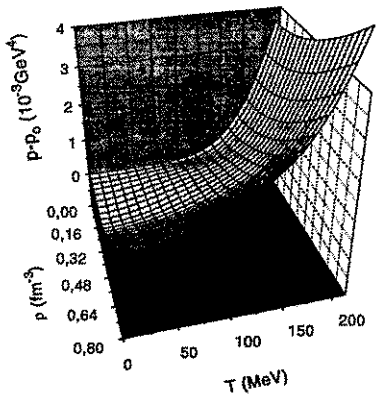

Fig. 2 *Pressure p of a constituent quark gas in dependence on the baryon density ϱ and temperature T relative to the value p_0 at $T{=}0$ and $\varrho{=}0$.*

[1] *Institut für Kern- und Hadronenphysik, FZR* and *Institut für Theoretische Physik, TU Dresden*

References

[1] R. Wünsch, K. Goeke, Th. Meissner, *Z. Phys.* **A 348** (1994) 111
[2] S.P. Klevansky, *Rev. Mod. Phys.* **64** (1992) 51
[3] M. Jaminon, B. Van den Bossche, *Nucl. Phys.* **A567** (1994) 865

Decay of Superdeformed Bands in Nuclei around ^{135}Nd

R. M. CLARKE[1], M. A. DELEPLANQUE[1], S. FRAUENDORF AND F. S. STEPHENS[1]

In almost all cases, the decay path of superdeformed (SD) bands into low deformation states is not yet established experimentally. An exception are nuclei in the mass 130 region. A prominent configuration dependence in the decay pattern is observed: The last observed spin in the SD band strongly depends on the nucleus. A particular striking example is ^{135}Nd, whose SD band [1], based on the $i_{13/2}$ neutron orbital, terminates suddenly at spin 25/2, although lower levels are seen in the neighboring odd N nuclei. Calculations of the deformation energy show that there are two competing minima, one is the axial SD band the other a triaxial one with lower deformation. At spin 25/2 the two have the same energy and the nucleus slides from the SD into the triaxial minimum, which has a configuration similar to the low deformation states into which it immediately decays. The deformation change corresponds to a "hop" by scattering a neutron and a proton pair. This picture explains the fragmentation of the decay and the increase of the lifetimes observed experimentally [1]. In adjacent nuclei the triaxial minimum lies higher and the decay out of the SD band is delayed. It is possible that the configuration dependence seen in the decay of SD bands in heavier nuclei can be understood in terms of subsequent hops.

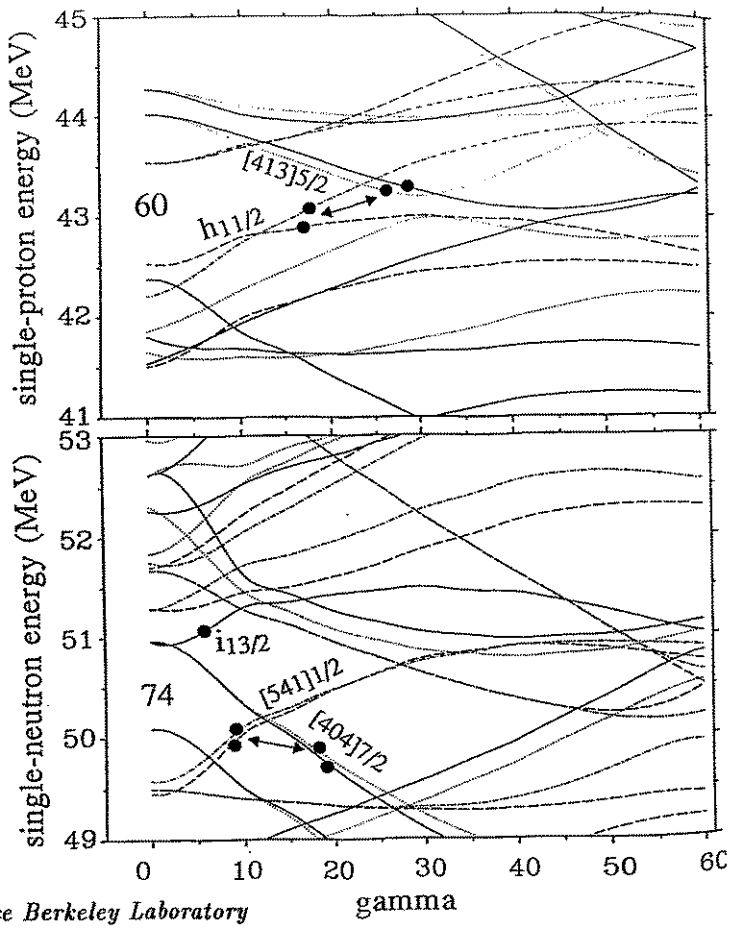

Fig. 1 *Single particle energies along a straight path in the (ϵ, γ) plane connecting the two minima at $(0.3, 8°)$ and $(0.22, 30°)$. The configuration change in ^{135}Nd when hopping from the high deformation to the low deformation minimum is indicated.*

[1] *Lawrence Berkeley Laboratory*

References

[1] M. A. Deleplanque *et al.*, subm. Phys. Rev. Lett.

Confirmation of the Shears Mechanism in Light Pb Isotopes

G. BALDSIEFEN[1] ,S. FRAUENDORF, H. HÜBEL[1] AND M. NEFFGEN[1]

The recently discovered $\Delta I = 1$ bands in the light Pb nuclei (c.f. e.g. [1]) are a challenge to standard nuclear structure theory, since they occur in almost spherical nuclei. The striking regularity is a consequence of the shears mechanism suggested in ref. [2]: High j proton (neutron) particles and high j neutron (proton) holes prefer a perpendicular orientation of their angular momenta, since this maximizes the spatial overlap of their wavefunctions. Moving up the band, most of the angular momentum is gained by gradually aligning these angular momentum vectors.

The shears mechanism is an example of "Magnetic Rotation", discussed in ref [3], which is expected in weakly deformed nuclei, when the high j levels of particle type and the high j levels of hole type are combined. In contrast to ordinary rotation, it is characterized by: regular $\Delta I = 1$ sequences with a low but rather constant moment of inertia $\mathcal{J}^{(2)}$, large B(M1) values and very small B(E2) values. The regularity is not a consequence of the anisotropy of the density distribution, as for ordinary rotational bands, but rather it is caused by a very anisotropic current distribution.

Very important experimental signatures of the shears bands are contained in their lifetimes for γ decay. Tilted Axis Cranking (TAC) calculations predict [2]: Very low B(E2) values (almost spherical) and strong but decreasing B(M1)values (closing of the blades reduces the transversal magnetic moment). Lifetimes have been measured in ^{199}Pb [4]. For the first time both the decreasing of the B(M1) values and the very small deformation (the B(E2) values correspond to $\beta < 0.08$) could be experimentally demonstrated. The agreement with TAC calculations is very good.

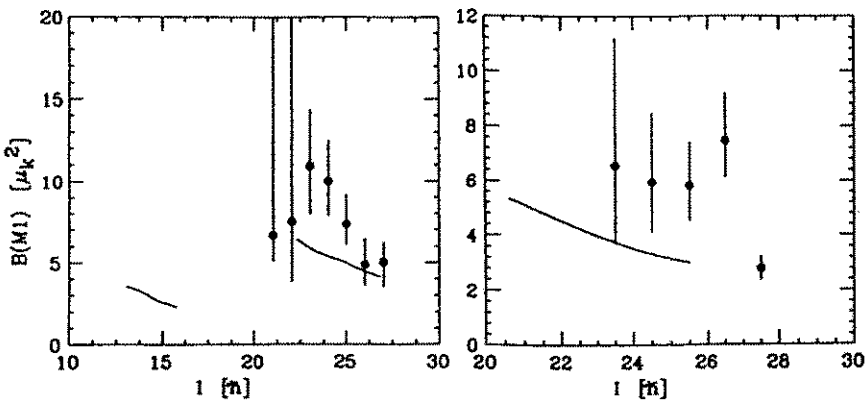

Fig. 1 *Experimental B(M1) values for two shears bands in ^{199}Pb compared to TAC calculations (full drawn lines).*

[1] *Institut für Strahlen - und Kernphysik, Universität Bonn*

References

[1] G. Baldsiefen *et al.* Nucl. Phys. **A 574** (1994) 521
[2] S. Frauendorf, Nucl. Phys. **A557** (1993) 259c
[3] S. Frauendorf, Proc. Int. Conf. on Large γ - ray detectors, Berkeley 1994, in print
[4] M. Neffgen *et al.*, to be publ.

Origin of the $\Delta I = 4$ staggering in Superdeformed Bands

S. FRAUENDORF AND J. MENG[1]

It has recently been found that some superdeformed $\Delta I = 2$ bands in the mass 150 and 190 regions [1,2] show a $\Delta I = 4$ staggering, i. e. the curve found by interpolating the sequence $I = I_0 + 4n$ is by a few keV displaced form the curve obtained by interpolating the sequence $I = I_0 + 2 + 4n$. This energy displacement has been interpreted as a consequence of an inherent fourfold symmetry. Hamamoto and Mottelson [3] ascribe the staggering to a nonaxial deformation that makes the *long* axis of the nucleus to a fourfold (C_4) symmetry axis. In their approach the bands are described by the rotational hamiltonian

$$H = A_1 I_1^2 + A I_3^2 + B_1 (I_1^2 - I_2^2)^2, \quad A = A_3 - A_1 = \frac{1}{2}(\frac{1}{\mathcal{J}_3} - \frac{1}{\mathcal{J}_1}) \qquad (1)$$

It is found that a sizable staggering appears only if $B_1/A > 10^{-2}$.
We have used Tilted Axis Cranking (TAC) [4] to investigate whether a deformation of the C_4 type is able to generate staggering. TAC permits to calculate the classical energy. This function $E(I, \vartheta, \phi)$ is compared with the energy obtained from the rotational hamiltonian (1) by substituting the classical vector $\vec{J}$ for the angular momentum operator $\vec{I}$.
We use the TAC routhian

$$h' = h_{mho}(\varepsilon_2) - \hbar\omega_o \varepsilon_{44} \rho^2 (Y_{44} + Y_{4-4}) - \vec{\omega} \cdot \vec{j}, \quad \vec{\omega} = \omega(\sin\vartheta\cos\phi, \sin\vartheta\sin\phi, \cos\vartheta) \qquad (2)$$

to calculate the classical energy $E(I, \vartheta, \phi) = \langle h' \rangle + \vec{\omega} \cdot \vec{J}$, where h_{mho} is the Nilsson hamiltonian, $\hbar\omega_o$ the oscillator energy and ρ the radius in units of the oscillator length.
As an example, we study $Z = 80$ and $N = 114$ with the deformations $\varepsilon_2 = 0.42$ and ε_{44}=0.1 at the angular momentum $J = 39$ corresponding to $\omega \approx 0.3 MeV$. At $\phi = 45°$ the angular momentum components are given by the relation $J_1 = \mathcal{J}_1 \omega \sin\vartheta \;\; J_3 = \mathcal{J}_3 \omega \cos\vartheta$, where $\mathcal{J}_1 = 0.13 keV^{-1}$ is found. The function $J_3(\vartheta)$ shows steps, indicating rearrangements of particles. The determination of $\mathcal{J}_3$ becomes to certain extend ambiguous. Our calculations place $\mathcal{J}_3$ in the interval $0.02 keV^{-1}$ to $0.07 keV^{-1}$ and, hence, $4keV < A < 21keV$. The function $E(J, \vartheta = 90°, \phi)$ follows the expected $(\cos(2\phi))^2$ dependence to a good approximation. For the coefficient we find $B_1 J^4 = 50keV$ and $370keV$ for the yrast and the lowest neutron p - h excitation, which correspond to $B_1 = 2 \times 10^{-5} keV$ and $1 \times 10^{-4} keV$, respectively. Even if the lower limit $A = 7keV$ is assumed the ratio $B_1/A \sim 10^{-4} ... 10^{-5}$.
In conclusion, assuming a substantial C_4 distortion for superdeformed ^{194}Hg we are able to construct a classical hamiltonian that has the form of the rotational hamiltonian used by Hamamoto and Mottelson to describe the $\Delta I = 4$ staggering. However, the calculated ratio B_1/A is by far to small to generate a staggering of the observed order of magnitude.

[1] *Postdoc from Institute for Theoretical Physics, Academica Sinica, Bejing, China*

References

[1] S. Flibotte *et al.* Phys. Rev. Lett, **71** (1993) 4299
[2] B. Cederwall *et al.* Phys. Rev. Lett, **72** (1994) 3150
[3] I. Hamamoto and B. Mottelson, Phys. Lett. **B333** (1994) 294
[4] S. Frauendorf, Nucl. Phys. **A557** (1993) 259c

Resonance Phenomena in a Statistical Model [D]

E. Sobeslavsky, F.-M. Dittes and I. Rotter[1]

Within a simplified S-matrix model [1] we investigate the resonance behaviour of an open quantum system as a function of the coupling strength between bound and unbound states. Here, *simplified* means that we follow the S–matrix poles corresponding to an effective Hamiltonian [2] $H^{eff} = H_0 - i\pi\alpha\sum_{c=1}^{\Lambda} V_c V_c$, where both the $N \times N$ matrix H_0, and the components of the coupling vectors V_c are properly chosen from a Gaussian distribution. N denotes the number of bound states (we restrict ourselves to $N = 15$), while $\Lambda = 3$ is the number of decay channels coupled to the bound states.
Increasing the coupling parameter, α, we trace the situation with well isolated resonances to that one with strongly overlapping resonances. Fig. 1 shows the elastic cross sections, $\sigma_{11} = \mid 1 - S_{11}(E) \mid^2$, and Argand diagrams for $\alpha = 0.002$, 0.015, 2.0 (the Argand diagrams being the energy dependent location of the S-matrix values in the (ReS_{11}, ImS_{11}) - plane for real values of E). At $\alpha = 0.002$ the resonances are well isolated. The separation of different time scales starts at $\alpha \approx 0.015$. At $\alpha = 2.0$ the cross section shows dips instead of resonances.
Regarding the cross sections and the Argand diagrams together with the landscapes of the S-matrix (not shown here), we conclude that at high level density different S-matrix poles become relevant if different energy resolutions are used. Our investigations show how gross, intermediate and fine structures arise in the cross section. These structures can be described only if the interferences between all resonances are taken into account.

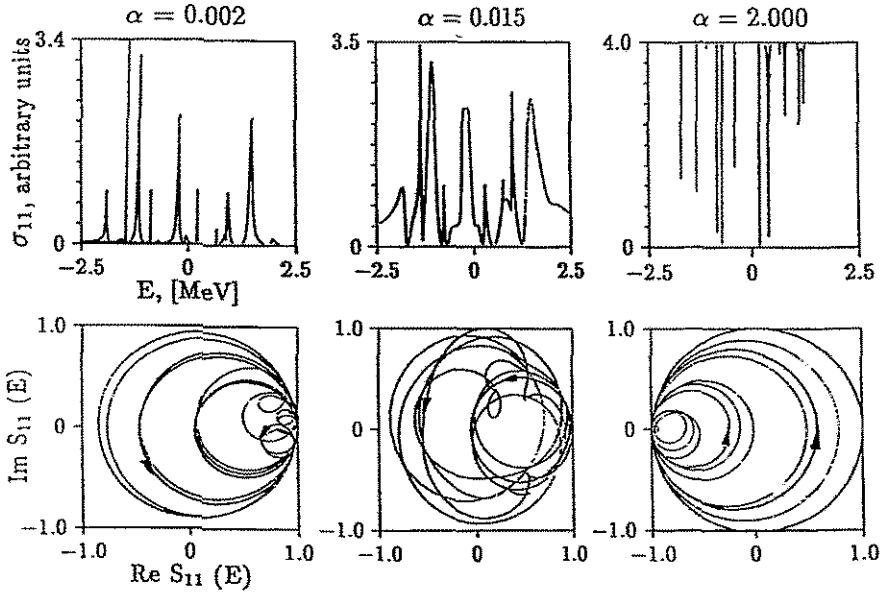

Fig. 1 *Cross sections and Argand diagrams for typical coupling parameters (see text)*

[1] *Institut für Theoretische Physik, TU Dresden* and *Institut für Kern- und Hadronenphysik, FZR*

References

[1] F.-M. Dittes, I. Rotter and T. H. Seligman, Phys. Lett. **A 158** (1991) 14
[2] W. Iskra, I. Rotter and F.-M. Dittes, Phys. Rev. **C 47** (1993) 1086

Level Repulsion in the Complex Plane [D,W]

M. MÜLLER, F.-M. DITTES, W. ISKRA[1] AND I. ROTTER[2]

We investigate the behaviour of resonances in a model quantum system Q – described by an N-dimensional Hilbert space – coupled to Λ decay channels as a function of the coupling strength α between the eigenstates of the (originally closed) system Q and these channels. The effective Hamiltonian describing this situation is of the form [1,2] $H^{eff} = H_0 - 2i\alpha \sum_{c=1}^{\Lambda} V_c V_c$, where H_0 denotes the Hamiltonian of Q itself, whereas $V_c \equiv \{V_c^i\}_{i=1,\ldots,N}$ is the (normalized to length one) coupling vector of Q to the c-th channel.

The (complex) eigenvalues of H^{eff} determine both the positions and the widths of the resulting resonance states. It is known that an increase of α causes a significant reorganization of the spectrum, leading to a separation of resonance lifetimes. Since large α correspond to a large overlap of the states, it is believed that the latter mechanism is relevant for the spectra of heavy nuclei [3].

In the present work we investigate the formation of broad and narrow ("trapped") structures in detail. We point out, that the underlying mechanism for it is the consecutive repelling of states (eigenvalues of H^{eff}) in the complex plane. The relevant scattering process of two resonances is investigated analytically for one decay channel in dependence on the symmetry of V. In particular, we show that a complete symmetry of V leads to a degeneracy of the resonances, both in position and in width. At the degeneracy point the wave functions of the states become unnormalizable, and the velocities (with respect to α) of the eigenvalues of H^{eff} diverge.

We investigate the behaviour of the cross section σ^{tot} near such critical points and emphasize that a direct extraction of widths and positions of the resonances might be misleading due to their strong interference. This is illustrated in Fig. 1 for the case of two resonances and one open channel for different values of α. The coupling vector has been chosen symmetrically, $V^1 = V^2 = 1/\sqrt{2}$, and the critical value of α equals 1. For comparison the Breit–Wigner profiles with resonance parameters corresponding to the eigenvalues of H^{eff} are drawn (dashed lines).

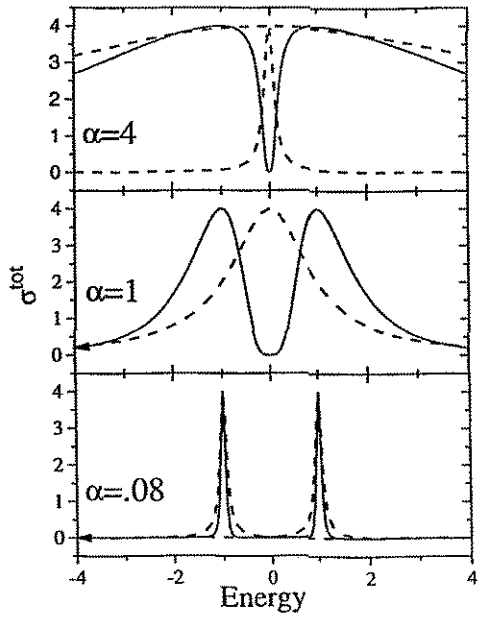

Fig. 1 *Cross section σ^{tot} in the case of two resonances.*

[1] *Soltan Institute for Nuclear Studies, PL-00-681 Warszawa, Poland*

[2] *Institut für Theoretische Physik, TU Dresden* and *Institut für Kern- und Hadronenphysik, FZR*

References

[1] C. Mahaux and H. A. Weidenmüller, *"Shell-Model Approach to Nuclear Reactions"*, North–Holland, Amsterdam, 1969

[2] F.-M. Dittes, H. L. Harney and I. Rotter, Phys. Lett. **A 153** (1991) 451

[3] I. Rotter, Rep. Prog. Phys. **54** (1991) 635

Localization in Random Band Matrices with Powerlaw Shape of the Band

F.-M. DITTES, Y. V. FYODOROV[1,3], A. D. MIRLIN[2,3], J. QUEZADA[4] AND T. H. SELIGMAN[4]

The ensemble of random band matrices is defined as a set of large $(N \times N)$ matrices with elements $H_{ij} = G_{ij} \cdot a(\mid i-j \mid)$, $i,j = 1,\ldots,N$, where the G_{ij} are independently distributed Gaussian variables – so that the matrix G belongs to the Gaussian Orthogonal Ensemble – whereas $a(\mid i-j \mid)$ is some function tending to zero for $\mid i-j \mid \to \infty$ and determining the shape of the band.

Random band matrices generalize, therefore, the usual random matrices where the function a would be a constant. They were first introduced as an attempt to describe intermediate level statistics for Hamiltonian systems in a transitional regime between complete integrability and fully developed chaos. Afterwards, they found applications in various contexts ranging from atomic physics [1] to solid state physics [2], and especially in the course of investigations of the quantum behavior of driven chaotic systems [3].

Most frequently, the function $a(\mid i-j \mid)$ is considered to be fast (at least, exponentially) decreasing when $\mid i-j \mid$ exceeds some typical value b called the bandwidth. Matrices of this sort are known to have eigenfunctions extended over all basis states when $b \sim N$, whereas for $b \ll N$ the eigenfunctions become localized. They arise naturally in the description of Anderson localization of a quantum particle in a random potential and of its dynamical analogues [4].

In the present work, we study the case intermediate between that of constant a and that of exponentially fast vanishing $a(\mid i-j \mid)$ by assuming a powerlike decrease of $a(\mid i-j \mid)$ for large $\mid i-j \mid$: $a(\mid i-j \mid) \sim |i-j|^{-\alpha}$. Such matrices describe slowly decaying correlations between distant states and appear in the description of certain chaotic systems as well as in solid state problems [5].

We provide both analytical arguments and extended numerical evidence showing the peculiarities of powerlike $a(\mid i-j \mid)$. In particular, we find a crossover from the region of localized ($\alpha > 3/2$) to completely extended ($\alpha < 1/2$) eigenvectors. In the region $1/2 \leq \alpha \leq 3/2$ eigenvectors are of complex nature and share features typical for both localized and extended states.

[1] *Fachbereich Physik der Universität-Gesamthochschule Essen*

[2] *Institut für Theorie der Kondensierten Materie, Universität Karlsruhe*

[3] *Petersburg Nuclear Physics Institute, Gatchina, Russia*

[4] *IFUNAM Laboratorio de Cuernavaca, Cuernavaca, Mexico*

References

[1] M. Feingold, in *"Quantum Chaos – Quantum Measurement"*, ed. P. Cvitanovic et al., NATO ASI Series C, v. 358, Kluwer 1992, p. 167

[2] P. Devillard, J. Stat. Phys. **62** (1991) 373

[3] F. M. Izrailev, in *"Quantum Chaos – Quantum Measurement"*, loc. cit., p. 89

[4] S. Fishman, D. R. Grempel and R. E. Prange, Phys. Rev. Lett. **49** (1982) 509

[5] J. V. Jose and R. Cordery, Phys. Rev. Lett. **56** (1986) 290; G. Yeung and Y. Oono, Europh. Lett. **4** (1987) 1061

Wave Functions, Evolution Equations and Evolution Kernels in Light–Ray QCD

D. MÜLLER[1], D. ROBASCHIK[1], B. GEYER[1], F.-M. DITTES AND J. HOŘEJŠI[2]

It is generally accepted that quantum chromodynamics (QCD) allows the theoretical description of scattering processes at large momentum transfer, where the hard scattering subprocess can be treated perturbatively, whereas for the remaining parts of the process one has to use "parton distribution functions" or "wave functions". These functions are not calculable perturbatively, but have to be determined phenomenologically. Nevertheless additional information on them can be obtained because they satisfy evolution equations with respect to the involved momenta.

In the present work evolution equations for nonperturbative wave functions and distribution functions of QCD are derived on a unified basis using the framework of non-local light cone expansion. For this purpose generalized distribution amplitudes are introduced as matrix elements of light-ray operators. The evolution equations for these amplitudes follow from the renormalization group equation of the considered operators. This implies that the evolution kernels can be obtained from the anomalous dimensions of the corresponding operators.

On the basis of these general considerations the evolution equation for the exclusive virtual Compton scattering amplitude in the Bjorken region is derived. Furthermore, the evolution equations for the quark distribution function with the known Altarelli-Parisi-Lipatov kernel as well as for hadron wave functions with the Brodsky-Lepage (BL) kernel are obtained.

We point out that the general evolution kernels are extended BL kernels containing the standard BL kernel (for the usually considered restricted domain of definition). Especially, it is possible to derive the Altarelli-Parisi-Lipatov kernel as a limiting case of the extended BL kernel. It is shown that the calculation of the BL kernel as evolution kernel in QCD is sufficient for the determination of the extended BL kernel.

The mentioned connection is valid to all orders of perturbative QCD. This allows a consistency check of the existing two-loop calculations of the BL and the Altarelli-Parisi kernels in QCD [1]. Technical basis of the obtained results are analytical and support properties of the anomalous dimensions of light-ray operators obtained with the help of the α-representation of Green's functions (for a detailed report see [2]).

[1] *Fachbereich Physik der Universität Leipzig*

[2] *Nuclear Centre, Charles University Prague, ČR*

References

[1] F.-M. Dittes et al., Phys. Lett. **209 B** (1988) 325

[2] D. Müller, D. Robaschik, B. Geyer, F.-M. Dittes and J. Hořejši, Fortschr. d. Phys. **42** (1994) 101

Investigation of an Ensemble near the Elastic Threshold [D]

M. MÜLLER, E. PERSSON, I.ROTTER[1]
W. ISKRA[2]

The structure of discrete nuclear states is described by the Hamilton operator $H = H_0 + V$. H_0 is the shell model hamiltonian and V is the residual interaction between the nucleons, which describes the *internal mixing* of the states. Eigenvalues and eigenfunctions of H are real and provide the energies and wavefunctions of the states. The states used in the calculation are many particle states with 2p-2h excitations. They can have an energy above the elastic threshold for neutron scattering.

In the continuum shell model, these states are coupled to the continuum of decay channels. This gives a finite lifetime against particle decay to the states above the threshold. The structure of the states is described by an effective Hamilton operator $H^{eff}_{QQ} = QHQ + QVP \cdot G^{(+)}_P \cdot PVQ$ [2] where Q and P are projection operators onto the closed system states and the continuum respectively. $G^{(+)}_P$ is the Green function for the motion of a particle in the continuum. In contrast to H, the operator H^{eff}_{QQ} is non-hermitean and has complex eigenvalues, $\tilde{\varepsilon}_R = \tilde{E}_R(E) - \frac{i}{2}\tilde{\Gamma}_R(E)$, where E is the system energy. If the fixpoint equation $\tilde{E}_R(E_R) = E_R$ $(E_R \geq 0)$ is solved can E_R and $\Gamma_R = \tilde{\Gamma}_R(E_R)$ be interpreted as energy and width of the resonance R respectively. For states below the elastic threshold, $\tilde{\Gamma}_R(E > 0)$ is a measure of the collectivity of the states. The second term of H^{eff}_{QQ} describes the *external mixing* of the states via the continuum of decay channels, the value of which is determined by both the residual interaction V and the level density (degree of resonance overlapping).

The external mixing of nuclear states via the continuum is investigated numerically at energies near the elastic threshold. It is for two states and one open channel:

$$W^{ext}_{RR'} = \int dE' \, \langle \Phi_R | V | \xi^{c(+)}_{E'} \rangle \, \frac{1}{E^{(+)} - E'} \, \langle \xi^{c(+)}_{E'} | V | \Phi_{R'} \rangle \, .$$

Here, Φ_R are eigenfunctions of QHQ and ξ^c_E are channel wavefunctions describing the motion of one unbound particle relative to the residual nucleus. While the imaginary part of $W^{ext}_{RR'}$ is zero at energies below the elastic threshold (residuum of the integral), the real part, consisting of the principal value integral, does not vanish at these energies. Therefore, even discrete states below the threshold may be mixed via $W^{ext}_{RR'}$.

We investigate the possible influence of states below the elastic threshold to states above this threshold. The complex eigenvalues of the effective hamiltonian are studied as a function of the parameter α^{ex} which determines the strength of the coupling to the continuum. α^{ex} is varied from 0.05 to 10 is steps of 0.05. An ensemble of 190 states with $J^\pi = 1^-$ is used. Only one neutron channel is considered as open. The system energy is always kept at 4MeV, i.e the fixpoint equation is not solved. The closed system energies (i.e eigenvalues of the hermitean QHQ) are shifted to around the elastic threshold.

Fig 1: The widths and the energies of all states for all α^{ex}. The trapping effect (formation of two time scales at large α^{ex}) can clearly be seen. It has been shown that the actual shape of this eigenvalue picture is only weakely dependent on the position of the elastic threshold and on the system energy.

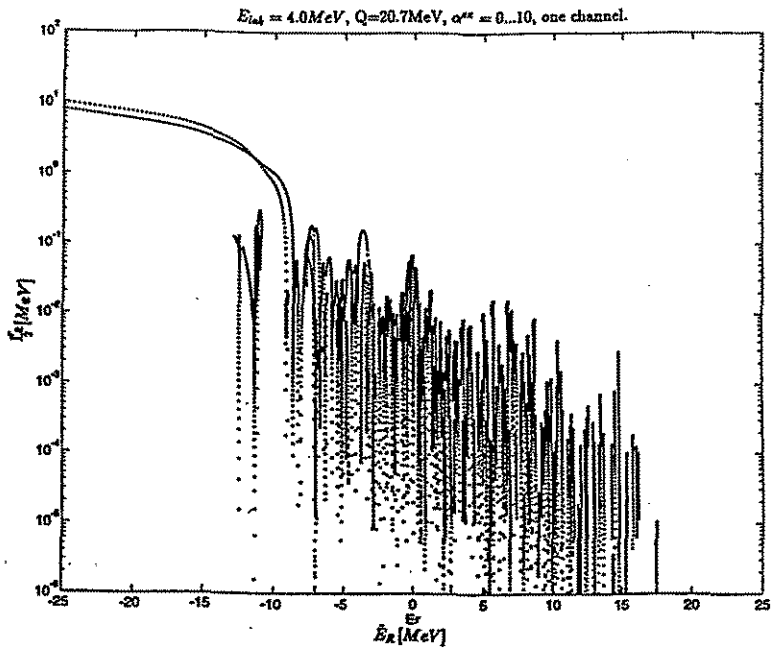

Fig 2: The closed system energies for states above the elastic threshold are increased by 5Mev and the energy of states below this threshold are decreased by 3MeV. This splits the ensemble in a discrete and a resonant part. For small α^{ex} the states are so narrow that the gap effectively splits the ensemble in two independent parts. For sufficiently large α^{ex} though, we can clearly see that the broadest of the resonant states gets trapped by the discrete states.

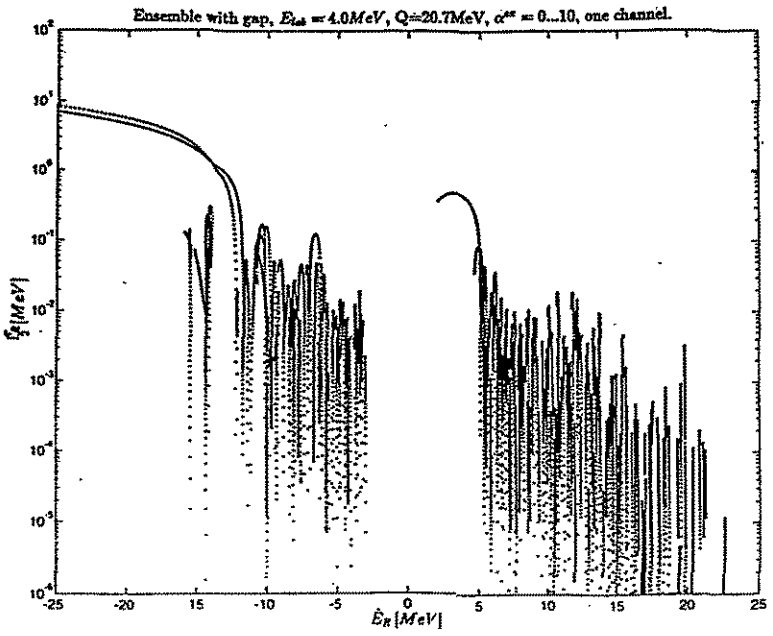

The result that THE DISCRETE STATES CAN TRAP THE RESONANT STATES is of special interest for the neutron resonances lying in the very neighbourhood of the elastic neutron threshold. The result also implies that some care must be taken to the discrete states when interpreting a measured neutron spectrum close to the elastic threshold.

[1] *also Technische Universität Dresden, Institut für Theoretische Physik, D-01062 Dresden.*
[2] *also Soltan Institute for Nuclear Studies, PL-00-681 Warszawa, Poland*

References

[1] W. Iskra, M.Müller, I. Rotter J. Phys. G, 19(1993)2045; **20**(1994)775
[2] I. Rotter Rep. Prog. Phys. 54(1991)632

Magnetic Properties of Sodium Clusters

S. FRAUENDORF, S. M. REIMANN[1] AND V.V.PASHKEVICH[2]

It is possible to measure the magnetic moments of atomic clusters by the deflection in a strong (1T) Stern-Gerlach magnet. Fractions of a Bohr magneton μ_B are detectable. The magnetic moment probes the angular momentum composition of the delocalized valence electron wavefunctions in alkali clusters. The components of the magnetic moment in units of μ_B are given by

$$\mu_i = -\langle 0|l_i + 2s_i|0\rangle + \left(\sum_n \frac{|\langle n|l_i + 2s_i|0\rangle|^2}{E_n - E_o} - m \int \rho(\vec{x})(x_{i+1}^2 + x_{i+2}^2) d^3x \right) \omega_i \quad i \text{ cyclic}$$

with $|0\rangle$ and $|n\rangle$ beeing the ground and excited states of the valence electron system. The magnetic field B is expressed by $\omega = \mu_B B$, which is $0.579 \times 10^{-4} eV$ for B=1T.
The first term describes the paramagnetism. We have calculated the paramagnetism of Na clusters containing up to 100 atoms. The shapes are found by means of the shell correction methods of ref. [2]. It is found that μ can reach several μ_B provided the clusters have axial shape ($l_3 = \Lambda \neq 0$; the symmetry axis is 3). The paramagnetic deflection of odd clusters varies strongly with N reflecting the filling of the levels in the deformed potential. The Λ- values are sensitive to the cluster shape and the radial profile of the potential.
A particular striking effect is the quenching of the orbital paramagnetism ($\langle l_i \rangle = 0$) when the odd cluster takes on a triaxial shape. Using the method of refs. [3,4] we have calculated the triaxiality of Na clusters in the range N = 10...200. Triaxial shapes are found for clusters around $N = 12, 16, 24, 32, 48, 72, 82, 96, 106, 150$. In these regions the orbital paramagnetism is sytematically quenched for several adjacent clusters, what may be used as experimental evidence for triaxial shapes.
The second and third term describe the diamagnetism, which appears in even axial clusters with filled Λ- quadruplets or even triaxial clusters. For spherical shape the first term is zero and the cluster becomes an ideal diamagnet, like a superconductor. However, the persistent currents are a consequence of the quantization of the valence electron motion and not of pair correlations. For deformed shape the two terms partially compensate. Thus, an axial cluster has one ideal diamagnetic axis and two axes of incomplete diamagnetism. The diamagnetic susceptibility of axial and triaxial clusters containing up to 200 atoms has been studied, using the shapes calculated by means of the shell correction methods of ref. [2] and [3,4].
A first report of the results is given in ref. [4]. We are investigating the influence of ionic structure, thermal damping and the transition to the dissipative regime with eddy currents, characteristic for the nonsuperconducting metals, in large clusters.

[1] *ITP Universität Regensburg, Germany*
[2] *LTP JINR, Dubna, Russian Federation*

References

[1] W. de Heer, Thesis, UCB Berkeley and privat communication
[2] S. Frauendorf, V.V. Pashkevich, Z. Phys **D26** (1993) S 98
[3] S.M. Reimann, M. Brack, K. Hansen, Z. Phys. **D28** (1993) 235
[4] S. Frauendorf, S. M. Reimann and V.V.Pashkevich, Surface Review and Letters, in print, contribution to this annual report

Triaxial Shapes of Sodium Clusters [1]

S. Frauendorf, S. M. Reimann[1] and M. Brack[1]

Combining a modified Nilsson-Clemenger model with the shell correction method, the energy surfaces of sodium clusters with sizes up to $N = 200$ atoms are calculated for triaxial quadrupole and a special combination of hexadecapole deformations. Generalizing the Kohn - Sham - Nilsson approach of ref. [1] to triaxial clusters, the model parameters are fitted to the single-particle spectra obtained from microscopic jellium model calculations for spherical clusters, using the local density approximation. The ground-state shapes and energies are determined by simultaneous minimization with respect to three shape parameters. A significant fraction of the clusters is predicted to be triaxial. The binding energies turn out to be more sensitive to the hexadecapole than to the triaxial deformations. The deviations from the axial shape do not generate a systematic even odd staggering of the binding energies.

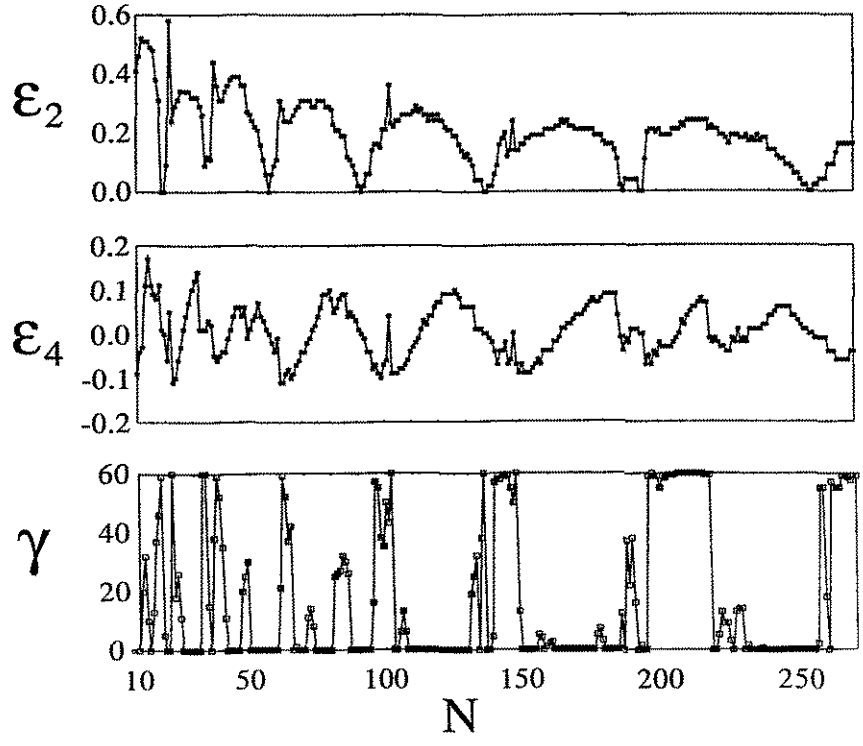

Fig. 1 *Ground state deformations for Na clusters containing $N < 200$ atoms. The parameter ε_2 measures the quadrupole deformation (elongation), ε_4 the hexadecapole deformation (waist line development) and γ the triaxiality of the cluster.*

[1] *ITP Universität Regensburg, Germany*

References

[1] S. Frauendorf, S. M. Reimann and M. Brack, Surface Review and Letters, in print and Z. Phys. **D** submitted

[2] S.M. Reimann, M. Brack, K. Hansen, Z. Phys. **D28** (1993) 235

Shapes and Free Energies of Molten Sodium Clusters

S. FRAUENDORF AND V.V.PASHKEVICH[1]

The shell correction method introduced in ref. [1] to calculate the energy and shapes of alkali atom clusters at zero temperature is extended to finite T. The free energy F is obtained as the sum

$$F = F_{LD} + \delta F.$$

Here, F_{LD} is the free energy of a classical drop of liquid Na with the experimental bulk values of the specific free energy and the surface tension. The shell correction δF is calculated from the free energy of the valence electrons in the average potential generated by them and the positive ions. A new method is proposed that permits to calculate very efficiently the *canonical* partition function of N electrons in the potential. It is combined with a new averaging procedure that eliminates the smooth part of the *canonical* free energy of the valence electrons. Equilibrium shapes are determined by minimizing $F(\alpha, \alpha_4)$ and $F(\alpha, \alpha_3)$ simultanously with respect to the deformation parameters (α, α_4) (quadrupole, hexadecapole distortion) and (α, α_3) (quadrupole, octupole distortion).
Assuming temperatures $T = 500 - 700^o K$, typical for cluster formation in a supersonic jet, and $T = 0$, we have studied the shapes and free energies of neutral even Na clusters with mass number $N = 10 - 700$. For $N < 100$ the shapes are practically independent of T. For heavier clusters the thermal fluctuations begin to wash out the deformation of open shell clusters. This is a consequence of the thermal avaraging of the shell structure, which is responsible for cluster deformation. The supression of deformation occurs as an extension of the regions of spherical shape around the magic numbers. These regions extend with T and N. In the mass region $N \sim 700$ only about one half of the clusters belonging to one shell are still deformed. They are localized in the middle of the shell, having deformations that are somewhat reduced as compared to the $\alpha, \alpha_4, \alpha_3$ values for $T = 0$.
The function $\Delta_2 F(N) = \frac{1}{8}(F(N+2) - 2F(N) + F(N-2))$ is calculated from the F values obtained by minimization with respect to the deformation parameters. It shows the positive spikes at the closed shells, which are known from the study of $F(N)$ assuming spherical shape [2]. As a new feature negative spikes are found somewhat below and above the magic numbers. These spikes are caused by the onset of deformation in the open shell. Such a behaviour is seen in the experimental values of $d \ln I(N)/dN$ [3], where $I(N)$ are the experimental abundances of hot Na clusters measured in ref. [4].
First results are published in ref. [5]. Since $F(T)$ is a thermodynamical potential it permits to calculate the level density, which, due to the renormalization to the experimental values of F, contains both the ionic and electronic contributions. Unimolecular evaporation rates are beeing studied using the nuclear statistical reaction theory.

[1] *LTP JINR, Dubna, Russian Federation*

References

[1] S. Frauendorf, V.V. Pashkevich, Z. Phys **D26** (1993) S 98
[2] M. Brack, O. Genzken, K. Hansen Z. Phys. **D21** (1991) 65.
[3] S.M. Reimann, M. Brack, K. Hansen, Z. Phys. **D28** (1993) 235
[4] S. Bjørnholm et al. , Phys. Rev. Lett. **65**(1991) 1627
[5] S. Frauendorf and V.V.Pashkevich, Surface Review and Letters, in print

"Shears bands" in ^{199}Pb and ^{200}Pb
(Nucl. Phys. A574 (1994) 521)

Baldsiefen, G., H. Hübel, W. Korten, D. Mehta, N. Nenoff, B.V. Thirumala Rao, P. Willsau, H. Grawe, J. Heese, H. Kluge, K.H. Maier, R. Schubart, S. Frauendorf and H.J. Maier

Abstract: High-spin states in ^{199}Pb and ^{200}Pb have been investigated by in-beam γ-ray spectroscopy using several different reactions. In addition to an extension of the spherical level scheme, eight (possibly ten) regular sequences of dipole transitions are found. They are built on oblate proton 2p2h states that are coupled to neutron $i_{13/2}$ excitations. The experimental results are compared to tilted-axis cranking calculations. A new way of generating regular bands is suggested, that combines collective rotation with a continuous and simultaneous reorientation of neutron and proton spins into the direction of the total angular momentum.

Hadron sources of the lepton pair production in proton-deuteron interaction at the initial energies 1 - 5 GeV
(Yad. Fiz. 57 (1994) 924)

Bratkovskaya, E.L., B. Kämpfer, A.V. Molochkov, B.L. Reznik, A.I. Titov

Abstract: Predictions on elementary cross sections for dielectron production in *pd*-reactions at initial energies of 1 - 5 GeV are presented. We consider Δ,η,ω Dalitz decays and direct vector ρ,ω meson decays, where the Δ and η decays are more significant. Calculating of the delta production we take into account delta mass dependence of the Δ-production matrix element whereas in the delta decay probability the vector dominance model was incorporated. Those assumptions are essential for description of the in dielectron distributions with invariant mass near ρ/ω resonance region.

Interpretation of bands in ^{163}Er within the tilted rotation scheme enhanced E1 decay strength
(Nucl. Phys. A571 (1994) 337)

Brockstedt, A., J. Lyttkens-Lindén, M. Bergström, L.P. Ekström, H. Ryde, J.C. Bacelar, J.D. Garrett, G.B. Hagemann, B. Herskind, F.R. May, P.O. Tjom, S. Frauendorf

Abstract: High-spin data are presented for levels in ^{163}Er and in particular the structure of three high-K rotational bands are discussed and interpreted within the tilted rotation scheme. Large observed B(E1) values are interpreted in terms of coupling to octupole degrees of freedom.

Long-time behavior of the semiclassical baker's map
(Phys. Rev. E49 (1994) 963)

Dittes, F.M., E. Doron, U. Smilansky

Abstract: We study the long-time behavior of the quantized baker's map in the semiclassical approximation. Our main object of investigation is the trace of the (n-step) time-evolution operator. We express this trace as a phase-space integral which equals the semiclassical expression in terms of periodic orbits. This enables us to follow the evolution explicitly up to the time at which the semiclassical traces start to diverge exponentially from the quantum ones. Our data indicate that this breakdown time scales with h in a way close to $h^{-1/2}$.

Consequences of neutron-proton interactions on backbending
(Phys. Rev. C50 (1994) 196)

Frauendorf, S., J.A. Sheikh, N. Rowley

Abstract: The influence of neutron-proton correlations on backbending is investigated in a single-j-shell model. It is shown that these correlations are quenched if the neutrons and protons fill a high-j intruder orbital asymmetrically. This is due to the repulsive neutron-proton correlation energy in these configurations and is responsible for the observed forking of the ground state band into proton and neutron S bands.

Effects of flow on intermediate mass fragments in central gold on gold collisions
(Phys. Lett. B337 (1994) 53; Erratum Phys. Lett. B340 (1994) 267)

Heide, B., H.W. Barz

Abstract: The fragment-fragment correlation is investigated for nearly central collisions of *Au* on *Au* at 150 MeV per nucleon. The properties of the fragmenting source are determined within the Boltzmann-Ühling-Uhlenbeck approach. The final decay is described by a statistical multifragmentation model including secondary decay and Coulomb expansion. An anisotropic radial flow is needed to reproduce the energy spectra, the relative velocity distribution of the fragments and their correlation function.

Selforganization in the nuclear system and irreversibility
(Progress of Theoretical Physics, Suppl. 116 (1994) 385)

Iskra, W., M. Müller, I. Rotter

Abstract: The properties of the atomic nucleus are investigated from the point of view of selforganization. The nucleus is described as an open quantum mechanical many-body system embedded in the continuum of decay channels. The information entropy is calculated in relation to two different sets of basic wavefunctions: I_β is obtained from the wave-functions of the resonance states in relation to the shell model states and I_γ is calculated by

means of the partial widths in relation to the decay channels. Both information entropies are calculated as a function of the coupling strength of the nuclear states to the continuum of decay channels. The I_β characterize the mixing of the wavefunctions of the resonance states in relation to the shell model basis while the I_γ are connected with the irreversibility of the scattering process. As a result, neither I_β nor I_γ are a proper measure for quantum chaos. Additional information on lifetimes and level density is necessary.

Self-organization in the nuclear system: II. Formation of a new order
(J. Phys. G: Nucl. Part. Phys. 20 (1994) 775)

Iskra, W., M. Müller, I. Rotter

Abstract: The information entropy of the atomic nucleus is calculated from the wave functions of the resonance states. The transition from low- to high-level density is traced as a function of the coupling strength between the discrete nuclear states and the environment of decay channels. In the critical region of the coupling strength where a redistribution inside the nucleus takes place, information entropy in relation to the discrete states of the closed system is created. Beyond the critical value, a few relevant short-lived modes exist together with long-lived noise. This result is in full correspondence to the maximum information entropy principle of synergetics formulated by Haken. The noise is characterized by disorder expressed by a large information entropy while the relevant modes have a high order and take, correspondingly, a small part of the information entropy of the whole system. The entropy excess accompanying the formation of the new order is used inside the system for creation of noise. Further, the noise is not structureless and the corresponding information entropy is smaller than its maximal value.

Bubble free energy during the confinement transition
(Yad. Fiz. 57 (1994) 187)

Jenkovszky, L.L., B. Kämpfer, V.M. Sysoev

Abstract: By integrating the thermodynamic Gibbs-Tolman-Konig-Buff equation, we derive an expression for the surface tension $\sigma(R)$ and demonstrate that the use of its simple asymptotic ($y = R/\delta \gg 1$) form $\sigma(R) = \sigma_\infty(1 - 2\,\delta/R)$ is questionable in case of small droplets, typical of the deconfinement phase transition. The misuse of the asymptotics may affect calculations of the droplet free energy and, consequently, the estimated supercooling or superheeting of the hot and dense nuclear matter.

Kinetics of an expanding pion gas and low-mass dilepton emission
(Phys. Rev. C49 (1994) 1132)

Kämpfer, B., P. Koch, O.P. Pavlenko

Abstract: We study the space-time dependence of muon pair production from dense, nonequilibrium pion matter in the framework of a Boltzmann type transport model which properly includes effects of Bose statistics. Starting from an initially supersaturated pion gas with a

large positive effective chemical potential we find that this pion chemical potential stays approximately constant during the evolution. As a consequence, such a scenario leads to an increased dilepton yield near the kinematical threshold for muon pair production via pion annihilation. Depending on the lifetime of the dense hadron matter formed in relativistic heavy ion collisions, this component can be observed above the background of muon pairs from resonance decays and the ρ,ω bump. In such a way the measurement of the dimuon invariant mass spectrum could help to understand the initial state and the dynamical evolution of ultrarelativistic heavy ion collisions.

Photon production in an expanding and chemically equilibrating gluon-enriched plasma
(Z. Phys. C62 (1994) 491)

Kämpfer, B., O.P. Pavlenko

Abstract: Photon production in a longitudinally and transversely expanding gluon plasma with initially little quark admixture is considered. Chemical equilibration of quarks and gluons is followed by rate equations. The yields of hard photons with $E \geq 2$ GeV are insensitive to chemical equilibration and depend mainly on the initial thermalized state. Medium-energy photons with $E \sim 1$ GeV are more frequently produced in case of faster equilibration, despite of faster cooling. For an assumed fast equilibration we follow the evolution of matter through mixed and hadron phases. The transverse momentum kick, due to transverse expansion, of photons from hadron matter is shown to be reduced for an equation of state with reduced latent heat. The photon yield in the region $E > 1$ GeV from deconfined matter dominates for conditions, estimated to be achieved at RHIC, in case of a weakly first-order confinement transition.

Transverse momentum dependence of dileptons from parton matter produced in ultrarelativistic heavy-ion collisions
(Phys. Rev. C49 (1994) 2716)

Kämpfer, B., O.P. Pavlenko

Abstract: The $M_\perp$ scaling property of the dilepton spectrum from early parton matter in ultrarelativistic heavy collisions is analyzed for various mechanisms of initial parton production. If there is no essentially additional scale in the parton distribution, we find even for strong off-equilibrium parton matter approximate scaling, while such scales as low-momentum cutoff or parton masses cause strong scaling violations.

Probing early parton kinetics by photons, dileptons and charm
(Nucl. Phys. A566 (1994) 351c)

Kämpfer, B., O.P. Pavlenko

Abstract: Kinetic processes in pre-equilibrium parton matter are considered. We investigate chemical quark equilibration and parton thermalization, and their influence on electromagnetic and charmed probes.

The spin-dependent deuteron structure function within an effective meson-nucleon theory
(Phys. Lett. B321 (1994) 271)

Kaptari, L.P., K.Yu. Kazakov, A.Yu. Umnikov, B. Kämpfer

Abstract: A consistent theoretical approach is suggested for the description of deep inelastic scattering of polarized leptons off polarized deuterons within the operator product expansion method and an effective meson-nucleon theory. Our approach represents a method to extract the nucleon structure functions from nuclear (deuteron) data. Recent deuteron data on the spin structure function $g_1(x)$ are fairly well described.

Wave functions, evolution equations and evolution kernels from light-ray operators of QCD
(Fortschr. Phys. 42 (1994) 101)

Müller, D., D. Robaschik, B. Geyer, F.-M. Dittes, J. Horejsi

Abstract: The widely used nonperturbative wave functions and distribution functions of QCD are determined as matrix elements of light-ray operators. These operators appear as large momentum limit of nonlocal hadron operators or as summed up local operators in light-cone expansions. Nonforward one-particle matrix elements of such operators lead to new distribution amplitudes describing both hadrons simultaneously. These distribution functions depend besides other variables on two scaling variables. They are applied for the description of exclusive virtual Compton scattering in the Bjorken region near forward direction and the two meson production process. The evolution equations for these distribution amplitudes are derived on the basis of the renormalization group equation of the considered operators. This includes that also the evolution kernels follow from the anomalous dimensions of these operators. Relations between different evolution kernels (especially the Altarelli-Parisi and the Brodsky-Lepage kernels) are derived and explicitly checked for the existing two-loop calculations of QCD. Technical basis of these results are support and analytically properties of the anomalous dimensions of light-ray operators obtained with the help of the α-representation of Green's functions.

Selforganization and disorder in an open quantum system
(Acta Physica Polonica 25 (1994) 711)

Müller, M., I. Rotter, W. Iskra

Abstract: The properties of the atomic nucleus are investigated from the point of view of selforganization. The transition from low to high level density is traced as a function of the coupling strength between the discrete nuclear states and the evironment of decay channels. A redistribution inside the nucleus takes place in a small region around some critical value of the coupling strength. Beyond the critical value, a few relevant short-lived modes exist together with long-lived states (*slaving principle of synergetics*). In the critical region of the coupling strength, information entropy, calculated from the resonant states in relation to the discrete states of the closed system, is created (*maximum information entropy principle*). The

long-lived states are characterized by disorder, which is expressed by a large information entropy. The relevant modes have a high order and take, correspondingly, a small part of the information entropy of the whole system.

High-K bands in the ^{166}Yb region
(Phys. Rev. C50 (1994) 1360)

Oliveira, J.R.B., S. Frauendorf, M.A. Deleplanque, B. Cederwall, R.M. Diamond, A.O. Macchiavelli, F.S. Stephens, J. Burde, J.E. Draper, C. Duyar, E. Rubel, J.A. Becker, E.A. Henry, M.J. Brinkman, A. Kuhnert, M.A. Stoyer, T.F. Wang

Abstract: High-K bands have been observed in the ^{166,167,168}Yb isotopes following the ^{124}Sn(^{48}Ca, $xn\gamma$) reaction. The $\nu h_{11/2}$ band in ^{167}Yb has been extended to higher spins. The high-K bands in the even-even isotopes were observed for the first time and show very high $B(M1)/B(E2)$ ratios. Configuration assignments for the new bands are proposed. The results are interpreted within the tilted cranking model.

An effective model of the quark-gluon plasma with thermal parton masses
(Phys. Lett. B 337 (1994) 235)

Peshier, A., B. Kämpfer, O.P. Pavlenko, G. Soff

Abstract: A model is presented which reproduces the pure SU(3) gauge theory on the lattice for thermodynamical quantities. It exploits only thermal quark and gluon masses $m(T) \alpha g(T)T$ and no other interaction or bag constant. The latent heat at confinement temperature is much smaller compared with the bag model parametrization; this modifies drastically the cooling velocity of the quark-gluon plasma and the duration of the deconfinement phase. The effective thermal quark masses lead to a kinematical threshold and violate the M_T scaling of the transverse dilepton spectrum from the plasma.

Microscopic analysis of two-body correlations in light nuclei
(Nucl. Phys. A573 (1994) 93)

Peter, A., W. Cassing, J.M. Häuser, A. Pfitzner

Abstract: Within a nonperturbative dynamical two-body approach - based on coupled equations of motion for the one-body density matrix and the two-body correlation function - we study the distribution of occupation numbers in a correleated system close to the ground-state, the relaxation of single-particle excitations and the damping of collective modes. For this purpose the nonlinear equations of motion are solved numerically within a finite oscillator basis for the first time adopting short-range repulsive and long-range attractive two-body forces. We find in all cases that the formation of long- and short-range correlations and their mixing is related to the long- and short-range part of the nucleon-nucleon interaction which dominate the resummation of loop or ladder diagrams, respectively. However, the proper description of relaxation or damping phenomena is found to require both types of diagrams as well as the mixed terms simultaneously.

Vibrations versus collisions and the iterative structure of two-body dynamics
(Nucl. Phys. A577 (1994) 753)

Pfitzner, A., W. Cassing, A. Peter

Abstract: We adopt a truncated version of two-body dynamics by neglecting three-body correlations, as is supported by microscopic numerical calculations. Introducing orthogonal channel correlations for the pp- and the pn-channel and integrating the latter in terms of vibrational RPA-states we derive a retarded two-body equation. Its solution is nonperturbative with respect to loops, ladders and mixed contributions. In the stationary limit we obtain an equation for a generalised effective interaction which iterates both the *G*-matrix and the polarisation matrix. An in-medium scattering approach transparently demonstrates the collisional damping of the vibrations.

On size and shape of the average meson fields in the semibosonized Nambu & Jona-Lasinio model
(Z. Phys. A 348 (1994) 111)

Wünsch, R., K. Goeke, Th. Meissner

Abstract: We consider the bosonized form of a two-flavor Nambu & Jona-Lasinio model involving scalar-isoscalar and pseudoscalar-isovector quark-quark interaction. Solitonic meson fields are obtained by minimizing the effective Euclidean action. In dependence on the constituent quark mass, which is the only free parameter in the model, we evaluate a series of meson profiles and compare them with a properly parameterized reference profile. We show that the self-consistent fields do in fact practically not depend on the constituent quark mass. Their shape can be very well approximated by this reference profile which interpolates between the correct asymptotic behavior for small and large radii. To demonstrate the accuracy of the approximation we evaluate several static properties like energy, mean square radius, axial-vector constant and delta-nucleon mass splitting using both self-consistent and reference profiles. The agreement is found to be very well in the physically relevant mass region.

2 Experimental Medium Energy Physics

Test of the COSY-TOF-Start-Detector MARS at the COSY Beam[B,K]

A. SCHÜLKE, E. KUHLMANN[2], P. MICHEL, K. MÖLLER[1,2], B. NAUMANN, L. NAUMANN, A. SCHAMLOTT

The first beam time at the COSY Time-of-Flight spectrometer TOF in spring 1994 with a 455 MeV proton beam was used mainly to perform functional tests of the various components of the spectrometer. In this first test measurement the TOF spectrometer was used in a configuration consisting of the central-endcap-hodoscope [1](stop detector) and (alternatively) one of the two versions of the start detector [2],[3]. Here a short account is presented on the results of methodical investigations of the Rossendorf start detector MARS. The configuration used in the measurements is shown schematically in Fig.1.

In this configuration the complete B-ring and four elements of the A-ring of the start detector were used. The four segments of the A-ring were arranged in a cross-like geometry. They served for monitoring the primary beam. From beam diagnostics as well as data analysis it turned out that the (up to now uncooled) beam was not of the desired quality. Data analysis revealed that only 6% of all hits detected can be assigned to pp-reactions. All other hits had to be discarded since there was no geometrical link between target position, B-ring and the central hodoscope for these hits. This means that the particles registered originate from beam halo rather than nuclear reactions.

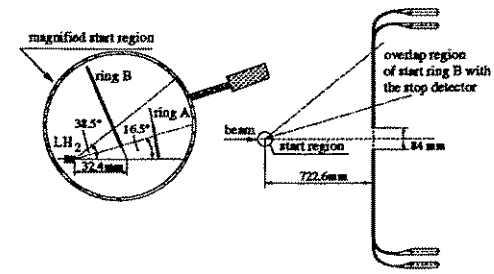

Fig.1 *Schematical view of the configuration used in the first measurement.*

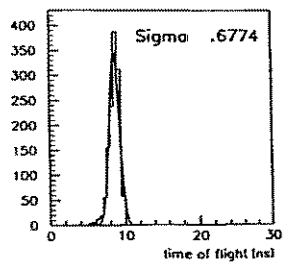

Fig.2a *Start-stop time-of-flight spectrum.*

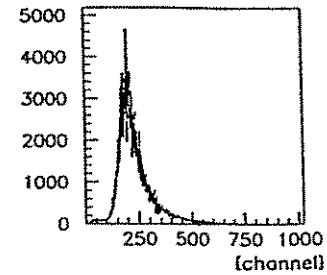

Fig.2b *Start detector ADC spectrum.*

Since TOF is a time-of-flight spectrometer one of the crucial properties of the spectrometer is the time resolution. In Fig.2a a TDC spectrum is presented showing the time of flight between a start detector segment and a certain pixel of the central hodoscope (timing information is extracted from the wedge-like element). The TDC spectrum was generated in data analysis on the basis of the parasitic beam halo particles because these particles have a small energy spread. The time resolution obtained under these conditions turned out to be 1.6 ns (FWHM). This time resolution is composed of both the start and the stop detector resolution. The arrangement used in the test measurement did not allow to separate the time resolution of the start detector from the total resolution. In fact there was no necessity to do this since the time resolution of the start detector had been measured accurately under clean conditions in an earlier experiment [2].

As concerns the energy resolution of the start detector (Fig.2b) so it is quite satisfactory with signals well above noise. In a next step the geometrical adjustment of the start

detector was investigated. Neighbouring segments of the start detector B-ring are designed to have small overlap to assure 100% efficiency if it is operated as a veto detector [4]. Fig.3 illustrates a central projection of the overlap regions of the B-ring measured with particles arising from the target point. The signature chosen for this projection was two hits ($M_B = 2$) in neighbouring segments of ring B. The obvious left-right asymmetry in Fig.3 is caused by beam imperfections (asymmetric beam halo).

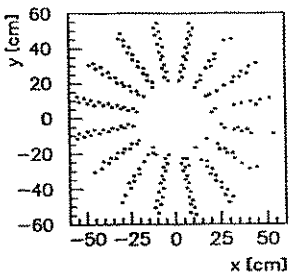

Fig. 3 *Central projection of the overlap regions of the start ring on the stop detector from the target point.*

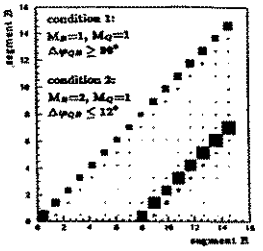

Fig. 4 *Coincidence matrix of start detector.*

The results of the data analysis of the measurement are represented in form of a correlation matrix (coincidence matrix) for the start detector segments (Fig.4). This kind of representation was introduced in connection with an earlier test of the start detector MARS [4]. In Fig.4 all those hits are represented of the total bulk of data which fulfill the 2 conditions indicated in the picture. Condition 1 says: 2 particles are registered (one hit in the B-ring, one hit in the central hodoscope) with relative azimuthal angle $\Delta\varphi_{BQ} > 90°$. Particles fulfilling condition 1 correspond to the entries on the main diagonal in Fig.4. Part of the hits on the main diagonal (with signature $\Delta\varphi_{BQ} \approx 180°$, $\Delta\Theta < 16.5°$) are due to elastic pp-scattering.

The hits of the coincidence matrix outside the main diagonal correspond to condition 2. According to this condition two particles are detected in ring B with one of these particles registered additionally in the central hodoscope. The main feature of the coincidence matrix is the straight line starting at the point (0,8). This line corresponds to elastic pp-scattering. It is obvious from Fig.4 that elastic scattering can easily be separated from background. In Fig.5 as an example the hit pattern of an elastic event is shown (2 hits in the start detector B-ring, 1 hit in the stop detector).

For data analysis an adapted version of the Bochum TOF data analysing program system was used which was developed by members of the Bochum-TOF-group on the basis of a program package from M. Gasthuber (University of Hamburg) [5].

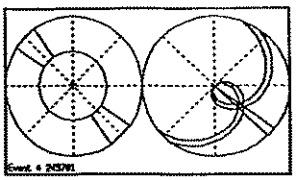

Fig. 5 *Hit pattern of an elastic event.*

[1] *Institut für Kern- und Hadronenphysik, FZR*
[2] *Institut für Kern- und Teilchenphysik, TU Dresden*

References

[1] M. Dahmen et al., Nucl. Instr. and Meth. **A348** (1994) 97-104
[2] P. Michel et al., Annual Report 1992 Jül-2726, p. 5
[3] T. Czarnecki et al., Annual Report 1993 Jül-2879, p. 13
[4] P. Michel et al., Annual Report 1993 Jül-2879, p. 15
[5] M. Steinke, H. Brand COSY-TOF-NOTES BO-4.5-1994

Properties of the extracted COSY beam[B,K]

P. JAHN[1], B. NAUMANN, M. ROGGE[1]

In May 1994 the first accelerated COSY beam of 1.09 GeV/c protons was delivered to the target position at the Time-of-Flight Spectrometer (TOF) using the extraction beamline with a length of about 56 meters (Fig. 1). Since that time this extraction channel has been investigated. Its optimal adjustment requires the knowledge of the beam input parameters. Therefore the beam emittances near the extraction region in horizontal (x) and vertical (y) planes were measured.

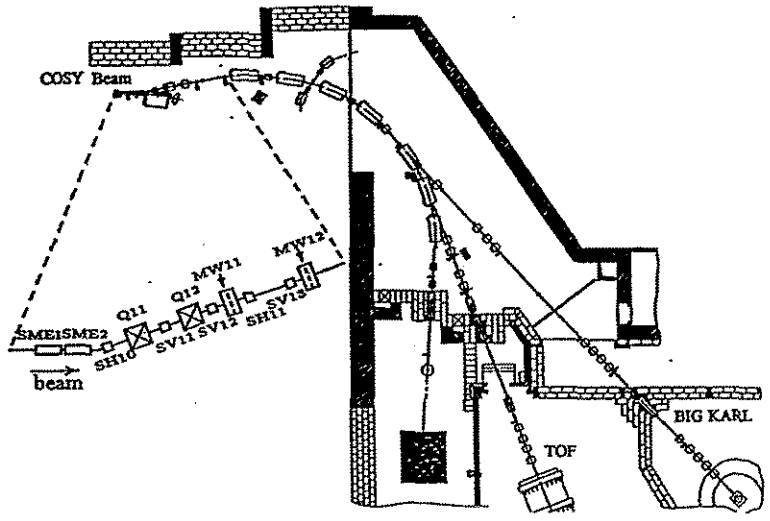

Fig.1 *The extraction beamlines with the target places at COSY [1]. The elements on the first 7 meters of the beamline using for the emittance measurements are magnified.*

Usually for emittance measurements in particle beams a description by Twiss parameters is chosen [2]. We used another equivalent method starting from the imaging laws of thin lenses, to get additional and more detailed information about the intensity distributions in metrical and angular spaces. Using this approximation, the calibration constant for a quadrupole lens can be found with good accuracy. The beam extension at the known position of the steerer SH10 has been imaged by the quadrupole lens Q12 on the multiwire proportional chamber MW12 and the calibration constant of Q12 has been obtained. The focal length of the calibrated quadrupole Q12 is changed by setting the lens current. Q12 images the beam extension at a well defined beam position along the extraction channel on MW12. With the approximation of a thin lens the magnification for imaging can be obtained as a function of the Q12 calibration constant and the set lens current. Horizontal and vertical planes in our case can be observed independently since the beam focussed in one plane is not defocussed in the other plane so much that parts of the beam touch the beam tube. The envelope of the beam in each plane can be described by three parameters, as are i) the distance of the minimum beam extension (waist) from the middle of the magnetic extraction septum (SME1,SME2) of COSY $z_{waist}^{horizontal}, z_{waist}^{vertical}$, ii) the beam extensions x_{waist}, y_{waist} and iii) the beam divergences x', y'. With the described imaging method we calculated the beam extensions x and y at various beam positions z using half the FWHM values of the imaging extensions measured by the chamber MW12. The waist positions $z_{waist}^{horizontal}, z_{waist}^{vertical}$ and the beam parameters on the waist positions x_{waist}, y_{waist}

and x', y' can be calculated with the following equations, which are valid near the waist position z_{waist} [3]

$$x^2 = (x_{waist})^2 + (z - z_{waist}^{horizontal})^2 \cdot (x')^2 \quad \text{and} \quad y^2 = (y_{waist})^2 + (z - z_{waist}^{vertical})^2 \cdot (y')^2.$$

The horizontal and vertical beam extensions x and y shown in Fig.2 have been calculated using half the FWHM values of the imaging extensions on the multiwire proportional chamber MW12 during the September run.

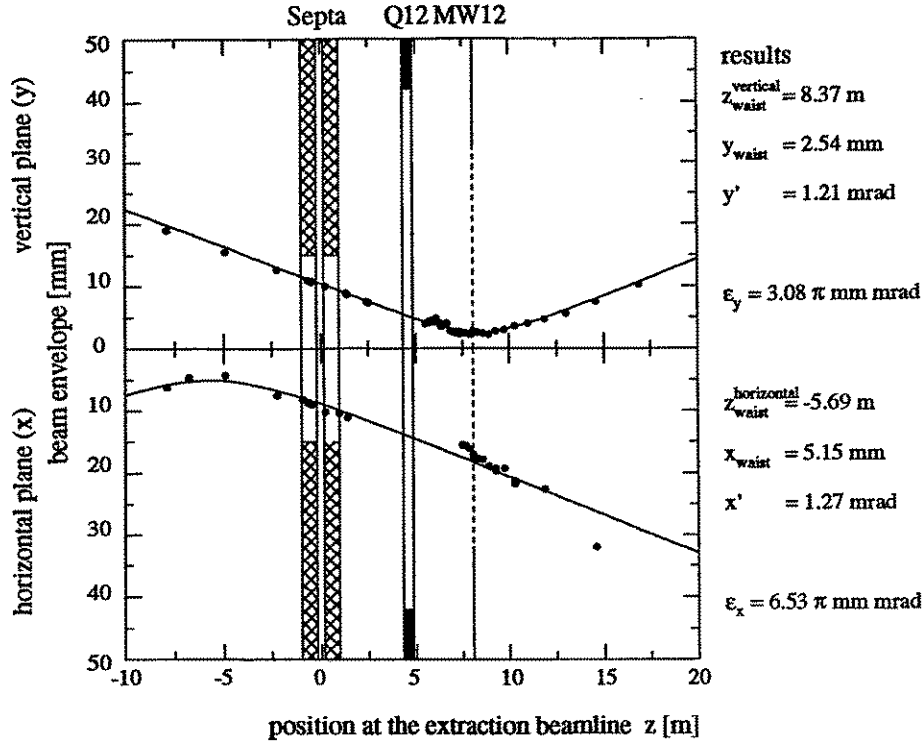

Fig.2 *Horizontal and vertical beam extensions x and y in the COSY beam extraction region for determination of horizontal and vertical emittances ε_x and ε_y.*

The emittances here were obtained as

$$\varepsilon_x = \pi \cdot x_{waist} \cdot x' = \pi \cdot 5.15\ mm \cdot 1.27\ mrad = 6.53\ \pi\ mm\ mrad$$
$$\varepsilon_y = \pi \cdot y_{waist} \cdot y' = \pi \cdot 2.54\ mm \cdot 1.21\ mrad = 3.08\ \pi\ mm\ mrad.$$

For the 95% width the ε_x and ε_y result in 28 π *mm mrad* and 10 π *mm mrad* respectively. This is considerably more than the design value of $\varepsilon = 2.5\ \pi$ *mm mrad* for the beamline to the experimental areas TOF and BIG KARL [4]. The positions of the waists in three measurements up to September 1994 has not changed much and was about 6 m before the middle of the magnetic septum in the horizontal plane and about 9 m after it for the vertical plane.

[1] *Institut für Kernphysik, Forschungszentrum Jülich*

References

[1] U. Bechstedt et al., Annual Report 1993, Jülich, 1994, Jül-2879, p.198

[2] Beam Diagnostics: CERN Accelerator school, Aarhus, 1986, p.99

[3] K.L. Brown et al.,TRANSPORT Manual, Geneva, 1980, CERN 80-04, p.176

[4] S. Martin and C.A. Wiedner, Annual Report 1991, Jülich, 1992, Jül-2590, p.255

Subthreshold Production of K^- Mesons at the 0° Facility [B,K]

H. Müller, T. Kirchner, Ch. Schneider, Ch. Schneidereit, M. Büscher[1], K. Sistemich[1], V.I. Komarov[2], A. Sibirtsev[2]

The production of particles in proton-nucleus reactions at energies below the corresponding threshold for free nucleon-nucleon interactions is a typical cooperative nuclear phenomenon, which is at present far from being understood. Contradictory physical pictures are used to interpret subthreshold production as for example the consideration of high-momentum components in the nuclear wave function, or the inclusion of clusters consisting of several target nucleons, or the discussion of multi-step processes. A common feature of all approaches consists in the close relationship between the structure of the involved nuclei and the interaction mechanism. It is of principal importance for a correct description of nuclear reactions at relativistic energies to disentangle these two sides of the collision process. Subthreshold production is expected to be a sensitive tool for this purpose.
There are further reasons, peculiar to the type of the considered particle, which make the investigation of K^- production especially interesting:

- K^- mesons may be produced via resonances. Well established resonances of this type are the $\Phi(1020)$ meson and the $\Lambda(1520)D_{03}$ resonance.
- Other candidates are the $f_0(980)$ and the $a_0(980)$ mesons the nature of which is still under discussion. It is not clear if they can be considered as usual $q\overline{q}$ states of the quark model or if they should be interpreted as K^+K^- molecules.
- There are recent discussions about a possible admixture of $s\overline{s}$ components in the ground state wave function of nucleons. As a logical conclusion one may speculate about consequences for strangeness production also at subthreshold energies.

So far, K^- subthreshold production has been investigated in the reactions $C+C$, $Si+Si$, and $Ca+Ca$ at incident energies between 1 and 2.1 GeV/nucleon [1], but no data are available on K^- subthreshold production in hadron-induced reactions. Detailed knowledge of this type of reaction is necessary for the understanding of heavy-ion interactions.
We propose to measure the energy-dependence of K^- production in proton-nucleus reactions below the nucleon-nucleon threshold at 2.5 GeV incident energy in order to contribute to the solution of the above mentioned problems. The planned 0° Facility together with the expected beam quality of COSY offers good conditions for carrying out also difficult coincidence measurements. Positively and negatively charged particles are separated in the 0° Facility and will be measured at the opposite sides of the magnet [2].
Since there are no data available, we are compelled to rely completely on model calculations in preparing the experiments. In order to minimize the uncertainties of such an approach two quite different models, the folding and the Rossendorf Collision (ROC) model, were applied. The inclusive K^- spectra as calculated by the two models are compared in Fig. 1 (for details see [3]). There is a discrepancy of about one order of magnitude in the cross section. This can be considered as a realistic estimate of the uncertainties we have to cope with. The measurement of such an inclusive spectrum is usually considered as a first step to differentiate between models. However, there are problems because of the high background arising from other reaction channels. For both charge states of the

kaon the production cross section is about two orders of magnitude smaller than that of pions (and protons). The problem is well-known from the planned investigation of K^+ subthreshold production [4]. In order to reduce the amount of data a fast trigger will be used in the K^+ experiment for finding on-line the true K^+ events out of the background. This system allows a π^+ suppression of more than 4 orders of magnitude. We intend to use the same fast trigger also for the measurement of correlated K^+ and K^- mesons [2]. Then at the "negative" side of the magnet only a relatively simple fast trigger for K^- mesons will be necessary, because the difference in the cross sections for K^- and π^- mesons becomes much less if they are measured in coincidence with identified K^+ mesons as can be seen from Fig. 2.

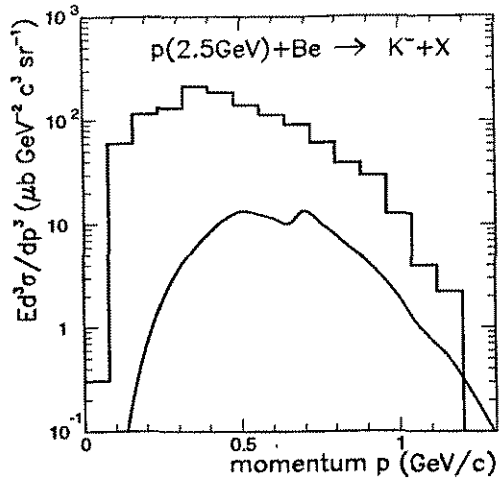

Fig. 1 *Folding-model (curve) and ROC-model (histogram) predictions for the K^--momentum spectra produced in pBe collisions at $T_p = 2.5$ GeV, integrated over kaon-emission angles $\Theta \leq 10°$*

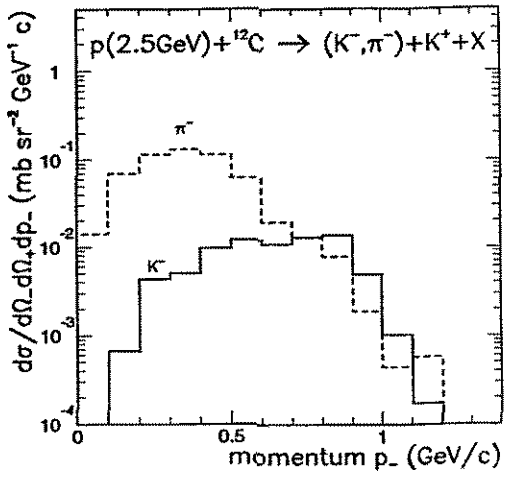

Fig. 2 *ROC model predictions for the momentum spectra of K^- and π^- mesons correlated with K^+ mesons at angles $\theta \leq 10°$ and momentum interval $0.15 \leq p_+ \leq 0.6$ GeV/c*

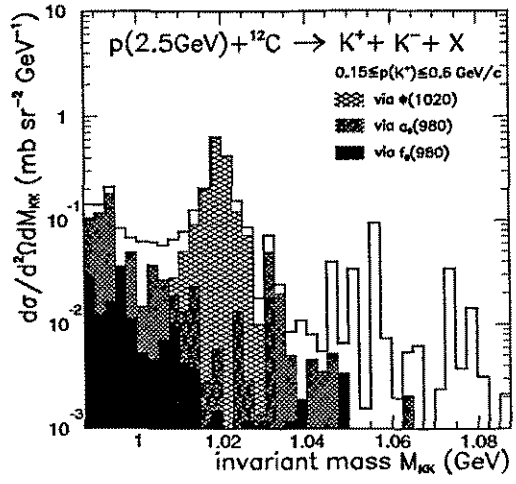

Fig. 3 *Predicted invariant K^+K^- mass spectrum integrated over emission angles $\theta \leq 10°$ and the contributions from $\Phi(1020)$, $a_0(980)$ and $f_0(980)$ indicated*

In the invariant mass spectrum (see Fig. 3) a rather clear signal from the production of the K^+K^- pair via the $\Phi(1020)$ resonance can be seen. The region below 1020 MeV is mainly populated via the $a_0(980)$ and $f_0(980)$ resonances. If it turns out that these two resonances are not usual $q\bar{q}$ quark model states then a much smaller cross section in this mass region must be expected. Thus, the measurement of K^+-K^- correlations is expected to yield valuable information about the mechanism of subthreshold production as well as

about the nature of the involved resonances.

[1] *Forschungszentrum Jülich, Institut für Kernphysik*
[2] *Joint Institute for Nuclear Research, Laboratory of Nuclear Problems 141980 Dubna, Moscow region, Russia*

References

[1] J. Caroll, Nucl. Phys. **A488** (1988) 203c
[2] M. Büscher, H. Müller, contribution in this report
[3] A. Sibirtsev et al., Z. Phys. **A351** (1995), in print
[4] W. Borgs et al., COSY Proposal #18 Jülich 1990

Conceptual Studies for a K^--Detection System at the 0° Facility [B,K]

M. BÜSCHER[1], H. MÜLLER

The 0° Facility which is currently being built will allow to simultaneously measure positively and negatively charged ejectiles which leave an internal target under forward angles $\vartheta \sim 0°$. It has been proposed [1,2] to measure the K^- production in pA reactions at energies close to and below the nucleon-nucleon threshold at $T_p = 2.5$ GeV. In this article we describe a concept of a detection system for the proposed studies.
For the detection of the K^+ (K^-) mesons and for the reduction of the background consisting mainly of π^+ and p (π^-) and of particles scattered in the magnet iron the following concept is suggested: The K^+ mesons will be detected in the side-detector system which will offer a K^+-detection efficiency of $\sim 15\%$ (including decay-in-flight between target and detectors) and a background suppression of more than 4 orders of magnitude. It covers a momentum range of $p_{K^+} \sim 150 \ldots 600$ MeV/c and allows to select events where a K^+ meson is produced with almost no background from other reaction channels.
As shown in Fig. 2 of [1] roughly the same number of K^- and π^- are produced in events

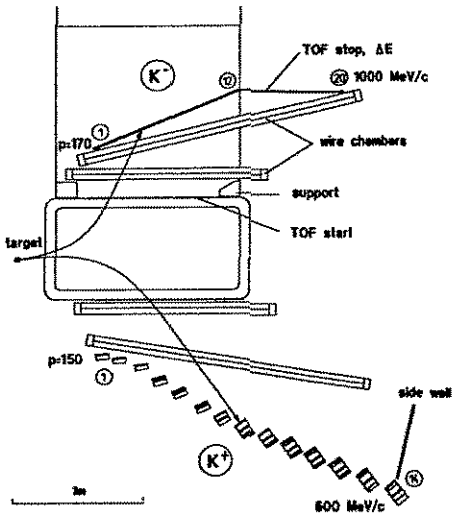

Fig. 1 *Principle layout of the proposed detection system for the K^+/K^- studies. For the detection of the K^+ mesons a system consisting of a TOF-start counter wall and 14 telescopes with TOF-stop, Cerenkov, ΔE and veto counters will be used. Negatively charged particles will be detected in a similar TOF system. For further background suppression the ΔE signal from the TOF-stop counters can be used.*

where a K^+ meson is formed. Thus, only a moderate background suppression has to be achieved by the detection system for the negatively charged particles. The principal layout of the $K^-(\pi^-)$ detection system can be seen in Fig. 1. The TOF-start counter wall can be similar to the one used for positively charged ejectiles, i.e. it consists of 18 scintillators with a height of $\sim$ 25 cm, a width of 5 cm and a thickness of 1...2 mm. For the TOF-stop counter wall 20 "standard" scintillators of 10 cm width and 1 cm thickness can be chosen. This wall allows to detect ejectiles in the momentum range p = 150...1000 MeV/c which is equal to the full momentum range accessible for negatively charged particles at the 0° Facility. According to ray-tracing calculations the detector heights must be between 40 cm (p = 150 MeV/c) and 80 cm (p $\geq$ 500 MeV/c) in order to cover the full vertical angular acceptance given by the spectrometer magnet. For further background suppression it is planned to also read out the ΔE signal from the TOF-stop counters, see below. Two wire chambers will allow to measure the particle flight paths for track reconstruction and for suppression of background particles scattered in the pole pieces of the spectrometer dipole.

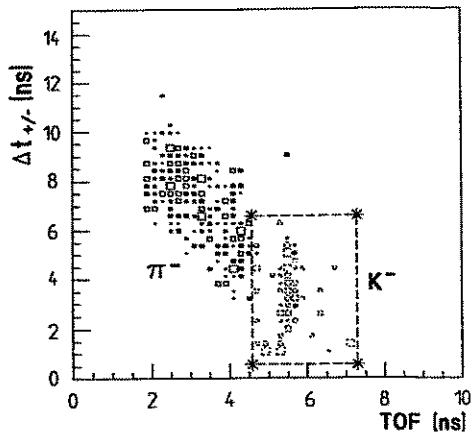

Fig. 2a *Simulated TOF spectra of correlated K^+/K^- and K^+/π^- events summed over all counters.*

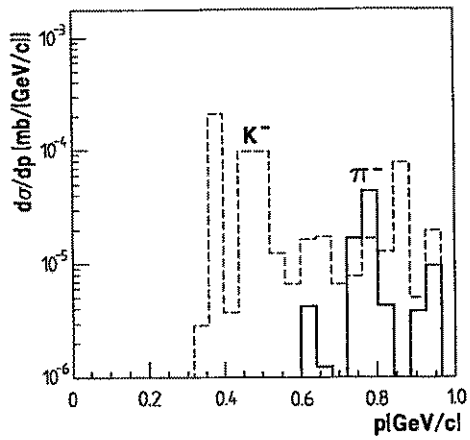

Fig. 2b *Momentum spectra of particles lying inside the gates shown in Fig. 2a.*

The performance of the full detection system has been simulated using "realistic" K^+/K^- and K^+/π^- events calculated with the Rossendorf Collision Model [1]. Only events where a K^+ meson is detected and a negatively charged ejectile reaches a TOF-stop counter were analyzed. Decay-in-flight and hadronic interaction in the magnet and detectors have not been simulated yet. Fig. 2a shows a 2-dimensional plot of the TOF of $K^-(\pi^-)$ versus the time difference $\Delta t_{+/-}$ between the detection of the K^+ and the $K^-(\pi^-)$ in the corresponding TOF-stop counters. It can be seen that - even if the sum over all counters (and, thus, ejectile momenta) is used - there is a good separation between the K^- and π^-. This allows to select K^- events by setting a 2-dimensional gate in the spectrum, see Fig. 2a. The resulting momentum spectra of particles lying inside this gate is shown in Fig. 2b. A comparison with Fig. 2 from [1] shows a clear suppression of the π^- events. Only for high-momentum ejectiles (p $\sim$ 800 MeV/c) there is a remaining π^- background. However, this background can also be totally rejected (on the level of statistics in our simulations) if one analyzes the TOF informations from Fig. 2a for individual stop counters. As an example, Fig. 3 shows the same spectrum as Fig. 2a

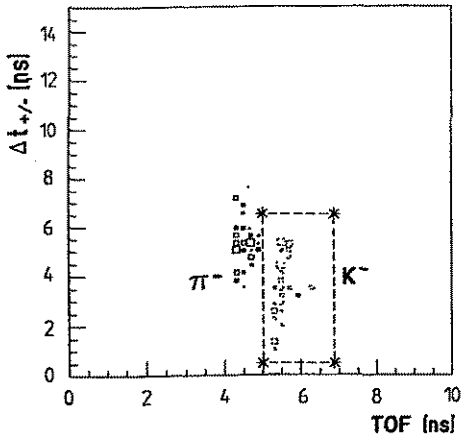

Fig. 3 *Same as Fig. 2a but only for counter #18 of the stop-counter wall for negatively charged particles.*

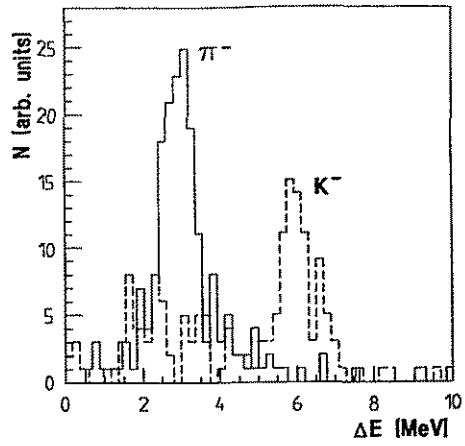

Fig. 4 *Energy-loss spectrum for K^- and π^- in TOF-stop counter #10 ($p \sim 400$ MeV/c).*

when only scintillator #18 of the negative stop-counter wall (p $\sim$ 800 MeV/c) is read out. Clearly, the separation between K^- and π^- is much better and the π^-events can completely be rejected. From Fig. 2b one can estimate the counting rates for correlated K^+/K^- events. Taking into account a total detection probability of 15% (30%) for $K^+(K^-)$ we expect 25 events per minute integrated over all momenta (p_{K^+} = 150...600 MeV/c, p_{K^-} = 170...1000 MeV/c). In addition to background suppression via TOF measurements it will be possible - especially for momenta p $\lesssim$ 600 MeV/c - to use the ΔE signal from the TOF-stop wall to distinguish between K^- and π^-. As an example Fig. 4 shows the ΔE spectrum in counter #10 (p $\sim$ 400 MeV/c) for K^+ and π^-. From this spectrum it can be concluded that an additional π^- suppression of at least 1 - 2 orders of magnitude for lower momenta will be possible.

Summarizing, the detection system presented here will allow to measure correlated K^+/K^- events from pA interactions at T_p = 2.5 GeV and even at lower beam energies where the cross sections decrease rapidly (see [1] and references therein). It is currently under investigation if the system can be installed "step by step" using first only the TOF-stop wall for K^- identification. In this case one would use the information on the time difference between emission at the target (calculated off line using the information on the K^+) and detection in the wall. This simpler setup should allow to measure at $T_p \approx 2.5$ GeV and moderate cross sections. For further measurements at lower energies, the full setup would be required.

[1] *Institut für Kernphysik, KFA Jülich*

References

[1] H. Müller et al., contribution to this report
[2] M. Büscher et al., Z. Phys. **A351** (1995), in print

Test of Prototype Telescopes for the 0° Facility in a Kaon Beam at ITEP Moscow [B,K]

R. Esser[1], L. v. Horn[1], D. Kopyto[1], H. Ohm[1], A. Franzen[1], M. Büscher[1], B. Prietzschk, B. Rimarzig, Chr. Schneider, V. Chernyshev[2], M. Chumakov[2], V. Koptev[3], S. Mikirtichyants[3], V. Kruglov[4]

At the 0° Facility [1] a TOF system as well as Cerenkov, ΔE and veto counters will be used to identify unambigously kaons among protons and pions which are produced with cross sections up to 6 orders of magnitude higher. A prototype of such a telescope has been tested at the synchrotron of the Institute of Theoretical and Experimental Physics (ITEP) in Moscow. The primary T = 2.5 GeV proton beam was used to produce secondary particles which were separated according to their momentum. Furthermore, these particles passed through two electrostatic separators where according to their masses clean proton, kaon and pion beams could be selected. All our measurements were done at p = 545 MeV/c, the lowest momentum where still a reasonable kaon rate was available and which is near the high-momentum end of the spectra which will be studied at the 0° Facility side detector. In this report we will concentrate on the perfomance of individual counters used. Detailed information about kaon identification and background rejection is given in [2]. The telescope employed in this experiment (see Tab. 1) was designed for a particle momentum around 500 MeV/c. We adapted it to the actual beam momentum by an optimization of the degrader thickness. A START counter as proposed in [3] made of Pilot U, 2 mm thick, 5 cm wide and 30 cm long was placed vertically close to the exit window of the beam line. For the approximately 30 cm long bent light guides Plexiglas GS 233 was used. The counter was read out by 1" photomultiplier tubes Philips XP2972 on both ends. A second scintillator strip was positioned horizontally in the center of the vertical START counter in order to act as an active collimator. This strip was directly read out by two 2" photomultiplier tubes Philips XP2020. This counter was used as reference for all time measurements since its simple geometry led to a better time resolution than was feasible with the START counter described above. The STOP counter, 1 cm thick, was placed 214 cm downstream of the START counter in a frame together with the remaining parts of the telescope (see at tab. 1). These components of a width of 10 cm and a height of 1 m were mounted vertically. Each end of the scintillators (STOP, ΔE_1, ΔE_2 and Veto) was glued to a fishtail light guide which was then coupled to a 2" photomultiplier tube XP2020. The data acquisition was based on a CAMAC system controlled by a PC 486. For each event all the amplitudes and the complete timing information were measured with LeCroy, FERA, QDCs and TFCs. The system gate signal was generated by a coincidence between the two START counters and the STOP counter, using analog meantimers to correct the timing signals for the light propagation time. The counting rate during all measurements was typically below 2×10^4 cps so that chance coincidences were negligible. Fig. 2 shows the time-of-flight spectrum for pions and protons measured with the unseparated beam. Due to the low production cross section kaon events are not visible in this plot. The spectrum indicates that the beam quality and the performance of the detector system are good.

Table 1 *Components of the telescope*

Counter	Thickness	Material
Horizontal start counter	0.4 cm	Pilot U
Vertical start counter	0.2 cm	Pilot U
Stop counter	1 cm	BC408
Cerenkov counter	5 cm	GS218
First degrader	7.3 cm	Fe
First ΔE counter	1.5 cm	BC408
Second ΔE counter	2.5 cm	BC408
Second degrader	1.2 cm	Fe
Veto counter	1 cm	BC408

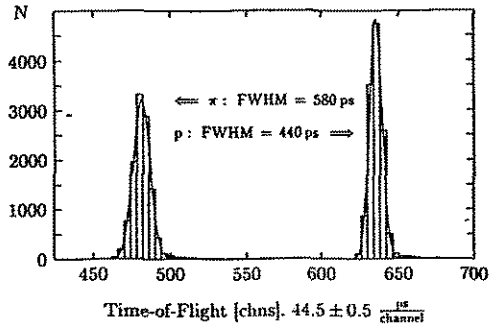

Fig. 2 *Time-of-flight spectrum measured with an unseparated beam. The spectrum represents raw data with no offline suppression.*

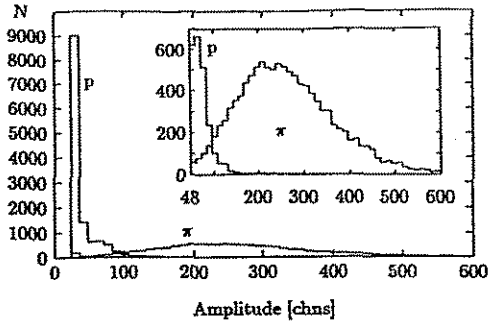

Fig. 3 *Charge-amplitude spectra of protons and pions measured with the Cerenkov counter. The inset is the portion of the spectrum for higher channel numbers where pions dominate.*

A ΔE spectrum is shown in [2]. Even with our preliminary Cerenkov counter using XP2020 for readout the spectra allow a good discrimination against pions, see Fig. 3. By the use of 3" photomultipliers the light collection efficiency will increase from 30% to 48%. The pion and proton spectra have been generated from the raw data by setting gates on the corresponding peaks in the TOF spectrum. The detection efficiency for protons is 18%, for pions it is 98%, implying a verry efficient pion suppression in experiments aimed at kaon detection. The distribution of

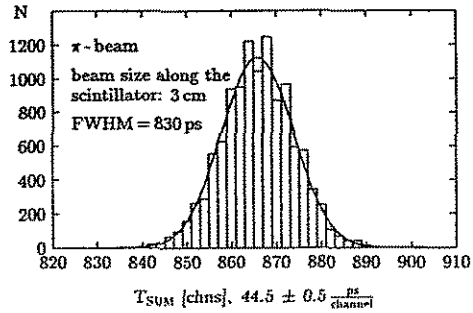

Fig. 4 *Timing distribution of the vertical START counter for pions.*

the pion events as a function of the time sum of both PMTs is shown in Fig. 4. The resolution of 830 ps FWHM still needs some improvement. Therefore we consider the following measures:

1. The amplitudes of the vertical START counter were limited to 200 mV for 545 MeV/c protons. Therefore the use of a constant fraction discriminator instead of a leading edge discriminator is mandatory. Furthermore the gain of the PMT XP2972 should be increased by modifying the voltage divider.

2. Because of the shorter wavelength of the light emitted by PILOT U the use of ultraviolet transmitting Plexiglass, e.g. GS218, instead of GS233 is expected to increase the light transmission by about a factor of 2. The time resolution will be improved accordingly. Alternatively, (standard) Plexiglass GS233 used together with scintillator materials with larger wavelengths (e.g.: BC408 or NE 122) might lead to a better timing resolution despite their longer time constants. They are 'slower' but according to [4] photoelectron statistics is the dominating factor of the timing resolution.

[1] *Forschungszentrum Jülich, Institut für Kernphysik*

[2] *Institut of Theoretical and Experimental Physics, Moscow, Russia*

[3] *PNPI Gatchina, St. Petersburg, Russia* [4] *JINR Dubna, Moscow, Russia*

References

[1] K. Sistemich, contribution to this report, p.

[2] A. Franzen, contribution to this report, p.

[3] R. Eßer et al., Ann. Rep., KFA-IKP 1993, p.41

[4] B. Kohlmeyer, DPG Physikertagung, Bonn, 1989

3 Experimental Nuclear Spectroscopy

Shell-Model States and Collectivity in $^{83}Br_{48}$ and $^{85}Rb_{48}$ [D]

R. SCHWENGNER, G. WINTER, J. REIF, H. PRADE AND L. KÄUBLER[1]

Excited states of the N=48 nuclei ^{83}Br and ^{85}Rb were studied with methods of in-beam γ–ray spectroscopy [1,2]. The level sequences in both nuclei have been interpreted in terms of the shell model using the model space $\pi(0g_{9/2}, 1p_{1/2}, 1p_{3/2}, 0f_{5/2})$ $\nu(0g_{9/2}, 1p_{1/2})$. Details of the calculations are described in [3].

The level energies and $E2$ transition strengths calculated for the positive-parity yrast states with $J^\pi \leq 21/2^+$ in ^{83}Br and ^{85}Rb are compared with the experimental ones in Fig. 1. The rotational-like level spacings of the sequence in ^{83}Br are well reproduced by the calculation. Moreover, the calculated $E2$ transition strengths are consistent with the slightly collective experimental values. In the wave function of the yrast states the configuration $\pi(0f_{5/2}\ 1p_{3/2})^{-4}\ \pi 0g^1_{9/2}\ \nu(0g^{-2}_{9/2})_{0,2}$ predominates where the protons in the negative-parity orbitals mainly form $0^+, 2^+, 4^+$ states and the two neutron holes couple to $J^\pi = 0^+, 2^+$. The large $B(E2)$ values appear in the shell model as a result of the coherent superposition of many components including excitations of the protons in the (fp) shell and of the $0g_{9/2}$ neutron holes.

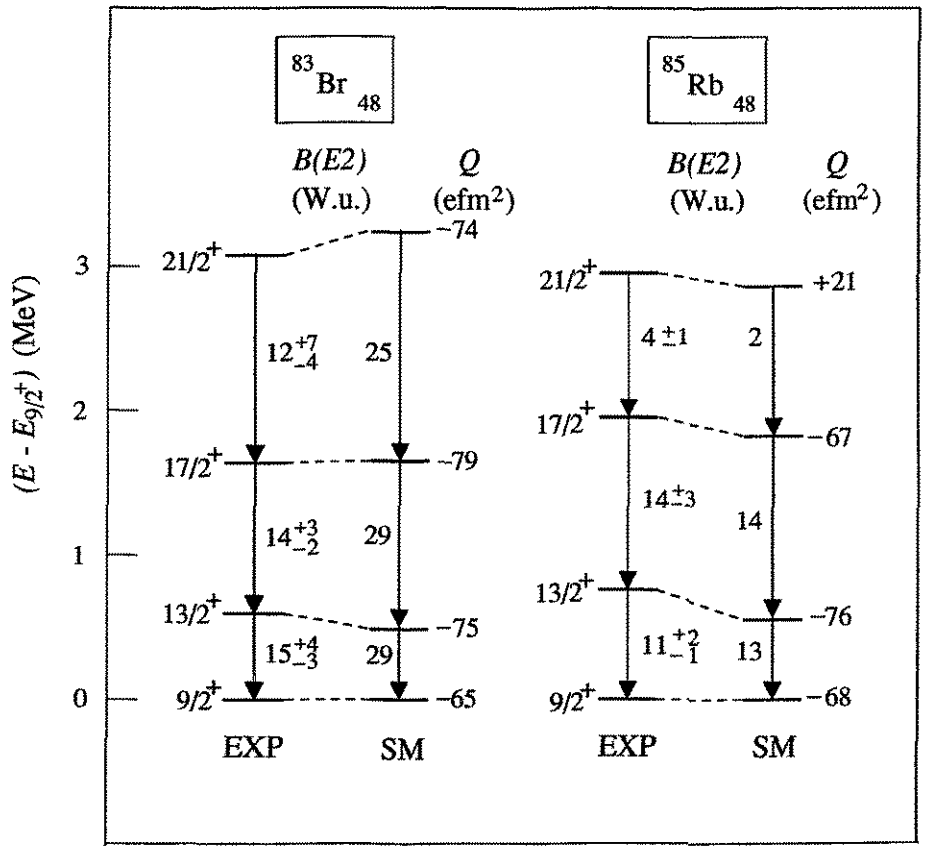

Fig. 1 *Comparison of experimental and calculated positive-parity yrast states up to spin 21/2 in* ^{83}Br *and* ^{85}Rb. *The transitions are labelled with E2 transition strengths in W.u. deduced in the present work; the numbers at the calculated levels are quadrupole moments in efm*^{2}.

The yrast states in ^{85}Rb up to $17/2^+$ and the $E2$ transitions between them are similar to those in ^{83}Br. These states include mainly the configuration $\pi(0f_{5/2}\ 1p_{3/2})^{-2}\ \pi 0g_{9/2}^1\ \nu(0g_{9/2}^{-2})_{0,2}$ which again reproduces the regular level spacings and $B(E2)$ values. In contrast to ^{83}Br, the structure changes at $J^\pi = 21/2^+$. The $21/2^+$ yrast state is formed mainly by coupling one proton moving in the $0g_{9/2}$ orbital to the fully aligned neutron configuration $(0g_{9/2}^{-2})_{8^+}$. This change causes a decrease of the spacing between the $17/2^+$ and $21/2^+$ states and a reduction of the $B(E2, 21/2^+ \rightarrow 17/2^+)$ value, which well reproduces the experimental findings. The change of the configuration is also reflected by the calculated quadrupole moments given in Fig. 1. Whereas the $9/2^+, 13/2^+, 17/2^+, 21/2^+$ states in ^{83}Br as well as the $9/2^+, 13/2^+, 17/2^+$ states in ^{85}Rb have negative quadrupole moments, the quadrupole moment of the $21/2^+$ state in ^{85}Rb is positive, which is caused by the fully aligned coupling of the two $0g_{9/2}$ neutron holes. In the picture of a quadrupole-deformed nucleus this means that the aligned coupling of the two $0g_{9/2}$ neutron holes causes a change of the nuclear shape from an oblate shape to a prolate one. In ^{83}Br there are two proton holes more in the (fp) shell than in ^{85}Rb and, consequently, there are more possibilities to generate states by aligning these low spins. The aligned coupling of the two $0g_{9/2}$ neutron holes and, thus, the change of the sign of the quadrupole moment is in this nucleus predicted at the $25/2^+$ state which has not been found in the experiment.

[1] *Institut für Kern- und Teilchenphysik, Technische Universität Dresden and Institut für Kern- und Hadronenphysik, Forschungszentrum Rossendorf*

References

[1] R. Schwengner et al., Annual Report 1992, **FZR-10** (1993) 82
and Annual Report 1993, **FZR-35** (1994) 47
[2] G. Winter et al., Annual Report 1992, **FZR-10** (1993) 83
[3] R. Schwengner et al., Nuclear Physics **A** (1995), in press

Fast M1 Transitions between Recoupled States in $^{85}Rb_{48}$ [D]

R. SCHWENGNER, G. WINTER, J. REIF, H. PRADE AND L. KÄUBLER[1]

Excited states of the N=48 nucleus ^{85}Rb have been investigated with methods of in-beam spectroscopy [1,2] and interpreted in terms of the shell model using the model space $\pi(0g_{9/2}, 1p_{1/2}, 1p_{3/2}, 0f_{5/2})$ $\nu(0g_{9/2}, 1p_{1/2})$ [3]. Properties of the positive-parity states with $I \leq 21/2$ are discussed in the preceding contribution [4].
The $21/2^+, ..., 33/2^+$ yrast states found in ^{85}Rb are compared with the shell-model predictions in Fig. 1.

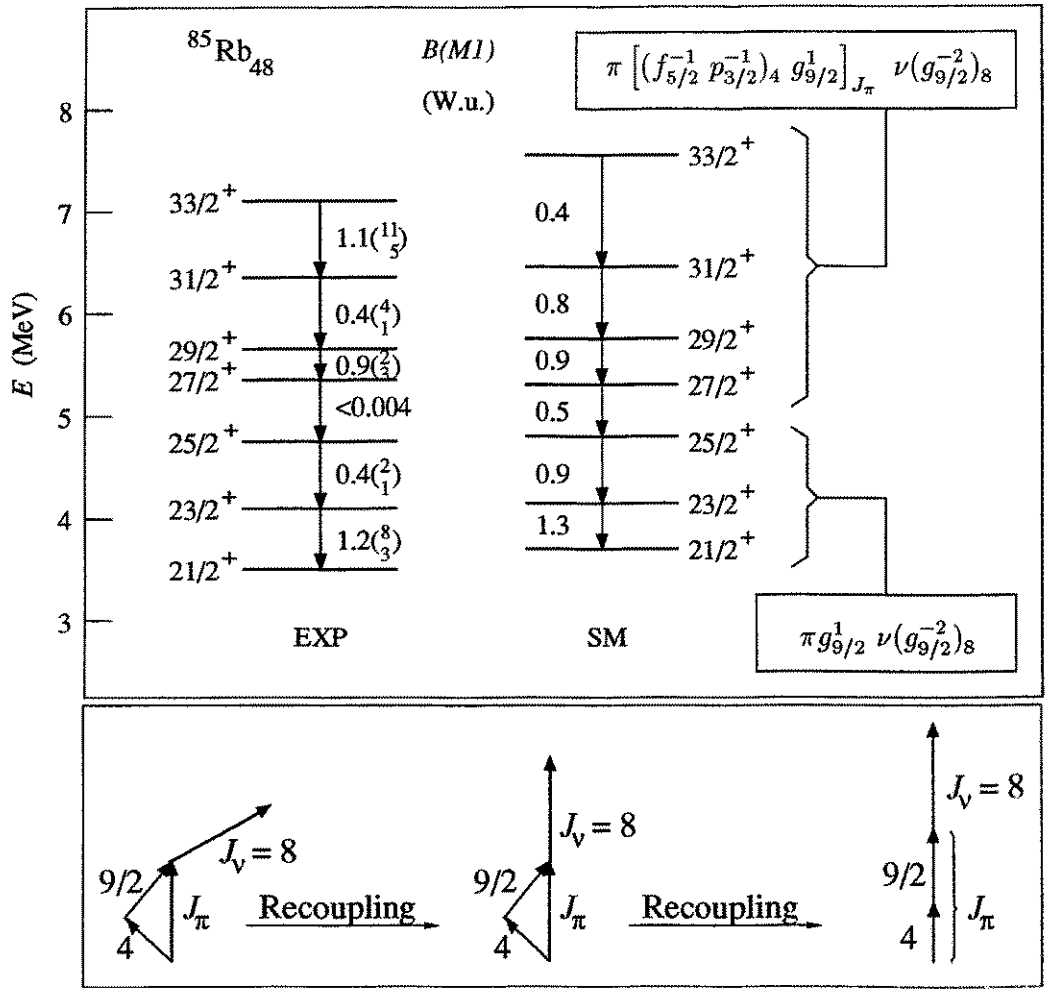

Fig. 1 *Comparison of experimental and calculated positive-parity states with $J \geq 21/2$ in ^{85}Rb. The transitions are labelled with $M1$ transition strengths in W.u. The experimental values were taken from [1]. States enclosed by braces belong to the respective configuration given and are generated from this configuration by recoupling the spins of the proton and neutron orbitals involved. In the bottom part this recoupling is schematically shown for the configuration of the $27/2^+, ..., 33/2^+$ states.*

The $21/2^+, 23/2^+$ and $25/2^+$ states are described by the configuration $\pi 0g_{9/2}^1$ $\nu(0g_{9/2}^{-2})_{8^+}$ including the fully aligned coupling of the two $g_{9/2}$ neutron holes. The generation of

levels with spins higher than 25/2 requires the breakup of an additional pair of nucleons. Indeed, the shell model predicts the configuration $\pi(0f_{5/2}^{-1}\ 1p_{3/2}^{-1})_{4^+}\ \pi 0g_{9/2}^{1}\ \nu(0g_{9/2}^{-2})_{8^+}$ for the formation of the $27/2^+$, $29/2^+$, $31/2^+$ and $33/2^+$ yrast states. As can be seen in Fig. 1, the large experimental $M1$ transition strengths of $B(M1) \approx (0.4 - 1.2)$ W.u. observed between most of these states are well reproduced by the calculations. In the shell-model description the $21/2^+$, $23/2^+$, $25/2^+$ states and the $27/2^+$, $29/2^+$, $31/2^+$, $33/2^+$ states belong to seniority $v = 3$ and $v = 5$ multiplets with the above configurations, respectively, and are formed by a recoupling of the spins of the involved proton orbitals and the neutron spin, which is schematically shown in the bottom part of Fig. 1. The large $B(M1)$ values then appear as a result of this recoupling. This description is consistent with the interpretation given in [1].

[1] *Institut für Kern- und Teilchenphysik, Technische Universität Dresden and Institut für Kern- und Hadronenphysik, Forschungszentrum Rossendorf*

References

[1] G. Winter et al., Zeitschrift für Physik **A334** (1989) 415
[2] G. Winter et al., Annual Report 1992, **FZR-10** (1993) 83
[3] R. Schwengner et al., Nuclear Physics **A** (1995), in press
[4] R. Schwengner et al., contribution to this report

Shell-Model Study of Shears Bands in Pb Isotopes [D]

S. Frauendorf, J. Reif and G. Winter

In several nuclei around ^{200}Pb regular sequences of enhanced magnetic dipole transitions have been found [1]. The analysis of the experimental findings in the framework of the tilted-axis cranking [1,2] has been suggested that the structure of these so-called shears bands is determined by the recoupling of the angular momenta of some few proton particles and neutron holes, respectively, both occupying high-j orbitals. From nuclei in the vicinity of closed shells it is well known that such a recoupling generates states which are connected by fast M1 transitions [3]. However, generally these states are not characterized by regular level spacings.

In order to investigate the origin of the regularity of the shears bands, shell-model calculations have been perfomed in the configuration space $(2s_{1/2}0h_{9/2}0i_{13/2})$ and $(2p_{1/2}2p_{3/2}1f_{5/2}0i_{13/2})$ for protons and neutrons, respectively. In the proton system only the stretched configuration $[(2s_{1/2})^{-2}(0h_{9/2})^{1}(0i_{13/2})^{1}]_{J^\pi=11^-}$ has been considered whereas for the neutrons the configurations $[(2p_{1/2}2p_{3/2}1f_{5/2})^{-m}(0i_{13/2})^{-n}]$ with $m = 0, ..., 12$ and $n = 1, 2$ have been investigated. Experimental single-particle energies have been used and the residual interaction has been calculated with the surface delta interaction, whose strength parameters have been adjusted to the spherical spectra of ^{202,204,206}Pb, ^{210}Po, ^{210}Bi and ^{206}Tl. The calculations reproduce fairly well the properties of the observed shears bands in ^{199,200}Pb. Regular level spacings are predicted by the model where the more active particles in high-j orbitals are involved the more regular the bands become. In agreement with the experimental results the calculated B(M1) values are in the order of several μ_N^2 for the ΔI=1 transitions and the crossover E2 transitions are very weak. In addition, the decrease of the B(M1) values with increasing spin is compatible with the experimental observations [4].

Furthermore, the calculations considering the neutron $[(0i_{13/2})^{-2}(fp)^{-m}]$ (m even) configurations show that the interaction between the neutrons occupying the low-spin (fp) orbitals and the $i_{13/2}$ orbital is essential to the occurrence of regular bands. If the (fp) shell is empty (or full) the shell-model levels show multiplet-like spacings. This irregularity is caused by changes of the orientation of the two $i_{13/2}$ neutron holes relative to each other. A gradual transition from the multiplets to more regular structures appears if the (fp) shell will be filled with particles (or holes). Regular bands occur only in the middle of the (fp) shell. In this case the two $i_{13/2}$ neutron holes are predominantly coupled to the aligned configuration with $J^\pi = 12^+$ and the wave function of the (fp) neutrons is mainly composed of states with $J^\pi = 0^+, 2^+, 4^+$. It seems that the (fp) neutrons affect the stretched coupling of the two $i_{13/2}$ neutron holes by the following feedback mechanism: On the one hand, the slightly deformed density distribution of the (fp) neutrons aligns the $i_{13/2}$ neutron holes, on the other hand, the spatial density distribution of the holes in the high-j orbital induces the deformation of the (fp) density. Regular bands appear only if this feedback is strong enough.

References

[1] G. Baldsiefen et al., Nucl. Phys. **A574** (1994) 521
[2] F. Frauendorf, Nucl. Phys. **A557** (1993) 259c
[3] R. Schwengner et al., contribution to this report
[4] G. Baldsiefen et al., contribution to this report

High-Spin States in ^{81}Y [B]

G. WINTER, R. SCHWENGNER, J. REIF, J. DÖRING[1], G.D. JOHNS[1], S.L. TABOR[1]
C.J. GROSS[2], C. BAKTASH[3], Y.A. AKOVALI[3], D.W. STRACENER[3], F.E. DURHAM[4],
D.G. SARANTITES[5], M. KOROLIJA[5], P.F. HUA[5], D.R. LAFOSSE[5],
A. MACCHIAVELLI[6], I.Y. LEE[6], W. RATHBUN[6], A. VANDERMOLEN[7]

High-spin states in ^{81}Y have been investigated in connection with the ^{58}Ni(^{32}S, $2\alpha p$) reaction at 135 MeV. Prompt coincidences between γ rays were observed with the early implementation of GAMMASPHERE (36 detectors) and recorded on tape if three or more γ rays were detected. In addition, evaporated charged particles were observed in the 96-element MICROBALL for channel selection. This study was initiated in order to extend the information on deformation and pairing in a nucleus with proton und neutron numbers close to 40.

Although the nucleus ^{81}Y is only formed with a small relative cross section the analysis of triple γ coincidences and of particle-gated γ-γ coincidences allowed us to expand the very recently published [1] level scheme considerably. In particular, when gating γ-γ coincidences by signals corresponding to the detection of two α particles and one proton in the MICROBALL γ rays from levels in ^{81}Y are found to dominate in the spectra.

Sequences of high-spin states with positive and negative parity and signature $\alpha = +1/2$ have been identified with spins up to $(49/2)\hbar$ at excitation energies up to 13 MeV. Sequences with signature $\alpha = -1/2$ could only be followed up to $(39/2)\hbar$.

The kinematic moment of inertia as derived from the level spacings within the positive-parity sequence observed in ^{81}Y is shown in Fig. 1 together with the corresponding data found [2] in the isotone ^{79}Rb. The rather constant moment of inertia for the $\alpha = +1/2$ sequence in ^{79}Rb is interpreted as arising from the gap at proton number 38 in the scheme of single-particle states for prolate deformation. The variation of the moment of inertia for the transitions within the $\alpha = -1/2$ sequence is not well understood.

Up to spin $27/2\hbar$ the new data for the positive-parity sequence in ^{81}Y imply a similar behaviour as observed in ^{79}Rb. For higher spin the curves for $\alpha = +1/2$ and $\alpha = -1/2$ are close to each other in both nuclei. But in ^{81}Y the effective moment of inertia is found to increase considerably with increasing spin.

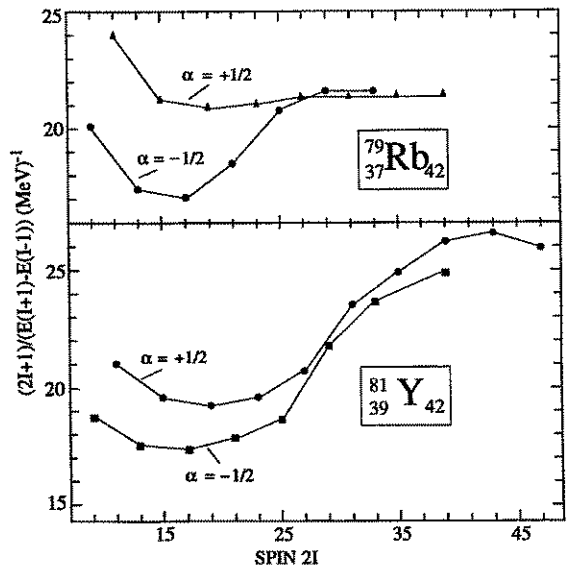

Fig. 1 *Kinematic moment of inertia as derived from the level spacings within the positive-parity sequences in* ^{79}Rb *and* ^{81}Y.

[1] *Florida State University.* [2] *UNISOR.* [3] *ORNL.* [4] *Tulane University.*
[5] *Washington University.* [6] *Lawrence Berkeley Laboratory.* [7] *Michigan State University.*

References

[1] T.D. Johnson et al., Z. Phys. **A 350** (1994) 189
[2] J.W. Holcomb et al., Phys. Rev. **C48** (1993) 1030

Excitations of the N=50 Core in $^{89}_{39}Y_{50}$ [D]

J. Reif, G. Winter, R. Schwengner, H. Prade and L. Käubler[1]

The high-energy properties of nuclei having magic proton or neutron numbers might be significantly influenced by particle-hole excitations of the closed core. Recently, the semi-magic nucleus ^{89}Y has been investigated using in-beam γ-ray spectroscopy [1] and the high-spin part ($I^\pi \geq 17/2^+$) of the deduced level scheme has been interpreted assuming the break-up of the N=50 core. In order to test this interpretation, shell-model calculations have been performed considering two configuration spaces: whereas the space SM-I has been generated out of the proton orbitals $0f_{5/2}, 1p_{3/2}, 1p_{1/2}$ and $0g_{9/2}$ only (^{78}Ni core) the space SM-II has been expanded by the neutron orbitals $1p_{1/2}, 0g_{9/2}$ and $1d_{5/2}$ (^{66}Ni core). For details of the used parametrization of the residual nuclear interaction see [2].

The results, both for the excitation energies (see Fig. 1) and electromagnetic transition probabilities (see Table 1), suggest for the positive-parity states above 4.5 MeV with $17/2 \leq I \leq 23/2$ considerable admixtures of the neutron $[(0g_{9/2})^{-1}(1d_{5/2})]$ excitation coupled to the odd proton occupying the $0g_{9/2}$ orbital.

The calculations predict that levels with higher spins are generated by raising one additional proton out from the negative-parity orbitals $0f_{5/2}$ or $1p_{3/2}$ to the $0g_{9/2}$ orbital causing a parity alteration. Therefore, negative parity is tentatively assigned to the experimetally observed states above 7.2 MeV with $23/2 \leq I \leq 31/2$.

Table 1 *Comparison of experimental and calculated $B(M1)$ values in ^{89}Y.*

$2I_i^\pi \rightarrow 2I_f^\pi$	$B(M1)_{exp}$ [a]	$B(M1)_{cal}$ [a]	
		SM-I	SM-II
$17^+ \rightarrow (15^+)$	≤ 2	48	0.3
$19^+ \rightarrow 17^+$	23^{+23}_{-2}	5	1430
$21^+ \rightarrow 19^+$	670^{+160}_{-110}	0.6	656
$(19^+) \rightarrow 21^+$	1224^{+1260}_{-414}	44	2400
$23^+ \rightarrow 21^+$	250^{+70}_{-35}	12	480

[a] Reduced transition probabilities are given in $10^{-3}\mu_N^2$.

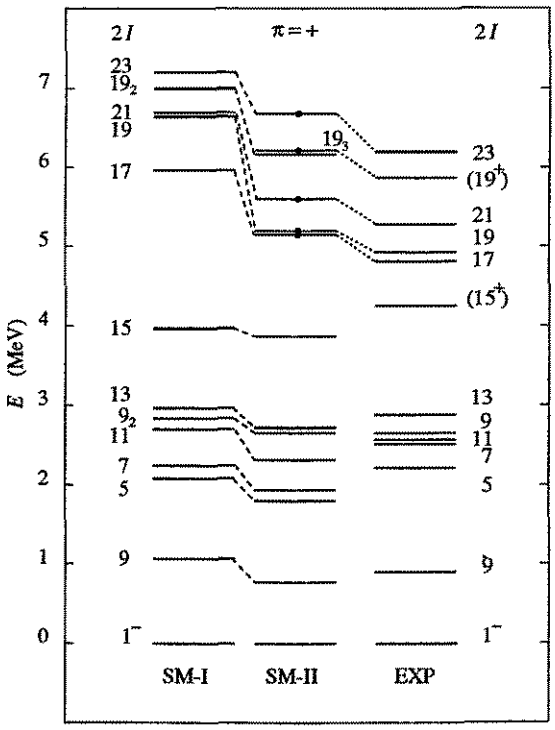

Fig. 1 *Comparison of experimental* (EXP) *and calculated* (SM-I and SM-II) *level energies of positive-parity states ($I \leq 23/2$) in ^{89}Y. All levels are labelled by $2I$. Levels marked with a dot are dominated by neutron-core excitations.*

[1] *Institut für Kern- und Teilchenphysik, TU Dresden and Institut für Kern- und Hadronenphysik, FZR*

References

[1] L. Funke et al., Nucl. Phys. **A541** (1992) 241
[2] G. Winter et al., Phys. Rev. **C49** (1994) 2427

Search for Collectivity in ^{109}Sn - a New Level Scheme[B]

L. KÄUBLER[1], H. PRADE, J. REIF, H. SCHNARE, R. SCHWENGNER, G. WINTER, H. GRAWE[2], J. HEESE[2], H. KLUGE[2], K.-H. MAIER[2], R. SCHUBART[2], K.-M. SPOHR[2]

The collective behaviour of nuclei near the magic numbers $N = Z = 50$ is mainly caused by 2p2h excitations across $Z = 50$. To look for high-spin states and to clarify the ground state problem [1], in-beam experiments to ^{109}Sn have been performed using the reactions ^{55}Mn(^{58}Ni,3pn) with $E_{^{58}Ni} = 240$ MeV (VICKSI accelerator of the HMI Berlin) and ^{106}Cd(α,n) with $E_\alpha = 23$ MeV (Rossendorf cyclotron). First results are given in [2,3]. The level scheme shown in Fig. 1 has been constructed on the basis of the following experimental results: $\gamma\gamma$-coincidences measured with the OSIRIS spectrometer in 0° geometry at the HMI (2mg/cm^2 thick Au-backed target), $\gamma\gamma$-coincidences (LEPS-GE(Li)) and γ-RF time distributions, measured in connection with the (α,n) reaction [1], the angular-distribution coefficients given in [4,5], and the K-conversion coefficients given in [6]. In comparison to the level schemes presented in [4-6], here the g.s. problem has been solved [1], all excitation energies have been revised and the level scheme has been extended essentially to higher spins. First very preliminary results of an experiment to ^{109}Sn (thin target, ^{54}Fe (^{59}Co,3pn reaction) with GAMMASPHERE at the LBL Berkeley [7] show 9 more transitions on top of the state at $E_x = 8121$ MeV giving a hint at smooth band termination [8] also in ^{109}Sn.

[1] *Institut für Kern- und Teilchenphysik, TU Dresden and Institut für Kern- und Hadronenphysik, FZR*

[2] *Hahn-Meitner-Institut Berlin*

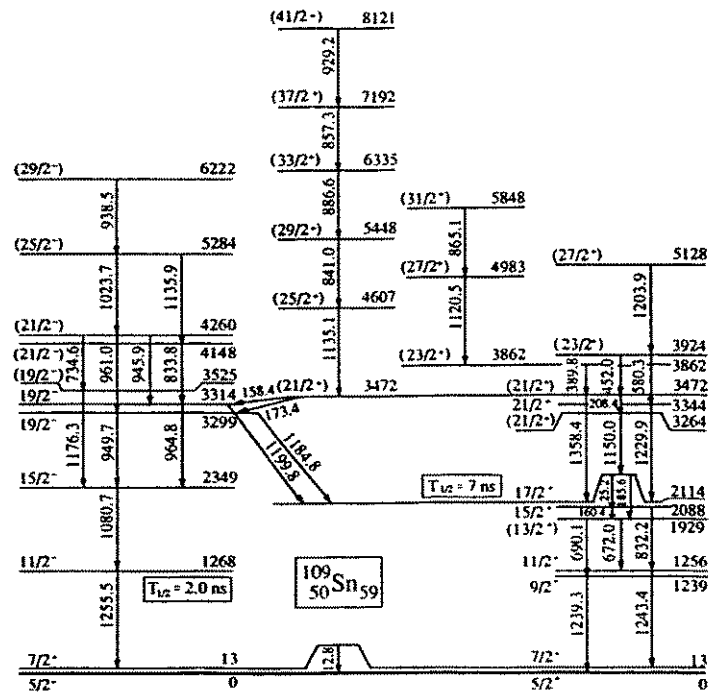

Fig. 1 *Level scheme for ^{109}Sn as deduced from the present experiments*

References

[1] L. Käubler et al., contribution to this report
[2] L. Käubler et al., Z. Phys. A, in press
[3] L. Käubler et al., Physica Scripta, in press
[4] O. Hashimoto et al., Nucl. Phys. **A318** (1979) 145
[5] M.G. Johnston et al., Proc. 4th Int. Conf. on Nuclei far from Stability, Helsingør, Denmark, 1981, p. 469
[6] G. Madueme et al., Physica Scripta **13** (1976) 17
[7] D.B. Fossan et al., proposal for an experiment to ^{109,110}Sn with GAMMASPHERE
[8] I. Ragnarsson et al., submitted to Phys. Rev. Lett.

Observation of the $7/2^+ \rightarrow 5/2^+$ Transition to the Ground State of ^{109}Sn [B]

L. KÄUBLER[1], H. PRADE, J. REIF, R. SCHWENGNER, G. WINTER, H. GRAWE[2], J. HEESE[2], H. KLUGE[2], K.-H. MAIER[2], R. SCHUBART[2], K.-M. SPOHR[2]

For ^{109}Sn the deexcitation of known levels to the ground state has not yet been observed. The behaviour of energies of the $5/2^+$ and $7/2^+$ single-particle states in $^{105-113}$Sn suggests a change of the g.s. angular momentum from $5/2^+$ to $7/2^+$ between ^{107}Sn and ^{111}Sn. In the literature different values for the g.s. of ^{109}Sn are given: $5/2^+$ or $7/2^+$ from the decay [1], 7/2 from atomic beam [2] and 5/2 from collinear laser experiments [3]. The $5/2^+$ and $7/2^+$ states in ^{109}Sn should be nearly degenerated. The α-particle beam (E_α = 23 MeV) of the Rossendorf cyclotron U-120 has been used to excite low-lying states in ^{109}Sn by means of the reaction ^{106}Cd(α,n), bombarding a 10 mg/cm^2 metallic target. To search for low-energy γ-rays, $\gamma\gamma$-coincidences between a LEPS and a Ge(Li) detector (V = 60 cm^3) have been measured (Δt = 140 ns) and sorted into a 2K $\times$ 2K matrix from which $\gamma\gamma$-coincidence spectra have been taken. As shown in the upper part of Fig. 1, an E_γ = 12.8 keV transition coincides with transitions deexciting states in ^{109}Sn [4] while such a transition has not been found in ^{114}Sn. This nuclid has been excited simultaneously in the experiment because of the contamination of the target with other Cd isotopes.

Starting with the $11/2^- \rightarrow 7/2^+$ transition, the construction of the level scheme for ^{109}Sn [4] leads to an energy difference of about 13 keV between the 1239.3 keV and 1243.4 keV transitions. On the basis of the level scheme [4], the results of our coincidence experiment, and of the direct measurement of the g.s. spin [3], the sytematics of $d_{5/2}$ and $g_{7/2}$ single particle states in tin nuclei and the results of shell-model calculations we suggest that the 12.8 keV transition deexcites the $7/2^+$ state to the $5/2^+$ ground state of ^{109}Sn.

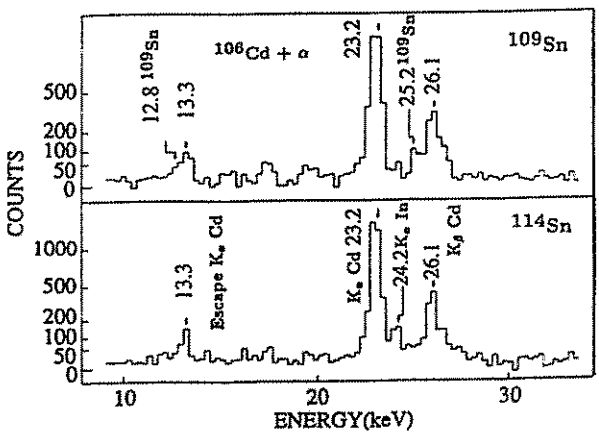

Fig. 1 *Comparison of $\gamma\gamma$-coincidence spectra for ^{109}Sn and ^{114}Sn. The spectra are sums of gates on E_γ = 160.4, 672.0, 832.2, 1080.7, 1229.9, 1243.4 and 1255.5 keV representative for ^{109}Sn and E_γ = 102.9, 272.3, 672.3, 627.5, 887.7 and 1299.9 keV representative for ^{114}Sn.*

[1] *Institut für Kern- und Teilchenphysik, TU Dresden and Institut für Kern- und Hadronenphysik, FZR*

[2] *Hahn-Meitner-Institut Berlin*

References

[1] S. Shastry et al., Phys. Rev. C1 (1970) 1835

[2] W. Hogervorst et al., Physica Scripta 9 (1974) 317

[3] J. Eberz et al., Z. Phys. A-Atomic Nuclei **326** (1987) 121

[4] L. Käubler et al., contribution to this report and references therein

Magnetic Quadrupole Transition Rates in ^{85,87}Rb

L. KÄUBLER[1], CH. PROTOCHRISTOV[2], M. MICHAILOVA[2]. J. REIF, W.-ANDREJTSCHEFF[2], L. FUNKE[3], L. KOSTOVA[2], H. PRADE, R. SCHWENGNER, G. WINTER

The knowledge about proton $1g_{9/2}$ states in N = 50 nuclei is scarce. Therefore the half-life of the $9/2^+$ isomer in ^{87}Rb has been measured [1], confirming the $g_{9/2}$ single-particle character of this state. In Table 1 the experimentally determined B(M2, $9/2^+ \rightarrow 5/2^-$) values obtained for ^{85}Rb and ^{87}Rb are compared showing a decrease by about a factor of three from ^{87}Rb to ^{85}Rb. Here we try to describe this behaviour by calculations within the particle-anharmonic core coupling (PACC) model and within large scale shell-model calculations (SM).

The PACC calculations have been performed with the computer code NUCLODD [3]. The model is described in detail in [4,5]. The quadrupole coupling constants κ_2 are determined to correspond to small deformation parameters $\beta = 0.13$ for ^{85}Rb and $\beta = 0.10$ for ^{87}Rb. The pairing gap $\Delta = 1.2$ MeV was fixed for both nuclei and the experimentally observed 0_1^+, 2_1^+, 2_2^+, 4_1^+ and 0_2^+ states of the adjacent even-even Kr and Sr core nuclei have been included in the calculations. The single-particle model space $1f_{5/2}$, $2p_{3/2}$, $2p_{1/2}$ and $1g_{9/2}$ with the energy differences $|\Delta E(2p_{3/2}-1f_{5/2})| = 0.4$ and 1.2 MeV, $|(\Delta E(2p_{1/2}-1f_{5/2})| = 1.0$ and 2.2 MeV and $|\Delta E(1g_{9/2}-1f_{5/2})| = 2.7$ and 4.4 MeV for ^{85}Rb and ^{87}Rb, respectively, has been used.

Table 1

Comparison of experimental B(M2) values, given in Weisskopf units, for $9/2^+ \rightarrow 5/2^-$ transitions in ^{85,87}Rb with the predictions of PACC and SM calculations (cf. the text). The gyromagnetic factors g_s^{free} are renormalized by a factor of 0.7.

Nucleus	E_x (keV)	$T_{1/2}^{exp}$	E_γ (keV)	$B(M2)^{exp}$ (W.u.)	$B(M2)^{th}$(W.u.) PACC	SM
$^{85}_{37}Rb_{48}$	514.0	1.0(1)μs[a]	514.0	0.045(4)	0.097	0.031
$^{87}_{37}Rb_{50}$	1578.1	6.0(1)ns	1175.3	0.12(2)	0.099	0.30

[a]) Taken from [2]

The SM calculations have been performed with the code RITSSCHIL [6]. In the case of ^{87}Rb the configuration space has been generated out of the $1f_{5/2}$, $2p_{3/2}$, $2p_{1/2}$ and $1g_{9/2}$ proton (π) orbitals relative to a hypothetic $^{78}_{28}Ni_{50}$ core without any truncation of the occupation possibilities for the nine active protons. For ^{85}Rb, the configuration space has been expanded by the neutron (ν) $2p_{1/2}$, $1g_{9/2}$ orbitals assuming a hypothetic $^{66}_{28}Ni_{38}$ core. The two neutron holes are coupled to a restricted proton configuration space where no more than two protons are allowed to occupy the $1g_{9/2}$ orbital [7]. For the effective nuclear interaction a set of parameters determined from a realistic interaction has been used [8].

Level energies in ^{85,87}Rb calculated in the PACC model are given in [9], for those obtained in the SM in [7] for ^{85}Rb and [8] for ^{87}Rb. Both models reproduce to some extent the experimentally observed lowering of the energy of the $9/2^+$ state from ^{87}Rb to ^{85}Rb and the $5/2^- - 9/2^+$ level distances. Discussing the B(M2, $9/2^+ \rightarrow 5/2^-$) values (Table 1), both models describe the experimental values within the right order of magnitude. The experimentally observed decrease of B(M2) from ^{87}Rb to ^{85}Rb is without further reduction of the renormalization factor for g_s^{free} only reproduced by the SM, whereas the PACC results remain nearly constant. The PACC calculations for ^{85}Rb give with $g_s^{eff} = 0.4\ g_s^{free}$ about the right B(M2) value. Such a strong renormalization of g_s^{free} is a feature of models, wich try to describe experimentally observed B(M2) values[10-13]. The explicit inclusion of core polarization effects within the PACC calculations is expected to improve the situation.

Large scale SM calculation are inherently based on a large number of mixing configurations. Thus, in the light of the shell-model calculations the decrease of the B(M2) values towards smaller neutron numbers can be understood as a consequence of the neutron excitations involved in the wave functions of ^{85}Rb which cause a decrease of the amplitudes of the main components contributing to the M2 transition, e.g. 57% $\pi\ (1f_{5/2}^5\ 2p_{3/2}^4)$ in ^{87}Rb and 23% $\pi\ (1f_{5/2}^5\ 2p_{3/2}^4)\ \nu\ (1g_{9/2})_{0^+}^{-2}$ in ^{85}Rb.

[1] *Institut für Kern- und Teilchenphysik, TU Dresden and Institut für Kern- und Hadronenphysik, FZR*

[2] *Institut for Nuclear Research and Nuclear Energy, Bulgarian Academy of Sciences*

[3] *Ingenieurgesellschaft IAF Dresden*

References

[1] Ch. Protochristov et al., Annual Report 1989, ZfK-731(1990)21
[2] H. Sievers, Nucl. Data Sheets **62** (1991) (271)
[3] M.M. Michailova, JINR-report E4-90-415 (1990) 1
[4] R.V. Jolos et al., Proc. Int. School on Nucl. Phys., Neutron Phys. and Nucl. Energy, Varna 1989, eds. W. Andrejtscheff and D. Elenkov, World Scientific 1990, pp. 171-189
[5] M. Michailova et al., J. Phys. **G12** (1986) L191
[6] D. Zwarts, Comput. Phys. Commun. **38** (1985) 365
[7] R. Schwengner et al., Nucl. Phys. A, in press
[8] J. Sinatkas et al., J. Phys. **G18** (1992) 1377
[9] L. Käubler et al., to be published
[10] H. Ejiri et al., Phys. Rep. **38C** (1978) 87
[11] A.I. Vdovin et al., Nucl.Phys. **A440** (1985) 437
[12] A.I. Vdovin et al., Izv. AN SSSR, ser. fiz. **49** (1985) 173
[13] L.G. Kostova et al., Z. Phys. **A342** (1992) 145

Experimental Setup for (γ,γ') Experiments at the S-DALINAC [B]

S. Skoda, M. Freitag, L. Käubler, T. Mylaeus, H. Prade, J. Reif, W. Schulze, R. Schwengner, G. Winter, J. Enders[1], P. von Neumann-Cosel[1], A. Richter[1], C. Schlegel[1], J. Eberth[2], M. Kabadiyski[2], N. Nicolay[2], H.-G. Thomas[2], M. Wilhelm[2], P. von Brentano[2] and A. Zilges[2]

The (γ,γ') experiments planned at the S-DALINAC electron accelerator will take place behind the injector in the accelerator hall. Electrons decelerated by a Ta sheet provide bremsstrahlung-γ-rays, which are collimated through a large Pb block. The bremsstrahlung with a continuous energy spectrum will be used to irradiate various targets and the resulting γ transitions from low-spin states shall be observed by one or two EUROBALL-CLUSTER-detectors.

The CLUSTER detector [1] comprises 7 encapsulated Ge-detectors in a common cryostate and a BGO-Compton-suppression shield. The BGO shield is used to suppress γ rays resulting from Compton-scattering in the 7 Ge detectors. To protect this shield from the high background due to γ rays scattered in the accelerator hall, a housing of 30 cm Pb around two CLUSTER detectors has been prepared (see Fig. 1). This results in 20-30 tons of Pb, which have to be installed and which constrict the space conditions even further. The housing will be assembled within a special steel frame that enables an adjustment of the horizontally mounted detectors to the beam-height of 156 cm and was designed to support 40 tons.

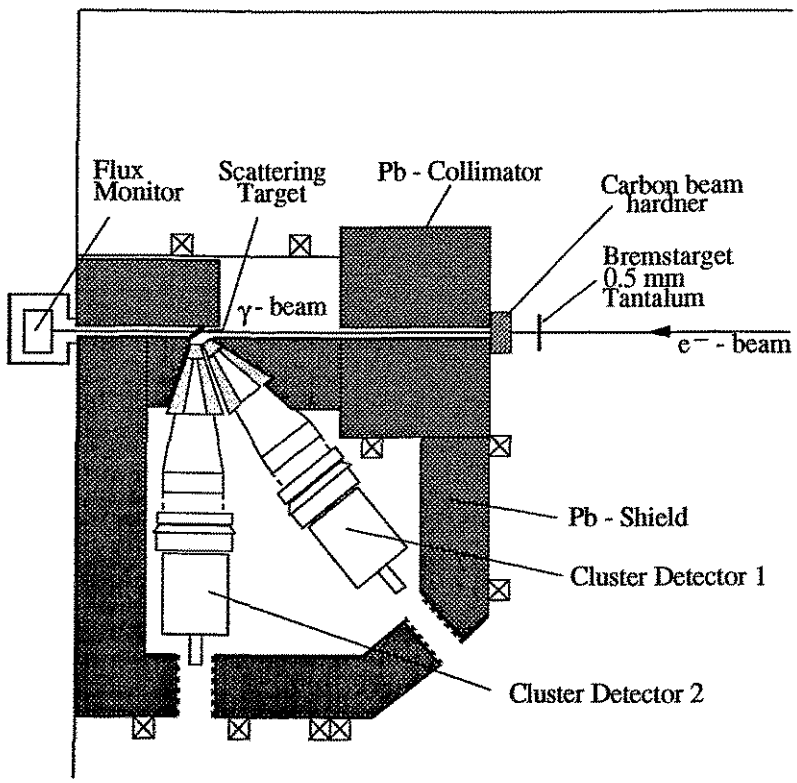

Fig. 1 *CLUSTER detectors in the* Pb *housing (horizontal cut at beam height)*

To prevent the γ rays emitted by the target from entering the front side of the BGO shield a Pb-collimator was built. Its inner opening follows the complicate honeycomb shape of the seven Ge detectors. Because of the restricted spacings the collimator has to be inserted into the housing separately from the CLUSTER and must be mounted and positioned inside the housing.
Moreover, a variable positioning of the CLUSTER detectors has to be provided to support different experimental conditions. The CLUSTER detector is mounted in a table top frame described in [2]. To allow for various positioning requirements the frame can be moved by height-adjustable rollerlegs. The friction on the relatively small rolling balls, due to the large weight of the detector system and the collimator, is reduced by ball-bearings. The electronics (NIM and CAMAC) and the analyzer system will be installed about 60 m from the detector.
The bremsstrahlung spectrum results in a high counting rate from undesirable γ rays of low energies while the transitions of interest at some 6 MeV have a small intensity. To allow for an as high as possible counting rate pure singles and coincidences shall be gated and processed separately. The coincidences are used to add back the energies detected in two or more Ge crystals after Compton scattering. The pure singles events will be accumulated on disk while the coincidence events will be stored on tape.

[1] *Institut für Kernphysik der TH Darmstadt, Schloßgartenstr. 9, 64289 Darmstadt*
[2] *Institut für Kernphysik der Universität zu Köln, Zülpicher Str. 77, 50937 Köln*

References

[1] EUROBALL III proposal, GSI 1992, ed. J. Gerl and R.M. Lieder
[2] J. Stephan and M. Freitag, Annual Report 1993, **FZR-35** (1994) 89

High-lying three-quasiparticle bands and signature splitting in ^{81}Rb
(Phys. Rev. C50 (1994) 1845)

Döring, J., R. Schwengner, L. Funke, H. Rotter, G. Winter, B. Cederwall, F. Lidén, A. Johnson, A. Atac, J. Nyberg, G.Sletten

Abstract: Two new high-lying level sequences of negative parity have been identified in the odd-proton nucleus ^{81}Rb by in-beam γ-ray spectroscopy using the reactions ^{79}Br(α,2n) at 27 MeV and ^{68}Zn(^{19}F,α2n) at 72 MeV. One sequence, dominated by $M1$ transitions, is interpreted as a three-quasiparticle band predominantly containing a neutron in the $p_{1/2}$, $p_{3/2}$, or $f_{5/2}$ subshell coupled to $g_{9/2}$ proton and $g_{9/2}$ neutron excitations. The other new level sequence forms the three-quasiparticle extension of the unfavored negative-parity band, but the states decay also by $E1$ transitions. The signature splitting points to a configuration where an aligned $g_{9/2}$ proton pair is involved.

Excited states built on the 6$^-$ isomer in $^{86}_{37}Rb_{49}$
(Phys. Rev. C 49 (1994) 2427)

Winter, G., R. Schwengner, J. Reif, H. Prade, J. Döring, R. Wirowski, N. Nicolay, P. von Brentano, H. Grawe, R. Schubart

Abstract: High-spin states of the doubly-odd nucleus ^{86}Rb containing 37 protons and 49 neutrons have been investigated via the reaction ^{82}Se(^{7}Li, $3n$) using ^{7}Li ions with energies between 30 and 35 MeV. The new level scheme is based on prompt $\gamma\gamma$-coincidences, angular distributions and directional correlation orientation ratios of γ-rays as well as on linear polarizations of some strong γ-rays and contains levels with excitation energies up to 7.9 MeV and tentative spins up to 16 $\hbar$. For fifteen of the levels lifetimes in the ps region have been determined by analyzing the Doppler shift of γ-rays. Several fast $M1$ transitions with $B(M1) > 0.3$ W.u. have been identified. The new high-spin level scheme of ^{86}Rb is interpreted on the basis of shell-model calculations in the configuration space $1p_{3/2}$,$0f_{5/2}$,$1p_{1/2}$, and $0g_{9/2}$ for the protons and $1p_{1/2}$,$0g_{9/2}$, and $1d_{5/2}$ for the neutrons. The energies of the observed levels with $I > 5$ as well as most of the observed electromagnetic transition probabilities could be well described. The excitation of a $0g_{9/2}$ neutron over the N=50 shell gap into the $1d_{5/2}$ orbital is predicted to cause remarkable alterations only for states with $I^\pi \geq 15^+$. Some of the reduced $M1$ transition probabilities calculated within the shell model are found to depend critically on the parametrization used to describe the residual interaction.

4 Experimental Heavy Ion Physics

Angular Correlations of Fission Fragments produced by ^{7}Li(43AMeV) + ^{232}Th [B]

C.-M. Herbach, D. Hilscher[1], P. Gippner[2], H.-G. Ortlepp[2], G. Pausch, K.D. Schilling, W. Wagner[2]

The heavy-ion reaction ^{7}Li(43AMeV) + ^{232}Th has been investigated [1] by using the 4π-spectrometer FOBOS [2]. In a first step, the folding angle $\vartheta_{ff}=\vartheta_1+\vartheta_2$ and the coplanarity angle α_{cop}=abs($\phi_1 - \phi_2$) have been analysed for the fission fragment (FF) coincidences, which had been recorded by different FF detection systems with in-plane (Fig. 1) and out-of-plane (Fig. 2) geometry.

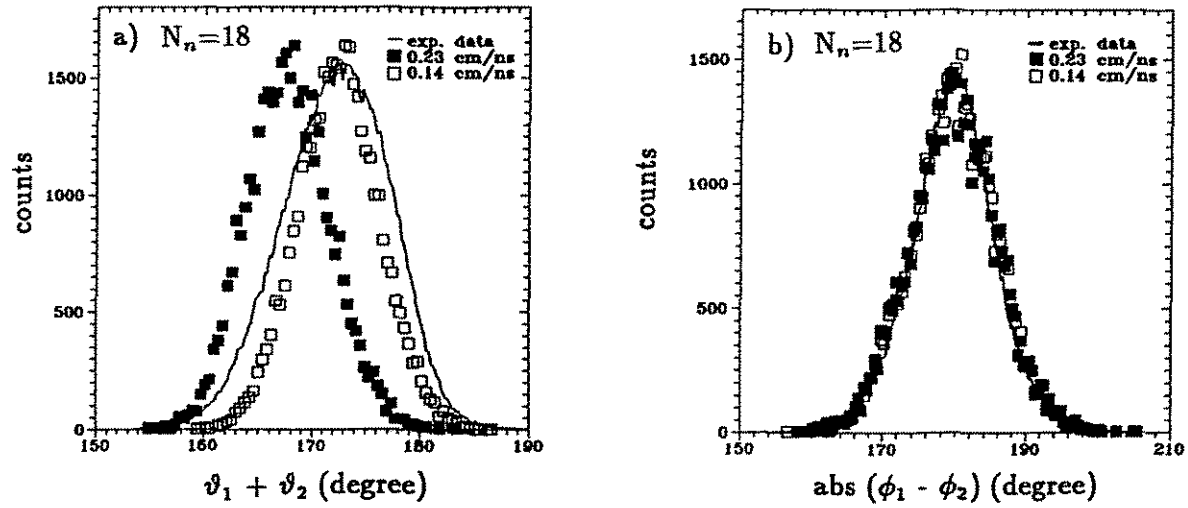

Fig. 1 *Measured and simulated angular distributions for the in-plane FF-detection*

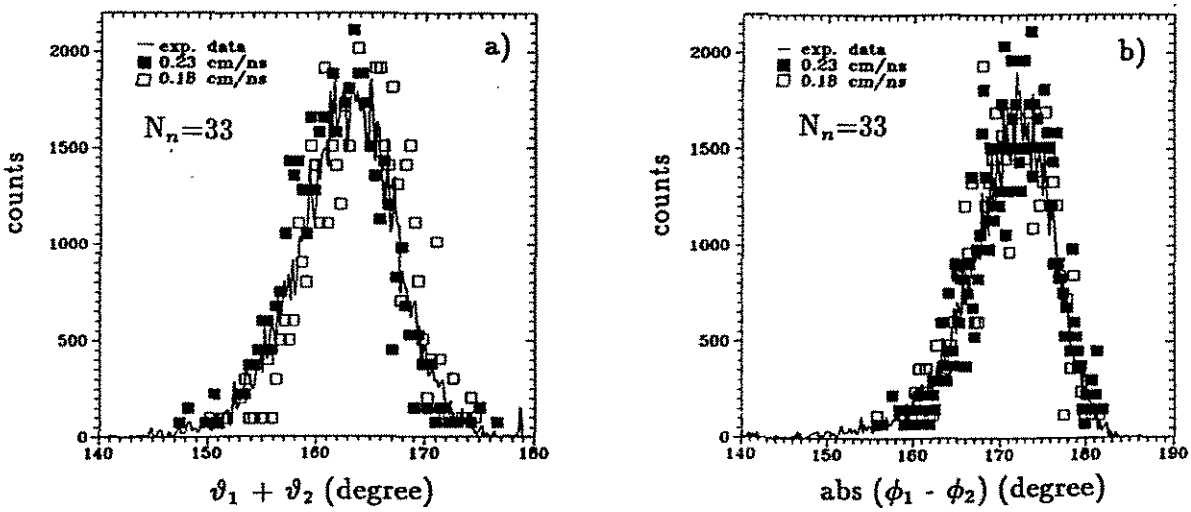

Fig. 2 *Measured and simulated angular distributions for the out-of-plane FF-detection*

In contrary to the folding angle (a), the coplanarity (b) is independent of the longitudinal velocity of the composite system and the distribution width can be studied as a measure of the transversal deflection of the fissioning nucleus. The observed FWHM (α_{cop})=11°-13° is comparable with the width of the ϑ_{ff}-distribution. This indicates a strong influence of the deflection on the FF angular correlations. For comparison, the

data measured with ^{252}Cf result in a value of FWHM (α_{cop})=3°.
In order to simulate the transversal deflection of the compound nucleus before fission, the recoil of isotropically emitted 6 MeV neutrons was considered. By variation of the neutron number N_n as the only parameter, a quite good agreement was achieved between the experimental and simulated coplanarity spectra. Moreover, the folding angle distribution measured by the out-of-plane detection system is also reproduced (Fig. 2a).
The optimized parameter N_n was found to be dependent on the linear momentum transfer (LMT): Small LMT=50% and large LMT=80% corresponds to N_n=18 and N_n=33, respectively. For comparision, an estimate for the neutron evaporation in accordance with [3] results in N_n=11 and N_n=18. However, besides neutron evaporation additional effects contribute to the broadening of the α_{cop}-distribution, as e.g. the angular divergence and the width of the beam at the target position as well as the angular straggling of the charged particles within the target material and the detector foils. Nevertheless, all these effects cause a qualitatively similar shape of the transversal momentum distribution, and the parametrization via isotropic neutron evaporation seems to be a satisfactory approximation to calculate the geometrical efficiency for coincidence measurements.
As usual [4], the FF angular correlation has been analysed to deduce the velocity of the fissioning system $v_{c.m.}$ and to estimate the LMT within the frame of the Massive Transfer Model. The detected FF yield has been corrected for geometrical acceptance. The data shown in Fig. 3 cover the whole range of the impact parameter from peripheral to central collisions. The smooth behaviour of the yield does not allow to distinguish between different groups for complete and incomlete fusion. The maximum at 0.15 cm/ns corresponds to the LMT of 55% and is in accordance with the transfered momentum of 160-180 MeV/c per nucleon of the projectile, which is predicted for the most probable LMT in central collisions at intermediate energies [5]. The large extension of the yield below zero and beyond the total projectil momentum is caused by the strong deflection of the composite system as discussed above.

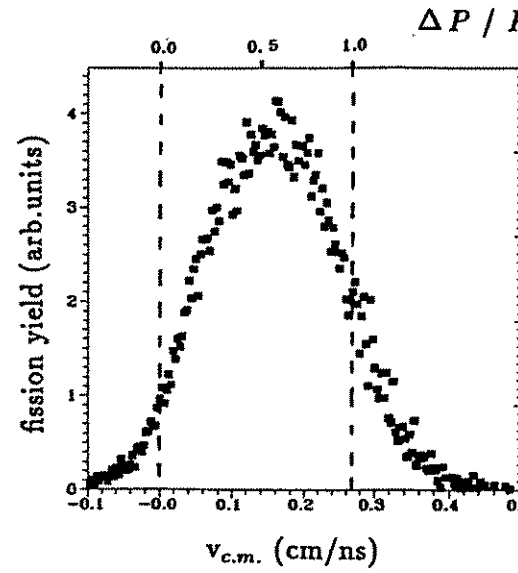

Fig. 3 *Longitudinal velocity of the fissioning system produced by $^{7}Li(43AMeV) + ^{232}Th$.*

[1] *Hahn-Meitner-Institut Berlin*

[2] *Joint Institute for Nuclear Research, Dubna* and *Institut für Kern- und Hadronenphysik, FZR*

References

[1] A.A. Aleksandrov et al.,contribution to this report
[2] H.-G. Ortlepp et al., Proc. Int. School-Seminar on Heavy Ion Physics, JINR Dubna, Russia, vol.2 (1993) 466
[3] W.W. Wilcke et al., At. Data and Nucl. Data Tab. **25** (1980) 389
[4] D. Guerreau, Int. School on Nucl. Phys. "Nuclear Matter and Heavy Ion Collisions", Les Houches, Report Ganil P89-07, 1989
[5] C. Gregoire and F. Scheuter, Phys. Lett. **146B** (1984) 21

Mass and Momentum Distribution of Fission Fragments produced by ^{7}Li + ^{232}Th at 43 AMeV bombarding Energy [B]

C.-M. HERBACH, D. HILSCHER[1], P. GIPPNER[2], H.-G. ORTLEPP [2], G. PAUSCH, K.D. SCHILLING, W.WAGNER[2]

Basic features of the 4π-spectrometer FOBOS [1] are the mass determination of heavy fragments deduced from time-of-flight (FWHM(TOF)<1ns) and kinetic energy ($E_{thresh.}$ <0.5 AMeV) measurements as well as the precise detection of the emission direction ($\Delta\vartheta$ <0.2°) by using position-sensitive counters. If the event is recorded completely, the measured single-particle parameters enable a kinematical analysis even for events with multiplicities larger than two.

Within the framework of [2], binary fission fragments (FF) produced by ^{7}Li(43AMeV) + ^{232}Th have been analysed. In order to verify the procedures, the longitudinal velocity of the fissioning system $v_{c.m.}$ has been evaluated both from the masses m and the velocity vectors $\vec{v}$ of the two FF by eqs. (1,2) and from the FF folding angle (Fig.1).

$$\vec{P} = m_1 \cdot \vec{v_1} + m_2 \cdot \vec{v_2} \qquad (1) \qquad \vec{v}_{c.m.} = \vec{P} \,/\, (m_1 + m_2) \qquad (2)$$

The second method is known as a satisfactory approximation to analyse binary fission in heavy-ion reactions [3]. It assumes symmetrical fission and a fixed relative FF-velocity. With the exception of the data at the lower and upper limits, the results are close to the dotted line of ideal agreement (Fig.1). This indicates the quality of the deduced single-particle data.

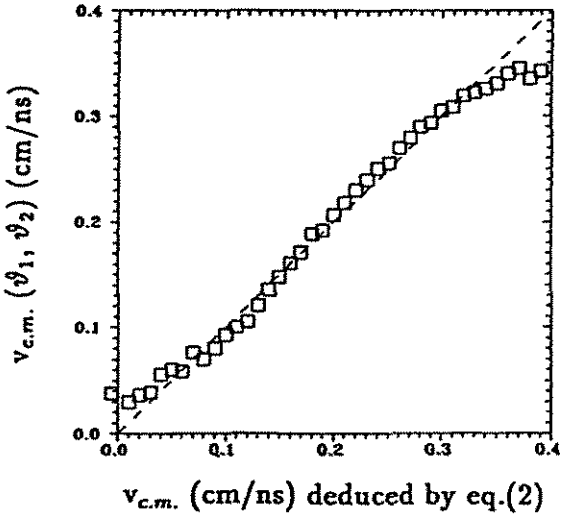

Fig. 1 Longitudinal velocity of the fissioning system $v_{c.m.}$ deduced both from kinematical analysis (x-axis) and from angle correlation (y-axis)

In contrast to the folding angle method, by kinematical analysis the momentum of the fissioning nucleus is calculated as a vector. As shown in Fig.2a, the fission of ^{232}Th bombarded by ^{7}Li originates from composite systems with a broad distribution of the transversal momentum FWHM(P_x)=FWHM(P_y)=700-800 MeV/c, which corresponds to 40% of the amount of the incident projectile momentum. For comparison, FF coincidences from ^{252}Cf have been analysed and resulted in FWHM(P_x)=FWHM(P_y)=200-250 MeV/c (Fig.2b). This value corresponds to 5% of the single-FF momentum and indicates an upper estimate of the experimental resolution.

The ratio between abs($\vec{P}$) and the incident projectile momentum has been used to study the dependence of the single-fragment mass distribution on the momentum transfer (Fig.3a). The observed linear decrease of the mean fragment mass as a function of the increasing momentum transfer results in an absolute decrease of the averaged fragment mass by about 12 amu comparing peripheral and central collisions. By assuming a maximum excitation energy of 290 MeV, the averaged energy taken away per evaporated nucleon is about 12 MeV. The fragment mass was measured with an experimental resolution of

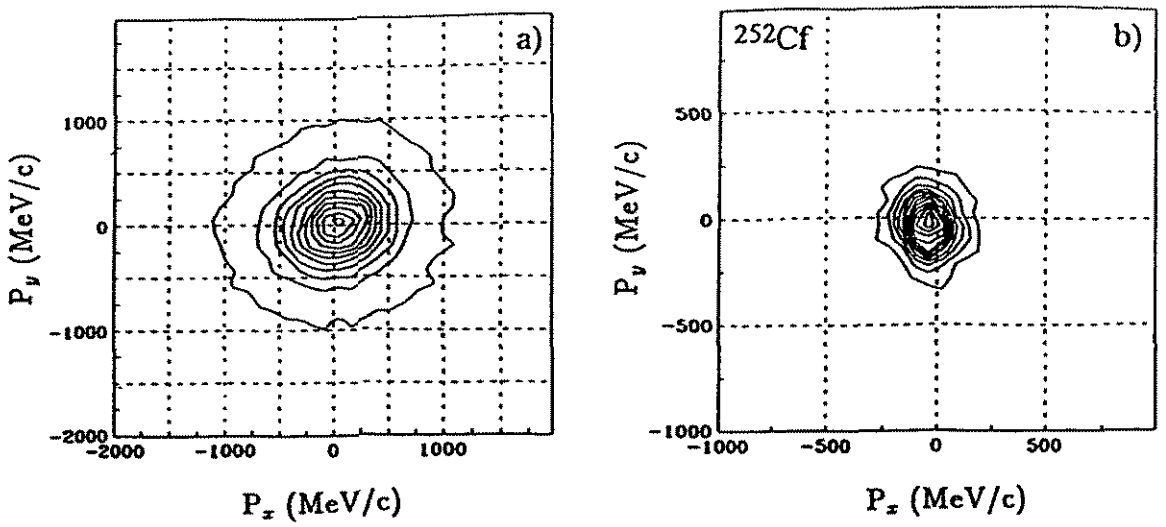

Fig. 2 Transversal components of the total momentum obtained from FF

FWHM(m)=16amu. The increase of the observed distribution width (Fig. 3b) at small momentum transfer is caused by contributions of asymmetric fission at low excitation energy. The minimal FWHM(m)=35amu is obtained at about 50% momentum transfer and is followed by a monotonous increase up to 50amu at complete fusion.

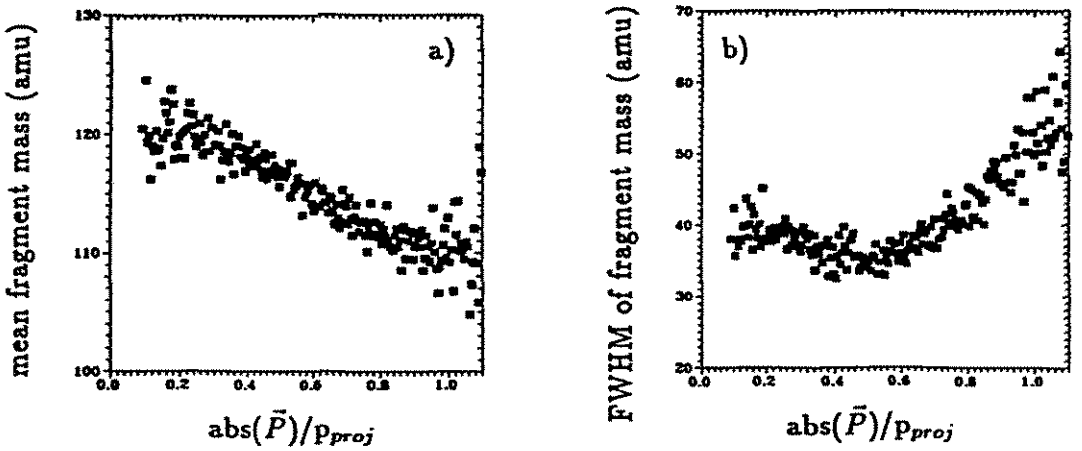

Fig. 3 Single-fragment mass distribution as a function of total momentum transfer

The relative FF-velocity distribution with the mean value of v_{ff}=2.4cm/ns and the FWHM(v_{ff})=0.25cm/ns agrees with the measurement at ^{252}Cm. The mean values increase very slowly at large momentum transfers. Evidently, the increased fragment velocity caused by the decreased fragment mass is superimposed by the reduction of the total kinetic energy by charged particle evaporation.

[1] *Hahn-Meitner-Institut Berlin*

[2] *Joint Institute for Nuclear Research, Dubna* and *Institut für Kern- und Hadronenphysik, FZR*

References

[1] H.-G. Ortlepp et al., Proc. Int. School-Seminar on Heavy Ion Physics, JINR Dubna, Russia, vol.2 (1993) 466

[2] A.A. Aleksandrov et al.,contribution to this report

[3] D. Guerreau; Int. School on Nucl.Phys. "Nuclear Matter and Heavy Ion Collisions", Les Houches, Report Ganil P89-07 (1989)

Correlations Between Intermediate Mass and Fission Fragments in the Reaction ^{7}Li(43 AMeV) on ^{232}Th Studied at FOBOS [B]

A.A. Aleksandrov [1], I.A. Aleksandrova [1], M. Andrassy [2], L. Dietterle [2], V.N. Doronin [1], P. Gippner [2], C.-M. Herbach, D. Hilscher [3], S.I. Ivanovskij [1], A. Matthies [2], D. May [2], H.-G. Ortlepp [2], G. Pausch, Yu.E. Penionzhkevich [1], V.N. Pokrovskij [1], G. Renz [2], K.D. Schilling, D.I. Shishkin [1], O.V. Strekalovskij [1], V.V. Trofimov [1], C. Umlauf [2], D.V. Vakatov [1], V.M. Vasko [1], W. Wagner [2], V.E. Zhuchko [1]

At present several questions concerning fission of hot nuclei [1] such as the influence of dynamics on time scales, the mechanism of dissipation and others are extensively discussed. One goal of the experiments presently being carried out at FOBOS is the further investigation of neck emission of light and intermediate mass fragments (IMF) observed in ref.[2].

A 270 μg/cm^2 thick ^{232}Th target deposited on a 50 μg/cm^2 Al_2O_3 backing was placed in the center of the FOBOS array [3] and bombarded by a ^{7}Li beam from the U-400M cyclotron of the FLNR. Fission fragments (FF) and IMF were recorded by 10 position-sensitive avalanche counters (PSAC) measuring the time-of-flight (TOF) and the emission angle and by 12 axial ionization chambers measuring the energy (E) and the Bragg-peak height (Z). Light charged particles (LCP) were recorded by 10 CsI(Tl) counters. Since the U-400M beam parameters did not allow a precise TOF measurement against the RF-signal of the cyclotron, two transmission avalanche counters placed near the target in direction of the modules 2 and 5 generated the timing reference signals. The geometrical arrangement of the FOBOS modules available at that time has been chosen according to Monte-Carlo simulations of binary and ternary fission after incomplete linear momentum transfer (LMT) (fig. 1).

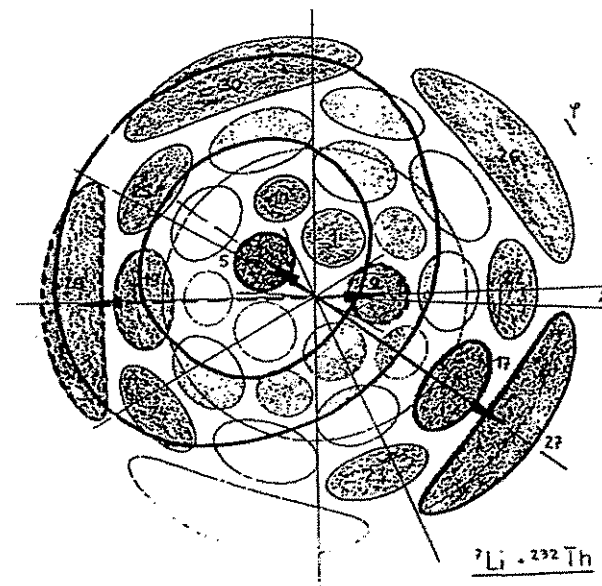

Fig. 1 *The geometrical acceptances of the FOBOS modules in polar coordinates (ϑ,ψ). The modules used are shaded (numbers). The dots are a result of simulation of neck particle emission assuming a mean LMT and considering one FF is recorded in module 5, the coincident FF in modules 17 or 27. Expected IMF are distributed within the ring-like region marked by thick full lines.*

The BIC and PSAC were operated in a gas flow-through regime at pressures of 200 Torr of P-10 gas mixture and 4 Torr pentane, respectively. The PSAC bias set at a value about 5 Volts below the onset of spark discharges guaranteed an efficient registration of fragments from FF down to alpha particles. Altogether 3.1 · 10^6 events with two FF have been recorded. They contain 230 triple (IMF-FF-FF) coincidences. The FF and IMF were selected by windows in the TOF-E and E-Z distributions. As a first result of

this experiment, yields of IMF-accompanied fission related to binary fission have been determined in dependence on the excitation energy (E^*) of the intermediate system and the angle between the fission axis and the direction of IMF emission (ϑ_{IMF-FF}). The 230 triple events allow only a rough division into certain intervals in E^* and ϑ_{IMF-FF}. The geometrical acceptance factors ϵ_{ijk} for all combinations with one FF in module i, a second FF in module j and an IMF in module k have been determined with the help of Monte-Carlo simulations. These simulations deliver mean excitation energies (E^*_{ijk}), which were assumed to be proportional to the LMT, as well as mean angles (ϑ_{ijk}).
With the numbers $N_{IMF(i,j,k)}$ of triple and $N_{FF(i,j)}$ of binary events for a certain combination of FOBOS modules (i,j,k), the measured IMF yield per fission (into the full solid angle 4π) becomes

$$Y_{i,j,k} = N_{IMF(i,j,k)}/(N_{FF(i,j)} \cdot \epsilon_{(ijk)}).$$

These yields have been selected into groups of low LMT ($\Delta p \approx 50\%$; $E^* \approx 150$ MeV) and high LMT ($\Delta p \approx 80\%$; $E^* \approx 230$ MeV). The yields for five mean angles ϑ_{IMF-FF} are shown in fig. 2. The $Y_{i,j,k}$ at low LMT do not show any significant dependence for ϑ_{IMF-FF} between 35° and 90°. The mean value of this IMF component amounts to $(0.7 \pm 0.1) \cdot 10^{-3}$ IMF-accompanied fissions per binary fission. At the higher LMT this value is increased to $(2.3 \pm 0.3) \cdot 10^{-3}$. The enhanced yield near $\vartheta_{IMF-FF} \approx 90°$ for higher E^* confirms the existence of a further IMF source, the strength of which increases with E^*, too. Possibly, these IMF were emitted from the neck region of the fissioning system at scission as has been claimed in ref. [2].

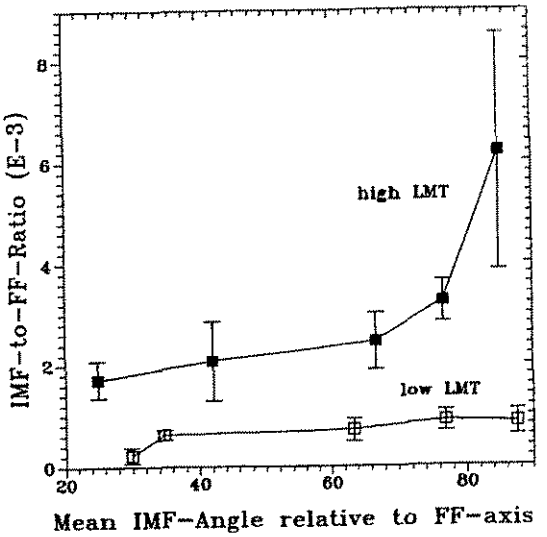

Fig. 2 *Yields $Y_{i,j,k}$ for certain mean IMF-angles ϑ_{ijk} according to low (open squares) and high (full squares) E^*_{ijk}.*

If we consider an interval $\Delta\vartheta_{IMF-FF} = 10°$ around $\vartheta_{IMF-FF} = 90°$ (fig. 2) a rough estimate of the probability for neck emission of IMF results in a value of several units times 10^{-4} per binary fission. It is higher by about one order of magnitude than in the case of low energy (spontaneous or thermal neutron induced) ternary fission [4].

[1] *Joint Institute for Nuclear Research, Dubna, Russia*
[2] *Institut für Kern- und Hadronenphysik, FZR und Joint Institute for Nuclear Research, Dubna*
[3] *Hahn-Meitner-Institut Berlin, Germany*

References

[1] D. Hilscher and H. Rossner, Ann. Phys. Fr. **17** (1992) 471
[2] D.E. Fields et al., Phys. Rev. Lett. **96** (1992) 3713
[3] H.-G. Ortlepp et al., Proc. Int. School-Seminar on Heavy Ion Physics, JINR Dubna, Russia, vol.2 (1993) 466
[4] J.P. Theobald et al., Nucl. Phys. **A502** (1989) 343c

Study of Fission and IMF Emission in the Reaction ^{14}N (34 AMeV) on ^{197}Au at FOBOS [B]

A.A. Aleksandrov [1], I.A. Aleksandrova [1], L. Dietterle [2], V.N. Doronin [1], S. Dshemuchadse, P. Gippner [2], C.-M. Herbach, S.I. Ivanovskij [1], D.V. Kamanin [1] ,A. Matthies [2], D. May [2], H.-G. Ortlepp [2], G. Pausch, Yu.E. Penionzhkevich [1], G. Renz [2], K.D. Schilling, D.I. Shishkin [1], O.V. Strekalovskij [1], V.V. Trofimov [1], C. Umlauf [2], D.V. Vakatov [1], V.M. Vasko [1], W. Wagner [2], V.E. Zhuchko [1], I.P. Zurin [1]

After the ^{7}Li + ^{232}Th experiment [1] the investigation of binary and ternary decay of heavy nuclei with excitation energies up to E* $\approx$ 300 MeV at FOBOS [2] has been continued using another reaction. A 500 μg/cm^2 thick gold foil has been bombarded by a ^{14}N beam of 34 AMeV delivered by the U-400M cyclotron of the FLNR. A second run at 55 AMeV is planned for 1995.

16 gas-filled modules of the FOBOS array were used. 80 CsI(Tl) detectors of the FOBOS scintillator shell [3] were operated in a slave mode with respect to the gas modules to detect light charged particles (LCP) and penetrating light fragments. Two small transmission avalanche counters near the target supplied timing reference signals for the TOF measurement [1]. One of them was fixed at ϑ=37° whereas the second one was positioned at ϑ=101° relative to the beam axis to trigger on backward emitted fragments. The ionization chambers (BIC) were operated with on-line mixed Ar + CH_4 gas at a pressure of 250 Torr, the avalanche counters (PSAC) at 4 Torr of pentane. Apart from the time-of-flight (TOF), direction (ϑ, ψ), energy (E) and Bragg-peak height (Z), the PSAC pulse-height (ΔE) of the fragments was additionally measured.

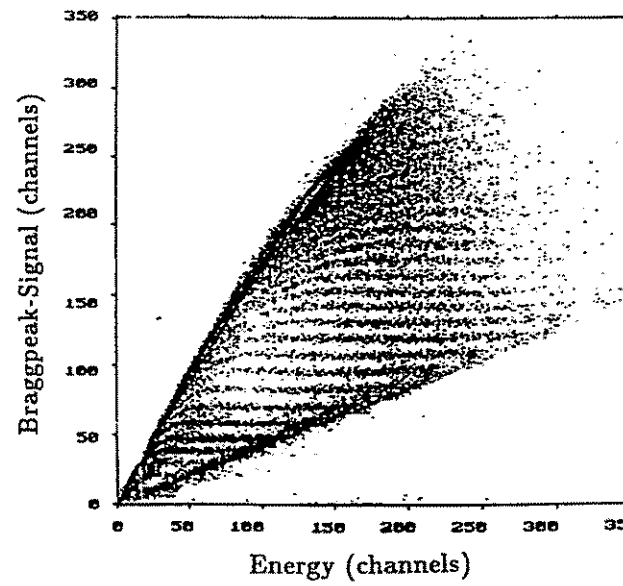

Fig.1 *Bragg-peak height vs. energy plot of particles recorded by a BIC at 37°. Z-branches from 2 to 25 are resolved. The transition to unresolved FF is smooth.*

Using the ΔE- and TOF-information it was possible to roughly identify slow particles which did not enter the BIC. About 2.5 · 10^6 events with two and 2 · 10^3 events with three fragments hitting the gas modules have been recorded. A first estimate of the ratio of triple (FF+FF+IMF) to binary (FF+FF) decays yields $\approx$ 2.5 · 10^{-3} for events with 80% momentum transfer. This value is comparable with the value obtained for ^{7}Li + ^{232}Th [1] . The larger statistics in this experiment, however, should allow a more detailed analysis. The CsI(Tl) detectors recorded one additional LCP in $\approx$ 50% of the events. A first scan of the data shows some interesting features to be analyzed in detail:

(i) There is a smooth transition from symmetric to very asymmetric fission (A_1 /A_2 $\approx$ 10) both in the yield and in the fragment energy (fig.1).

(ii) We observe either a heavy residue or fission fragments (fig.2) in coincidence with a sideward emitted light fragment (IMF).

(iii) Both, in symmetric and asymmetric fission there is a considerable probability of LCP emission in backward direction.

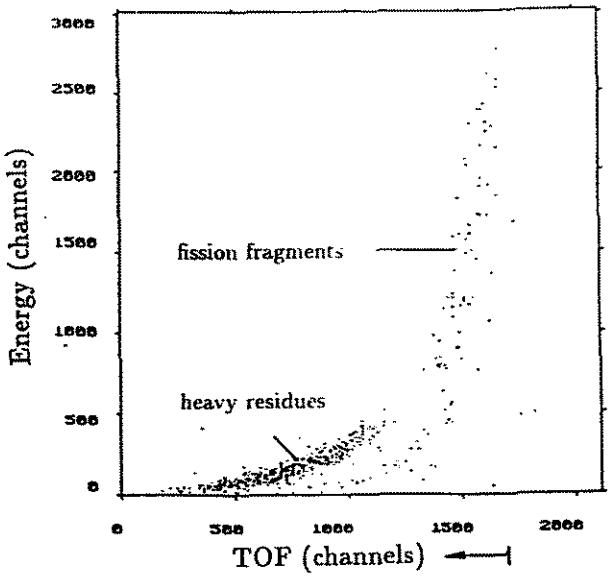

Fig.2 *Energy vs. TOF plot of a module at 37°. Only events in coincidence with IMF at 101° were selected. The two distinct groups can be interpreted as heavy partners of a binary process and fragments of their subsequent fission.*

New information about the competition between binary and ternary decay of hot nuclei with mass numbers A $\approx$ 190 at excitation energies $E^* \approx$ 300 MeV as well as about the probability for survival of a heavy residue is expected after the detailed analysis which is in progress now.

[1] *Joint Institute for Nuclear Research, Dubna, Russia*

[2] *Institut für Kern- und Hadronenphysik, FZR* and *Joint Institute for Nuclear Research, Dubna*

References

[1] A.A. Aleksandrov et al., contribution to this report

[2] H.-G. Ortlepp et al., Proc. Int. School-Seminar on Heavy Ion Physics, JINR Dubna, Russia, vol. 2 (1993) 466

[3] W. Wagner et al., Scient. Report 1991-1992 (Flerov Laboratory of Nuclear Reactions, JINR Dubna) E7-93-57 (1993) 244

Cold Spontaneous Fission of ^{244}Cm Studied at FOBOS [B]

Yu.V. Pyatkov[1], A.A. Aleksandrov[1], I.A. Aleksandrova[1], B.I. Andreev[1], S. Dshemuchadse, P. Gippner[2], C.-M. Herbach, E.M. Kozulin[3], A. Matthies[2], Yu.Ts. Oganessian[3], H.-G. Ortlepp[2], Yu.E.Penionzhkevich[3], G.Renz[2], K.D. Schilling, O.V. Strekalovskij[3], V.M.Vasko[3], W.Wagner[2]

Recent investigations on fission physics [1] provide an abundant material for new approaches to the conception of the mechanism of this process, in particular, of the role of cluster degrees of freedom. One of the promising ways is the investigation of mass and charge spectra of cold fragmentation products. It is well known that the fragment mass distributions of cold compact (CCF) and cold deformed (CDF) fragmentation are characterized by prominent structures [2]. In this work, the mass-energy distribution of ^{244}Cm spontaneous fission (CCF and CDF regions involved) has been measured applying the two-velocities (TOF-TOF) method. The experiment was performed at the FOBOS facility of the FLNR in Dubna. Two groups of 3 position-sensitive avalanche counters (PSAC) respectively were positioned under 180° to determine the velocity vectors (v_L, v_H) of complementary fission fragments and the angle between them.

A small transmission avalanche counter was placed near the ^{244}Cm source to generate a time reference signal. The flight path between the source and the PSAC was $\approx$ 50 cm. The distributions Y(E, M) and Y(TKE, M) have been obtained for 10^5 fission fragment coincidences, where M is the mass of one primary fragment, E is energy and TKE is the total kinetic energy of a complementary fragment pair. The experimental mass resolution for single mass peaks in the region of CCF was $\approx$ 3 amu (fig.1). This value agrees well with respective simulations where the actual thickness of the PSAC windows as well as the geometry of the experiment has been taken into account. A comparison of our data [7] with known characteristics of ^{244}Cm(sf) [3-6] gave satisfactory agreement. Note that a simultaneous measurement of masses and energies of primary fragments has been performed by the authors of ref.[4].

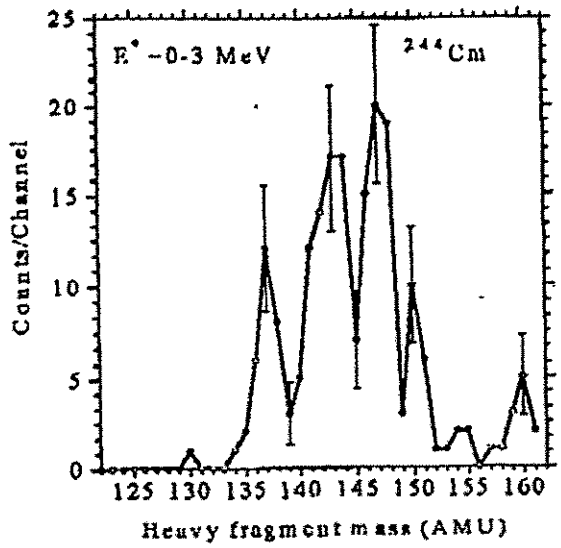

Fig. 1 *Primary fragment mass distribution of ^{244}Cm(sf) for the excitation energy window $E^* = 0$ - 3 MeV.*

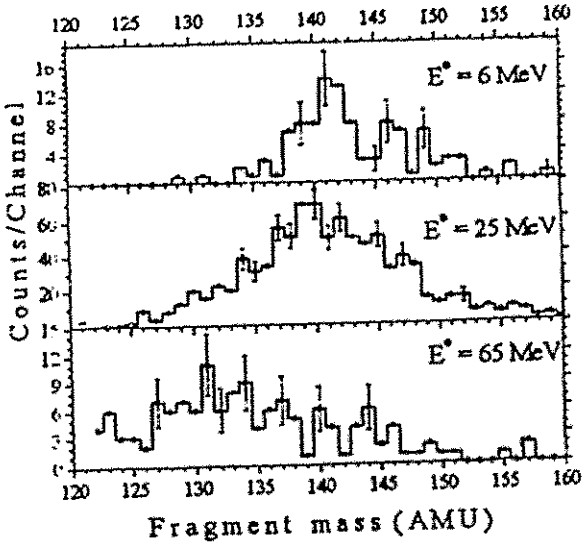

Fig. 2 *Primary fragment mass distribution of ^{244}Cm(sf) for 3 excitation energy windows.*

In order to analyze the dependence of the fine structure of the mass yields on the excitation energy E^* of the fissioning system at scission, the distribution Y(M, E^*) has been built up in intervals of $\Delta E^* = 1$ MeV for the energy range $E^* = 0$ - 80 MeV. Remember that $E^* = Q$ - TKE, where Q is the mean energy of the reaction for a fragment pair with mass numbers A_L and A_H.

For illustration, three cuts Y (M, E^*) at low, medium and high E^* are presented in fig. 2. It is seen that in the region of CCF usually connected with a compact prescission configuration the yields in the neighborhood of the double magic fragment $A_H = 132$ are highly suppressed. This fact was already mentioned in ref. [6]. Vice versa, masses around $A_H = 132$ prevail in the yields at high E^*. The fine structures substantially smoothed at mean values of E^* appear, if TKE decreases (E^* increases) what is usually ascribed to the manifestation of CDF. The pronounced peak at $A_H \approx 132$ - 134 is seen in a rather large range of E^* in the CDF region of ^{244}Cm(sf).

It has been found that the shift of the most probable mass $M_{Y_{max}}$ of the light fission fragment with E^* can be described as

$$E^* \sim M_{Y_{max}} - 95amu.$$

Summarizing the following experimental facts have been established:

(i) In ^{244}Cm(sf), the maximum yield of heavy fragments in the region of CCF appears at $A_H = 140$ - 148; masses around $A_H = 132$ (spherical shell) dominate the CDF region.

(ii) Inversely, in thermal neutron induced fission of ^{245}Cm (compound nucleus ^{246}Cm), the mass distribution peaks near $A_H = 132$ for CCF and near $A_H = 140$ for CDF.

(iii) In ^{244}Cm(sf), the most probable mass of the light fragment depends linearly on the excitation energy at scission.

It seems that all the mentioned properties can be interpreted in the framework of the cluster concept of the multi-valley fission model suggested in refs.[8, 9]. It should be stressed that the peculiarities discussed in the present paper are not specific for ^{244}Cm. Analogous phenomena have been observed in ^{252}Cf(sf) and ^{249}Cf(n_th, f) [10].

[1] *Moscow Engineering Physics Institute, Moscow, Russia*

[2] *Institut für Kern- und Hadronenphysik, FZR* and *Joint Institute for Nuclear Research, Dubna*

[3] *Joint Institute for Nuclear Research, Dubna, Russia*

References

[1] Proc. 2nd Int. Conf. on Dynamical Aspects of Nuclear Fission, Smolenice (1993)

[2] I. Kaufmann et al., Z. Phys. **A341** (1992) 319

[3] R. Schmidt and H. Henschel, Nucl. Phys. **A395** (1983) 15

[4] Yu.A. Barashkov et al., Sov. J. of Nucl. Phys. **13** (1971) 668

[5] I.S. Alkhasov et al., Sov. J. of Nucl. Phys. **11** (1970) 281

[6] F. Caitucoli et al., Nucl. Phys. **A394** (1983) 360

[7] Yu.V. Pyatkov et al., Proc. Workshop on Nuclear Fission and Fission-Product Spectroscopy, Château de la Baume, Seyssins France (1994)

[8] Yu.V. Pyatkov et al., Proc. Int. Conf. on Nuclear Structure and Nuclear Reactions at Low and Intermediate Energies, Dubna (1992) 347

[9] Yu.V. Pyatkov et al., Proc. Int. School-Seminar on Heavy Ion Physics, JINR Dubna, Russia, vol.1 (1993) 358

[10] Yu.V. Pyatkov et al., JINR Rapid Communications **N2** [59] (1993) 98

Test Measurements Performed With a Bragg Ionization Chamber [B]

M.-GEBHARDT[1], V.N. DORONIN[2], P. GIPPNER[3], H.-G. ORTLEPP[3], G. RENZ[3], D.I. SHISHKIN[2], W. WAGNER[3]

An ionization chamber with the electric field parallel to the particle trajectory, well known as a Bragg ionization chamber (BIC), is presented. Bragg curve spectroscopy (BCS) was first proposed by Gruhn et al. [1]. It is a well established method for nuclear charge identification of heavy- ion reactions products. The BIC allows to determine the nuclear charge and the energy of low-energetic heavy ions (E /A $\approx$ 0.8 + 2.8 AMeV).
In contrast to the usual technique of pulse shaping by a long and a short time constant, the real-time digital processing of the BIC was used. The basic idea of this method and the principle is described in ref. [2]. The results obtained in this work are useful for the operation of the detector modules of the 4π - spectrometer FOBOS built-up at the cyclotron facility U-400M [3] of the JINR Dubna for the study of medium- energy heavy-ion reactions.
First tests have been performed by use of a treefold alpha-particle source (^{238}Pu, ^{239}Pu and ^{244}Cm). All measurements were carried out at a BIC without the entrance window foil. Therefore it was not necessary to correct for energy straggling. The BIC consists of a cathode (K), a Frisch-grid (FG) and an anode (A). The distance between K and FG (FG and A) amounted to 24.8 cm (1 cm). Fig. 1 illustrates the principle of the drift time measurement.

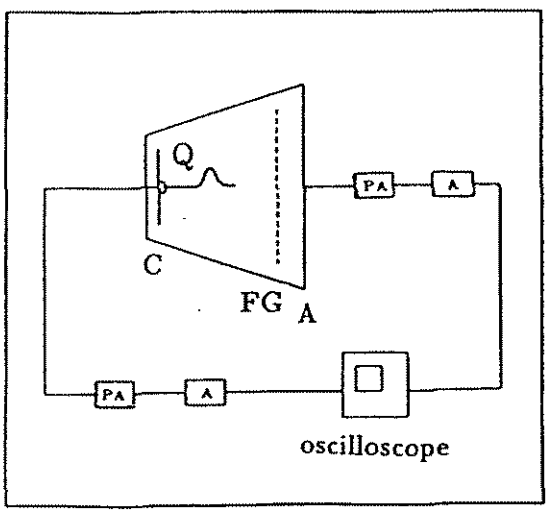

Fig. 1 *Principle of drift-time measurement*

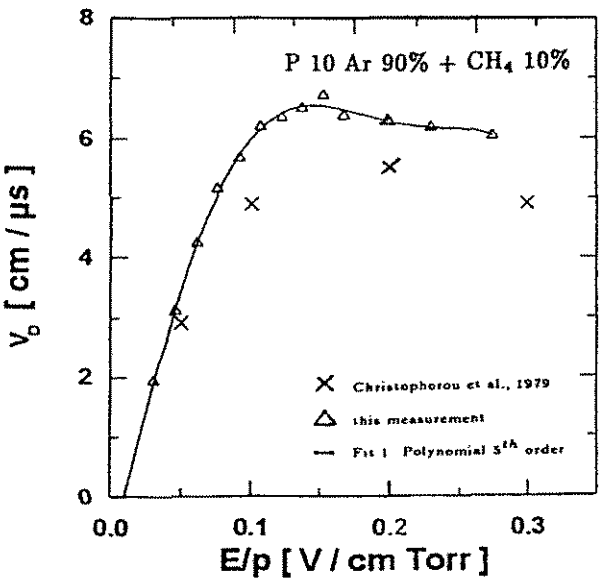

Fig. 2 *Drift velocity (v_D) measurement for a gas mixture P10*

The BIC is usually operated in a flow-though regime with P10 gas (90% Ar + 10% CH_4) at a pressure of $\approx$ 200 Torr. In the first run, we realized a stationary regime using gas from a storage bottle because at that time the device for on-line gas mixing was not yet ready. This resulted in a gas mixture P5 what has been estimated from a drift time measurement. Furthermore, we analysed the gas with the help of a mass spectrometer.

The drift velocity v_D was measured for different gas mixtures. Fig. 2 shows the v_D-measurement for P10 at a pressure of 200 Torr. The goal was to analyse the behavior of the BIC energy signal over a measuring period of 5 weeks. A decrease of the pulse height was expected as resulting from the gas residues originating from the BIC meterials and from the leakage rate.
Fig. 3 shows the decrease of the magnitude as a function of time. The decrease was about 1.25 % within a time intervall of 18 hours.
Furthermore, we analysed the change of the BIC signal due to adding of a defined amount of air to the chamber gas. These experiments have been done using alpha particles from a ^{239}Pu source. The chamber gas was P10 and we estimated the concentration of air with a mass spectrometer.
After adding of 1 Torr of air to the actual gas pressure, the energy signal decreased by 0.68%. Fig. 4 shows the measured energy spectrum.

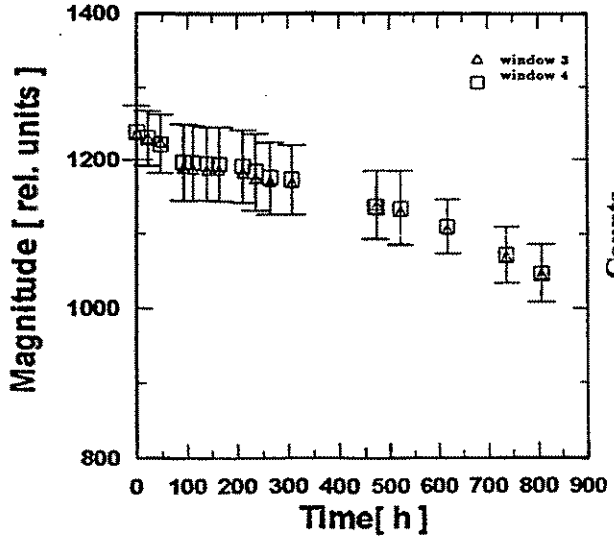

Fig. 3 *Decrease of the magnitude of the energy signal as a function of time*

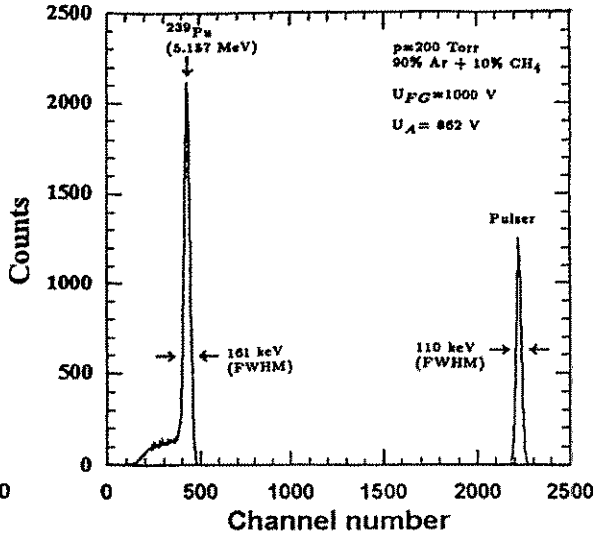

Fig. 4 *Energy spectrum of alpha particles from* ^{239}Pu

[1] *Johann Wolfgang Goethe Universität, Frankfurt, Germany*

[2] *Joint Institute for Nuclear Research, Dubna, Russia*

[3] *Institut für Kern- und Hadronenphysik, FZR* and *Joint Institute for Nuclear Research, Dubna*

References

[1] C.R. Gruhn et al., Nucl. Instr. and Meth. **A196** (1982) 33

[2] H.-G. Ortlepp and A. Romaguera, Nucl. Instr. and Meth. **A276** (1989) 500

[3] H.-G. Ortlepp et al., Proc. 5th Int. Conf. on Nucleus - Nucleus Collisions, Taormina, Italy (1994) (to be published in Nucl. Phys. A)

Usage of ARGUS as an Event Class Separator for IMF-Detection [B]

J. KRÜGER, H. FUCHS[1], D. KAMANIN[1], G. PAUSCH AND COLLABORATION OF FOBOS

The investigation of IMF production mechanisms [1] in the reaction $^{32}S(960\ MeV) + ^{197}Au$ has been continued with a comparison between experimental data and model predictions [2] about production cross-sections of projektilelike fragments Z=2, 4, 6 for different bins in momentum transfer, which was determined by a folding angle analysis.
For Z=4 and Z=6 a good agreement was found, whereas for Z=2 the experimental yields are higher. This is due to sequential decay of the projektile spectators, which had not been taken into account.
Protons and alpha particles play a different role in the process of direct projectile breakup [3]. This is underlined by the angular distributions for different momentum transfers (fig. 1). For small angles to the beam axis ($\vartheta < 35°$), high proton multiplicities indicate high momentum transfer, whereas high alpha multiplicities indicate medium momentum transfer. We conclude that the origin of protons is more connected with evaporation processes from the targetlike system and (due to the alpha-cluster structure of the sulfur projectile) alphas originate from direct projectile breakup processes.

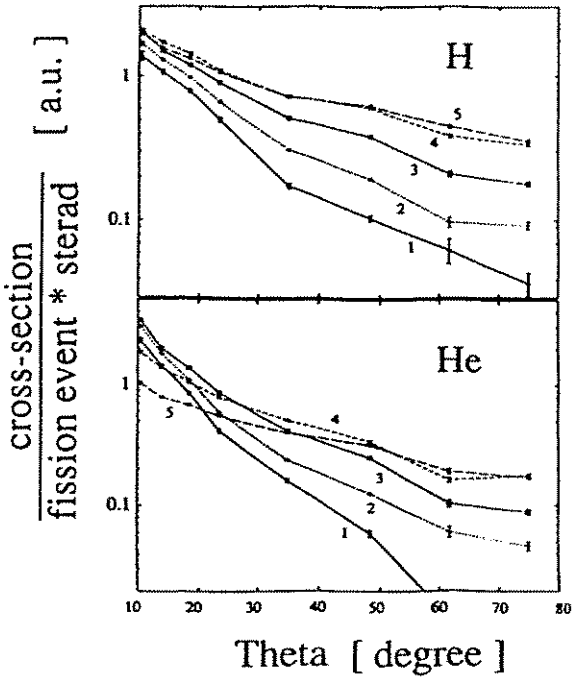

Fig. 1 *Angular distributions of H- and He-fragments for different bins in the momentum transfer, characterized by the velocity of the fissioning system v.*
1: 0 cm/ns < v ≤ 0.2 cm/ns
2: 0.2 cm/ns < v ≤ 0.4 cm/ns
3: 0.4 cm/ns < v ≤ 0.6 cm/ns
4: 0.6 cm/ns < v ≤ 0.8 cm/ns
5: 0.8 cm/ns < v

Total multiplicities for protons and alphas have been determined by two different methods:
a. parametrization and integration of the angular distributions
b. from the yields at ϑ=75°
Method b. can be used, because the yield at this angle for isotropic evaporation (velocity v_e) from a moving source (velocity v_s) is only weakly dependent on the ratio v_e/v_s, if only $v_e > v_s$ is valid. The results are shown in fig. 2.

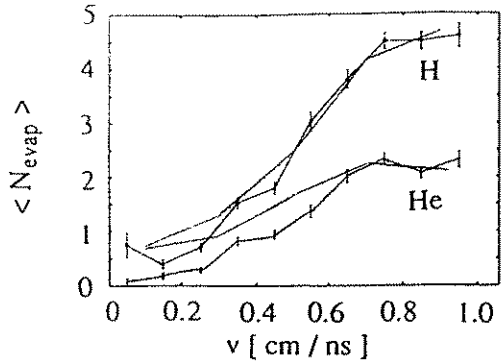

Fig. 2 *Average total multiplicities for evaporation from the targetlike system. The curves without errorbars were derived by method (a), the curves with errorbars by method (b).*

From the folding angle analysis of the fission fragments we determined three criteria for low (I), medium (II) and high (III) momentum transfer: (ϵ-fraction of total events)

I. energy sum > 700 MeV and H-multiplicity = 0 and He-multiplicity=0, ϵ = 1.62%

II. 200 MeV < energy sum < 500 MeV and He-multiplicity $\geq$ 4, ϵ = 0.61%

III. 40 MeV < energy sum < 50 MeV and H-multiplicity $\geq$ 3, ϵ = 0.37%

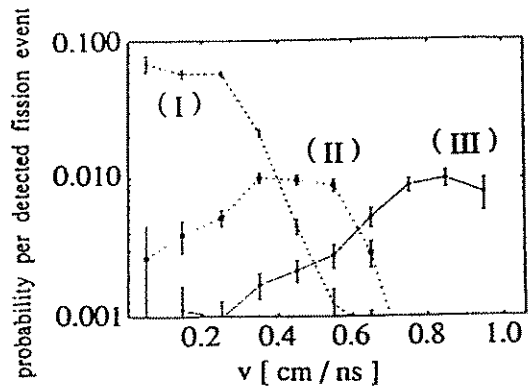

Fig. 3 *Velocity spectra of fissioning systems, selected by the given criteria (see text)*

For the computation of the energy sum all particles Z=1...16 with higher energy than in the "punch-through"-point of the phoswich detector (which belongs to the respective stopping energy in 500 microns pilot-U plastic material) were taken. These filter conditions allow the determination of the momentum transfer independent of the detection of fission fragments. By sorting the complete analysis data under this criteria, we will be able to obtain angular distributions, production cross sections, mass and velocity spectra of IMFs produced in collisions with different impact parameters and different excitation energies of the emitting source. In the frame of this work, the calibration of the phoswich detectors had been extended. Energy values for all identified particles Z=1...16 and all detectors are available now. A missing momentum analysis is still in progress.

[1] *Hahn-Meitner-Institut Berlin*

References

[1] G. Pausch et al., Annual Report 1992, FZR 93-10 (1993)99
[2] K. Möhring et al., Nucl. Phys. A 533 (1991)333
[3] J. Krüger et al., Annual Report 1993, FZR-35 (1994)61

Velocity Correlations of Intermediate Mass Fragments - a Key to the Space-Time Extent of the Multifragmenting Source in Central Heavy-Ion Collisions[B]

R. KOTTE, B. KÄMPFER[1], J. MÖSNER, W. NEUBERT, D. WOHLFARTH
FOR THE FOPI COLLABORATION

Measurements of intermediate mass fragments (IMFs) produced in central Au + Au reactions have been performed at the SIS at GSI by the FOPI collaboration using the phase I setup of the 4π detector system in the projectile energy range 100-400 A·MeV. The events are preselected by cutting the bins PM3-PM5 [1] of the total measured charged particle multiplicity (corresponding to impact parameters of $b/b_{max} < 0.5$ in sharp-cutoff approximation). Central collisions are selected by an additional cut on high values (bin ERAT5) of the ratio E_{rat} [2] of total transverse and longitudinal energies in the forward c.m. hemisphere ($b/b_{max} < 0.2$).

The data are interpreted within the Coulomb dominated final state interaction model. This model is designed to determine the space-time structure of the multifragmenting source of the reaction products by analysing IMF-IMF velocity correlations [3]. However, the code is also well suited as event generator. Only a few parameters allow the description of the asymptotic momentum distributions by propagation of an initial configuration characterized by (i) the total charge of the source which is assumed to be $Z_s = 2 \cdot Z_{Au}$, (ii) a slope parameter α describing the experimental charge distribution, which is approximated by an exponential function $dN/dZ \sim A_Z \cdot exp(-\alpha Z)$ for IMFs with $Z \geq 3$ from central events, plus two additional up-scale parameters $A_{1,2}$ for Z=1, 2 particles, (iii) a radial collective expansion with linear velocity profile between the center and the surface of the source which gives rise to an averaged flow energy $\langle E/A \rangle_{flow}$, (iv) a temperature parameter T determining the random initial thermal motion with Maxwellian velocity distribution, which is not a free parameter but constrained by energy conservation when the parameters in items (ii) - (iii) are fixed, and finally v) the radius of the source R_s which can be translated into a freeze-out density. R_s is the essential parameter extracted from fits to correlation functions (cf. right panel of Fig. 1).

With the input parameters given in Table 1 the Coulomb trajectory model quite well reproduces for central Au+Au reactions both the single-particle distributions and the two-particle observables [3-5].

One of the main results of the correlation analysis performed for central Au + Au collisions is the observation of rather constant averaged next-neighbour distances of the IMFs within the source at break-up time (cf. right column of Table 1) giving rise to a freeze-out density which does not depend on the projectile energy in the range under consideration.

Table 1: Input parameters of the Coulomb trajectory model.

projectile energy E/A [MeV]	charge distr. steepness α 1	temperature parameter T [MeV]	mean radial flow energy $\langle E/A \rangle_{flow}$ [MeV]	sharp sphere source radius R_s [fm]	next-neighbour IMF distance $\langle d_{IMF} \rangle$ [fm]
100	0.5	15	9	$13.3^{+0.8}_{-0.4}$	8.57 ± 0.3
150	0.7	25	12	$12.0^{+1.0}_{-0.5}$	8.55 ± 0.4
250	0.9	35	25	$11.0^{+1.6}_{-0.8}$	8.62 ± 0.6
400	1.1	55	40	$10.5^{+2.0}_{-1.0}$	8.63 ± 0.8

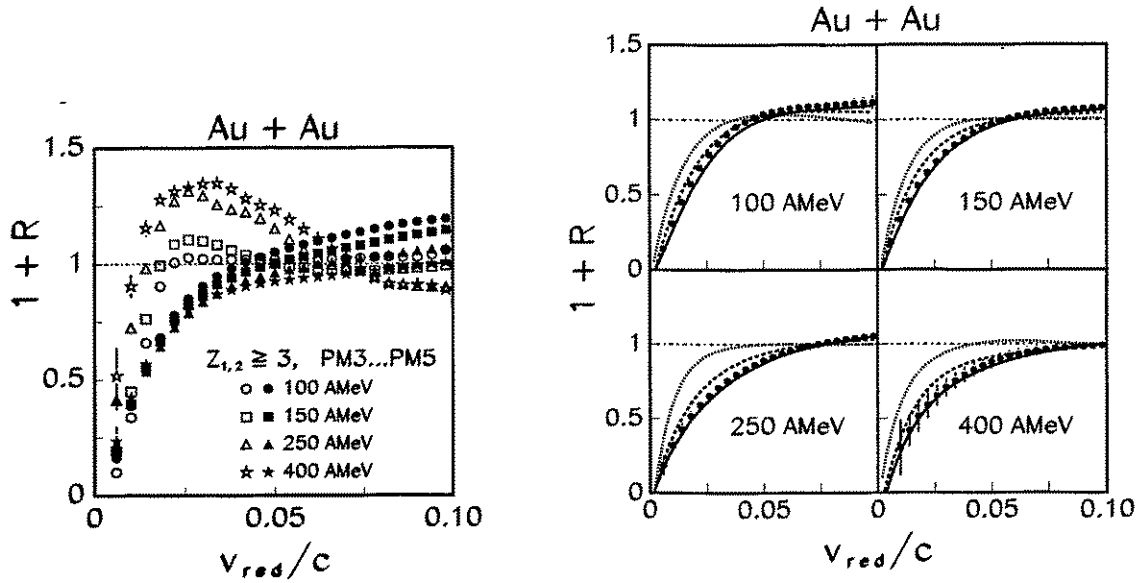

Fig. 1 *Left panel: The experimental relative-velocity correlations of IMFs produced in semi-central collisions (selected by the PM3–PM5 cut) of Au + Au at various beam energies. Open symbols: without event rotation before mixing. Full symbols: with regard of the reaction plane, i.e. rotation into a unique reaction plane before event mixing. Right panel: The experimental relative-velocity correlation function of IMF pairs from central (ERAT5) events of the reaction Au + Au at various beam energies (dots). The events are rotated into a unique reaction plane before mixing. The full, dashed and dotted lines correspond to simulations using the parameters of Table 1, but the radius parameters* $R_s = 10$, *16, and 30 fm, respectively.*

[1] *Institut für Theoretische Physik, TU Dresden und Institut für Kern- und Hadronenphysik, FZR*

References

[1] J.P. Alard et al. (FOPI collaboration), Phys. Rev. Lett. **69** (1992) 889
[2] S.C. Jeong et al. (FOPI collaboration), Phys. Rev. Lett. **72** (1994) 3468
[3] R. Kotte, B. Kämpfer, J. Mösner, W. Neubert, D. Wohlfarth et al., FZ Rossendorf preprint, FZR-56 (1994), to be published in Phys. Rev. C
[4] B. Kämpfer, R. Kotte, J. Mösner, W. Neubert, D. Wohlfarth et al., Phys. Rev. C **48** (1993) R955; Proc. of the XXII Int. Workshop on Gross Properties of Nuclei and Nuclear Excitations, Hirschegg, Austria 1994, p. 113, (ed. H. Feldmeier, GSI Darmstadt)
[5] B. Kämpfer, R. Kotte, J. Mösner, W. Neubert, and D. Wohlfarth, FZ Rossendorf Annual Report 1993, FZR-35 (1994) 63; R. Kotte, B. Kämpfer, J. Mösner, W. Neubert, and D. Wohlfarth, GSI Darmstadt Annual Report 1994, GSI 95-1

Simulation of Relative-Angle Distributions by the Copenhagen Statistical Multifragmentation Model [B]

W. NEUBERT, V. LIPS[1], H. OESCHLER[1], R. KOTTE, J. MÖSNER AND D. WOHLFARTH

Velocity correlations of Intermediate Mass Fragments (IMF) supply information on the space-time structure of the fragmenting source [1]. The complementary relative-angle correlation is a possible way to disentangle both the time and space dependence as demonstrated for coincident IMF pairs produced in the reaction α on Au [2]. The spatial extent of the fragmenting source is related to the freeze-out density. Simulations carried out with the Berlin version of the Statistical Multifragmentation Model (SMM) [3] showed that the relative-angle distribution remains nearly unchanged if the freeze-out density is varied between ρ/ρ_0=0.1 and ρ/ρ_0=0.3. We checked this important conclusion independently by using the Copenhagen SMM [4] which is also based on a spontaneous breakup scenario. The calculations were performed with the 'variable volume' version of this code which allowed to vary the breakup density in the wide range from ρ/ρ_0=0.04 to ρ/ρ_0=0.4. As input to the SMM the mass (A=150) and the charge (Z=62) of the fragmenting system were taken from intranuclear cascade (INC) calculations for the reaction α+Au at 3.6 AGeV. The excitation energy of 5 MeV/u was found under constraint of a proper reproduction of the IMF mass distribution. With that the basic input parameters are compatible with [2] and the relative-angle correlations were calculated for IMF pairs within the mass interval 5< $A_{fragment}$ ≤12. A filter routine which considers both the charge and the energy dependence of the registration efficiency of the involved counters [2] has been applied to the simulated IMF events.Although the results given in Fig. 1 show some dependence on the breakup density the stated weak sensitivity on ρ/ρ_0 [2] may be confirmed. The relative-angle distribution simulated with ρ/ρ_0=0.16 comes close to the experimental data and confirm the findings of ref. [5].

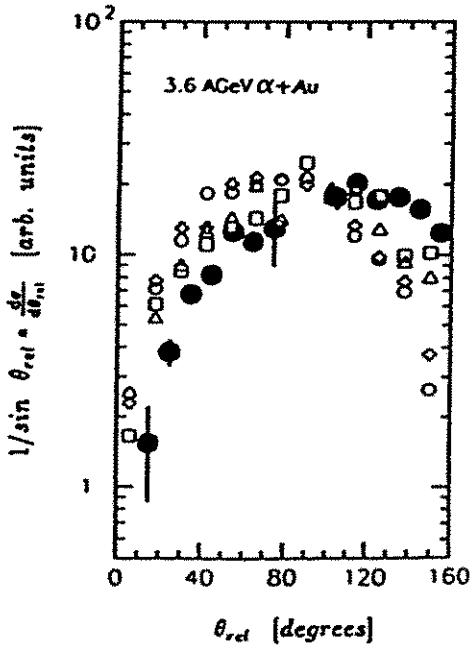

Fig. 1 *Relative-angle distributions simulated for various densities*
●*:experimental data[2],* ○*:*ρ/ρ_0*=0.04,*
✧ *:* ρ/ρ_0*=0.08,* △*:* ρ/ρ_0*=0.16,*
□*:*ρ/ρ_0*=0.4*

[1] *Institut für Kernphysik, Technische Hochschule Darmstadt*

References

[1] B. Kämpfer et al., Phys. Rev. C48 (1993) R955
[2] V. Lips et al., Phys. Letters B338 (1994) 141 and thesis TH Darmstadt (1994)
[3] D.H.E. Gross, Nucl. Phys. A428 (1985) 313c; Rep. Progr. Phys. 53 (1990) 605
[4] J.P. Bondorf et al., Nucl. Phys. A443 (1985) 321; Nucl. Phys. A444 (1985) 460
[5] B. Li, D.H.E. Gross, V. Lips, H. Oeschler, Phys. Letters B335 (1994) 1

Experimental Results from the Reaction Au+Au at 1 GeV/u [B]

J. BIEGANSKY, J. MÖSNER, W. NEUBERT AND D. WOHLFARTH

The FOPI detector system at GSI Darmstadt was used to investigate the reaction Au + Au at a beam energy E_{beam} = 1GeV/u. The goal was the investigation of pion production as well as the continuation of the systematic studies of central event samples performed for lower energies between 100-800 MeV/u [1]. Results are presented with emphasis on the forward plastic wall (plawa) data. This plastic scintillator array covers $1^0 < \vartheta_{lab} < 30^0$ and consists of an outer (512 strips, 1024 phototubes, $\vartheta_{lab} > 7^0$) and an inner part (252 paddles, $\vartheta_{lab} < 7^0$). The mean number of detected charged particles (pmul) increases with the centrality of the event, characterized by the quantity E_{rat} [2] which is defined as the ratio of transversal-to-longitudinal energy. As known from *QMD* model calculations [3] one can assign E_{rat} values > 0.9 to impact parameters b $\leq$ 4fm.

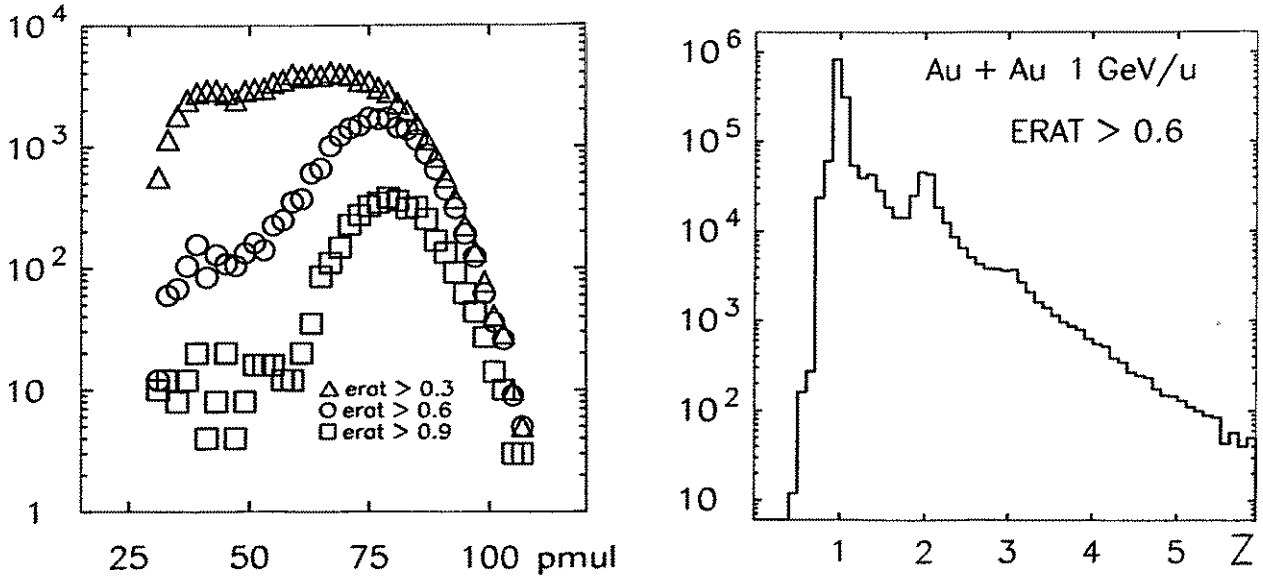

Fig. 1 *Multiplicity and charge distribution as measured with the plastic wall.*

In Fig. 1 lower multiplicities are suppressed if a higher degree of centrality is required according to an enlarged geometrical overlap of the colliding nuclei leading to a bigger number of produced particles.

Particles with charges up to Z=3 can be resolved by fitting the energy loss to time-of-flight correlation plots (ΔE-TOF method). As expected from model calculations [4], mainly light particles are produced at this energy. The identification of charged particles with Z > 3 was impossible because of the low abundance of heavier particles and due to the detector response at this incident energy. Fluctuations in the energy loss signal, secondary reactions and double hits [4] lead to distorted energy loss and velocity informations and therefore spoil the charge resolution.

In order to evaluate the charged particle yield distribution we used a multi-Gaussian decomposition procedure [5] which allows to take different background shapes into account. The charge distribution was fitted assuming an exponential distribution $\frac{dn}{dZ} \sim e^{-\lambda * Z}$ and the slope parameter λ was determined to λ=2.8$\pm$0.2.

Further investigations concerning sideward flow of the system require the determination of the reaction plane in order to quantify effects that are not equally distributed in the azimuth angle ϕ_{lab}. The azimuthal orientation of the reaction plane ϕ_{rplane} offers a relative frame for each event and is derived from the ϕ-asymmetry in the transversal momentum (P_t) distribution [6]. Then P_t can be decomposed into an in-plane fraction (P_x) and an out-of-plane fraction (P_y).

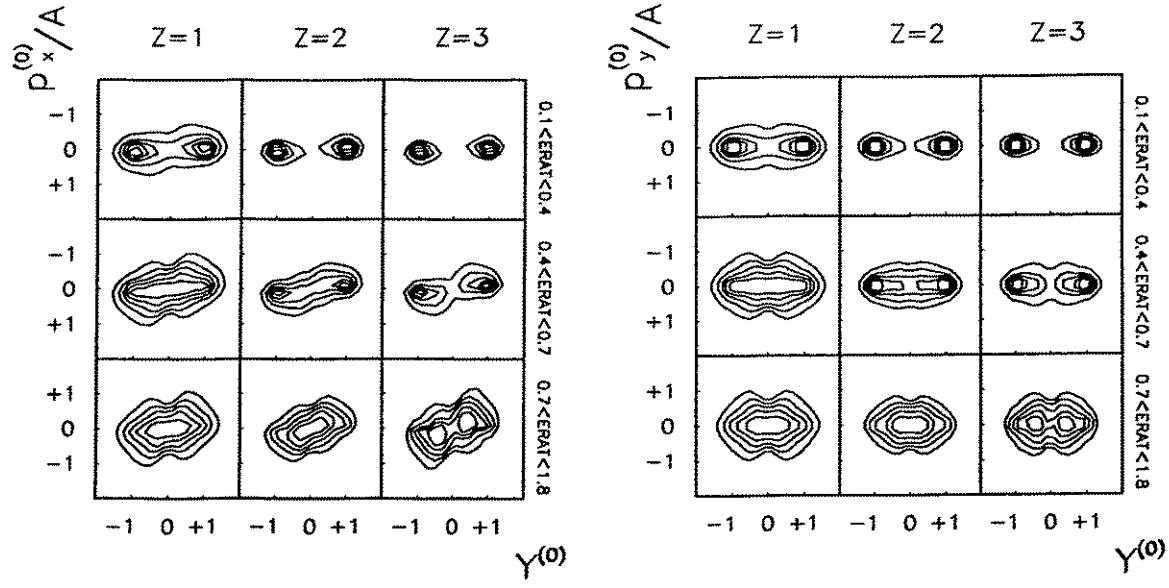

Fig. 2 *Momentum distributions of different particles (columns) and different centrality cuts (rows) as measured with the plastic wall*

Fig. 2 shows two-dimensional plots of the scaled transverse momenta $P_x^{(0)}$ and $P_y{}^{(0)}$ versus rapidity $Y^{(0)}$ for different particle charges and bins of E_{rat} (extended to the backward hemisphere by reflection). The superscript $^{(0)}$ denotes normalization to the projectile momentum per nucleon or to the projectile rapidity in the center-of-mass frame,respectively. With increasing centrality of the collisions both sources are shifted from target rapidity ($Y^{(0)} = -1$) and projectile rapidity ($Y^{(0)}$=+1) to a common source at center-of-mass rapidity $Y^{(0)}$=0 due to the enhanced degree of *stopping*. Furthermore, the in-plane fraction $P_x^{(0)}$ is shifted to larger momenta compared to $P_y^{(0)}$ for an increasing charge and E_{rat} indicating that the apparent flow angle increases with decreasing impact parameter. This behaviour is enhanced for heavier fragments compared to the lighter particles since the contribution from the thermal motion is of minor importance.

References

[1] T. Wienold, Thesis, University of Heidelberg, GSI Report GSI-93-28 (1993)
[2] W. Reisdorf, Proc. Int. Conf. Hirschegg 1992
[3] J. Aichelin, Phys. Rep.**202** (1991)
[4] U.Sodan, Thesis, University of Heidelberg (1994)
[5] G. Winter, ZfK-Report **182** (1969)
[6] P. Danielewicz and G. Odyniec, Phys. Lett. B **110** (1985) 146

Application of the Statistical Multifragmentation Model (Moscow version) to Symmetric Heavy Ion Collisions [B]

W. NEUBERT, A.S. BOTVINA[1], J. BIEGANSKY, R. KOTTE, J. MÖSNER AND D. WOHLFARTH

The efforts to improve the statistical multifragmentation models (SMM) were realized in the development of the 'Moscow code' [1]. This code solves some numerical problems of the original Copenhagen SMM code [2] in case of highly excited large fragmenting systems. This was achieved by changing to the grand canonical treatment if the excitation energy exceeds a critical level. The Moscow code has been proved to give adequate descriptions of intermediate mass fragment production in proton-nucleus [3] and peripheral heavy ion collisions [4].

The following extensions of the hitherto existing code version were necessary to describe the experimental data for the reaction Au on Au obtained with the FOPI detector system (phase I) installed at the SIS/GSI Darmstadt:

1) a collective expansion with a linear velocity profile between the center and the surface of the breakup volume was superimposed on the thermal motion to simulate the considerable amount of radial flow,
2) an acceptance filter routine which considers the geometrical structure and the basic detector properties of the forward plastic wall of the FOPI detector.

This updated code was applied to the experimental data obtained in the energy range from 150 AMeV to 1.0 AGeV with emphasis on this two limiting energies as 'check points'. In order to compare with the model we refer to observables obtained in central event samples. The corresponding selection criteria are desribed in detail in ref. [5]. The calculations were carried out on the assumption that the two colliding Au nuclei overlap completely. This scenario may be justified at 150 AMeV beam energy for which exist well established experimental data [5]. The fragment charge distribution is properly reproduced by assuming a thermal excitation energy of E^*=12 MeV/u (Fig. 1). The slope parameter obtained from an exponential fit $dN/dZ \sim \exp(-\lambda \cdot Z)$ to the calculated Z distribution matches the experimental one (Fig. 2). We remark that the corresponding baryonic entropy amounts to S/A=1.96 which is slightly larger than that obtained in [6] with the phase space code FREESCO. The mean kinetic energies of fragments with $Z \geq 3$ are reproduced by a radial flow component of about 18 MeV/u (Fig. 3) which matches the results of ref. [5]. Moreover, the assumption of complete overlap was applied to simulate observables obtained in central collisions at higher beam energies. The increasing steepness of the Z distributions could be verified up to the largest value $\lambda = 2.8 \pm 0.2$ obtained at 1.0 AGeV [7], (Fig. 2). We found a linear relationship between the slope parameter and the thermal excitation energy (Fig. 4). However, one should be cautious because other observables (e.g. the total charged particle multiplicity) are obviously overestimated at such high excitation energies. A considerable reduction of the system size occurs during the nonequilibrium stage. Preliminary BUU calculations performed for 1.0 AGeV incident energy yield an equilibrated source of ~180 nucleons. If this value is used as input of the SMM the multiplicity is considerably reduced. However, excitation energies of about 55 MeV/u to are necessary reproduce the steepness of the Z distribution. A preliminary analysis of the shapes of the kinetic energy spectra of the registered particles with Z=1,2,3 yield a large amount of radial flow (~100 MeV/u).

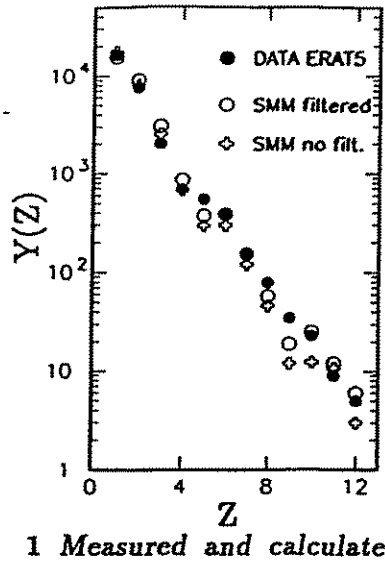

Fig. 1 *Measured and calculated fragment charge distributions for Au+Au at 150 AMeV.*

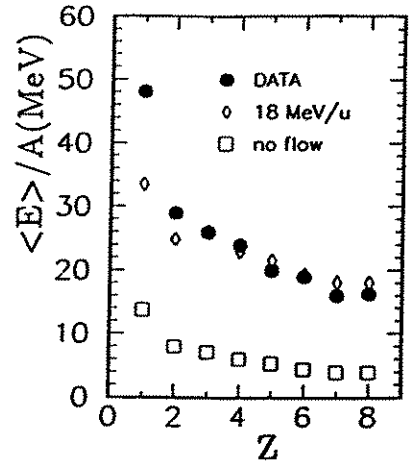

Fig. 3 *Measured and calculated mean kinetic energies per nucleon of fragments produced at 150 AMeV, DATA from ref.[5].*

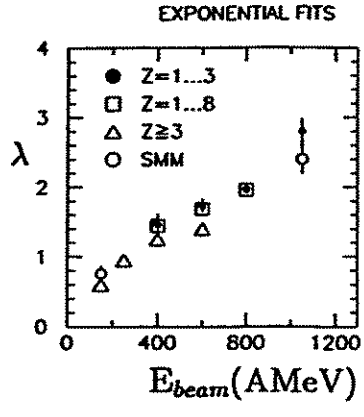

Fig. 2 *Compilation of slope parameters λ describing the Z distribution of fragments from Au+Au. ERAT5 cut (explanation see [5]) for the experimental data, open circles denotes the calculated values.*

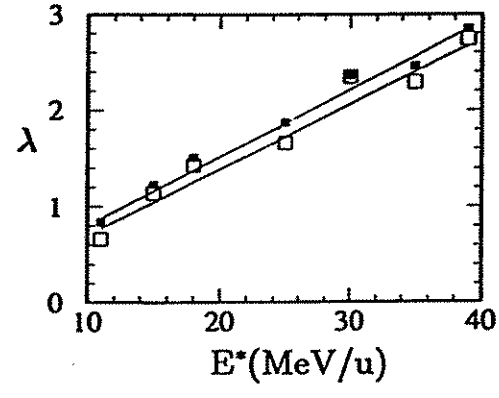

Fig. 4 *Relation between exponential slope parameter of the Z distribution and excitation energy of the system A=394, Z=158. Black squares: no filter, open squares: with acceptance filter, straight lines are weighted averages of linear fits.*

[1] *Hahn-Meitner Institut Berlin GmbH*
(on leave from Institute for Nuclear Research, Moscow, Russia)

References

[1] A.S. Botvina et al., Nucl. Phys. A475 (1987) 663
[2] J.P. Bondorf et al., Nucl. Phys. A443 (1985) 321, Nucl. Phys. A444 (1985) 460
[3] A.S. Botvina, A.S. Iljinov and I.N. Mishustin Nucl. Phys. A507 (1990) 649
[4] M. Begemann-Blaich et al., Proc. XXXII Int. Winter Meeting Bormio 1994, p.107
[5] S.C. Jeong and FOPI coll., Phys. Rev. Letters 72 (1994) 3468
[6] M. Dzelalija et al., submitted to Phys. Rev. C (1995)
[7] J. Biegansky et al., contribution to this report

Production of Intermediate Mass Fragments in 1 GeV Proton-Nucleus Collisions [B,W]

W. NEUBERT, M.N. ANDRONENKO[1] AND A.S. BOTVINA[2]

The cascade-fragmentation-evaporation model was used to simulate the measured fragment charge distributions obtained from Al, Ni, Ag and Au targets [1]. The nonequilibrium stage of the reaction was simulated by an intranuclear cascade code (INC). An ensemble of excited residual nuclei is supplied for a given projectile, incident energy, impact parameter and target. The corresponding data files provide the size and excitation energy of each residual nucleus which is actually decaying, as input of the Moscow version [2] of the Statistical Multifragmentation Model (SMM). In addition, the residual nuclei are allowed to release a part of their excitation energy before they enter into the SMM. Since we analyse data obtained in inclusive measurements we refer to randomly distributed impact parameters. But we found that only that part of events undergo a breakup into several pieces which is generated at impact parameters smaller than $b = 0.3 \cdot R$ ($R = r_0 \cdot A^{1/3}$). Fig. 1 shows the mean values of the calculated excitation energy distributions selected for b=0.3r_0 and randomly distributed impact parameters. Here we compare also calculated and experimental excitation energies which have been evaluated from the momentum transfer determined from the shifts in the kinetic energy spectra measured in forward and backward geometry [1]. The INC underestimates the experimental values, even for the smallest impact parameter. We tried to remove this discrepancy by an alternative choice of the input parameters for the SMM: (i) the mean excitation energy per nucleon was taken from the experiment and (ii) the mean masses come from the INC output.

A comprehensive comparison of experimental and calculated fragment charge distributions is shown in Fig. 2. In all given cases preequilibrium emission prior to multifragmentation was excluded. The cascade-multifragmentation approach allows for Al a nearly perfect reproduction of the experimental charge distribution. We remark that even the pronoun-

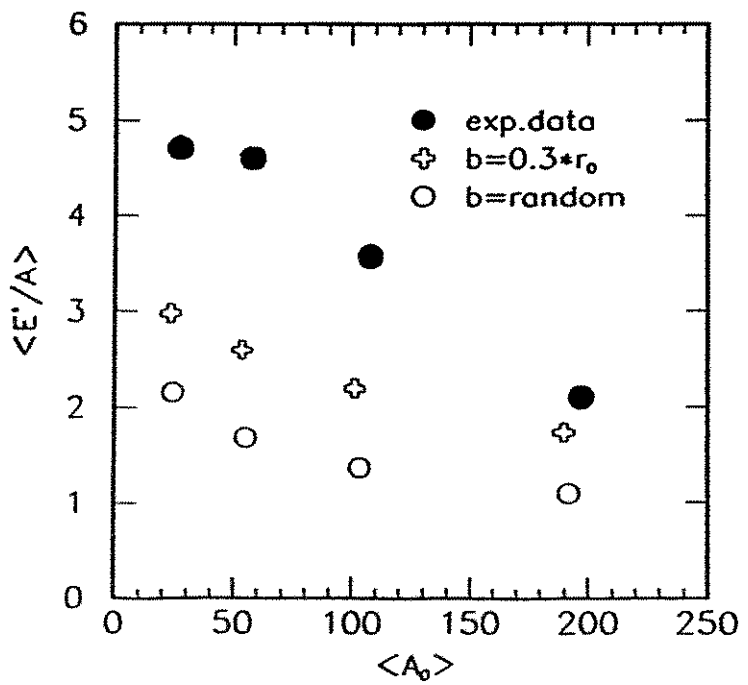

Fig.1 *Mean excitation energies per nucleon for 1 GeV p + Al, Ni, Ag and Au targets. The experimental values are normalized to the target mass.*

ced cluster depletion around Z~5 [3] can be verified. However, we observe a systematic overestimation of clusters with $Z > 10$ for Ni and heavier targets. This effect enhances obviously in the calculations carried out with increased excitation energies. The consideration of preequilibrium emission seems partly to remove this discrepancy as checked for the target nucleus Ag.

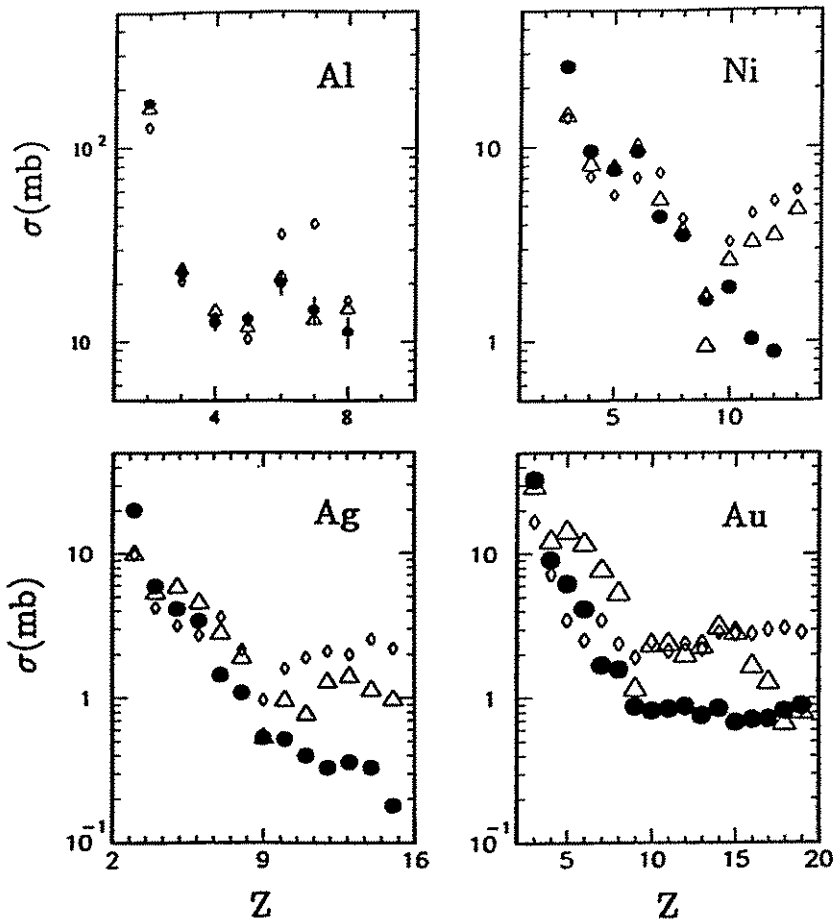

Fig.2 *Charge distributions of Intermediate Mass Fragments for 1 GeV proton collisions with Al, Ni, Ag and Au. The calculated yields are normalized to the sum over the experimental fragment cross sections. Black points: experimental data, triangles: INC (random impact paramters) output tansferred to the SMM, without preequilibrium emission, rhombus: fixed input for the INC (experimental excitation energy, mean masses from the INC).*

[1] *St. Petersburg Nuclear Physics Institute, Gatchina, Russia*

[2] *Hahn-Meitner Institut Berlin GmbH*

(on leave from Institute for Nuclear Research, Moscow, Russia)

References

[1] L.N. Andronenko et al., St. Petersburg Nuclear Physics Institute, report NP-38-1980, Gatchina 1994

[2] A.S. Botvina, A.S. Iljinov and I.N. Mishustin, Nucl. Phys. **A507** (1990) 649

[3] G. Röpke et al., Phys. Rev. **C31** (1985) 1556

Calculation of Isotopic Yield Ratios of Intermediate Mass Fragments and their Relation to the Baryonic Entropy [B,W]

W.Neubert, M.N. Andronenko[1], R. Kotte, J. Mösner and D. Wohlfarth

The possibility of determining the entropy via isotopic yield ratios of clusters with $Z \geq 3$ has been demonstrated in ref. [1]. The greater part of previous analyses has been done by using the Quantum Statistical Model (QSM) [2] which treats the breakup of an infinite nuclear system at thermal equilibrium. Recently it was found [3] that the isotopic yield ratios become insensitive to the baryonic entropy S/A for nuclei with A<60 as far as the QSM is considered. Statistical Multifragmentation Models (SMM) which describe the fragmentation of finite size nuclei overcome this limitation. Here, it is reported on the application of the hybrid model described in the preceding contribution [6]. Within its first stage, i.e. the intranuclear cascade (INC), this model allows for an impact parameter sampling of the observables. The INC code was run for 1 GeV protons as projectile, different targets and several impact parameters. The output file containing the mass distributions and the excitation energies of the 'residual' nuclei formed upon completion of the INC was used as input for the SMM code [4]. The freeze-out density was fixed to $\rho = 0.3\rho_0$. Here we refer to isotopic distributions of He, Li, Be and B produced in collisions of protons with Al, Ni, Ag, Au and U targets. The inclusive experimental data [5] are compared with calculations for randomly distributed impact parameters ($0 \leq b \leq$ target radius). In Fig. 1a, b, c both the experimental and the calculated isotopic yield ratios are plotted in analogy to [1] as function of the neutron-to-proton ratio of the combined system of projectile and target which in the case of protons as projectile reduces to $N_T/(Z_T+1)$ (T refers to the target). The straight line is the mean average of an exponential fit to a compilation of published data (refs. cited in [3]) for incident proton energies from 210 MeV to 350 GeV. The experimental data [3] and the calculated ones (triangles) are in satisfactory agreement. However, there is a tendency to underestimate the yield ratios with increasing target mass. It is supposed that the excitation energies of the fragmenting nuclei prepared by the INC are too low (compare also [6]). Therefore, an alternative input (denoted by (*)) is used for the SMM: (i) the mean values of the mass and charge distributions given by the INC for semicentral collisions (b=0.3 target radius) and (ii) the mean values of the excitation energies were taken from the experiment [5]. This approach (rhombus) improves the yield ratios of the Li and B isotopes but the Be ratios become too large. In this context we remark that the INC delivers in the central collision limit (b=0.1 target radius) residual nucleus distributions as input of the SMM which give no further improvement. The $^{9,10}Be/^{7}Be$ ratios were found to be even 20% lower than for randomly distributed impact parameters. A further improvement between experimental data and calculations may be achieved only by adjusting the parameters of the multifragmentation scenario. The Be ratio depends remarkably on the freeze-out density in the excitation energy domain nearby the multifragmentation threshold as found in calculations for the Ag target. Further calculations are required with regard to heavier target nuclei.

Using the input set denoted by (*) the relation between the isotopic ratios and the baryonic entropies is shown in Fig. 2a, b, c. In the range from Al to U a pronounced correlation between both quantities for all considered fragment species was found. There is a linear relation insofar the isotopes differ by one neutron $\Delta N=1$. The shape of the relation turns to an exponential one if the $\Delta N=2$ ratios $^{9,10}Be/^{7}Be$ are considered.

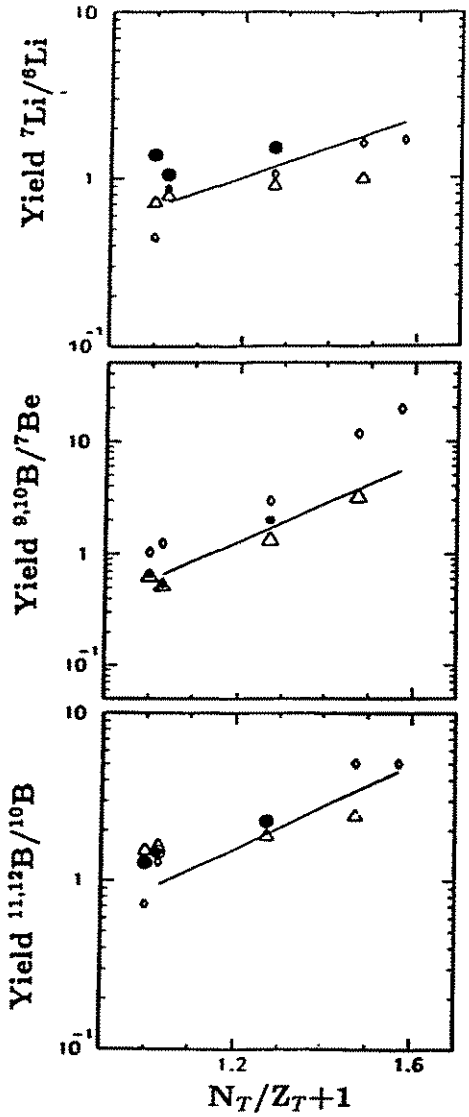

Fig.1 *Isotopic yield ratios of Li, Be and B. Black point- exp. data [3], triangles- calculated, rhombs- calculated with input (*), straight line- fit of compilated exp. data.*

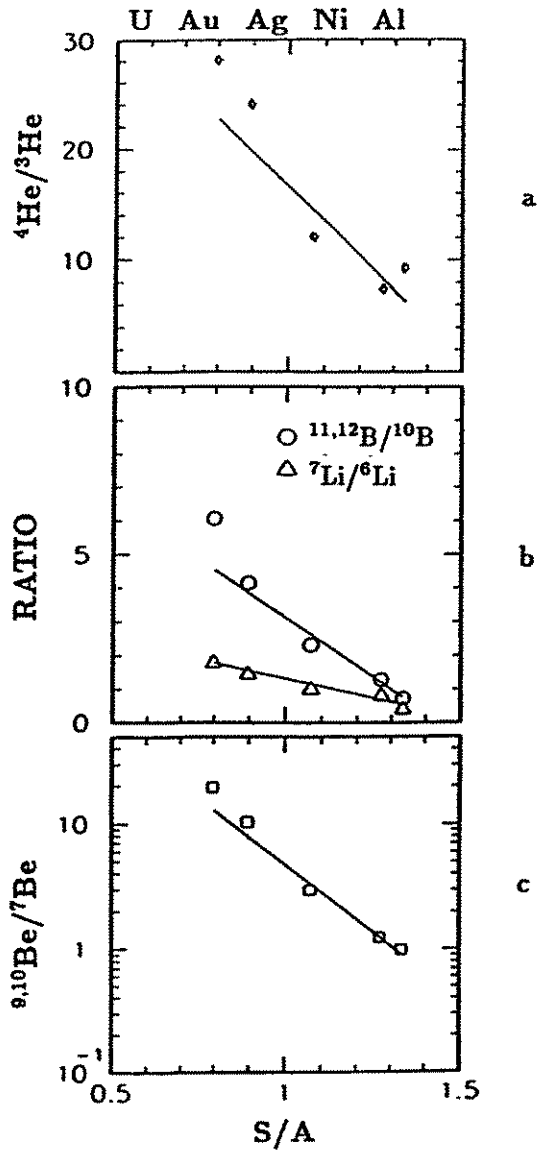

Fig.2 *Correlations of isotopic yield ratios and baryonic entropy, straight lines- reproduction by fits.*

[1] *St. Petersburg Nuclear Physics Institute, Gatchina, Russia*

References

[1] R. Wada et al., Phys. Rev. Letters **58** (1987) 1829
[2] D. Hahn and H. Stöcker, Nucl. Phys. **A476** (1988) 718
[3] L.N. Andronenko et al., Z. Phys. **A350** (1994) 1
[4] A.S. Botvina et al., Nucl. Phys. **A507** (1990) 649
[5] L.N. Andronenko et al., report NP-38-1980, Gatchina 1994
[6] W. Neubert et al., contribution to this report

Entropy Production in the Reaction ^{4}He+Au at 3.6 AGeV [B,G]

W. NEUBERT, H. OESCHLER[1], V. LIPS[1] AND J. KONOPKA[2]

Two statistical models were used to determine the entropy that matches the observables obtained in the reaction ^{4}He+Au at 3.6 AGeV performed at the synchrophasotron of the JINR in Dubna using the FASA setup [1][2]. The method is based on the measured fragment mass distribution and the associated multiplicities of Intermediate Mass Fragments (IMF). Here, we report on the utilization of the Copenhagen Statistical Multifragmentation Model (SMM). An approach like this one requires a definite size of the system which is actually decaying. This was achieved by INC calculations yielding a breakup system consisting out of A_{part}=150 and Z_{part}=62. In the following, these values represent basic input parameters of the SMM. We used in the calculations the 'variable volume version' of the Copenhagen code in which the breakup volume depends on the fragment multiplicity. We investigated the shape of the mass distributions and the associated IMF multiplicity both as a function of the excitation energy and the nuclear density. The range of both input parameters gathers from preceding investigations [2][3]. The interesting physical quantities were calculated for 22 pairs of input parameters which span an irregular grid over the range of relevant excitation energies (from 4.5 MeV/u to 7.0 MeV/u) and freeze-out densities (from $0.06\cdot\rho_0$ to $0.375\cdot\rho_0$). Each grid point delivers mass distributions of fragments which have lost their excess excitation energies by secondary particle emission (calculated by Weisskopf's statistical compound evaporation model).
These mass distributions were fitted by a power law ansatz $dN/dA \sim A^{-\tau}$ in the mass interval from A=10 to A=40 where full detection efficiency is realized. The obtained parameters τ and the associated IMF multiplicities are shown in Figs. 1a and 1b. Then we transformed the isolines which correspond to the experimental values $\tau=2.\pm0.04$ and IMF multiplicity = 5.1 ± 0.8 into the corresponding plot of the associated entropies (Fig. 1c). Both the values of τ and the IMF multiplicity allow to fix the range of entropies within the limits $1.48 \leq S/A \leq 1.6$ for densities between $0.1\rho_0$ and $0.3\rho_0$. Unfortunately, the error bar of the IMF multiplicity (±0.8) is no expedient to restrict the entropy more effectively. Complementary calculations [5] with fixed density were carried out in the framework of the Quantum Statistical Model (QSM). The entropy was found to be $0.7 \leq S/A \leq 1.1$ for densities of $0.1\rho_0$ to $0.3\rho_0$ in reference to the shape of the mass distribution alone. We performed additional calculations with the fixed-volume version of the Copenhagen SMM in order to draw a direct parallel with the QSM results. Fig. 2 summarizes the results in a representation where the IMF multiplicity per participating nucleon is given as function of the baryonic entropy. The shape of both model predictions is similar except an upward shift of about 0.4 units on the S/A scale with respect to the QSM. Besides, QSM predicts for comparable conditions higher IMF multiplicities than the SMM. In Fig. 2 the multiplicity limits for ^{4}He+Au are displayed together with experimental data obtained from a sample of central events in Au on Au collisions [3]. In terms of the QSM, the common ordinate for both reactions is possible because the N/Z ratio of both decaying systems is similar. The striking point is, that in both types of reactions the maximum IMF multiplicity for an equilibrated source is not yet attained. The reaction ^{4}He on Au at slightly higher incident energies seems to be most favourable for the maximum yield of IMFs.

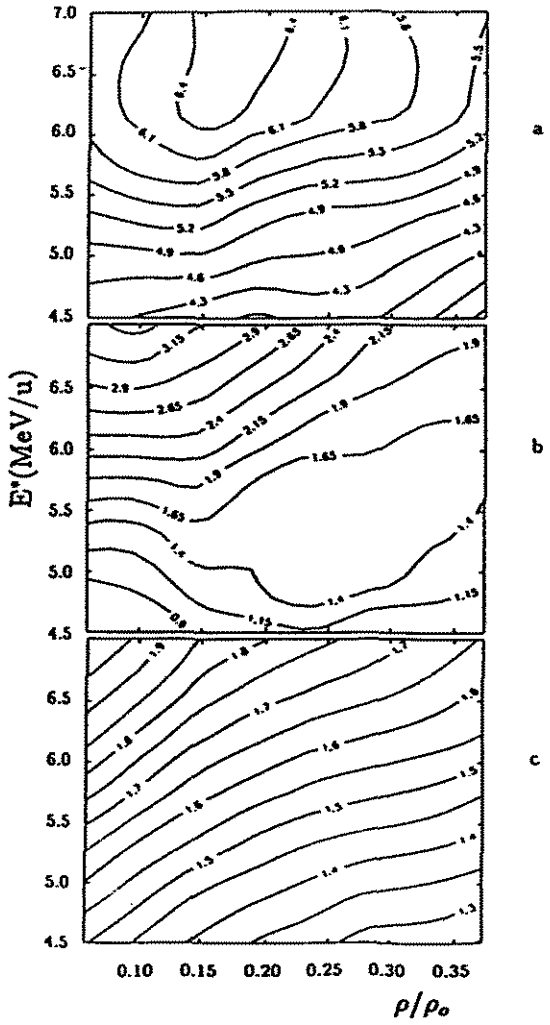

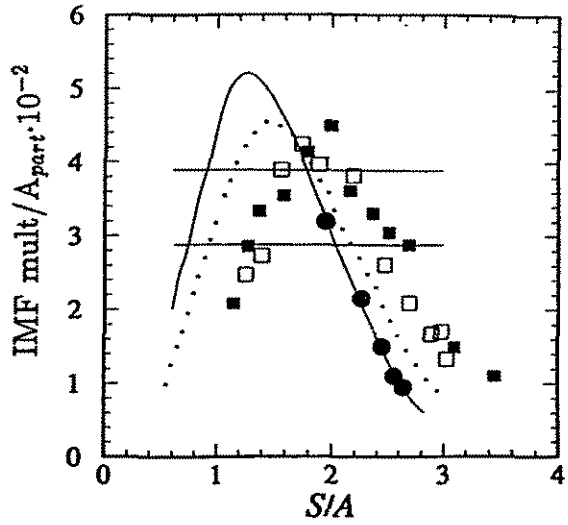

Fig.2 *IMF multiplicity per participating nucleon as function of the baryonic entropy (A_{part}=150). Black squares: Copenhagen code, fixed ρ/ρ_0=0.1, open squares: the same with ρ/ρ_0=0.3. Continues line: QSM, ρ/ρ_0=0.3, dotted line: QSM, ρ/ρ_0=0.1, black dots: Au+Au, 150-800 AMeV [4]. The horizontal bars show the range of the measured IMF multiplicity. Complementary experimental data of the reaction α on Au restrict the valid entropies to the rising part of this plot.*

Fig.1 *Calculated mean IMF multiplicities (a), power law parameters (b) and baryonic entropy (c) as function of the thermal excitation energy and nuclear density of a fragmenting nucleus with A_{part}=150.*

[1] *Institut für Kernphysik, Technische Hochschule Darmstadt*
[2] *Institut für Theoretische Physik, J.W. Goethe-Universität, Frankfurt am Main*

References

[1] S.P. Avdeyev et al., Nucl. Instrum. Methods Phys. Res. **A332** (1993) 194
[2] V. Lips et al., Phys. Rev. Letters **72** (1994) 1604
[3] V. Lips et al., Phys. Letters **B338** (1994) 141
[4] Ch. Kuhn et al., Phys. Rev. **C47** (1993) 2782
[5] J. Konopka et al., to be submitted to Phys. Letters

Isotope Ratios of Light Fragments as Thermometers in Au + Au Collisions at 600 AMeV [B]

T. MÖHLENKAMP, J. POCHODZALLA,[3] A. SCHÜTTAUF,[2] W. SEIDEL, A. WÖRNER,[1] E. ZUDE,[1] FOR THE ALADIN/LAND-COLLABORATION

The temperature determination of highly excited nuclear systems is indispensable for a detailed understanding of the decay mechanism of these systems. For nuclei, a temperature can not be pre-determined but has to be reconstructed from observable quantities. For this purpose an experiment was performed with the ALADIN forward spectrometer system of the GSI facility. The breakup of the kinematicly well separated projectile spectators, formed in Au + Au collisions at 600 AMeV, was investigated. Time-of-flight and charge information of all charged fragments were provided by the TOF-wall. The TP-MUSIC detector [1] equipped with 18 multiwire proportional counters allowed the measurement of the charges, positions and angles of fragments with Z$\geq$2. Combining this tracking information with the time-of-flight measurement the masses of light fragments could be determined with a resolution of about ΔA_{FWHM}=0.3.

For a nuclear system at low density and in chemical and thermal equilibrium a measure of the temperature of the system may be obtained via double ratios of two isotope pairs differing by one neutron each [2]. Following this work we define a temperature $T_{HeLi,0}$ in terms of the yield ratios ^{3}He/^{4}He and ^{6}Li/^{7}Li

$$T_{HeLi,0} := 13.32/ln(2.182 \cdot \frac{Y_{6Li}/Y_{7Li}}{Y_{3He}/Y_{4He}}). \quad (1)$$

In order to test the influence of the Fermi-Dirac statistics and the sequential decay of primary, excited fragments we analyzed calculations with the quantum statistical model [3]. These calculations indicate that $T_{HeLi,0}$ depends almost linearly on the actual temperature T of the system. The ratio $T_{HeLi,0}$/T varies between about 0.95$\pm$0.05 and 0.75$\pm$0.05 for breakup densities between $0.1 \cdot \rho_0$ and $0.5 \cdot \rho_0$. Results of sequential evaporation calculations with the code GEMINI [4] also confirm a nearly linear relation between $T_{HeLi,0}$ and the *initial* temperature of the system $T = \sqrt{k \cdot \langle E_0 \rangle / \langle A_0 \rangle}$, where k denotes the inverse level density parameter. In line with QSM calculations for higher densities the ratio $T_{HeLi,0}/T \approx 0.7$. Finally, also the microcanonical multifragmentation model of Gross and co-workers [5] predicts a rather constant ratio of 0.7$\pm$0.05 between $T_{HeLi,0}$ and the thermodynamic temperature of the system. In order to account pragmatically for the systematic underprediction of the temperature by the quantity $T_{HeLi,0}$, we define the final isotope temperature via $T_{HeLi} = 1.2 \cdot T_{HeLi,0}$. Thus, T_{HeLi} provides - within the models mentioned - a common temperature scale in the evaporation, fragmentation as well as the vapor regime of nuclear systems.

The mass and the excitation energy of the decaying pre-fragments were determined by a total energy balance, suggested by Campi and co-workers [6].

$$E_0 = (\sum_i m_i + \sum_i K_i) - (m_0 + K_0) \quad (2)$$

Here, the sum runs over all fragments within an event where m_i is the fragment mass and K_i its kinetic energy. m_0 and K_0 denote the initial mass and kinetic energy of the pre-fragment. Averaging Eq. 2 over a given event sample determined by a bin in Z_{bound}

and Z_{max} the average kinetic energies of the individual fragment charges were evaluated from the transverse width of the momentum distributions [7].

Figure 1 shows the isotope temperature as a function of the total excitation energy per nucleon. Measured excitation energy - temperature pairs of this caloric curve are shown by the solid points. Data for target residues produced at intermediate energies between E/A=30 and 84 MeV are shown by the open circles. In the latter case, the excitation energies were also deduced from an energy balance [8] and T_{HeLi} was evaluated using the coincident light particle yields associated with emission from the target remnant. Because of the exponentially decreasing production rate of ^{3}He towards low excitation energies and the finite width of the excitation energy distribution temperatures can not be determined for excitation energies below approximately 2 AMeV. The only value for T_{HeLi} in the evaporation regime below 2 AMeV excitation energy is provided by the ^{22}Ne+^{181}Ta fusion reactions at E/A=8.1 MeV [9] (open triangle). The caloric curve shown in Fig. 1 can be divided in three distinctly different portions. The rise of T_{HeLi} for excitation energies below 2 AMeV is compatible with the low-temperature approximation of a fermionic system $T = \sqrt{10 \cdot \langle E_0 \rangle / \langle A_0 \rangle}$, which is representative for the evaporation from a nucleus at normal density (solid line). The isotope temperature stays rather constant at a value of about 5 MeV for excitation energies between 3 and 10 AMeV. For higher excitation energies, again an increasing temperature towards larger excitation energies is found (dashed line), where the slope of 2/3 alludes to a gas of classical, elementary particles. Depending on the low density equation-of-state the freeze-out in this vapor regime occurs between 0.15 and 0.3 of normal nuclear density. The observed caloric curve agrees qualitatively with predictions of the Copenhagen multifragmentation model [10] and resembles the one of the paradigm of a phase transition - the first-order phase transition of bulk H_2O.

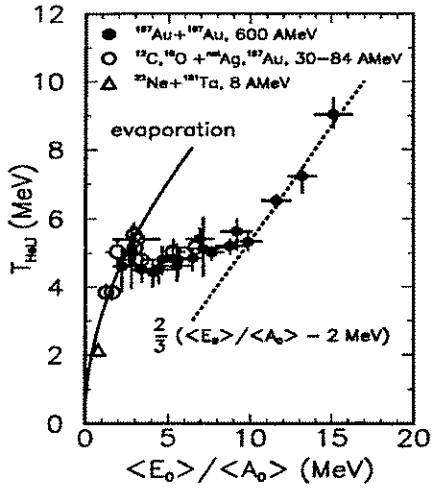

Figure 1: *Isotope temperature T_{HeLi} as a function of the excitation energy per nucleon.*

[1] *Gesellschaft für Schwerionenforschung Darmstadt*

[2] *Institut für Kernphysik, Universität Frankfurt*

[3] *Heisenberg fellow of DFG*

References

[1] T. Möhlenkamp *et al.*, FZ-Rossendorf, IKH, Annual Report 1993 page 97.

[2] S. Albergo *et al.*, Nuovo Cimento A **89**, 1 (1985).

[3] D. Hahn and H. Stöcker, Nucl. Phys. **A476**, 718 (1988).

[4] R.J. Charity *et al.*, Nucl. Phys. **A483**, 371 (1988).

[5] D.H.E. Gross, Prog. Part. Nucl. Phys. **30**, 155 (1993) and references therein.

[6] X. Campi, H. Krivine, and E. Plagnol, Phys. Rev. C **50**, R2680 (1994).

[7] E. Zude *et al.*, PhD thesis (University of Mainz) 1994.

[8] R. Trockel *et al.*, Phys. Rev. C **39**, 729 (1989) and
R. Trockel, PhD thesis (University of Heidelberg) 1988.

[9] C. Borcea *et al.*, Nucl. Phys. **A415**, 169 (1984).

[10] J. Bondorf *et al.*, Nucl. Phys. A **444**, 460 (1985).

Mass Determination Using the ALADIN Spectrometer [B]

T.MÖHLENKAMP, M.BEGEMANN-BLAICH,[1] W.F.J.MÜLLER,[1] TH.RUBEHN,[1]
A.SCHÜTTAUF,[2] W.SEIDEL, A.WÖRNER[1] FOR THE ALADIN-COLLABORATION

In previous experiments with the ALADIN forward spectrometer, charge and tracking information was achieved for fragments with charges of 8 and above [1] from the decay of the projectile spectator. This together with the known magnetic field of the ALADIN magnet allowed the determination of particle momenta. Additionally, the time of flight of the particles was measured with a separate detector device, therefore their masses could be determined.

For the new experimental setup, 18 multiwire proportional counters [2] were added to the anode sections of the TP-MUSIC III detector to extend the mass reconstruction down to very light particles. These proportional counters were sensitive to particles with charges larger than 1. A position resolution in the bending plane of the magnet of 1.7 mm and 0.7 mm FWHM for Z=2 and Z=10 was obtained, the angular resolution was 3.5 and 1.3 mrad, respectively. It turned out that for fragments with charges up to approximately 15, the accuracy of the tracking information and therefore of the momentum resolution was better than that of the anode sections, which had a lower charge threshold of 8 but reached their best tracking resolution only for fragments with charges of 20 and above. Due to a better calibration method, the time resolution of the TOF-wall was improved and varied between 250 and 150 ps FWHM. For 600 AMeV, the mass resolution was therefore 0.3 and 0.6 mass units FWHM for Z=2 and Z=10, respectively, and individual masses could be resolved for fragments up to mass 25, as it is shown in Fig. 1 for the system Au + Au. The mass separation of these light particles opens new possibilities for the investigation of the decay mechanism of excited nuclear matter, p.e. via the isotopic composition of the fragments [3] or via higher order momentum correlations between particles from the decay of spectator matter.

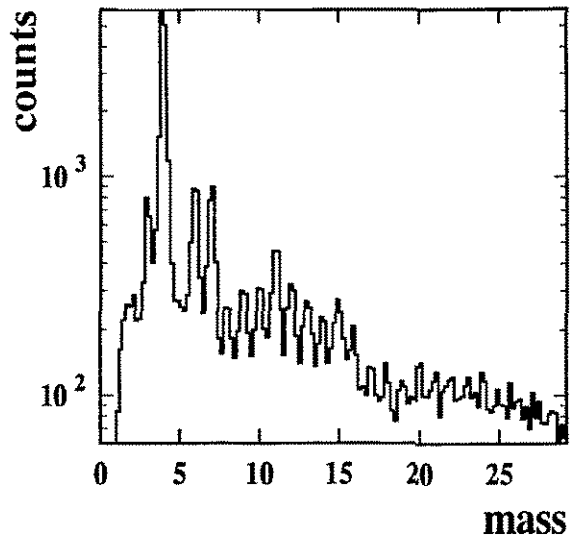

Figure 1: Mass distribution of fragments with $A < 30$ for collisions of Au + Au at 600 MeV/u. The distribution is not corrected for the tracking efficiency.

[1] *Gesellschaft für Schwerionenforschung Darmstadt*
[2] *Institut für Kernphysik, Universität Frankfurt*

References

[1] V.Lindenstruth *et al.*, GSI scientific report 1991 p.362

[2] W.Seidel *et al.*, GSI scientific report 1991 p.359 and Jahresbericht 1991, FZR 92-09, p.298

[3] T.Möhlenkamp *et al.*, contribution to this annual report

Isotopic ratios of intermediate mass fragments produced in p + A reactions at 1 GeV
(Zeitschrift für Physik A350 (1994) 1)

Andronenko, L.N., M.N. Andronenko, A.A. Kotov, W. Neubert, D.M. Seliverstov, I.I. Strakovsky, L.A. Vaishnene

Abstract: Isotopic ratios were measured for Li, Be and B produced in p + Al, p + Ni and p + Ag reactions. The experimental data were analysed in the framework of the Quantum Statistical Model in order to relate the isotopic yield ratios to the baryonic entropy.

The response of a large CsI(Tl) detector to light particles and heavy ions in the intermediate energy range
(Nucl. Instr. Meth. in Phys. Res. A344 (1994) 378)

Fomichev, A.S., I. David, S.M. Lukyanov, Yu.E. Penionzhkevich, N.K. Skobelev, O.B. Tarasov, A. Matthies, H.-G. Ortlepp, W. Wagner, M. Lewitowicz, M.G. Saint-Laurent, J.M. Corre, Z. Dlouhý, I. Pecina, C. Borcea

Abstract: Particle dependent response of a CsI(Tl) scintillation detector with an entrance surface of 314 cm^2 has been investigated using a secondary beam facility at the energy range from 2 to 77 MeV/A. The mass and charge identification of particles with Z = 1-18 has been performed by means of time-of-flight and energy measurements. The dependence of light output on E, Z and A has been studied. Using a pulse shape analysis possibility of identify the masses of momentum separated particles with charges of Z = 1-7 is presented.

Collective expansion in central Au + Au collisions
(Phys. Rev. Lett. 73 (1994) 3367)

Hsi, W.C., G.J. Kunde, J. Pochodzalla, W.G. Lynch, M.B. Tsang, M.L. Begemann-Blaich, D.R. Bowman, R.J. Charity, F. Cosmo, A. Ferrero, C.K. Gelbke, T. Glasmacher, T. Hofmann, G. Imme, I. Iori, J. Hubele, J. Kempter, P. Kreutz, W.D. Kunze, V. Lindenstruth, M.A. Lisa, U. Lynen, M. Mang, A. Moroni, W.F.J. Müller, M. Neumann, B. Ocker, C.A. Ogilvie, G.F. Peaslee, G. Raciti, F. Rosenberger, H. Sann, R. Scardaoni, A. Schüttauf, C. Schwarz, W. Seidel, V. Serfling, L.G. Sobotka, L. Stuttge, S. Tomasevic, W. Trautmann, A. Tucholski, C. Williams, A. Wörner, B. Zwieglinski:

Abstract: Energy spectra for intermediate mass fragments produced in central Au + Au collisions at E / A = 100 MeV indicate a collective expansion at breakup. For the first time, values for this collective expansion energy per nucleon are extracted independently for each charge. Typically, these values are one-third to one-half on the incident kinetic energy per nucleon in the c.m. system, but they decrease with Z_f, suggesting that all fragments do not participate equally in the collective expansion.

Collective motion in selected central collisions of Au on Au at 150 A MeV
(Phys. Rev. Lett. 72 (1994) 3468)

Jeong, S.C., N. Herrmann, Z.G. Fan, R. Freifelder, A. Gobbi, K.D. Hildenbrand, M. Krämer, J. Randrup, W. Reisdorf, D. Schüll, U. Sodan, K. Teh, J.P. Wessels, D. Pelte, M. Trzaska, T. Wienold, J.P. Alard, V. Amouroux, Z. Basrak, N. Bastid, I.M. Belayev, L. Berger, M. Bini, Th. Blaich, S. Boussange, A. Buta, R. Caplar, C. Cerruti, N. Cindro, J.P. Coffin, R. Dona, P. Dupieux, J. Erö, P. Fintz, Z. Fodor, L. Fraysse, S. Frolov, Y. Grigorian, G. Guillaume, S. Hölbling, A. Houari, F. Jundt, J. Kecskemeti, P. Koncz, Y. Korchagin, R. Kotte, C. Kuhn, M. Ibnouzahir, I. Legrand, A. Lebedev, C. Maguire, V. Manko, P. Maurenzig, G. Mgebrishvili, J. Mösner, D. Moisa, G. Montarou, I. Montbel, P. Morel, W. Neubert, A. Olmi, G. Pasquali, M. Petrovic i, G. Poggi, F. Rami, V. Ramillien, A. Sadchikov, Z. Seres, B. Sikora, V. Simion, S. Smolyankin, R. Tezkratt, M.A.Vasiliev, P. Wagner, Z. Wilhelmi, D. Wohlfarth, A.V. Zhilin

Abstract: Using the FOPI-facility complete data of Au on Au collisions at 150 AMeV were collected for charged products (Z = 1 to 15) at laboratory angles $1^\circ \leq \Theta_{lab} \leq 30^\circ$. Central collisions were selected applying various criteria. The kinetic energy spectra of fragments from an isolated midrapidity source are investigated in details for center of mass angles $25^\circ \leq \Theta_{cm} \leq 45^\circ$. The heavy products ($Z \geq 3$) are used to determine the collective energy which is found to be at least 10 AMeV.

Evidence for simultaneous breakup in reactions with relativistic α-projectiles
(Phys. Lett. B338 (1994) 141)

Lips, V., R. Barth, H. Oeschler, S.P. Avdeyev, V.A. Karnaukhov, W.D. Kuznetsov, L.A. Petrov, O.V. Bochkarev, L.V. Chulkov, E.A. Kuzmin, W. Karcz, W. Neubert, E. Norbeck, D.H.E. Gross

Abstract: The relative-angle distributions of IMFs, studied for the system α + ^{197}Au at 3.6 GeV/nucleon, show a strong suppression of small relative angles. By multi-body Coulomb trajectory calculations it is shown that the magnitude of this effect is very sensitive to the time scale of the IMF emission. The experimental angular distributions are well described assuming a fast breakup of the system with times less than 100 fm/c between IMF emissions.

Multifragmentation induced by relavistic alpha-projectiles
(Phys. Rev. Lett. 72 (1994) 1604)

Lips, V., R. Barth, H. Oeschler, S.P. Avdeyev, V.A. Karnaukhov, W.D. Kuznetsov, L.A. Petrov, O.V. Bochkarev, L.V. Chulkov, E.A. Kuzmin, W. Karcz, W. Neubert, E. Norbeck

Abstract: Multifragmentation of the system a + ^{197}Au has been studied at incident energies of 1 and 3.6 GeV/nucleon with the new 4π setup, FASA. Mass, energy, and velocity of a few fragments are measured with high precision using time-of-flight telescopes, while for the other fragments, global multiplicity information is obtained from 55 CsI(Tl) detectors covering the main part of 4π. Very high mean IMF (intermediate mass fragment) multiplici-

ties of $\langle M \rangle_{IMF} = 5.1 \pm 0.8$ are observed at the higher incident energy. Compared to the lower incident energy, they increase by 40 %, indicating an increasing energy deposition with increasing incident energy.

Multifragmentation in peripheral nucleus-nucleus collisions
(Acta Physica Polonica B 25 (1994) 425)

Trautmann, W., J.C. Adloff, M. Begemann-Blaich, P. Bouissou, J. Hubele, G. Imme, I. Iori, P. Kreutz, G.J. Kunde, S. Leray, V. Lindenstruth, Z. Liu, U. Lynen, R.J. Meuer, U. Milkau, A. Moroni, W.F.J. Müller, C. Ngo, C.A. Ogilvie, J. Pochodzalla, G. Raciti, G. Rudolf, H. Sann, A. Schüttauf, W. Seidel, L. Stuttge, A. Tucholski

Abstract: The complete fragmentation of highly excited nuclear systems into fragments of intermediate mass is observed in heavy-ion reactions at relativistic bombarding energies in the range of several hundreds of MeV per nucleon. Similar features are found for peripheral collisions between heavy nuclei and for more central collisions between a heavy and a light nucleus. The partition space explored in multifragment decays is well described by the statistical multifragmentation models. The expansion before breakup is confirmed by the analysis of the measured fragment energies of ternary events in their own rest frame. Collective radial flow is confined to rather small values in these peripheral-type reactions. Many conceptually different models seem to be capable of reproducing the charge correlations measured for the multifragment decays.

5 Technical and Methodic Developments

Activities of the Detector Laboratory

W. Enghardt, M. Freitag, J. Hutsch, G. Pausch, H. Prade, M. Sobiella

The Detector Lab Rossendorf provides experimental groups of the Institute for Nuclear and Hadronic Physics with infrastructure and technical support for development, manufacture and test of detector components to be used in nuclear physics experiments and medical applications. In 1994 the main activities have concerned

- the production of 20 double-grid avalanche counters (DGAC's) for the heavy-ion spectrometer FOBOS in Dubna [1],
- the construction of the gantry for a PET camera to be used for dose localization and beam monitoring in heavy-ion tumour therapy [2] – which is now completed,
- the manufacture of 9 table frames [3] for the EUROBALL cluster detectors of Germany and Sweden,
- technical support for the construction and manufacture of components for the start detector of the COSY 0°-Facility [4].

The winding machine [5] has been run to produce wire planes for the FOBOS counters. Some effort was made to improve the quality control of manufactured wire planes [6]. The progress achieved with the new technology for the FOBOS DGAC's is demonstrated in fig. 1.
Besides the research activities within the PET and KASCADE projects (see contributions in this volume) the design of a 4π Silicon Ball, EUROSIB, has been started. It will consist of 41 Si detectors of $\approx 1300\text{mm}^2$ (thickness 500μm, glued onto thin ceramics backings) which form a selfsupporting structure (fig. 2) similar to the Berlin Si-Ball [7]. Pulse-shape discrimination will allow to identify protons, alphas and heavier charged particles within a wide dynamic range [8]. This ball shall be operated as an ancillary detector for charged particles within the EUROBALL spectrometer [9].
In 1995 the Detector Lab is planned to be extended by labs for radiation physics and solid-state detectors. Furthermore the manufacture of very large wire planes for the COSY 0°-Facility requires a reconstruction of the cleanroom. This expansion of the infrastructure has been prepared by investments concerning e.g. a large optical table for detector assambly, a precise measuring stand for large-area wire planes, new filter boxes for the cleanroom, a test chamber with vaccum stand, and a small electronics pool.

References

[1] H.-G. Ortlepp et al., Report FZR 92–11 (1992).
[2] W. Enghardt et al., Phys. Med. Biol. **37** (1992) 2127.
[3] J. Stephan and M. Freitag, Annual Report 1993, FZR–35 (1994) 89.
[4] R. Esser et al., Annual Report 1993, FZR–35 (1994) 86.
[5] M. Sobiella et al., Annual Report 1993, FZR–35 (1994) 103.
[6] J. Hutsch et al., FOBOS Workshop '94, Cracow, June 1994
[7] W. Bohne et al., Annual Reports HMI–B 497 (1992) 92, and HMI–B507 (1993) 79.
[8] G. Pausch et al., contribution in this volume
[9] H. Grawe et al., Proposal for a 4π Silicon Ball for EUROBALL, July 1994

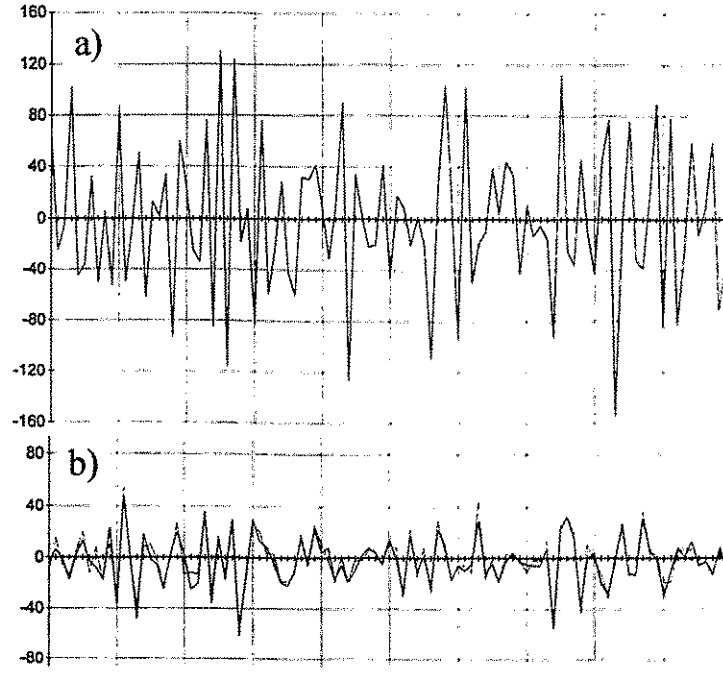

Fig. 1 *Quality control of wire planes for the FOBOS DGAC's: Wire distances are measured with a PC-controlled test stand [6] and analyzed with standard procedures.*
a) Deviation of measured wire distances (in μm) from the reference value, $d_{ref} = 1000\mu m$, for a DGAC produced in Dubna. The x-axis indicates the wire number.
b) The same for a DGAC grid produced in the Detector Lab Rossendorf.
Solid line: Wires on the winding frame.
Dotted line: Wires after soldering on the support frame.
The dispersion of wire distances is mainly due to the winding process, the influence of soldering is small.

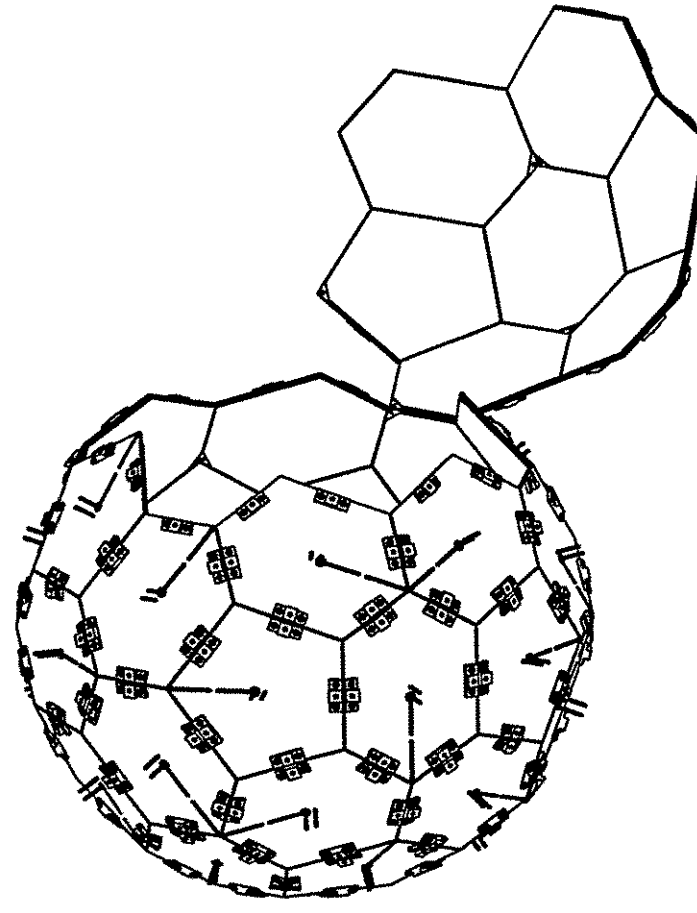

Fig. 2 *EUROSIB – a 42 element Si ball (41 detectors + beam entrance) consisting of $500\mu m$ detectors glued onto $630\mu m$ ceramics. Small Aluminum pieces form the selfsupporting structure. The total mass is $\approx 200g$.*

The Multiwire Chamber MWC 1 for the 0° Faciltity [B,K]

CH. SCHNEIDER, TH. KIRCHNER, H. MÜLLER, L. V. HORN[1], H. OHM[1], V. KRUGLOV[2]

The COSY 0° Facility is planned to consist of the spectrometer dipole D2, a start and stop scintillator arrangement and two multiwire chambers. The trigger decision and particle identification is based on the scintillator signals (time-of-flight and dE/dx measurements). Therefore the start scintillator is placed very close to the D2 magnet and the stop scintillator is positioned in the focal plane. The reconstruction of the particle trajectories will be done by means of the two wire chambers. Their main task is the position measurement of the particle tracks.

In this contribution we concentrate on the wire chamber MWC 1 which is located right behind the start counters. Since the achievable position resolution is restricted to about 5 mm mainly due to small angle scattering [1], we decided to build a chamber in which only anode readout is employed. So we can use conductive foils as cathodes. With the chosen wire distance of 2.54 mm we are below the necessary resolution and have an easy connection to the pin raster of the readout electronics, RAL 110, 111 [2]. For the cathodes we have looked for a material with high resistance in order to limit the current inside the chamber in the case of spark breakdowns. Furthermore the conductive material should have a high electron work function, because photo electrons produced in the cathode material increase the noise and worsen the operating conditions inside the chamber. From our point of view a foil with carbon as conductive material fullfils these conditions better than the usually used aluminium.

To test the counting behaviour of such a type of chamber we built a small test chamber with a sensitive area of 200 mm × 145 mm and wire distance of 2.5 mm. The wires with diameters 20 μm are made from tungsten covered by a thin gold layer. The mylar foil we used has a thickness of 26 μm with a 6 μm thick carbon layer on it. Test measurements with a 2.5 GeV beam consisting of pions, protons and kaons were performed at the ITEP Moscow. In this experiment our test chamber and a beam monitor were located between arrays of scintillation counters used as trigger for the efficiency measurement of the chamber.

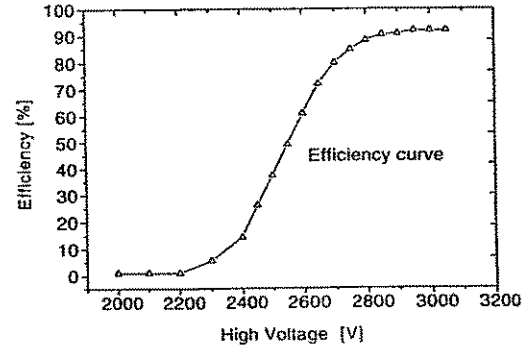

Fig. 1 *The Efficiency curve shows the ratio of counted to the triggered events in the chamber.*

If we compare the sensitive areas and spatial positions of the counters, the angular acceptances, along the vertical direction we get for the trigger counters 26°, for the test chamber 6.6° and for the beam monitor 6.5°. From the beam monitor we know that most parts of the gaussian like profile of the beam are inside the sensitive area of the beam monitor. The beam monitor can detect 88% of the full beam due to the size and position of its sensitive area. That's why we can detect with the given angular acceptance of the test chamber only about 90% of the full beam. From Fig. 1 we see that we measure 91% of all beam particles. This is about 100% efficiency in our estimation about the angular acceptance of the counters. A second indication that the detection efficiency is close to

100% is the plateau in Fig. 1 for high voltage > 2900 V. This result gives confidence in the reliability of the concept chosen for the chamber.

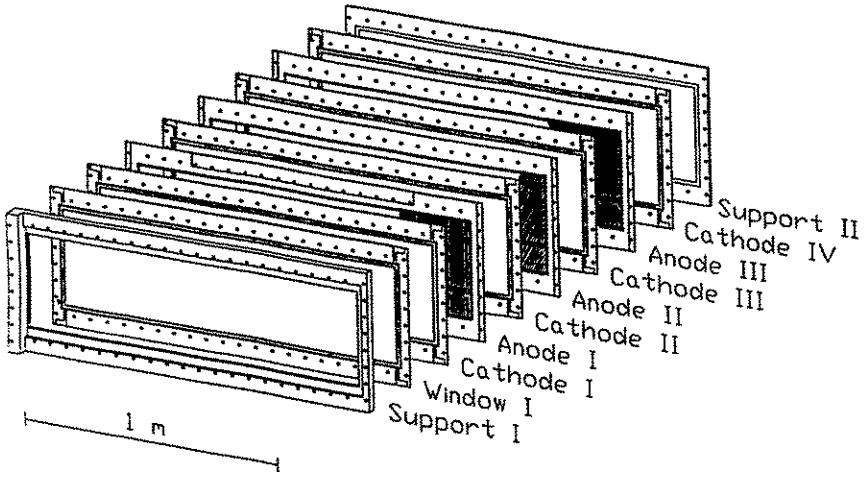

Fig. 2 *Components of the start chamber, the second window is fixed on the frame Support II*

The complete outline of the start chamber with a sensitive area of 1303 mm × 350 mm is shown in Fig. 2. The outer dimensions are 1403 mm × 510 mm. For the determination of the particle position in horizontal (x) and vertical (y) direction we have 3 anode planes with 512 wires each, denoted as Anode I-III in Fig. 2. The plane Anode I with the wires in vertical direction measures the x co-ordinate and the planes Anode II+III with inclined wires, ± 30°, the y co-ordinate.
Corresponding to the 3 anode planes we have 4 cathode planes denoted as Cathode I to IV. The frames of all anode and cathode planes are made from a fibre glass epoxy compound called Stesalit. Cathodes II and III have mylar foils with carbon layers on both sides, Cathodes I and IV have only one layer of carbon on the side that is oriented to the anode planes. Because the gap between anode and cathode is equal the width of a Stesalit frame the cathodes and anodes are mounted always on the same side of the Stesalit frames. In Fig. 2 these are the sides in direction to the frame Support I.
The anodes are on ground and the high voltage is on the cathodes, so the window foils should be again on ground potential to have electrostatic equilibrium conditions in the chamber. Therefore we use an additional cathode frame (Window I) as fixing frame for the front window to have the distance of 5 mm between the cathode and the window foil. The window foil consists of 25 μm Kapton. On the top sides two support frames (Support I, II) stabilise the chamber. Since the chamber MWC 1 is placed in the fringing field of the magnet D2 the support frames are made from stainless steel. The second gas isolating window is fixed on the frame Support II.

[1] *Institut für Kernphysik KFA Jülich*
[2] *JINR Dubna, Russia*

References

[1] Ch. Schneider et al., Annual Report 1993, Institut für Kernphysik KFA Jülich GmbH
[2] M. French et al., NIM A324 (1993)

Test Facility for Methodical Investigations of Long Scintillator Strips for use in the COSY-TOF-Spectrometer[B,K]

P. MICHEL, K. MÖLLER[1], A. SCHAMLOTT, A. SCHÜLKE

In next years a step by step extension of the COSY-Time-of-Flight spectrometer [1] is planned towards the final version of a 4π detector. The existing component of the endcap (central hodoscope) and these component presently under construction (ring-like hodoscope) consist of three layers of scintillating elements (one layer of wedge-like elements and two layers of right- and left-twisted Archimedian spirals correspondingly). Position determination is achieved by arranging the elements such as to form a grid of triangular pixels. An analogous configuration for the barrel sections (one layer of straight scintillator strips, two layers right- and left-bend strips correspondingly) turned out to be problematic because of the light pulse attenuation length in the bend elements being to small and because of technical difficulties in manufacturing the four meters long bend scintillator strips. Therefore there was the necessity of looking for an alternative concept avoiding the problems mentioned on one hand and maintaining the good spatial resolution properties determined by the geometrical pixel structure of the original version on the other hand. In the new concept special care was taken to solve the problem of on-line position determination. In a first step towards the realization of the new concept a methodical measurement was performed at CERN [2] to test two-sided read out of long straight scintillating strips using minimally ionizing particles. The position information of the detected particle was deduced from the signal time difference between the two ends. A time resolution of $\sigma = 0.45$ ns and a corresponding spatial resolution of $\sigma = 5$ cm were obtained. The on-line position measurement was carried out by a newly developed real time to digital converter (RTDC) [3] with conversion times in the range of a few nanoseconds.

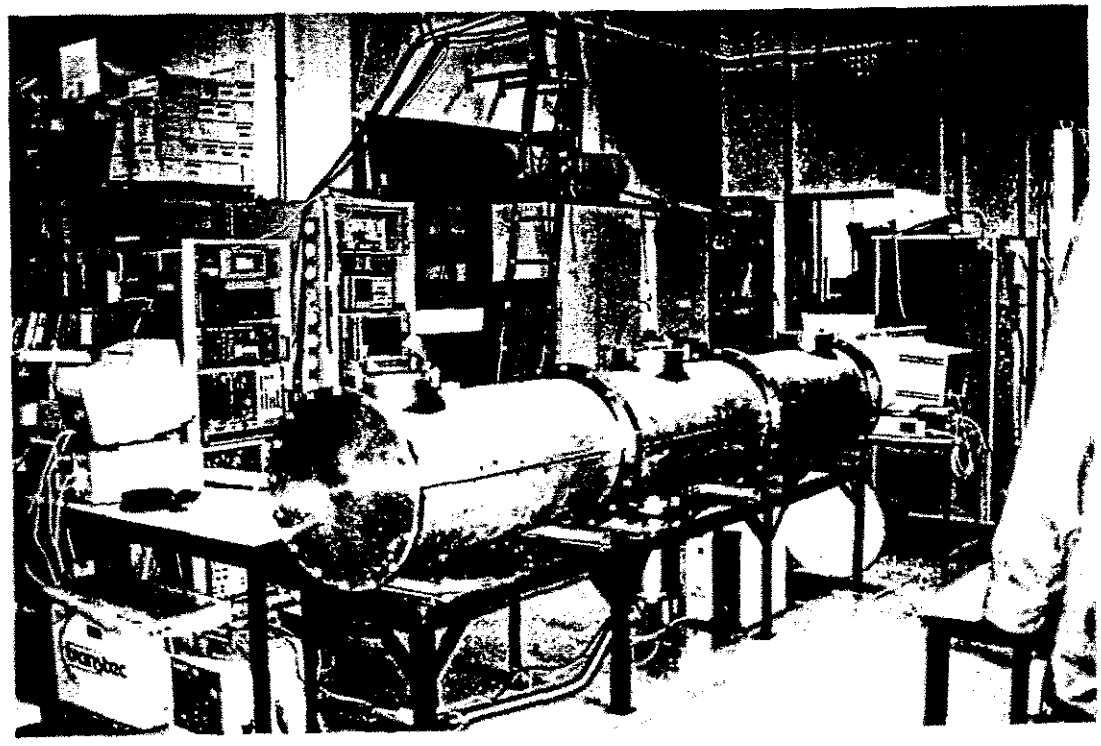

Fig. 1 *Test facility for the investigation of long scintillator strips*

From the test measurements at CERN one can draw the preliminary conclusion that the new concept could be an alternative for the original one. The new concept would mean that the three layer arrangement can be replaced by a single layer consisting of straight elements only. The final decision, however, on whether to realize the new concept or not requires the solution of quite a number of additional problems such as

1. Technical realization of 90°-read out
2. Check of the suitability of the existing light guide vacuum flanges
3. Vacuum behaviour of detector materials
4. Compensation of mechanical expansion of scintillator material caused by temperature increase
5. Ageing processes of scintillators under vacuum conditions

To investigate these problems a test facility was designed and manufactured (fig. 1). Its main component is a vacuum vessel which consists of three segments with total length of 3300 mm and inner diameter of 500 mm. Each segment has a radial flange connection (K250) for attaching the light guides. Different combinations of the segments in addition to different flange positions allow to adapt the apparatus to scintillators up to a length of 3280 mm. The configuration shown in fig.1 is adjusted to test scintillators of maximum length. For the investigation of the vacuum behaviour of the detectors the vessel can be evacuated down to high vacuum values of 10^{-8} mbar by means of a turbomolecular pump of type TURBOVAC 450 (Leybold). To generate fine vacuum the central fine vacuum pipe system of the laboratory is used. To perform ageing investigations of the detector materials pressure values in the range of 10^{-1} to 10^{-4} mbar must be kept constantly for long time periods (weeks). The pressure control in this case is carried out by a feed back system using pressure sensors (Pirani, Penning), a computer programmable control system (type OMRON CQM1) and an adjustable magnetic valve. The computer control of the system allows to automatically perform the following modes of operation: fine vacuum, high vacuum, pressure control, venting, standby and error checks. The control of the vacuum system is carried out menu-driven with a touch screen display (type OMRON NT20). The control programm comprises different options of diagnosis such as long term recording of measured vacuum data and automatic measurement of leaking and degassing rates. To determine the influence of temperature changes on the detector elements a possibility is provided to heat the vacuum vessel.

[1] *Institut für Kern- und Teilchenphysik, TU Dresden und Institut für Kern- und Hadronenphysik, FZR*

References

[1] E. Kuhlmann et al., Physica Scripta 48 (1993) 226

[2] P. Michel et al., Annual Report 1993, Instiut für Kern- und Hadronenphysik, FZ Rossendorf 1993; Annual Report 1993, IKP, Jül-2879

[3] F. Gabriel and P. Michel, FZR-30 (1994), FZ Rossendorf

A UV-Laser based Test System for the COSY-TOF-Spectrometer[B,K]

P. HERMANOWSKI[1], J. KRUG[1], R. LOKE[1], B. NAUMANN, L. NAUMANN

For online-monitoring and calibration purposes we are developing a UV-laser based test system [1], [2], [3]. The UV-light is led and distributed to scintillator counters by optical fibres, where light pulses similar to those originating from charged particles are produced. To obtain a uniform distribution of propagation time and light intensity in all detector channels we constructed a dedicated reflector head to couple the fibres to the scintillation counters (fig. 1).

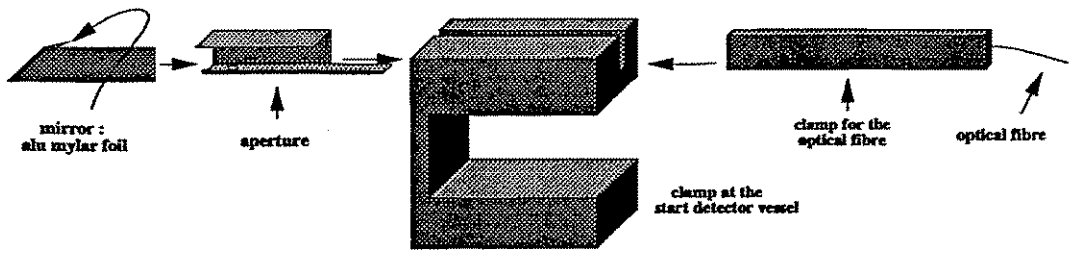

Fig. 1: *Schematic drawing of the reflector head*

It consists of a support to fix the fibre, an aperture and a mirror (alu mylar foil) to reflect the light towards the photomultiplier. By adjusting the mirror it is possible to regulate the light intensity. A setup of 32 fibres was connected to the counters of the start detector and tested during a test measurement in december 1994. The results we achieved are shown in figures 2 and 3.

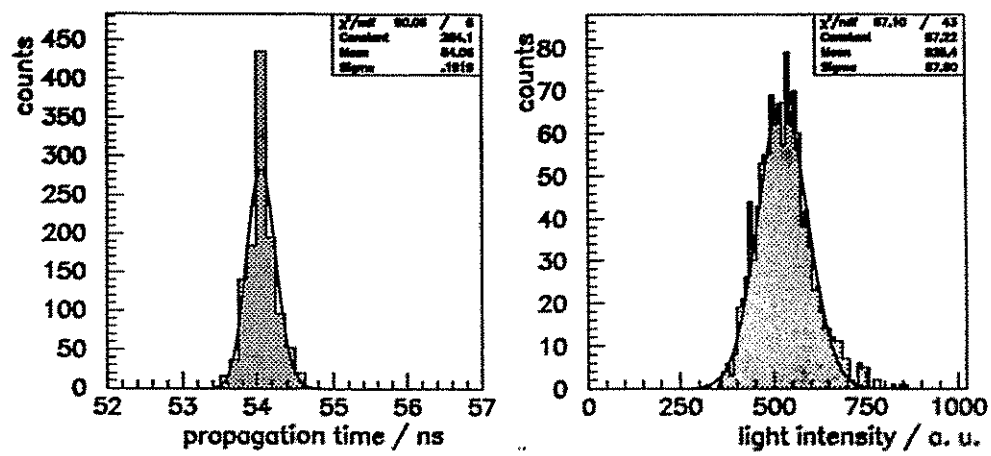

Fig. 2: *Typical TDC and QDC histograms of one channel. The time resolution is in the order of the intrinsic one of the photomultiplier XP2020*

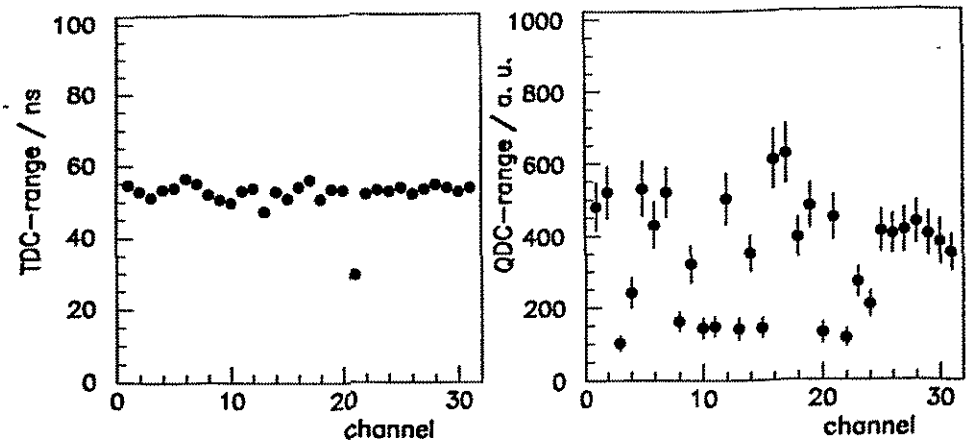

Fig. 3: *Time spread and light output of all 32 channels of the start detector*

[1] *Institut für Experimentalphysik I, Ruhr-Universität Bochum*

References

[1] P. Hermanowski et al., Annual Reports, FZ Rossendorf 1992 and 1993
[2] P. Hermanowski, Diplomarbeit, Bochum 1993
[3] R. Loke, Diplomarbeit, Bochum 1994

Status of the Evacuation and Gas Supply System of FOBOS [B]

G. RENZ [1], V.M. VASKO [2], P. GIPPNER [1], A. MATTHIES [1], V.N. DORONIN [2], D.I. SHISHKIN [2], C. UMLAUF [1], M. GEBHARDT [3]

The gas supply and exchange system of the position-sensitive avalanche counters (PSAC) [1] and Bragg ionization chambers (BIC) [2] worked very well during several weeks of experiments in 1994. Providing a full gas exchange inside the gas detector volumes within several hours, a pressure stabilization accuracy of better than 1 % has been achieved. The transition to the on-line mixing method for the P10 (90 % Ar + 10 % CH_4) gas mixture guaranteed a good long-time stability of the gas composition and, thus, of the electron drift time in the BIC. The gas is mixed by two independent electronic mass flow controllers for the gas components (fig.1). We have also the possibility to make an on-line check of the gas composition by means of a LEYBOLD Transpector gas analyzer [3]. For tuning the mixer output mass flow to the gas flow through the BIC regulation system, we used an additional controller at the BIC inlet collector.

A crucial problem of the FOBOS facility is the leakage rate Q through the thin entrance window foils of the great number of gas detectors. We have to find a compromise between foil thickness (quality), reasonable effective pumping speed S_{eff} and attainable ultimate pressure p_E inside the central vacuum chamber.

The gas diffusion rate of the 1.5 μm thick DuPont Mylar foils was found to be $Q/A = 3.7 \cdot 10^{-8}$ mbar·l/(s· cm^2) for unsupported test foils (area A=13 cm^2) at a difference pressure of 2.67 mbar. Therefore, extrapolating to a working gas pressure of 267 mbar, we expected a leakage rate of $Q = 4.2 \cdot 10^{-3}$ mbar · l/s for a BIC with an active window area of A = 1104 cm^2 and a value of $Q = 2.2 \cdot 10^{-3}$ mbar ·l/s for a BIC with A = 594 cm^2. Summing over all 30 BIC modules at 267 mbar results in a total value of Q=0.1 mbar· l/s for the expected leakage rate of the whole FOBOS facility. The contribution of the PSAC foils is negligible because of the much lower working pressure within the PSAC. The actual leakage rates measured during the FOBOS experiments in 1993/1994 turned out to be even one order of magnitude higher than the expected value of Q [4].

In order to increase the total pumping capacity, we decided to replace the old turbomolecular pumps situated at the beam entrance and exit of FOBOS by cryopumps HBK 3.2 A-P (S = 2600 l/s) [4]. In connection with the LEYBOLD TURBOVAC 1000 (S = 1000 l/s) set-up [2] directly mounted to the central vacuum chamber this resulted in an effective pumping speed of altogether 5000 l/s. Now, long-time leakage rates of even 13.3 mbar ·l/s can be managed supporting an ultimate vacuum of $p_E = 3 \cdot 10^{-3}$ mbar.

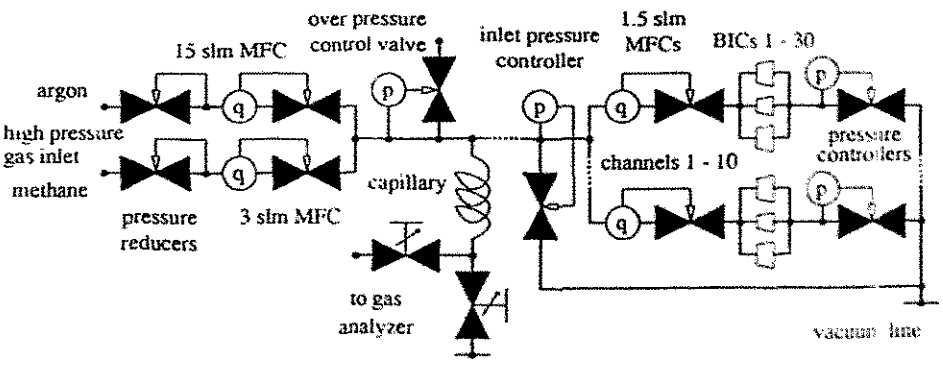

Fig. 1 *Scheme of the BIC on-line gas mixing and control system*

Simultaneously, many efforts were made to reduce the leakage rate of the BIC entrance windows by improving the quality of the foils and of the supporting grids. A special test facility was built in order to check the BIC windows under real experimental conditions and to study the phenomenon of foil aging. We tested 12 BIC with new 1.5 μm thick Mylar foils and found an average leakage rate of Q = $3.8 \cdot 10^{-3}$ mbar ·l/s in good agreement with the expected values.

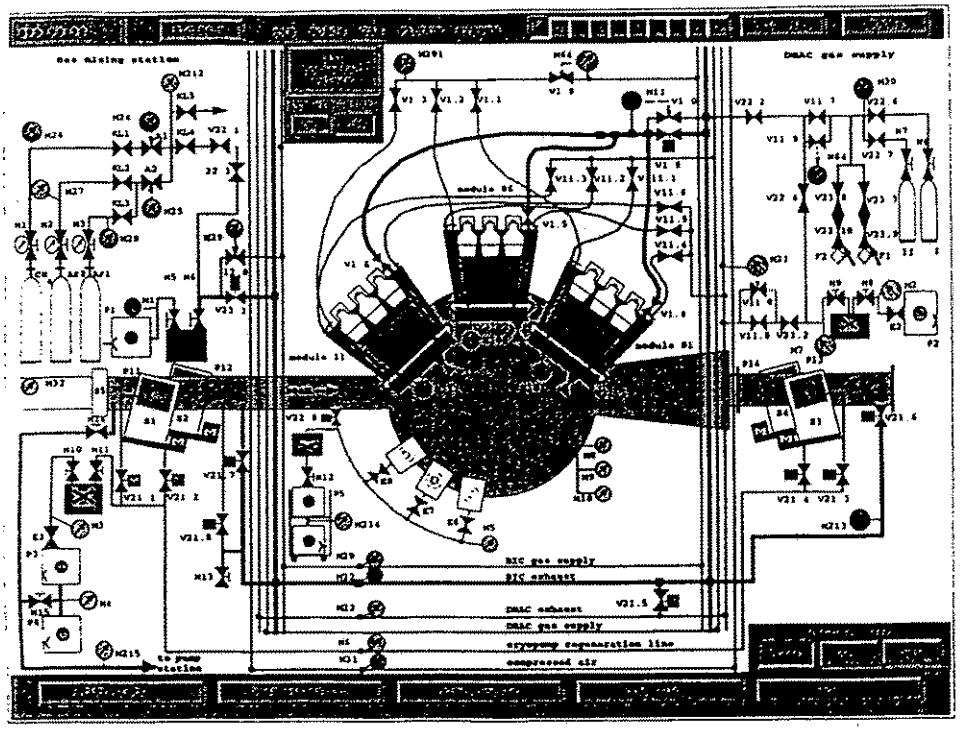

Fig. 2 *Visualization of the status of the FOBOS gas vacuum system on an X-terminal*

The SIEMENS SX automation system including the graphic visualization (fig. 2) was adapted to the new evacuation system. A supervision of the turbopump diagnostic signals via RS232 interfaces from the TURBOVAC NT20 control blocks [5] was included. Additionally to the 63 pressure measuring points we now measure and visualize all analog signals from the 11 mass flow controllers by multiplexing them to one DAC channel. Several hardware test and diagnostic routines were supplemented in order to control and ensure the status of the FOBOS gas-vacuum system on condition.

[1] *Institut für Kern- und Hadronenphysik, FZR* and *Joint Institute for Nuclear Research, Dubna*

[2] *Joint Institute for Nuclear Research, Dubna, Russia*

[3] *Physikalisches Institut der Johann Wolfgang Goethe Universität Frankfurt*

References

[1] G. Renz et al., Annual Report 1993 (FZ Rossendorf) FZR - 35 (1994) 90

[2] G. Renz et al., Annual Report 1993 (FZ Rossendorf) FZR - 35 (1994) 91

[3] LEYBOLD INFICON Inc., Transpector Gas Analysis System, Manual 2/1993.

[4] G. Renz et al., Scient. Report 1993-1994 (Flerov Laboratory of Nuclear Reactions, JINR Dubna) in press

[5] LEYBOLD AG, Operating Instructions, Turbotronik NT20 (1992)

Status of the FOBOS Scintillator Shell [B]

W. WAGNER [1], H.-G. ORTLEPP [1], D.V. KAMANIN [2], A. MATTHIES [1], O.V. STREKALOVSKIJ [2], V.E. ZHUCHKO [2]

The scintillator shell of the FOBOS array consists of 210 CsI(Tl) counters arranged behind the gas detectors to register light charged particles (LCP) and penetrating light fragments [1]. All the crystals were delivered by MONOCRYSTAL Kharkow, Ukraine, till the end of 1994. The photomultipliers, hollow light guides and biases as well as the high voltage supplies are at hand.

80 scintillation detectors have been installed at FOBOS. They were operated in the experiment ^{14}N (34 AMeV) + ^{197}Au in September 1994. To apply pulse-shape discrimination method [2] (fig. 1) and to match the timing conditions of the first level trigger [3] of FOBOS the scintillator signals have to be split and delayed. Therefore a special multichannel splitting-and-delay box has been developed at the RC Rossendorf which realizes output magnitude attenuation and a delay of 200 ns on the base of delay-line microchips.

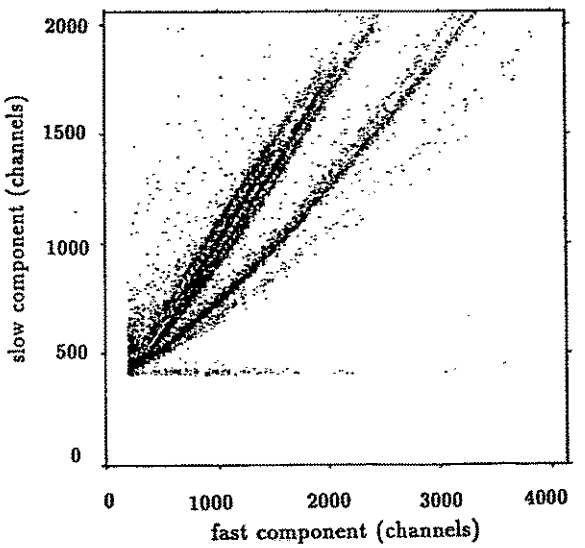

Fig. 1 *Pulse-shape discrimination matrix of a CsI(Tl) detector positioned at an angle $\vartheta = 37.4°$.*

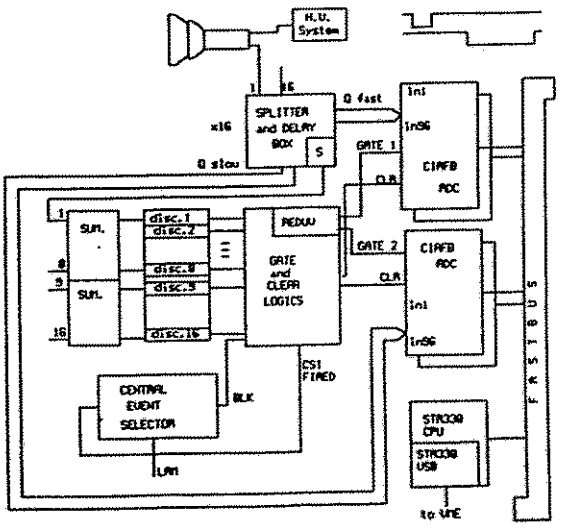

Fig. 2 *Blockscheme of the scintillator shell electronics.*

The FOBOS electronics has been upgraded by a FASTBUS minicrate containing four 96-channel current integrating ADCs (C.A.E.N. CIAFB F683C) and by control logics for the scintillator shell (fig. 2).

New control software has been developed to include the FASTBUS electronics into the VDB branch of the FOBOS data acquisition system [4].

Fig. 3 shows the image of one of the hexagonal shaped CsI(Tl) crystals of the scintillator shell when the coordinate information of the position sensitive avalanche counter (PSAC) of the respective FOBOS module has been recorded in coincidence with the scintillator signal.

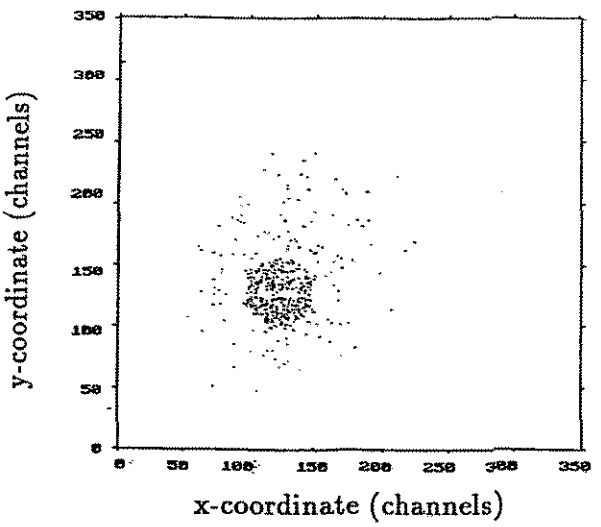

Fig. 3 *Coordinates matrix of the PSAC for events correlated with one of the scintillation detectors.*

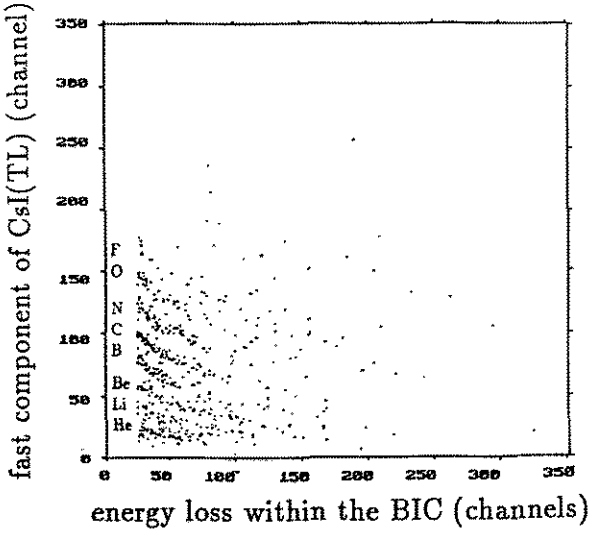

Fig. 4 *Particle identification matrix for fragments penetrating the BIC and stopped in the scintillator*

For penetrating light fragments particle discrimination was performed applying the ΔE-E-method to the energy loss (ΔE) of the fragments in the FOBOS ionization chamber (BIC) together with the light output of the fragments stopped in the scintillator (E) (fig. 4). By this way the dynamical range of the FOBOS detector is increased considerably. Furthermore this method can be used for energy calibration of the nonlinear response of CsI(Tl).

[1] *Institut für Kern- und Hadronenphysik, FZR* and *Joint Institute for Nuclear Research, Dubna*

[2] *Joint Institute for Nuclear Research, Dubna, Russia*

REFERENCES

[1] W. Wagner et al., Scient. Report 1991-1992 (Flerov Laboratory of Nuclear Reactions, JINR Dubna, E7-93-57 (1993) 244

[2] J. Alarja et al., Nucl. Instr. and Meth. **A242** (1986) 352

[3] H.-G. Ortlepp et al., Proc. Int. School-Seminar on Heavy Ion Physics, JINR Dubna, Russia vol. 2 (1993) 466

[4] ibid. [1] 249

The FOBOS Forward Array [B]

W. WAGNER[1], A. BUDZANOWSKI[2], B. CZECH[2], D. HILSCHER[3], J. HOLIK[2], H. HOMEYER[3], W. JANCZUR[2], H.-G. ORTLEPP[1], G. PAUSCH, O.V. STREKALOVSKIJ[4], L. ZRODLOWSKI[2]

For geometrical reason the minimum acceptance angle of the FOBOS spectrometer [1] is $\delta \approx 21°$. Mainly forward directed reaction products such like quasi-inelastic or projectile-like fragments, preequilibrium particles or heavy residues are not or ineffectively registered. On the other hand these particles carry valuable information about the transferred linear momentum in the nuclear reaction, the reaction plane, the excitation energy of the intermediate system, the recoil velocity etc..
Therefore it has been proposed to modify part of the former ARGUS detector [2] of the HMI Berlin for use as forward array at FOBOS.

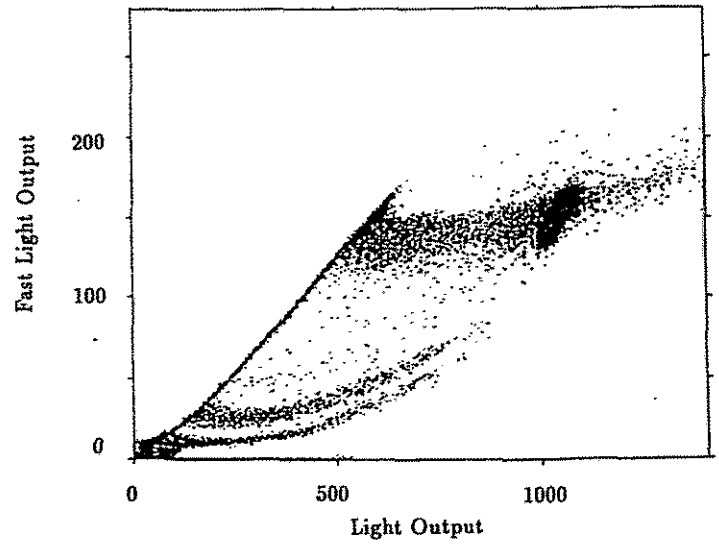

Fig. 1 *Scatterplot of a phoswich detector of the forward array applying pulse processing.*

Six rings of altogether 92 phoswich detectors consisting of 0.5 mm Pilot-U fast scintillator and 20 mm BGO are prepared to be installed into the forward cone of FOBOS.
The geometrical conditions are given in tab. 1. The thickness of the scintillators allows to stop protons (alpha particles) with energies up to $\approx 100 AMeV$. Particle charge identification is possible up to $Z \approx 15$ with a threshold for light charged particles (LCP) ($\approx 5 AMeV$).
The mechanism for adaptation of the forward array to FOBOS has been designed and produced at the INP Cracow and delivered to FLNR Dubna. The high voltage supply developed in CAMAC standard at Dubna is computer controlled under WINDOWS.

Table 1 *Geometry of the FOBOS forward array*

Ring	Detectors	ϑ
1	12	5 °
2	16	8 °
3	16	10.5 °
4	16	14 °
5	16	18.5 °
6	16	23.5 °

To include the forward array into the FASTBUS data acquisition system of the FOBOS scintillator shell [3] a simple pulse processing concept [4] has been modified for application

to phoswich detectors and tested at a ^{14}N beam.
It is planned to use the full configuration of the FOBOS array in the next beam experiment in 1995.

[1] *Institut für Kern- und Hadronenphysik, FZR und Joint Institute for Nuclear Research, Dubna*
[2] *Institute for Nuclear Physics, Cracow, POLAND*
[3] *Hahn-Meitner-Institut Berlin, GERMANY*
[4] *Joint Institute for Nuclear Research, Dubna, RUSSIA*

References

[1] H.-G. Ortlepp et al., Proc. Int. School-Seminar on Heavy Ion Physics, JINR Dubna, Russia, vol. 2 (1993) 466
[2] W. Terlau et al., Annual Report 1989 (HMI Berlin) HMI 482 (1990) 93
[3] W. Wagner et al., Scient. Report 1991-1992 (Flerov Laboratory of Nuclear Reactions, JINR Dubna) E7-93-57 (1993) 244
[4] J. Tōke et al., Report UR - NSRL - 394 (1993) University of Rochester, USA

Multihit Registration of Cosmic Particles with Digital Readout of Streamer Tubes[B]

U. Brandt[1], K. Daumiller[2], P. Doll[2], H. O. Klages[2], P. Kleinwächter, G. Kolb[1], J. Lang[1], L. Pentchev[3], D. Pröhl[4], S. Winkelmann[4]

In the KASCADE (KArlsruhe Shower Core and Array Detector)-project a streamer tube detection system is used to determine the flux of muons close to the core of extensive air showers [1]. The detectors will be arranged below a shielding of earth, iron and concrete of 16 radiation lengths. In a test set-up (similar like described in [2]) we investigated the properties of the streamer tubes (stability, plateau function, cathode transparency) as well as a digital readout electronics (cf. fig. 1) which is also applied at the multiwire proportional chambers of the KASCADE central detector [3,4]. The tubes have a length of 4 m, a 9 mm x 9 mm comb profile with a carbon layer of > 100 kΩ/cm^2 restistivity (cathode). Two anode wires are combined onto one track through the end plug of the chamber providing a spatial resolution of 20 mm vertically to the wires (anode 1-3 of fig. 1). As the other coordinate serve influence strips (cathode 1-3 of fig. 1, width 12 mm, pitch 16 mm) arranged perpendicular to the wires. The chambers are filled with an argon/isobutan = 1/3 mixture at atmospheric pressure. The high voltage applied to the cathode is 5kV. The discriminator thresholds of the entrance circuits of the motherboards as well as the delay time of the pulses which are held in the ASIC up

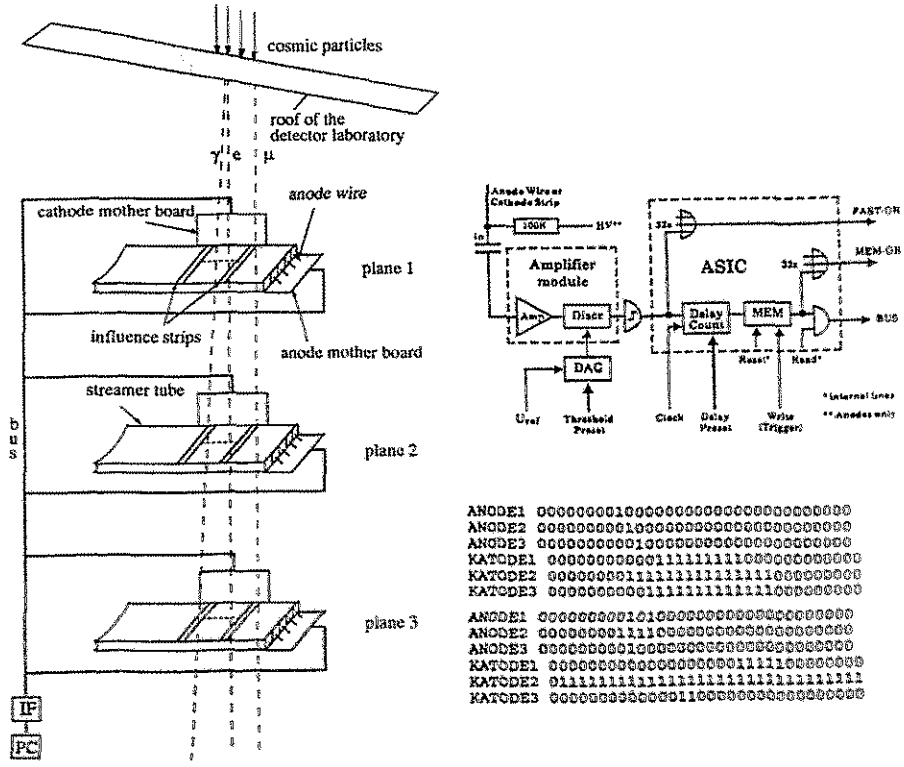

Fig. 1 Scheme of the experimental set-up (left), the digital frontend electronics and examples of readout pattern of the streamer tubes (right)

to the time where the trigger signal arrives, can be preset by means of the PC. The trigger is released from a twofold coincidence signal of scintillator counters placed above plane 1 and below plane 3, respectively. Fig. 1 shows typical examples of bit pattern obtained with the digital read out electronics. One can recognize a single hit event (upper case) clearly indicated by the anode structure of the streamer tubes. The corresponding cathode strips give a more or less broad response depending on the strip resistivity and the capacities of the strips with respect to the ground and the cathode profile. In the multihit case (lower part) one can distinguish between events on the anode wires and determine the position unambiguously. However, it is impossible to do this with the influence strip coordinates if the particle tracks are too close together. This can be overcome only by analog readout of the influence strips [5, 6].

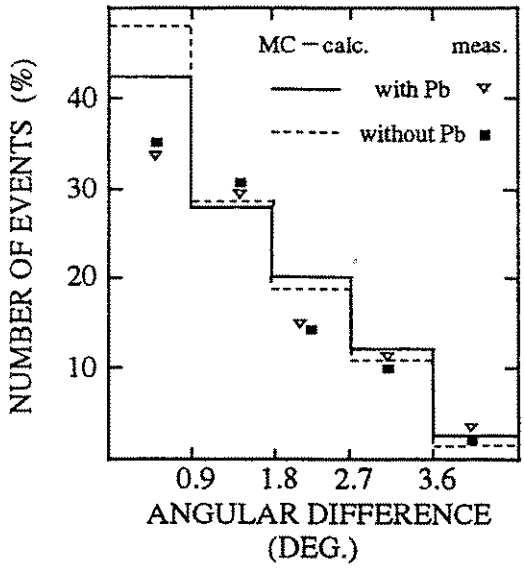

Fig. 2 Comparision of the scattering distribution of cosmic particles (single hits) with MC-calculations (see text)

With the help of fig. 2 one can discuss the scattering behaviour of the cosmic particles (only single hits) passing the roof of the detector laboratory in the experimental set-up described in [2]. The measured distributions of the track deflections with respect to the middle plane of the streamer detectors are compared with corresponding GEANT simulations taking into account the data of cosmic particle flux at sea level [7] and the real experimental conditions (e. g. a 5 cm lead layer between plane 2 and 3). In this way the histogramms obtained corresponds to a percentage of muons of 93% with a mean energy of 640 MeV which strike the set-up. The rest are essentially high energy electrons with a mean energy of 380 MeV. The gammaquanta give no response in the streamer tubes. The contribution of hadrons is negligible.

[1] *Universitt Karlsruhe,* [2] *Forschungszentrum Karlsruhe,*
[3] *Academy of Science, Sofia, Bulgaria*
[4] *Zentralabteilung Forschungs- und Informationstechnik, FZR*

REFERENCES

[1] P. Doll et al.: KfK 4686 (1989)
[2] U. Brandt et al.: Annual Report 1993, Institute of Nuclear and Hadronic Physics, FZR
[3] M. Kretschmer, KfK 5295 (1994)
[4] H. Koepernik et al.: Internal Report, FZR
[5] G. Bauer et al.: Nucl. Instr. and Meth. A260 (1987) 101
[6] Z. Krumstein, N. Khovansky, CERN/Dubna, private communication
[7] J. F. Ziegler, Nucl. Instr. and Meth. 191 (1981) 419

Status of the Fastbus Components in the Experiment Data Acquisition System at COSY Jülich [B,K]

S. Dienel[1], K.W. Leege[1], W. Oehme[1], H. Müller, B. Prietzschk, B. Rimarzig, Ch. Schneidereit, N. Brummund[2], M. Karnadi[2], H.R. Koch[2], R. Nellen[2], K.H. Watzlawik[2], M. Drochner[2], P. Wüstner[2], K. Zwoll[2]

For the experiments at COSY a unified architecture of the data acquisition systems (DACQ) has been proposed. The Fastbus components of the DACQ were in Rossendorf implemented and successfully tested (see [1]) by using a relatively simple arrangement based on components developed at Jülich and Rossendorf [2,3]. In 1994 an analogous system has been installed in Jülich for giving the experimenter the possibility to check the DACQ thoroughly. A further goal consisted in a qualitative improvement of the DACQ. Therefore, the existing DACQ was extended by several hard- and software components. So the DACQ software was ported to the workstation type "ALPHA" and is now available on both MIPS and ALPHA machines. For this purpose we had to develop a new interface of the so called CosyLog process, which is now based on UNIX sockets instead of semaphores like before.

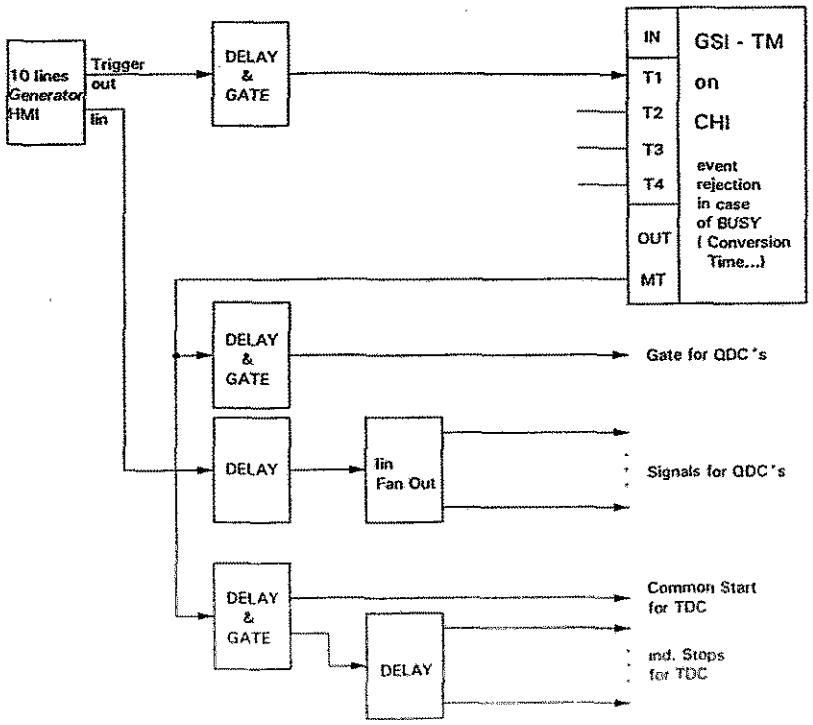

Fig. 1 *The new test arrangement using GSI Trigger Module*

The software systems were extended by also. Some new features we unified the user interface of the software and optimized the Readout-Procedures in the frontend system. The Fastbus modules of Phillips Scientific are very powerful but also sensitive to errors. Therefore we have built in a better error handling and error detection in the EMS-Server and workstation software.

Last year the so called GSI-Trigger module became available for the Fastbus system. We have integrated it into the DACQ by developing new facilities for handling the trigger both in the workstations software as well as in the EMS-Server. So it was possible to improve the trigger system of our test experiment mentioned above as shown in Fig. 1. Using the GSI-Trigger modules it is possible to increase the rate of measured events without any side effects.
Additionally we tried to improve the on-line data analysis. Instead of using PAW [4] a first version of a special visualization tool called "ROLAND" [5] was implemented. It combines an OSF/Motif interface with the facilities of the CERNLIB [4]. In this way the visualization of measured data becomes simpler, because ROLAND detects the histograms, supplied via Shared Memory, by the event decoding process automatically.

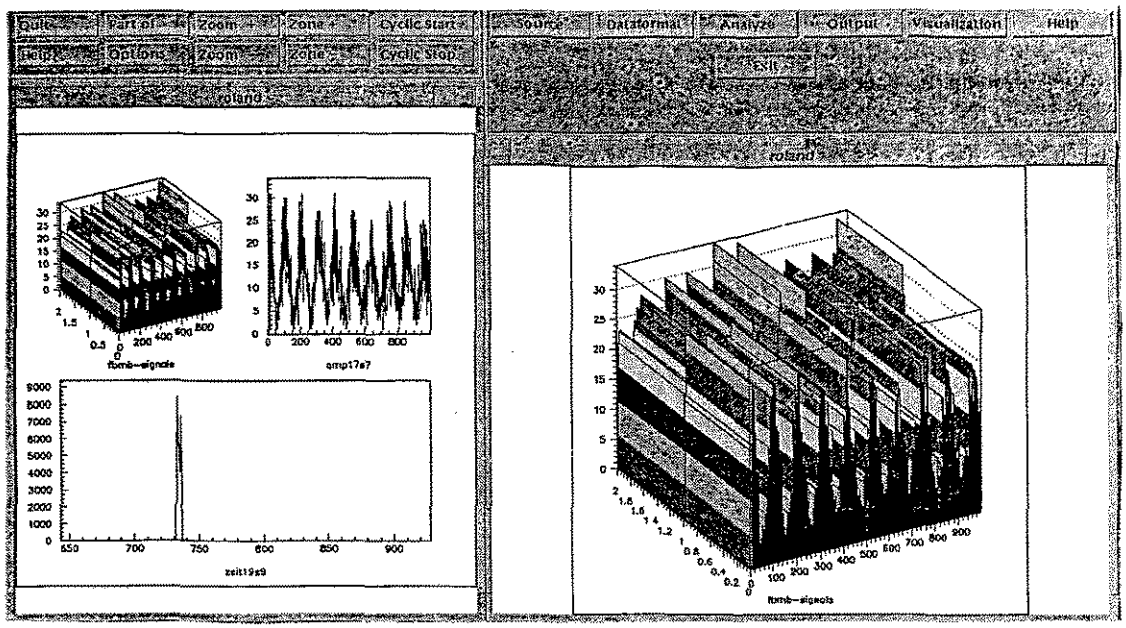

Fig. 2 *An example of visualization with ROLAND*

The user interface of ROLAND and some pictures of test signals are shown in Fig. 2.
It is planned to apply the described DACQ system for testing wire chambers built in the Rossendorf detector laboratory with the aim to thoroughly check and improve the DACQ.

[1] *Zentralabteilung Forschungs- und Informationstechnik, FZR*
[2] *Institut für Kernphysik DV, Forschungszentrum Jülich*

References

[1] S. Dienel et al., Annual Report 1993, FZR 94-35, p. 104
[2] K.H. Watzlawik et al., Annual Report 1992, KFA- Jülich, p.
[3] K. Zwoll et al., IB-KFA-ZEL 501293
[4] R. Brun et al., CERN Program Library, CERN, Geneva Swizerland, 1993
[5] J. Fleischer, Diplomarbeit, Hochschule für Architektur und Bauwesen, Weimar/FZR, 1994

ATHENE94 - a new Program for Universal Analysis of Multiparameter-Event Data [B]

D.V. VAKATOV[1], C.-M. HERBACH

Advanced monitoring and OFF-line analysis of the multiparameter data recorded by measurements at the 4π-spectrometer FOBOS [1] require a universal software package, which would enable the user to solve a maximum of different tasks by using an interactive plainly structured interface. The optimum between universality and simplicity certainly depends on the amount of collected data and the number of parameters which have to be displayed event by event. Usually, the data are stored not only into inclusive spectra but also must be filtered by different parameter correlations. In the case of measurements with the complete FOBOS-array, more than 1000 parameters have to be analyzed from a data-base of about 10 GByte per experiment. Most of the informations are deduced from two-dimensional data representations (matrixes) with typical resolution of some hundred channels per parameter. In this context, it is of special importance to accumulate in the memory a large number of matrixes simultaneously, to switch between them during the visualization at the display and to change the scaling of parameters without any loss of information.

Up to now, most of FOBOS data analysis has been performed with the program ATHENE [2,3], which operates at IBM-PC/AT computers and uses the extended memory in order to store the collected spectra. With the CPU Intel486-DX66 about 800 events/sec can be accumulated in the permanent spectra memory of 50 matrixes per 350x350 channels. Some special features e.g. concerning the calibration of the FOBOS data have been included additionally into the current PC-version. However, the essential increase of the experimental data-base requires the use of a more powerful computer, which enables both interactive dialog and the data analysis in a batch-job mode.

Based on the concept of the PC-version, the new program ATHENE94 has been developed on SUN- and DEC-stations; it also can be easily modified to operate on any computer provided with UNIX-like [4] operational system, if C++[5] and FORTRAN compilers as well as MOTIF/X11 [6] and CERNLIB [7] libraries are available. The interactive dialog and the graphical data representation are accessible from a remote X-terminal.

The data processing is carried out in a real-time mode. For this purpose, the program is subdivided into two internal UNIX-processes, which interact with each other via UNIX pipes and shared memory: one process provides the user with the friendly menu-based MOTIF [6] interface and HIGZ [7] science graphics, another one is responsible for the data analysis including reading, conversion, filtering, booking into histograms and saving the processed data into the output file. The input has been carried out to read the experimental raw data files recorded in the HOOPSY [8] format and in the format of the program OLYMP [9], and the latter is also used as the standard output data structure. In addition, special attention has been paid to ease one to modify the appropriate part of the program in order to attach his own data input and output procedures.

Experimental data can be represented in form of various histograms and colored scatterplots. The maximum quantity of different spectra and the number of the included channels are only limited by the available memory, and the distribution of the memory between the different spectra can be ordered by the user in a dynamical way.

The current draft program version includes various operations as e.g. the zooming of graphical representation, the graphical mouse supported setting of selection gates (polygons, rings, boxes and cuts), the storing of figures to PostScript and TEX metafiles as

well as the linear data calibration. Arbitrary logical expressions can be composed on the base of the interactively defined graphical gates. The initialized selection criteria can be used as a filter during the storing of data events into histograms or output-files. The user specific program initialization can be written to disk in form of ASCII-files and then can be restored at any time.

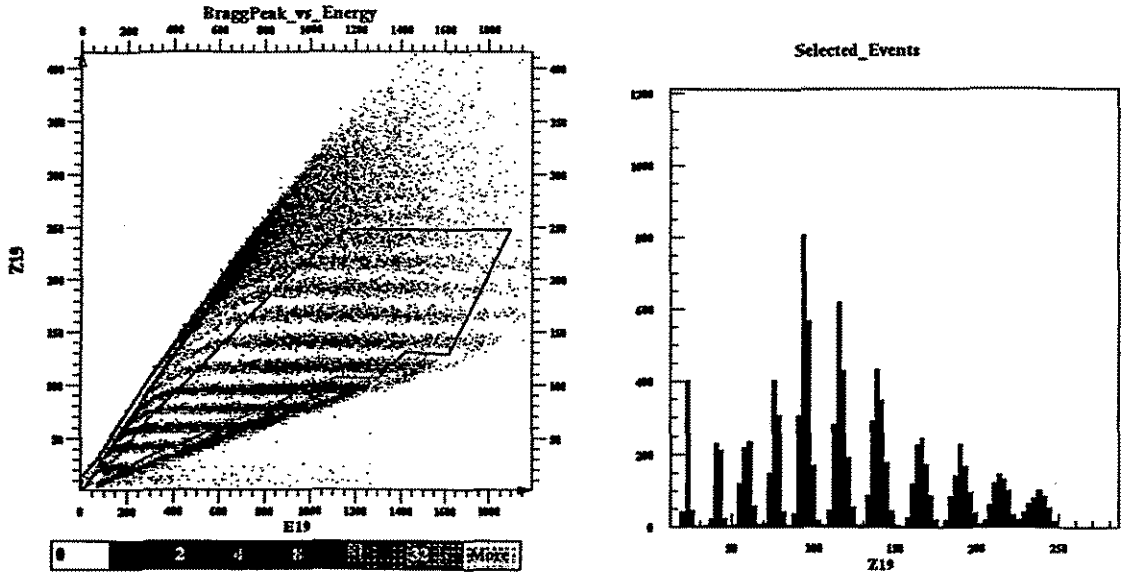

Fig. 1 *Example of data representation with ATHENE94; a gate within the scatter-plot (a) has been used to filter the events which are recorded into the histogram (b)*

Further efforts will be made in order to include user specific procedures for numerical data transformations and to manage the switch into a batch-job mode.

[1] *Joint Institute for Nuclear Research, Dubna*

References

[1] H.-G. Ortlepp et al.; Proc. Intern. School-Seminar on Heavy Ion Physics, Dubna, Russia, May 10-15, 1993, Vol.2, p.466
[2] C.-M. Herbach and C. Umlauf, Annual Report 1991, FZR 92-09 (1992) 61
[3] C.-M. Herbach and D.V. Vakatov, Proc. of the FOBOS-Workshop 1994, Cracow, Poland, June 28-30, 1994, Report FZR-65 (1995) 56
[4] Belyakov M.I. et al, "The Portable Operational System", Radio i svyaz, Moscow, 1991
[5] Bjarne Stroustrup, "The C++ Programming Language", Addison-Wesley, 1986
[6] OSF/Motif Programmer's Reference Manual, rev. 1.0, Open Software Foundation, Eleven Cambridge Center, Cambridge, MA 02142
[7] HIGZ User's Guide, CERN Geneva, 1993
[8] G. Roescher et al.; Report HMI-436, Berlin, 1986
[9] OLYMP User's Manual, Report HMI, Berlin, 1992

Computer Controlled Vacuum System for the COSY-TOF-Spectrometer[B,K]

R. KLEIN[2], P. MICHEL, K. MÖLLER[1], CH. NAKE[2], B. NAUMANN, L. NAUMANN, A. SCHAMLOTT, A. SCHÜLKE

To minimize background production, energy loss and multiscattering the start and stop detector components of the COSY-TOF-spectrometer [1] are placed in a modular vacuum vessel with a maximum volume of 60 m^3. Vacuum pressure less than 10^{-2} mbar is necessary for precise nuclear physics experiments. The installation of the LH_2 -target [2] in each of the two versions of the start detector [3,4] requires a sufficently low vacuum pressure in the order of 10^{-5} mbar around the cold target cell to suppress the growth of residual gas condensates at the target windows [5]. Such condensates would falsify the original composition of the target material. The spectrometer vessel operates at fine vacuum conditions (10^{-2} mbar). Between the Rossendorf start detector and the vessel a Mylar foil is installed to separate the high vacuum and the fine vacuum regions. To reduce background from the primary beam the Mylar foil was chosen as thin as possible (20 μm).

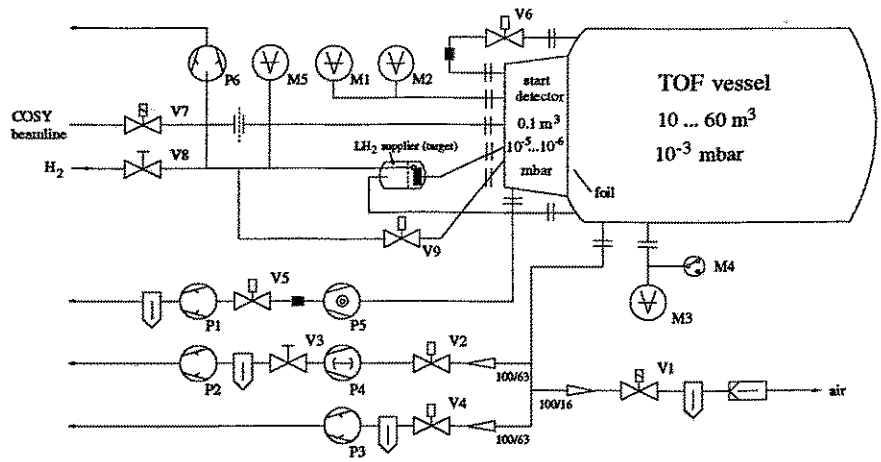

Fig.1: Schematical layout of the COSY-TOF-Spectrometer vacuum system
V - valve; P - pump; M - vacuum gauge;

To avoid limitation of the acceptance of the spectrometer a large area foil is necessary (ø600 mm). In the normal working regime of the spectrometer the pressure difference between the start detector and the vessel is small and no visible deformation of the foil occurs. But if in the case of technical trouble the pressure difference rises to a few millibars the foil is deformed substantially. This can lead to serious damage of the sensitive start detector elements (hollow light guides, target cell etc.). For this reason a bypass valve (V6) is provided to limit the pressure difference between the start detector chamber (M2) and the vessel region (M3). To automate vacuum equipment as a whole a computer controlled system was designed and installed. The layout of the COSY-TOF-spectrometer vacuum system is shown in fig.1. To make the control system independent of operator mistakes or system crashes a memory programmable controller - system OMRON [6] - was chosen. It consists of a CQM1 central processing unit and a lot of binary and analog I/O-units. A pseudo graphical touch screen panel (OMRON NT20) is used as a modern user interface. Controller unit, touch screen panel, vacuum measuring device and contactors for the pumps are housed in a 19 inch crate. The electropneumatic valves are controlled

by 24 V DC. At changing the experimental set-up it is necessary to separate the control and the vacuum system. Therefore all pumps except the turbo molecular pump and most of the valves are placed on a mobile platform and the control system is mounted in a mobil rack in the TOF area. For remote check of the vacuum system while the beam is active it is possible to display the system state, measuring values, recording informations and errors via a V24-line on a PC in the TOF counting room. To avoid mishandling by unauthorized persons a remote control of the system from this room was not installed intentionally. The control of the vacuum system is carried out menu-driven with the touch screen panel. The main menu entries *FineVac, HighVac* and *Venting* make it possible to evacuate as well as to ventilate the vacuum system automatically. In these modes of operation a complex error supervision is active which controls the following conditions:

- pressure difference between the two recipients
- limit positions of the valves
- response signals of the pumps (e.g. overload)
- trouble information of the vacuum measuring device
- availability of compressed air
- 24 V DC power supply

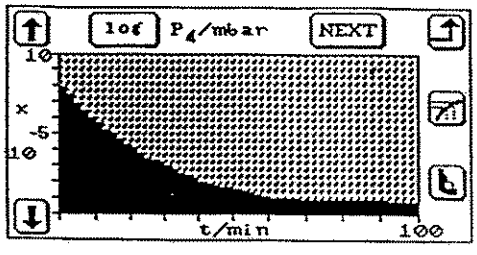

Fig. 2: Recorder information of vessel pressure (displayed on the NT20-panel)

All these errors cause closing valves (except bypass valve), opening the bypass valve and switching off the pumps. If the high vacuum is reached an enable signal is generated to allow filling the LH_2 -target. For venting a signal "LH_2 - target empty" is required, moreover a signal for COSY-Control is generated. In the *Service* mode each valve and each pump can be steered separately.

The system state and the pressure values can be displayed. The error supervision is suppressed. This mode is protected by a keycode, so an unintentional operating is impossible. In all operating modes the state of the vacuum system can be displayed in a vacuum scheme. It is also possible to store and display all pressure values over the time (up to a time scale of a few days - *Recorder*, see fig. 2) and to show pressure gradients for instance to measure leaking rates or the pump performance. The described vacuum control system was tested successfully during a two weeks COSY-TOF run in 1994. It is planned to integrate the LH_2 - target handling into the control system in near future.

[1] *Institut für Kern- und Teilchenphysik, TU Dresden und Institut für Kern- und Hadronenphysik, FZR*
[2] *FZ KFA Jülich, IKP*

References

[1] S. Brand et al., IKP, Jül-2462 (1990)
[2] V. Jaeckle et al., NIM **A349** (1994) p. 15
[3] K. Kilian et al., IKP, Jül-2590 (1991)
[4] T. Czarnecki et al., IKP, Jül-2879 (1993)
[5] L. Naumann, B. Naumann and A. Schamlott, COSY-TOF-Notes, RO-3 (1993)
[6] OMRON Sysmac CQM1 Programming Manual, Rev. 1993

Activities of the Electronics Group

K. Heidel, B. Prietzschk, B. Rimarzig

The Electronics Group, part of the department "Experimental Technique" in the Institute of Nuclear and Hadronic Physics, has been involved in projects concerning the development and manufacture of detector systems for nuclear physics experiments at COSY, Juelich, and at the heavy-ion cyclotron U-400M in Dubna (Russia). The main activities in 1994 are summarized as follows:

1. The use of light-emitting diodes (LED's) for calibrating scintillation detectors has been prepared by methodic work. A test stand with three scintillation detectors, coupled to photomultipliers (PM's), was built up which allows to check count-rate and temperature stability of energy and timing signals generated by a radioactive source or LED's. Stable pulse generators for LED operation were developed.

2. Detector case and PM base for the XP 2020 photomultiplier were developed. These photomultipliers will be exploited for the stop counters of the COSY 0°-facility [1]. About 200 PM tubes have been tested and certified.

3. Layouts of the wire planes for double-grid avalanche counters (DGAC's) of the FOBOS spectrometer in Dubna [2], as well as layouts for wire planes of 1.4 m lenght to be used in the start chamber of the COSY 0°-facility, were developed.

4. The serial production of printed-card boards for the wire planes, of 3-fold constant-fraction discriminators (CAMAC modules), energy/timing amplifiers and generator boards (SMD technology) for the FOBOS DGAC's was completed.

5. A fast zero-crossing discriminator for application in pulse-shape discrimination schemes [3] was developed and produced in a small series.

To produce double-grid avalanche counters for the heavy-ion spectrometer FOBOS, and to build up the start detector for the COSY 0°-facility, the construction of large wire planes was necessary. The DGAC's have pentagonal and hexagonal shapes measuring 324 mm and 425 mm in diameter, respectively. The wire planes of the 0°-facility start detector are rectangular and have a size of 1400 mm x 500 mm. These exotic wire planes make most exotic demands on the precision of PCB (printed-card board) manufacturing. For the construction, the electronic CAD system P-CAD [4] has been used which delivers all the necessary computer-aided manufacturing (CAM) files. Its tight integration with manufacturing is of major importance for success in such delicate design projects.
Besides these activities, the physicists of the institute have been provided with service and support for their experiments.

References

[1] W. Borgs et al., COSY Proposal # 18, 1991.
[2] H.-G. Ortlepp et al., Report FZR 92–11 (1992).
[3] K. Heidel et al., contribution in this report.
[4] P-CAD Productivity Across The Board, ALTIUM (USA), PC–098.

Pulse-Shape Discrimination for Particle Identification in 4π Silicon Balls

G. Pausch, W. Bohne[1], A. Buscemi[2], G. DeAngelis[2], G. DePoli[2], H. Grawe[1], D. Hilscher[1], M. Moszynski[3], G. Röschert[1], R. Schubart[4], D. Wolski[3], R. Zanon[2]

The efforts to exploit pulse-shape discrimination (PSD) for identification of charged particles in planar Si detectors [1] have been continued, stimulated by the proposal to build a 4π Si-ball for charged particle detection as an ancillary detector for EUROBALL [2]. In a test experiment carried out at ISL (VICKSI) in Berlin we irradiated Si detectors manufactured for the Berlin Si-Ball BSB [3] and for the Legnaro ΔE–E Si-Ball ISIS [4] *i)* with light charged particles produced in fusion-evaporation reactions (150 MeV ^{36}Ar + Ni), and *ii)* with heavier fragments produced by 510 MeV ^{36}Ar projectiles in mixed targets consisting of C, Ni, Ag, and Au (Table 1). All detectors were operated in the rear-side injection mode [5]. The most important results can be summarized as follows:
1) Excellent resolution was obtained with a PSD scheme similar to the zero-crossing technique which is well known from n/γ discrimination with scintillation detectors [6]: Two subsequent differentiations ($\tau_{RC} \approx$ 100...200ns) of the charge signal provide a bipolar pulse. The zero-crossing time t_{ZC} is measured relative to a rise-time compensated constant-fraction timing of the bipolar pulse. No external time reference is necessary.
2) Best particle resolution was found with a detector bias slightly above the voltage for total depletion (fig. 1), i.e. if low-energy ions are stopped in a region of very weak electric field (increased rise-time and pulse-shape differences [5]). However, the huge rise-time variation which supports PSD means a non-linear energy calibration due to the ballistic deficit (fig.2). If precise energy information is of interest one needs spectroscopy amplifiers (SPA) with ballistic deficit correction (BDC) [7].
3) The 500μm Eurisys detectors show excellent resolution for p/α discrimination as well as for heavy-ion identification (fig. 1). This is consistent with previous experience from detector tests [1] and experiments with the BSB.
4) There is no doubt that the concept of a Si-Ball with PSD is practicable.

Table 1 *Si detectors used in the test experiment*

Det. No.	Detector Type	Manufacturer	Thickness [μm]	Recomm. Bias [V]	Particle Resolution
1	ISIS "ΔE" [a]	Micron Semiconductor	130	22	moderate
2	ISIS "E" [a]	Micron Semiconductor	1000	123	no
3	BSB Type C [b]	Eurisys Measurements	500	70	excellent
4	BSB Type C [b]	Eurisys Measurements	500	70	excellent

[a] $\approx$ 1000mm^2, transmission mount, used in rear-side injection mode
[b] $\approx$ 750mm^2, glued with the high-field (front) side onto a 630μm ceramics backing

[1] *Hahn-Meitner-Institut Berlin, Bereich Festkörperphysik*
[2] *Istituto Nazionale Fisica Nucleare Legnaro, Italy*
[3] *Soltan Institute for Nuclear Studies Swierk-Otwock, Poland*
[4] *Universität Göttingen*

References

[1] G. Pausch et al., Nucl. Instr. and Meth. **A 349** (1994) 281, and refs. therein.
[2] H. Grawe et al., Proposal for a 4π Silicon Ball for EUROBALL, July 1994
[3] W. Bohne et al., Annual Reports HMI–B 497 (1992) 92, and HMI–B507 (1993) 79.
[4] G. DeAngelis, EUROBALL LCP Det. Meeting, Bordeaux, May 1994 (slide report).
[5] G. Pausch et al., Nucl. Instr. and Meth. **A 337** (1994) 573.
[6] T.K. Alexander, F.S. Goulding, Nucl. Instr. and Meth. **13** (1961) 244.
[7] M. Moszynski, G. Duchêne, Nucl. Instr. and Meth. **A 308** (1991) 557.

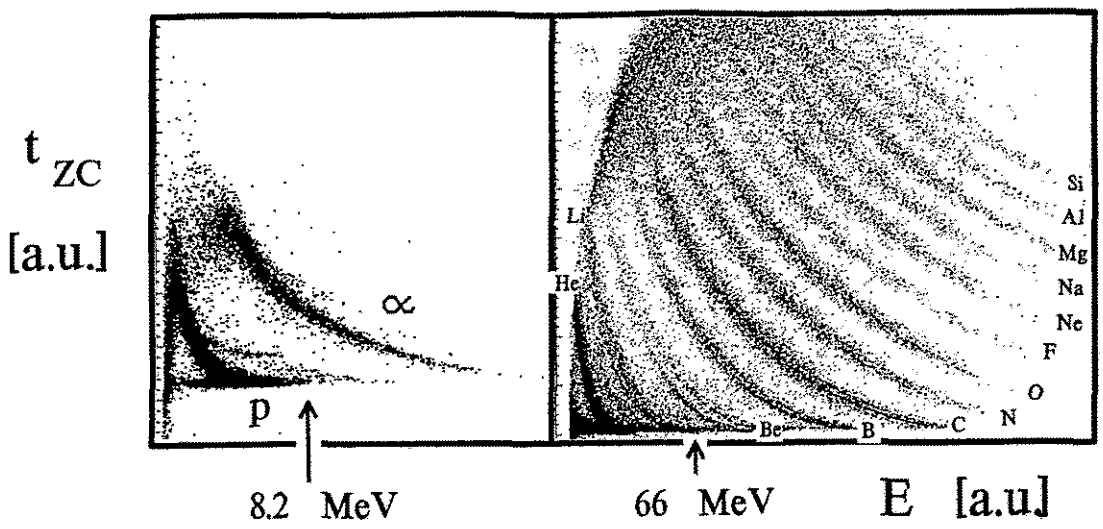

Fig. 1 *Scatterplots of the zero-crossing time t_{ZC} (y axis) versus energy deposition E (x axis) obtained with a PSD scheme similar to [6]:*
a) p/α discrimination (reaction 150 MeV ^{36}Ar + Ni, det. 3 at $\theta_{lab} = 110°$, bias 80 V)
b) Heavy ion identification (510 MeV ^{36}Ar + {C+Ni+Au}, det. 4 at 25°, bias 80 V)

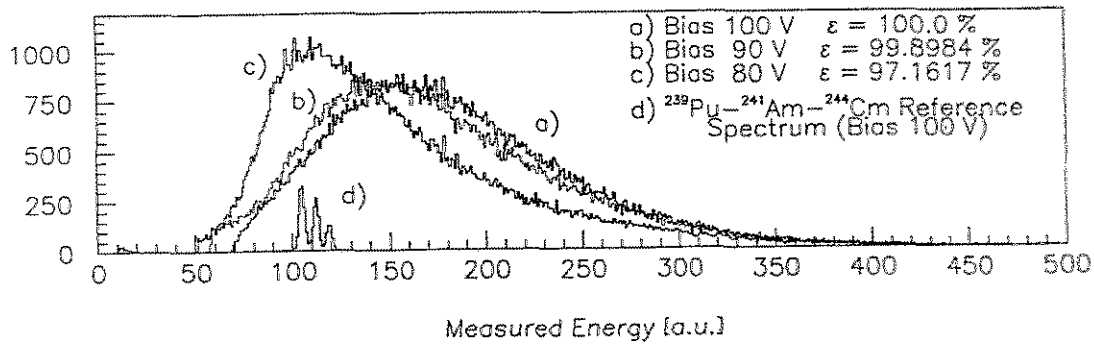

Fig. 2 *Energy spectra of α particles from 150 MeV ^{36}Ar + Ni at $\theta_{lab} = 110°$ measured with a spectroscopy amplifier ($\tau = 0.5\mu s$) for detector 3 with bias voltages of a) 100 V, b) 90 V, c) 80 V. The ballistic deficit due to larger rise times of the charge signal at lower bias shifts the measured amplitudes (parameter E) to lower values and causes a non-linear energy calibration. Nevertheless the counting efficiency ε for α particles stays nearly constant.*

Development of a Zero-Crossing-Detector for the Particle Identification

K. Heidel, T. Friese[1], H.-G. Ortlepp[2], G. Pausch

Pulse-shape discrimination has proved to be an excellent method to identify charged particles detected in planar Si detectors [1]. The time difference between the leading edge and the zero crossing of a bipolar pulse generated e.g. by means of a spectroscopy amplifier is, at a given energy, a function of charge and mass of the detected ion [2].
To support applications of this technique we developed a zero-crossing-detector. In contrast to the Constant Fraction Discriminator CFT 5386 [3] this circuit generates two logic output signals-one for the leading-edge-timing which is produced by a level discriminator (LD) and one for the zero-crossing point which is determined by a zero crossing discriminator (ZC). The LD have a adjustable front panel threshold. The block diagramm is given in Fig. 1. The bipolar input pulse is feed to a dual ultrafast comparator AD 96687, protected with a diode network, and the edge-trigger is activated by the LD and closed by the ZC. Now the shaper is started and generates for the ZC a signal of 20 ns width. The timing of this signals is modified by using a combination of a dual D-Flip-Flop. The requiried output signals are NIM-standard negative signals.
The circuit using the low current design was constructed on a printed circuit board produced in ECL technology. Each module, containing three separate channels, occupies a double slot in a CAMAC crate. A control of the LD threshold and the zero level of the ZC by CAMAC commands is prepared. Technical data are given in Table 1 and the timing scheme is shown in Fig. 2.

Table 1 *Technical data*

Input Pulse	bipolar, 0mV...2700mV
Input Imped.	2KΩ, dc-coupled
Output Pulse	NIM at 50Ω
Threshold	0mV...100mV, adjustable
Supply	6V(100mA), -6V(700mA)
Channels	three, ad with LED

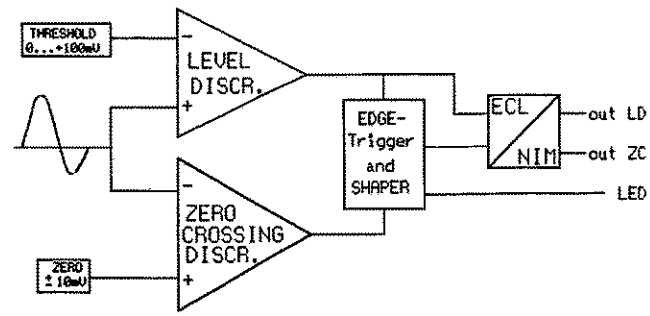

Fig. 1 *The circuit block diagramm*

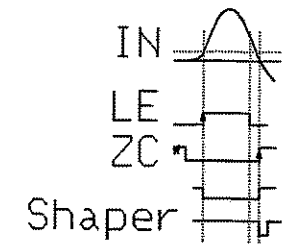

Fig. 2 *Timing scheme of the ZC-circuit*

[1] *Hahn-Meitner-Institut Berlin*
[2] *Institut für Kern- und Hadronenphysik FZR and Joint Institute for Nuclear Research, Dubna*

References

[1] G. Pausch et al., Nucl. Instr. and Meth. **A 349** (1994) 281, and refs. therein
[2] G. Pausch et al., his report
[3] K. Heidel et H.-G. Ortlepp, Annual report 1993, **FZR-35**, 113

Real Time Particle Separation in Scintillators[B,K]

P. MICHEL, K. MÖLLER[1], A. SCHAMLOTT, A. SCHÜLKE

A technique for online time measurement on the basis of a Real Time to Digital Converter (RTDC) was developed in last years [1].

This technique allows conversion times of a few nanoseconds for time to digital conversion in contrast to conventional methods with conversion times in the order of microseconds. The new method developed was used succesfully for online position determination in long scintillation counters [2].

Recently a further application of the method was tested consisting in fast particle separation in scintillation counters. The goal was to integrate particle separation in the online trigger. To achieve high trigger rates the time required for particle separation should be less than 100 ns.

In the first step of processing the photomultiplier signal is shaped (integrated and differentiated) in an Ortec 885 spectroscopic amplifier. After that the pulse is converted to a logical NIM signal by a leading edge discriminator (LeCroy 4413) with variable pulse length (Time over Threshold Mode).

If the discriminator thresholds are very low the NIM pulse length is proportional to the time intervall to be measured. This signal is used to start the RTDC.

Particles with different specific energy loss generate different pulse shapes in some types of scintillators (Stilben, BaF_2 ...). Thus it is possible to distinguish particles by pulse shape analysis. There is a lot of methods to do this, for example by measuring both the leading and trailing pulse components. A simple method consists in measuring the time interval between the on-set of the pulse and the center of gravity as well as the amplitude of the pulse. This method was used in the present case. The timing signal is measured as follows (Fig. 1). The stop signal is derived from simple negation of the start pulse.

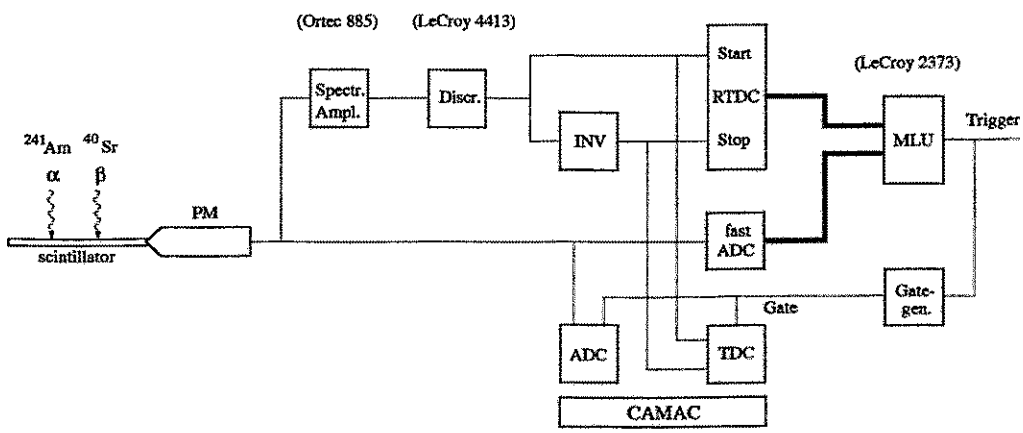

Fig. 1 *Electronic scheme of online particle separation.*

By means of the RTDC the time interval between the start and stop pulse is digitized. This time information and the digitized amplitude information are combined to form a

16 bit word. This word is used as an input adress of a 16 × 16 bit Memory Look up Unit (MLU, LeCroy 2373). If the whole memory is filled with logical "1" every input event produces an output signal of the MLU which is used as trigger signal.

In Fig. 2a a two-dimensional spectrum is shown representing events arising from the simultaneous irradiation of a thick stilben crystal with electrons from a ^{90}Sr-source and alpha-particles from a ^{241}Am-source. To ensure that the energy spectra of alpha-particles and electrons are completely mixed (i.e. have comparable amplitudes) the energy of the alpha-particles is reduced by a thin polyethylene foil. Thus a simple particle separation by setting energy thresholds is impossible. By means of a two-dimensional plot, however, a very good separation of alpha-particles and electrons is possible (Fig. 2a).

The trigger output signal of the MLU induces event read out and entering in the two-dimensional ADC-TDC plot. By suitable setting of the MLU memory table any event sample can be specified and selected. Since the output word of the MLU consists of 16 bit a large variety of event specific trigger signals can be formed. In the simplest case the memory is filled with "0" or "1" meaning "YES" or "NO" for the trigger. In Fig. 2b an example for this simple case is illustrated. Memory cells corresponding to the region above the indicated line are filled with logical "0" and the remaining cells with logical "1". This way only electrons are admitted for further online data processing.

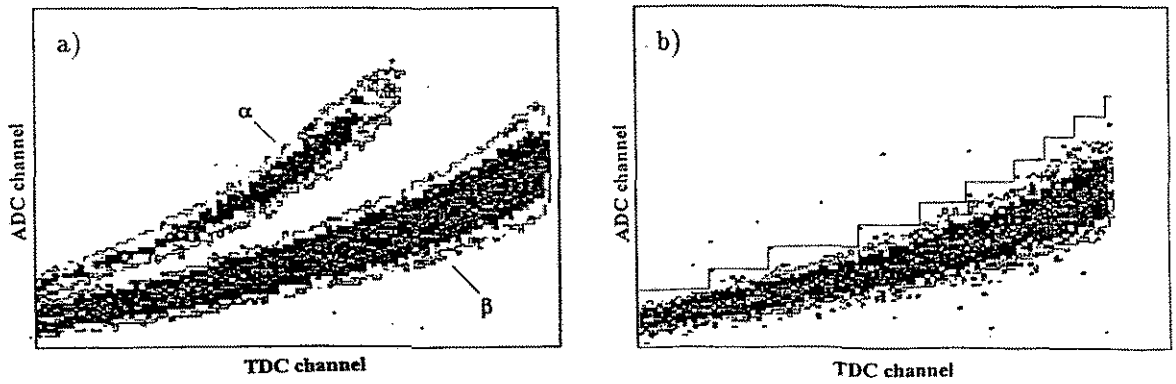

Fig. 2 *Two dimensional spectra: (a) total events (b) only electrons selected*

The digitized time information of the RTDC is available for use in the MLU about 10 ns after forming the stop signal. The digitalization of the pulse amplitude can be realized in the order of some ten nanoseconds by a fast ADC (for example LeCroy 4508). Since the transit time of the MLU amounts to about 35 ns a trigger time of less than 100 ns is within reach leading to trigger rates of $10^7 s^{-1}$. To reach this limit fast scintillators, for example BaF_2, with signal trailing times less than 1 ns are necessary. We plan to test the method described using these scintillator materials.

[1] *Institut für Kern- und Teilchenphysik, TU Dresden und Institut für Kern- und Hadronenphysik, FZR*

References

[1] F. Gabriel, P. Michel, FZR-30, 1994, Preprint FZ Rossendorf

[2] P. Michel, K. Möller, A. Schamlott, A. Schülke, FZR Annual Report 1993, Institut für Kern- und Hadronenphysik, p.84

A Positron Emission Tomograph for the on–line Control of Heavy Ion Tumour Therapy [B]

W. ENGHARDT[1], B. HASCH, K. LAUCKNER, J. PAWELKE, M. SOBIELLA, L. BYARS[2]

On the basis of our investigations on the technical aspects of in–beam positron emission tomography [1] and on the generation of β^+–emitters in organic targets by swift light ions [2,3] a positron emission tomograph for the on–line monitoring of the heavy ion therapy has been designed. For reasons of reliability during the planned clinical application the tomograph has been built up from components of the ECAT EXACT and ECAT EXACT High Resolution PET scanners of SIEMENS/CTI, Knoxville TN. The device is a limited angle, double head tomograph (Fig. 1). At the treatment place the heads will be mounted above and below the patient couch. Each head is build up from 8×4 position sensitive BGO block detectors [4] which are subdivided into 8×8 crystals of 20.0×6.25×6.25 mm^3. The coordinates of the crystals fired and a time label are fed into the coincidence processor that detects true and delayed (for random correction) coincidences in 12 ns wide coincidence windows. Valid coincidence events are transferred via a fibre optics cable to the Real Time Sorter (RTS) where they are stored either in histogram or in list mode. A SPARC 10 workstation connected via Ethernet to the RTS controls the whole device and runs tomographic reconstruction programs. At present the gantry for mounting the system at the treatment place is constructed, system tests are performed and the reconstruction software is prepared.

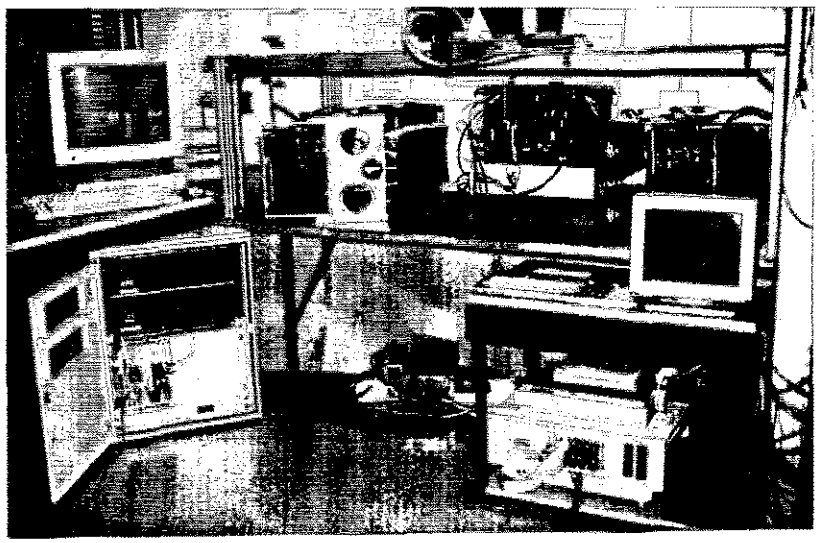

Fig. 1 *Preliminary installation of the PET scanner in the detector laboratory.*

[1] *Uniklinikum der TU Dresden und Institut für Kern- und Hadronenphysik, FZR*
[2] *Byars Consulting, Knoxville, TN, USA*

References

[1] J. Pawelke, Ph.D. Thesis, TU Dresden, 1995
[2] W. Enghardt et al., Phys. Med. Biol. **37** (1992) 2127,
[3] W. Enghardt et al., Annual Report 1993 **FZR-35** (1994) 114
[4] J.G. Rogers et al., IEEE Trans. Nucl. Sci. **NS–39** (1992) 1063

Performance Requirements for in-beam PET Scanners [B]

J. PAWELKE, W. ENGHARDT[1]

PET is regarded as an essential component for treatment plan verification as well as therapy monitoring in the experimental heavy ion tumour therapy unit at GSI [1], whereby five principal considerations appear important in the design of an in-beam PET scanner:

(1) The strictly 3D tumour conform treatment requires a positron camera which is capable of performing in-beam 3D tomography. For this purpose a positron camera consisting of two large-area detectors or an incomplete transaxial tomograph providing gaps for the therapy beam is well suited. Additionally a tomographic reconstruction algorithm specially developed for this limited angle PET application has to be implemented.
(2) Bismuth germanate (BGO) is the detector material of choice for PET today and can be operated at focused ion beams without any significant detector activation.
(3) The registration of the high background of γ-radiation which occurs during the particle extraction from the accelerator has to be suppressed in order to get PET images of appreciable quality acquired directly at the beam of high energetic heavy ions. However, a pulsed ion accelerator allows the detection of short-lived β^+-emitting isotopes with high efficiency during the irradiation in the pauses between particle extraction.
(4) Additionally to the detector properties the commercially support (e.g. hardware and software for on-line data analysing and reducing as well as methods of quality control) is of great importance for setup and operation of the tomograph in clinical use.
(5) A BGO based tomograph can perform the measurement of the endpoint of a β^+-emitting ion beam for an in-vivo treatment plan verification with an accuracy better than 1 mm. The maximum dose applied in the patient thereby is smaller than 10 mGy.

A tomograph which fulfils the requirements mentioned before has been built up at the FZR [2] and will be transferred to the GSI in autumn of 1995 and integrated in the treatment place according to the drawing shown in Fig.1.

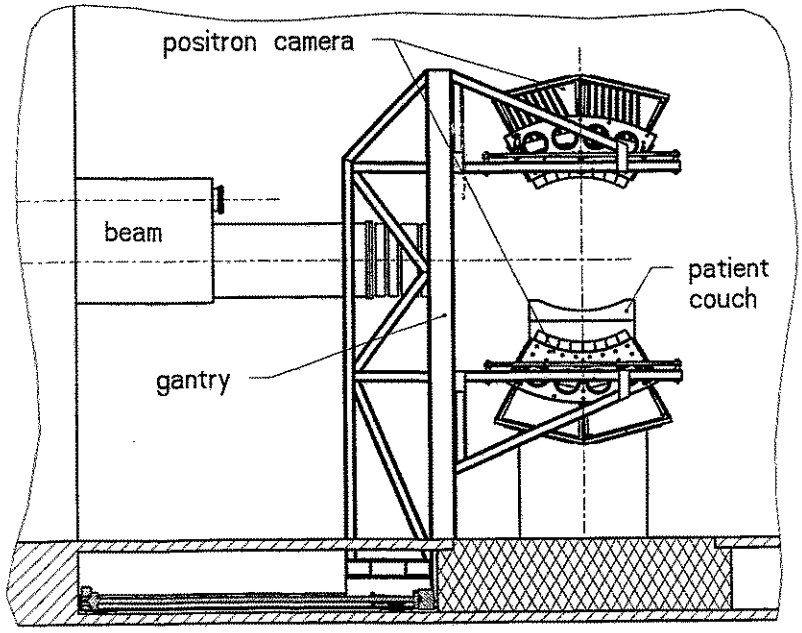

Fig. 1 *Treatment place at GSI Darmstadt.*

[1] *Uniklinikum der TU Dresden und Institut für Kern- und Hadronenphysik, FZR*

References

[1] G. Kraft, G. Gademann (eds.), Report **GSI-93-23**
[2] W. Enghardt et al, this Annual Report

The Gantry Movement Control of the PET Scanner at the GSI Therapy Unit [B]

R. HINZ, W. ENGHARDT [1] J. PAWELKE

The installation of the experimental heavy ion tumour therpy facility is in progress [1]. It includes the integration of a PET scanner for treatment plan verification as well as therapy monitoring [2]. The gantry of the PET scanner is moved by a linear axis driven by a stepping motor from a parking position to the measurement position and vice versa. An OS-9 computer controls the stepping motor. The acquisition of PET data takes place on the real time sorter, a SUN workstation system. That's why inter process communication over internet between the programs on these machines is necessary to coordinate the execution of the programs. This communication should be reliable and hardware independent, because the applications run under different operation systems and on different processors.

The preferred alternative to network applications using BSD sockets are Remote Procedure Calls (RPC) in connection with External Data Representation (XDR) standard [3] [4]. RPC implement a high-level client to server communication system designed to hide the details of the underlying network mechanisms. XDR is the standard for machine-independent description and encoding of data necessary for transferring data between different computer architectures.

A remote procedure call is very similar to an ordinary local procedure call. That is, the caller process sends a call message containing the parameters of the procedure to to the server process and waits for a reply message containing the results of the procedure. A RPC compiler helps programmer to write RPC applications simply and directly. It accepts the program interface definition written in RPC language, which is similar to C, and produces a C language output including a header file with common definitions, a server skeleton, a client stub and a file with the XDR filter routines for both parameter and results. The developer writes server procedures and links them with the server skeleton to get an executable server program. To create an excutable client program, the programmer writes an ordinary main program that makes local procedure calls and links it with the client stub.

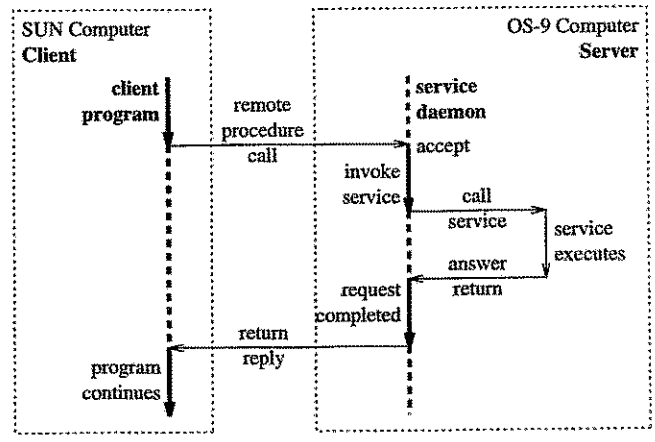

Fig. 1 *Network communiction with RPC*

[1] *Uniklinikum der TU Dresden und Institut für Kern- und Hadronenphysik, FZR*

References

[1] G. Kraft, G. Gademann (eds.), GSI Report **93-23**
[2] W. Enghardt et al., Phys. Med. Biol. **37** (1992) 2127
[3] Network Programming Guide, Sun Microsystems Inc. 1990
[4] The OS-9/OS-9000 NFS/RPC User's Manual, Microware Systems Corp. 1993

The Determination of Particle Ranges from β^+-Emitters Generated by Nuclear Fragmentation[B]

B.G. HASCH, W. ENGHARDT[1], L. SIHVER[2]

The depth-dose distribution of heavy ions in matter is characterized by the Bragg peak some tenth of a millimetre before the primary projectiles come to rest. The controlling of the heavy ion tumour therapy concerning the spatial dose deposition by means of positron emission tomography (PET) therefore requires the determination of the ranges of the primary projectiles from the range distribution of the β^+-active projectile fragments produced while relativistic heavy ions are stopped in matter. Our recent procedure for that purpose is based on a 3D Monte Carlo simulation including all essential physical processes in the successive modelling of the transport of heavy ions, positrons and annihilation photons through a target taking into consideration the characteristics of the measurement regime and photon detection. The refinement of the code described in [1] with changes in the stopping power calculation [2] and the parametrisation of the total and the partial fragmentation cross sections [3,4] is resulting in simulated range distributions which are in respect to the position of the peak of positron emitting projectile fragments and with regard to the shape in quite good agreement with the experimental data. Expecting the same relationship between the position and shape of the range distribution on one hand and the range of the primary projectiles on the other for the simulation and the experiment [6], the mean values of the peak of positron emitting projectile fragments for both distributions were calculated. Table 1 shows that this relatively simple procedure leads to a rather good prediction of the range of the primary projectiles in the experimental range distribution if the shift between the experimental and the simulated range distribution is taken into account.

System Proj.,Targ.	Energy MeV/u	Experiment Mean [mm]	Experiment Range [mm]	Simulation Mean [mm]	Simulation Range [mm]
^{20}Ne,PMMA	300	88.6±0.8	86.2±0.2	90.6±0.9	87.3±0.3
^{16}O,PMMA	330	124.0±0.7	127.3±0.3	126.0±0.8	128.9±0.5
^{12}C,Graphit	270	82.8±0.9	88.2±0.3	82.8±0.8	88.0±0.5

Table 1: *Comparison of the mean value for the peak of positron emitting projectile fragments in the experimental and simulated range distribution. The range of the primary projectiles and its error which are associated with the experiment are calculated with the stopping code ATIMA [5], whereas the range in the simulation is based on the Salamon stopping code [2].*

[1] *Uniklinikum der TU Dresden und Institut für Kern- und Hadronenphysik, FZR*
[2] *GSI Darmstadt*

References

[1] B.G. Hasch, W. Enghardt, Annual Report 1993, **FZR-35**(1994)116
[2] W. Heinrich et al., GSI Preprint **91-30** (1991)
[3] L. Sihver et al., Phys. Rev. **C47** (1993) 1225
[4] L. Sihver, to be published.
[5] Th. Schwab, Ph.D. Thesis, GSI-Report **91-10** (1991)
[6] W. Enghardt et al., Annual Report 1993, **FZR-35**(1994)114

The Implementation of an Iterative Reconstruction Scheme to Limited Angle Positron Cameras [B]

K. LAUCKNER, W. ENGHARDT[1], J. PAWELKE, M. SOBIELLA

The on-line treatment plan verification of the heavy ion tumour therapy can be performed by the technique of positron emission tomography [1]. In order to investigate the imaging properties of a limited angle positron camera under the special conditions of a very high γ-radiation background directly at a relativistic heavy ion beam, a step motor driven handling system (simulator) [2] has been installed behind the fragment separator at the Gesellschaft für Schwerionenforschung.

The limited angle 3D reconstruction algorithm [3] that has been originally developed for reconstructing positron emitter distributions measured in-beam by means of a positron camera of large area high density avalanche chambers, has been adopted to the simulator. Mainly the calculation of the 3D-backprojections from the measured coincidence data and the iterated solutions requires necessary modifications. According to the detector movement in a first step the backprojection is constructed in the frame rotated by an angle ϕ with respect to the fixed frame of the image space and in a second step the backprojected distribution is transformed into the image space. The 3D-matrix obtained as a result of the superposition of the backprojections from all detector positions is the basis for applying the algorithm [3].

The reconstruction algorithm has been applied to measurements of a ^{22}Na point sources of 2mm diameter and 380 kBq activity. In Fig.1 the projections of the radioactivity distribution onto the axis of one of the reconstructed results are shown. The spatial resolution (FWHM) in dependence on the number of iterations is analyzed by a Gaussian fit.

At present the algorithm is implemented to the double-head positron camera which is built up from two detector heads each consisting of 8x4 detector blocks.

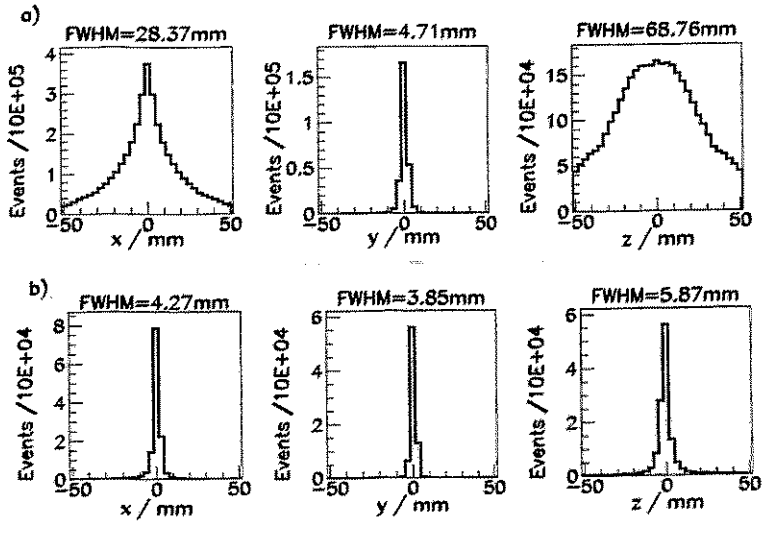

Fig. 1 *Results of the reconstruction for point source. a) 0. solution of iteration, b) reconstruction after 50 steps of iteration*

[1] *Uniklinikum der TU Dresden und Institut für Kern- und Hadronenphysik, FZR*

References

[1] Llacer J., Nucl. Sci. Appl. 3(1988)111
[2] Pawelke J. et al, Annual Report FZR(1992)142
[3] Enghardt W. et al, Phys. Med. Biol., 37(1992)791

Particle identification in a wide dynamic range based on pulse-shape analysis with solid-state detectors
(Nucl. Instr. Meth. in Phys. Rev. A349 (1994) 281)

Pausch, G., W. Bohne, D. Hilscher, H.-G. Ortlepp, D. Polster

Abstract: Heavy ions detected in a planar silicon detector were identified by exploiting a recently proposed combination of the pulse-shape and the time-of-flight techniques. We were able to resolve charge numbers up to $Z = 16$ within a wide dynamic range of $\approx$ 1:5, and to identify even isotopes for the elements up to magnesium. The simple scheme of signal processing is based on conventional electronics and cheap enough to be exploited in large multidetector arrays.

Particle identification in solid-state detectors by means of pulse-shape analysis - results of computer simulations
(Nucl. Instr. Meth. in Phys. Rev. A337 (1994) 573)

Pausch, G., W. Bohne, D. Hilscher

Abstract: A simple semi-empirical model has been used to simulate pulse shapes in silicon detectors for heavy-ion spectroscopy. The model describes qualitatively the results of a previous experiment which was performed to study the feasibility of pulse-shape analysis for identifying intermediate-mass fragments in single silicon detectors. The observed limits of the dynamic range for particle identification can be understood within the model. These limitations are predicted to be overcome by injecting the ions into the rear side of a totally depleted detector, and by combining the time-of-flight and the pulse-shape techniques to establish a new scheme of signal processing. With this technique. Z identification should be possible down to 0.5 AMeV for ions with mass numbers $A \leq 30$.

II Publications and Talks

1 Publications

Andronenko, L.N., M.N. Andronenko, A.A. Kotov, W. Neubert, D.M. Seliverstov, I.I. Strakovsky and L.A. Vaishnene:
Isotopic ratios of intermediate mass fragments produced in p + A reactions at 1 GeV;
Z. Phys.A350 (1994) 1

Baldsiefen, G., H. Hübel, W. Korten, D. Mehta, N. Nenoff, B.V.Thirumala Rao, P. Willsau, H. Grawe, J. Heese, H. Kluge, K.H. Maier, R. Schubart, S. Frauendorf and H.J. Maier:
"Shears bands" in ^{199}Pb and ^{200}Pb;
Nucl. Phys. A574 (1994) 521

Barz, H.W., G.F. Bertsch, P. Danielewicz, H. Schulz and G.M. Welke:
Transport treatment of an expanding pion gas in ultrarelativistic heavy ion collisions;
in "Hot and dense nuclear matter"; eds. W. Greiner, H. Stöcker and A. Gallmann, Plenum Publ. Cooperation, New York, 1994, p. 687

Barz, H.W., B.L. Friman, J. Knoll and H. Schulz:
Flavour-kinetic model for particle production in ultra-relativistic heavy-ion collisions;
in "Statistical Description of Transport in Plasma, Astro- and Nuclear Physics, Edt. J. Misquich, G. Pelletier and P. Schuck, Nova Science Publishers, Inc., 1994, p. 407

Bratkovskaya, E.L., B. Kämpfer, A.V. Molochkov, B.L. Reznik, A.I. Titov:
Hadron sources of the lepton pair production in proton-deuteron interaction at the initial energies 1-5 GeV;
Yad. Fiz. 57 (1994) 924

Bratkovskaya, E.L., A.I. Titov, B. Kämpfer:
Dielectron production as a probe for nuclear exotic states and nuclear interactions at intermediate energies:
in "Hadrons and Nuclei from QCD", edited by K. Fujii et al., p. 1
World Scientific Singapore - New Jersey - London - Hong Kong (1994)

Brockstedt, A., J. Lytkens-Lindén, M. Bergström, L.P. Eckström, H. Ryde, J.C. Barcelar, J.D. Garrett, G.B. Hagemann, B. Herskind, F.R. May, P.O. Tjom, S. Frauendorf:
Interpretation of bands in ^{163}Er within the tilted rotation scheme;
Nucl. Phys. A571 (1994) 337

Dittes, F.-M., E. Doron and U. Smilansky:
Long-time behavior of the semiclassical baker's map;
Phys. Rev. E49 (1994) R963

Döring, J., R. Schwengner, L. Funke, H. Rotter, G. Winter, B. Cederwall, F. Lidén, A. Johnson, A. Atac, J. Nyberg and G. Sletten:
High-lying three-quasiparticle bands and signature splitting in ^{81}Rb;
Phys. Rev. C50 (1994) 1845

Fomichev, A.S., I. David, S.M. Lukyanov, Yu.E. Penionzhkevich, N.K. Skobelev, O.B. Tarasov, A. Matthies, H.-G. Ortlepp, W. Wagner, M. Lewitowicz, M.G. Saint-Laurent, J.M. Corre, Z. Dlauhy, I. Pecina, C. Borcea:

The response of a large CsI(Tl) detector to light particles and heavy ions in the intermediate energy range;
Nucl. Instr. Meth. in Phys. Res. A344 (1994) 378

Frauendorf, S., A. Sheikh, N. Rowley:
Consequences of neutron-proton interaction on backbending;
Phys. Rev. C50 (1994) 196

Heide, B. and H.W. Barz:
Effects of flow on intermediate mass fragments in central gold on gold collisions;
Phys. Lett. B337 (1994) 53; Erratum Phys. Lett. B340 (1994) 267

Hensel, F., W. Enghardt, H.M. Prasser:
Verfahren zur Messung der integralen Massenfeuchte in Zweiphasenströmungen;
Patentschrift P4423665.4, Deutsches Patentamt, 7. Juli 1994

Hsi, W.C., G.J. Kunde, J. Pochodzalla, W.G. Lynch, M.B. Tsang, M.L. Begemann-Blaich, D.R. Bowman, R.J. Charity, F. Cosmo, A. Ferrero, C.K. Gelbke, T. Glasmacher, T. Hofmann, G. Imme, I. Iori, J. Hubele, J. Kempter, P. Kreutz, W.D. Kunze, V. Lindenstruth, M.A. Lisa, U. Lynen, M. Mang, A. Moroni, W.F.J. Müller, M. Neumann, B. Ocker, C.A. Ogilvie, G.F. Peaslee, G. Raciti, F. Rosenberger, H. Sann, R. Scardaoni, A. Schüttauf, C. Schwarz, W. Seidel, V. Serfling, L.G. Sobotka, L. Stuttge, S. Tomasevic, W. Trautmann, A. Tucholski, C. Williams, A. Wörner and B. Zwieglinski:
Collective expansion in central Au + Au collisions;
Phys. Rev. Lett. 73 (1994) 3367

Iskra, W., M. Müller and I. Rotter:
Selforganization in the nuclear system: II. Formation of a new order;
J. Phys. G20 (1994) 775

Iskra, W., M. Müller and I. Rotter:
Selforganization in the nuclear system and irreversibility;
Progress of Theoretical Physics, Suppl. 116 (1994) 385

Jenkovszky, L.L., B. Kämpfer, V.M. Sysoev:
Bubble free energy in a first-order phase transition;
Yad. Fiz. 57 (1994) 187

Jeong, S.C., N. Herrmann, Z.G. Fan, R. Freifelder, A. Gobbi, K.D. Hildenbrand, M. Krämer, J. Randrup, W. Reisdorf, D. Schüll, U. Sodan, K. Teh, J.P. Wessels, D. Pelte, M. Trzaska, T. Wienold, J.P. Alard, V. Amouroux, Z. Basrak, N. Bastid, I.M. Belayev, L. Berger, M. Bini, Th. Blaich, S. Boussange, A. Buta, R. Caplar, C. Cerruti, N. Cindro, J.P. Coffin, R. Dona, P. Dupieux, J. Erö, P. Fintz, Z. Fodor, L. Fraysse, S. Frolov, Y. Grigorian, G. Guillaume, S. Hölbling, A. Houari, F. Jundt, J. Kecskemeti, P. Koncz, Y. Korchagin, R. Kotte, C. Kuhn, M. Ibnouzahir, I. Legrand, A. Lebedev, C. Maguire, V. Manko, P. Maurenzig, G. Mgebrishvili, J. Mösner, D. Moisa, G. Montarou, I. Montbel, P. Morel, W. Neubert, A. Olmi, G. Pasquali, M. Petrovici, G. Poggi, F. Rami, V. Ramillien, A. Sadchikov, Z. Seres, B. Sikora, V. Simion, S. Smolyankin, R. Tezkratt, M.A. Vasiliev, P. Wagner, Z. Wilhelmi, D. Wohlfarth and A.V. Zhilin:

Collective motion in selected central collisions of Au on Au at 150 AMeV;
Phys. Rev. Lett. 72 (1994) 3468

Kämpfer, B., P. Koch, O.P. Pavlenko:
Dynamics of an expanding dense pion gas and low-mass dilepton emission;
Phys. Rev. C49 (1994) 1132

Kämpfer, B., B. Lukács, G. Paál:
Cosmic phase transitions;
Teubner-VerlagStuttgart-Leipzig (1994)
TEUBNER-TEXTE zur Physik, Band 29 (1994)

Kämpfer, B., O. P. Pavlenko:
Probing early parton kinetics by photons, dileptons and charm;
Nucl. Phys. A566 (1994) 351c

Kämpfer, B., O.P. Pavlenko:
Transverse momentum dependence of dileptons from parton matter produced in ultrarelativistic heavy-ion collisions;
Phys. Rev. C49 (1994) 2716

Kämpfer, B., O.P. Pavlenko:
Photon production in an expanding and chemically equilibrating gluon-enriched plasma;
Z. Phys. C62 (1994) 491

Kaptari, L.P., K.Yu. Kazakov, AYu. Umnikov, B. Kämpfer:
The spin-dependent deuteron structure function within an effective meson-nucleon theory;
Phys. Lett. B321 (1994) 271

Lips, V., R. Barth, H. Oeschler, S.P. Avdeyev, V.A. Karnaukhov, W.D. Kuznetsov, L.A. Petrov, O.V. Bochkarev, L.V. Chulkov, E.A. Kuzmin, W. Karcz, W. Neubert and E. Norbeck:
Multifragmentation induced by relavistic alpha-projectiles;
Phys. Rev. Lett. 72 (1994) 1604

Lips, V., R. Barth, H. Oeschler, S.P. Avdeyev, V.A. Karnaukhov, W.D. Kuznetsov, L.A. Petrov, O.V. Bochkarev, L.V.Chulkov, E.A. Kuzmin, W. Karcz, W. Neubert, E. Norbeck, D.H.E. Gross:
Evidence for simultaneous breakup in reactions with relativistic α-projectiles;
Phys. Lett. B338 (1994) 141

Müller, D., D. Robaschik, B. Geyer, F.-M. Dittes and J. Horejsi:
Wave functions, evolution equations and evolution kernels from light-ray operators of QCD;
Fortschritte der Physik 42 (1994) 101

Müller, M., I. Rotter and W. Iskra:
Selforganization and disorder in an open quantum system;
Acta Physica Polonica 25 (1994) 711

Oliveira, J.R.B., S. Frauendorf, M.A. Deleplanque, B. Cederwall, R.M. Diamond, A.O. Macchiavelli, F.S. Stephens, J. Burde, J.E. Draper, C. Duyar, E. Rubel, J.A. Becker, E.A. Henry, M.J. Brinkman, A. Kuhnert, M.A. Stoyer, T.F. Wang:
High-K bands in the ^{168}Yb region;
Phys. Rev. C50 (1994) 1360

Pausch, G., W. Bohne, D. Hilscher:
Particle identification in solid-state detectors by means of pulse-shape analysis - results of computer simulations;
Nucl. Instr. and Meth. in Phys. Research A337 (1994) 573

Pausch, G., W. Bohne, D. Hilscher, H.-G. Ortlepp, D. Polster:
Particle identification in a wide dynamic range based on pulse-shape analysis with solid-state detectors;
Nucl. Instr. and Meth. in Phys. Research A349 (1994) 281

Pawelke, J.:
Beiträge zum Einsatz der Positronen-Emissions-Tomographie in der Leichtionen-Tumortherapie;
Dissertation, TU Dresden, 1994

Peshier, A., B. Kämpfer, O.P. Pavlenko, G. Soff:
An effective model of the quark-gluon plasma with thermal parton masses;
Phys. Lett. B 337 (1994) 235

Peter, A., W. Cassing, J.M. Häuser, A. Pfitzner:
Microscopic analysis of two-body correlations in light nuclei;
Nucl. Phys. A573 (1994) 93

Pfitzner, A., W. Cassing, A. Peter:
Vibrations versus collisions and the iterative structure of two-body dynamics;
Nucl. Phys. A577 (1994) 753

Trautmann, W., J.C. Adloff, M. Begemann-Blaich, P. Bonission, J. Hubele, G. Imme, I. Iori, P. Kreutz, G.J. Kunde, S. Leray, V. Lindenstruth, Z. Lin, U. Lynen, R.J. Meijer, U. Milkau, A. Moroni, W.F.J. Müller, C. Ngo, C.A. Ogilvie, J. Pochodzalla, G. Raciti, G. Rudolf, H. Sann, A. Schüttauf, W. Seidel, L. Stuttge and A. Tucholski:
Multifragmentation in peripheral nucleus-nucleus collisions;
Acta Physica Polonica B25 (1994) 425

Winter, G., R. Schwengner, J. Reif, H. Prade, J. Döring, R. Wirowski, N. Nicolay, P. von Brentano, H. Grawe and R. Schubart:
Excited states built on the 6^- isomer in $^{86}_{37}Rb_{49}$;
Phys. Rev. C49 (1994) 2427

Wünsch, R., K. Goeke, Th. Meißner:
On size and shape of the average meson fields in the semi-bosonized Nambu & Jona-Lasinio model;
Z. Phys. A348 (1994) 111

2 Conference Contributions and Research Reports

Aleksandrov, A.A., I.A. Aleksandrova, M. Andrassy, L. Dietterle, V.N. Doronin, P. Gippner, C.-M. Herbach, D. Hilscher, S.I. Ivanovskij, A. Matthies, D. May, H.-G. Ortlepp, G. Pausch, Yu.E. Penionzhkevich, V.N. Pokrovskij, G. Renz, K.D. Schilling, D.I. Shishkin, V.E. Shuchko, O.V. Strekalovskij, V.V. Trofimov, C. Umlauf, D.V. Vakatov, V. M. Vasko, W. Wagner:
First experiments with FOBOS;
Poster, 5th Int. Conf. on Nucleus-Nucleus Collisions, Taormina, Italy, May/Jun. 1994

Andrassy, M., L. Dietterle, V.N. Doronin, P. Gippner, K. Heidel, C.-M. Herbach, D. Hilscher, S.A. Ivanovskij, J. Krüger, A. Matthies, D. May, H.-G. Ortlepp, G. Pausch, Yu.E. Penionzhkevich, G. Renz, K.D. Schilling, D.I. Schischkin, V.E. Shuchko, O.V. Strekalovskij, V.V. Trofimov, C. Umlauf, D.V. Vakatov, V.M. Vasko, W. Wagner, T. Wilpert:
Analyse von leichten, intermediären und Spaltfragmenten in der Reaktion ^{7}Li (43 AMeV) + ^{232}Th mit dem Multidetektorsystem FOBOS;
Verhandlungen der DPG 6 (1994) 1888

Andronenko, L.N., M.N. Andronenko, L.A.Vaishnene, Y.I. Gusev, A.A. Kotov, K.V. Lukashin, W. Neubert, D.M. Seliverstov and I.I. Strakovsky:
Formation of intermediate mass fragments on targets of Au, Ag, Ni and Al by 1 GeV protons (in russian);
Preprint NP-38-94, St. Petersburg Nuclear Physics Institute, Gatchina

Barz, H.W. and B. Heide:
Effects of anisotropic flow on the velocity correlations of intermediate mass fragments;
Proc. Int. Workshop on Gross Properties of Nuclei and Nuclear Excitations XXII, Hirschegg, Austria, Jan. 1994, (ed.) H. Feldmeier, p. 119

Begemann-Blaich, M. and W. Trautmann for the ALADIN/LAND/Miniball and ALADIN/LAND Collaborations:
Multifragmentation at relativistic energies: new results from ALADIN;
GSI-Nachrichten, GSI 05-94, p. 4-18

Botwina, A.S., I.N. Mishustin, M. Begemann-Blaich, T. Hofmann, J. Hubele, G. Imme, I. Iori, P. Kreutz, W.D. Kunze, V. Lindenstruth, U. Lynen, A. Moroni, W.F.J. Müller, C.A. Ogilvie, J. Pochodzalla, G. Raciti, H. Sann, A. Schüttauf, W. Seidel, W. Trautmann, A. Wörner:
Multifragmentation of spectators in relativistic heavy-ion reactions;
GSI-94-36, Preprint, June 1994

Brandt, U., K. Daumüller, D. Doll, H.O. Klages, P. Kleinwächter, G. Kolb and P. Manfraß:
Cosmic ray tracking by streamer tubes;
Verhandlungen der DPG 6 (1994) 1934

Brandt, U., K. Daumiller, P. Doll,, R. Gumbsheimer, H. Hucker, H.O. Klages, P. Kleinwächter, G. Kolb and J. Lang:
Untersuchungen zur Streifenauslese und zur Detektorstabilisierung von Streamertube-Detektoren für das KASCADE-Experiment;
Verhandlungen der DPG 6 (1994) 1934

Büscher, M., W. Cassing, A. Franzen, B. Kamys, V.I. Komarov, V. Koptev, S. Kopyto, H. Müller, M. Nioradze, O.W.B. Schult, A. Sibirtsev and K. Sistemich:
Investigation of subthreshold K^+ production in p + A reactions with the 0° facility at COSY Jülich;
Proc. Int. Conf. on Mesons and Nuclei at Intermediate Energies, Dubna, Russia, May 1994

Büscher, M., W. Cassing, B. Kamys, V.I. Komarov, V. Koptev, H. Müller, A. Sibirtsev, K. Sistemich:
Investigation of nuclear medium effects on elementary-particle reactions with the 0° facility at COSY-Jülich;
Proc. Int. Conf. on Physics with GeV - Particle Beams, Jülich, Aug. 1994

Cassing, W.,A. Franzen, B. Kamys, V.I.Komarov, V. Koptev, S. Kopyto, H. Müller, M. Nioradze, O.W.B. Schult, A. Sibirtsev, K. Sistemich:
Investigation of subthreshold K^+ production in p+A reactions with the 0° facility at COSY-Jülich;
Proc. Int. Conf. on Mesons and Nuclei at Intermediate Energies, Dubna, Russia, May 1994

Dittes, F.M.:
Transfer operator description of semiclassical maps;
Poster, Int. Symposium "Chaos and Mesoscopic Systems", Dresden, Jun. 1994

Dittes, F.M.:
New results on the semiclassical baker's map;
Poster and Proceedings: Workshop on Applications of Chaos in Many-Body Quantum Physics, Seattle, USA, Jun. 1994

Dittes, F.M., E. Doron und U. Smilansky:
Neue Ergebnisse zur semiklassischen Bäcker-Abbildung: Unitaritätsverletzung, Langzeitverhalten und Korrelationen klassischer Wirkungen;
Verhandlungen der DPG 6 (1994) 551

Dönau, F., P. von Brentano, S. Frauendorf, A. Gelberg and O. Vogel:
Tilted axis cranking description of four quasi-particle bands in Xe- and Ba-nuclides;
Proc. Int. Conf. on Physics from Large γ-ray Detector Arrays, Berkeley, USA, Aug. 1994, Vol. I, p. 152

Dönau, F., S. Frauendorf, O. Vogel, A. Gelberg, P. von Brentano:
Rotationsbanden mit geneigter Spinorientierung in geraden Xe- und Ba-Kernen;
Verhandlungen der DPG 6 (1994) 1941

Enghardt, W., B.G. Hasch, P. Manfraß, J. Pawelke, M. Sobiella, P. Blochberger, A. Friedrich, H. Geißel, H. Irnich, G. Kraft, A. Magel, W. Menfels, G. Münzenberg, F. Nickel, K. Popppensieker, I. Schall, D. Schardt, C. Scheidenberger, B. Voss, C. Ziegler:
PET for treatment plan verification and beam monitoring in light ion tumour therapy;
Proc. Int. Symp. on Heavy Ion Research: Space, Radiation Protection and Therapy, Sophia-Antipolis, France, Mar. 1994, p. 27

Eßer, R., K. Meyer, B. Veronik, H. Ohm, H. Seyfahrt, B. Prietzschk, B. Rimarzig, H. Müller:
Startdetektoren für das Flugzeitsystem der 0°-Facility an COSY;
Verhandlungen der DPG 6 (1994) 1818

Frauendorf, S., J. Meng, J. Reif:
Tilted cranking;
Preprint FZR-59 (1994)

Frauendorf, S.:
The decline of K-forbiddeness;
Proc. of the Int. Conf. on the Future of Nuclear Spectroscopy, Crete, Jun./Jul. 1993, Invited Lectures, ed. W. Gelletly, C. A. Kalfas, R. Vlastou, S. Harissopulos and D. Loukas, I. N. P., National Center for Scientific Research Domokritos, Athens, Greece, 1994, p. 111

Frauendorf, S., V.V. Pashkevich, S.M. Reimann:
Magnetic properties of sodium clusters;
Poster, ISSPIC 7, Seventh International Symposium on Small Particles and Inorganic Clusters, Kobe, Japan, Sep. 1994

Frauendorf, S., V.V. Pashkevich:
Shapes and free energies of molten sodium clusters;
Poster, ISSPIC 7, Seventh International Symposium on Small Particles and Inorganic Clusters, Kobe, Japan, Sep. 1994

Frauendorf, S., S.M. Reimann:
Potential energy surfaces of sodium clusters with quadrupole, hexadecapole and axially asymmetric deformations;
Poster, ISSPIC 7, Seventh International Symposium on Small Particles and Inorganic Clusters, Kobe, Japan, Sep. 1994

Gabriel, F., P. Michel:
Entwicklung eines TDC mit extrem kleiner Totzeit für schnelle Triggerprozesse;
Preprint FZR-30 (1994)

Gabriel, F., P. Michel, K. Möller, A. Schamlott, A. Schülke:
A real time to digital converter (RTDC) for on-line position measurement applied to the COSY-TOF stop detector;
Annual Report 1993, Jül-2879, KFA Jülich, IKP, 21

Gumalov, T.I., A.I. Titov, B. Kämpfer:
Neutral ρ meson properties in an isospin-asymmetric pion medium;
FZR-66 (1994)

Hasch, B.G., P. Manfraß, J. Pawelke, M. Sobiella, W. Enghardt, P. Blochberger, A. Friedrich, H. Geissel, H. Irnich, G. Kraft, A. Magel, W. Meufels, G. Münzenberg, F. Nickel, K. Poppensieker, I. Schall, D. Schardt, C. Scheidenberger, B. Voss, C. Ziegler:
PET for treatment plan verification and beam monitoring in light ion tumour therapy;
Poster, Proc. XI. Int. Conf. on Computers in Radiation Therapy, Manchester, Great Britain, Mar. 1994, p. 364

Hasch, B.G., K. Lauckner, P.Manfraß, J. Pawelke, M. Sobiella, W. Enghardt, H. Geissel, D. Schardt, L. Byars:
A positron camera for heavy ion therapy control;
Book of Abstracts, EORTC Heavy Particle Therapy Group Meeting, Heidelberg, Oct. 1994

Heide, B. and H.W. Barz:
Effects of flow on intermediate mass fragments in central gold on gold collisions;
FZR-Report 41 (1994)

Hilscher, D., W. Bohne, P. Figuera, H. Fuchs, F. Goldenbaum, U. Jahnke, D. Polster, H. Rossner, P. Ziem, J. Galin, B. Lott, M. Morjean, A. Peghaire, B. Quednau, T. von Egidy, F.J. Hartmann, S. Schmid, W. Schmid, K. Gulda, J. Jastrzebski, W. Kurcewicz, L. Pienkowski, G. Pausch, S. Proschitzki, J. Eades, S. Neumaier, Ye.E. Golubeva, A.S. Iljinov, D.I. Ivanov, V.G. Nedorezov, I.A. Pshenichov and A.S. Sudov:
First results on the decay of hot nuclei at low spin (PS 208);
Invited contribution to the LEAP'94,
Third Biennial Conference on Low-Energy Antiproton Physics, Bled, Slovenia, Sep. 1994

von Horn, L., D. Gotta, H. Ohm, K. Sistemich, Chr. Schneider, H. Müller, V. Kruglov:
Eine Vieldrahtproportionalkammer für den Einsatz an der 0°-Facility an COSY;
Verhandlungen der DPG 6 (1994) 1819

Hsi, W.C., G.J. Kunde, J. Pochodzalla, W.G. Lynch, M.B. Tsang, M.L. Begemann-Blaich, D.R. Bowman, R.J. Charity, A. Cosmo, A. Cosmo, A. Ferrero, C.K. Gelbke, T. Glasmacher, T. Hofmann, J. Hubele, G. Imme, I. Iori, J. Kempter, P. Kreutz, W.D. Kunze, V. Lindenstruth, M.A. Lisa, U. Lynen, M. Mang, A. Moroni, W.F.J. Müller, M. Neumann, B. Ocker, C.A. Ogilvie, G.F. Peaslee, G. Raciti, F. Rosenberger, H. Sann, R. Scardaoni, A. Schüttauf, C. Schwarz, W. Seidel, V. Serfling, L.G. Sobotka, L. Stuttge, W. Trautmann, A. Tucholski, C. Williams, A. Wörner and B. Zwieglinski:
Collective expansion in central Au+Au collisions;
Preprint Michigan State University, MSUCL-930, May 1994

Hübel, H., M. Neffgen, G. Baldsiefen, W. Korten, D. Mehta, N. Nenoff, U.J. van Severen, H. Grawe, H. Kluge, K.H. Maier, A. Korichi, M. Piiparinen, Jie Meng and S. Frauendorf:
Lifetimes of shears bands in ^{199}Pb;
Conf. on Physics on Large γ-Ray Detector Arrays, Berkeley, USA, Aug. 1994

Iskra, W., M. Müller and I. Rotter:
Radial pattern of nuclear decay processes;
Preprint FZR-39 (1994)

Iskra, W., M. Müller und I. Rotter:
Zeitskalen in Kernreaktionen;
Gruppenbericht, Verhandlungen der DPG 6 (1994) 1812

Iskra, W., M. Müller und I. Rotter:
Sättigung der Riesenresonanzstärke im Bereich sehr hoher Niveaudichte;
Verhandlungen der DPG 6 (1994) 1807

Iskra, W., M. Müller and I. Rotter:
The interplay of different time scales at high excitation energy;
2nd Int. Seminar on Interaction of Neutrons with Nuclei, Dubna, Russia, Apr. 1994, p. 20

Iskra, W., M. Müller and I. Rotter:
Selforganization and chaos in the nuclear system;
Applications of Chaos in Many-Body Quantum Physics, Seattle, USA, Jun. 1994

Jaeckle, V., Ch. Nake, K. Kilian, H. Machner, L. Naumann, P. Turek:
Weiterentwicklung des Flüssig-Deuteriumtargets mit extrem dünnen Folienfenstern;
Verhandlungen der DPG 6 (1994) 1798

Kämpfer, B., R. Kotte, J. Mösner, W. Neubert, D. Wohlfarth:
Velocity correlations of intermediate fragments produced in central collisions of Au on Au at 150, 250 and 400 AMeV: A key to space-time structure of fragmenting source;
Proc. Int. Workshop XXII, Hirschegg, Austria, Jan. 1994, p. 113

Kämpfer, B., O.P. Pavlenko, M.I. Gorenstein, A. Peshier, G. Soff:
Rapidity dependence of thermal dileptons resulting from hadronizing quark-gluon matter with finite baryon charge;
FZR-50 (1994)

Kaptari, L.P., A.Yu. Umnikov, F.C. Kahana, B. Kämpfer:
The tensor analyzing power T_{20} in deuteron break-up reactions within the Bethe-Salpeter formalism;
FZR-64 (1994)

Käubler, L., H. Prade, J. Reif, R. Schwengner, G. Winter, H. Grawe, J. Hesse, H. Kluge, K.-H. Maier, R. Schubart and K.-M. Spohr:
In-beam investigation of ^{109}Sn;
Verhandlungen der DPG 6 (1994) 1860

Käubler, L., H. Prade, J. Reif, R. Schwengner, G. Winter, H. Grawe, J. Hesse, H. Kluge, K.-H. Maier, R. Schubart and K.-M. Spohr:
In-beam investigation of ^{109}Sn;
Poster, Symposium on New Structure Phenomena in the Vicinity of Closed Shells, Stockholm-Uppsala, 1994

Kolomeizev, E. E., D.N. Voskresensky, B. Kämpfer:
Kaon polarization in nuclear matter;
Preprint FZR-40 (1994)

Komarov, V.I., A.Yu. Petrus, H. Müller:
Excitation of few-nucleon systems accompanied by "meson cooling";
Poster, Int. Conf. on Physics with GeV - Particle Beams, Jülich, Aug. 1994

Kotte, R., B. Kämpfer, J. Mösner, W. Neubert, D. Wohlfarth et al. (FOPI Collaboration):
Interplay of collective flow phenomena and velocity correlations of intermediate-mass fragments in collisions of Au + Au at E = 100-400 MeV;
Preprint FZR-56 (1994)

Kotov, A.A., L.N. Andronenko, M.N. Andronenko, Y.I. Gusev, K.V. Lukashin, W. Neubert, D.M. Seliverstov, I.I. Strakovsky and L.A.Vaishnene:
Target mass dependence of intermediate mass fragment production at 1 GeV proton-induced nuclear reaction;
Preprint NP-38-94, St. Petersburg Nuclear Physics Institute, Gatchina

Krüger, J., A. Budzanowski, H. Fuchs, C.-M. Herbach, D. Hilscher, H. Homeyer, D. Kamanin, A. Matthies, H.-G. Ortlepp, G. Pausch, W. Seidel, V. Shuchko, A. Siwek, V. Trofimov, A. Tutay, W. Wagner, R. Wolski, L. Zrodlowski:
Untersuchung der Projektilfragmentation und IMF-Emission im System ^{32}S (960 MeV) + ^{197}Au am erweiterten ARGUS-Detektor;
Verhandlungen der DPG 6 (1994) 1945

Kunde, G.J., W.C. Hsi, W.D. Kunze, A. Schüttauf, A. Wörner, M. Begemann-Blaich, Th. Blaich, D.R. Bowman, R.J. Charity, A. Cosmo, A. Ferrero, C.K. Gelbke, J. Hubele, G. Imme, I. Iori, P. Kreutz, V. Lindenstruth, M.A. Lisa, W.G. Lynch, U. Lynen, M. Mang, A. Moroni, W.F.J. Müller, M. Neumann, B. Ocker, C.A. Ogilvie, G.F. Peaslee, J. Pochodzalla, G. Raciti, T. Rubehn, H. Sann, W. Seidel, V. Serfling, L.G. Sobotka, J. Stroth, L. Stuttge, W. Trautmann, M.B. Tsang, A. Tucholski, G. Verde, C.W. Williams, E. Zude and B. Zwieglinski:
Fragment flow and the multifragmentation phase space;
GSI-94-46, Preprint, Aug. 1994

Michel, P., K. Möller, A. Schamlott, A. Schülke and the COSY-TOF collaboration:
Tests of the COSY-TOF start detektor MARS with electrons and 13 MeV protons;
Annual Report 1993, Jül-2879, KFA Jülich, IKP, 15

Michel, P., K. Möller, A. Schamlott, A. Schülke and the TOF-collaboration:
Investigation of light-readout straight scintillating stripes for the COSY-TOF stop detector;
Annual Report 1993, Jül-2879, KFA Jülich, IKP, 19

Müller, H.:
Statistical description of hadronic and nuclear interactions at medium energies;
Proc. Int. Conf. on Physics with GeV - Particle Beams, Jülich, Aug. 1994

Naumann, B. und L. Naumann:
Überlegungen zur Entwicklung eines Schauerdetektors am COSY-TOF-Spektrometer zum Nachweis der Photonen aus der Proton-Proton-Bremsstrahlung (Teil I);
Preprint: COSY-TOF-NOTES 2-R0-94

Neubert, W., H.W. Barz, R. Kotte, J. Mösner, D. Wohlfarth:
The reaction Au+Au at 150 A*MeV simulated by the Copenhagen statistical multifragmentation model,
Proceedings of the XXXII Int. Winter Meeting on Nuclear Physics, Bormio, Italy, Jan. 1994, p. 116

Pausch, G., W. Bohne, D. Hilscher, H.-G. Ortlepp, D. Polster:
Weiterentwicklung der Impulsformmethode zur Identifikation schwerer Ionen in Halbleiterdetektoren;
Verhandlungen der DPG 6 (1994) 1883

Pausch, G., W. Bohne, D. Hilscher, H.-G. Ortlepp, D. Polster:
Particle identification in a wide dynamic range based on pulse-shape analysis with solid-state detectors;
Preprint FZR-38 (1994)

Pawelke, J., B.G. Hasch, K. Lauckner, P. Manfraß, M. Sobiella, W. Enghardt, P. Blochberger, A. Friedrich, H. Geissel, H. Irnich, G. Kraft, A. Magel, W. Meufels, G. Münzenberg, F. Nickel, K. Poppensieker, I. Schall, D. Schardt, C. Scheidenberger, B. Voss, C. Ziegler:
In-beam PET imaging with different detectors;
Proc. Int. Conf. on Heavy Ion Research: Space, Radiation Protection and Therapy, Sophia-Antipolis, France, Mar. 1994, p. 26

Petrovici, M., D. Pelte, N. Herrmann, J. Ritman and the FOPI-Collaboration:
FOPIs route towards hot and dense nuclear matter;
GSI-Nachrichten, GSI 08-94, p. 3

Pfitzner, A., W. Cassing, A. Peter:
Competition of short- and long-range correlations in nuclear damping;
Proc. 7th International Conference on Nuclear Reaction Mechanisms, Varenna, Italy, Jun. 1994, p. 335

Pyatkov, Yu. V., A.A. Aleksandrov, I.A. Aleksandrova, B.I. Andreev, P. Gippner, C.-M. Herbach, E.M. Kozulin, A. Matthies, Yu.Ts. Oganessian, H.-G. Ortlepp, Yu.E. Penionzhkevich, G. Renz, K.D. Schilling, O.V. Strekalovskij, V.M. Vasko, W. Wagner:
Two-velocities measurements of fragment spectra in ^{244}Cm cold spontaneous fission on the FOBOS spectrometer;
Proc. Int. Workshop on Nuclear Fission and Fission Product Spectroscopy, Chateau de la Bourne, Seyssins, France, May 1994

Reif, J., G. Winter, R. Schwengner, H. Prade, L. Käubler, H. Grawe and R. Schubart:
Neutron-core excitations in the N=50 nuclei ^{86}Kr and ^{89}Y;
Verhandlungen der DPG 6 (1994) 1859

Reif, J., G. Winter, R. Schwengner, H. Prade, H. Grawe, R. Schubart:
Neutron-Core Excitations in $^{86}_{36}Kr_{50}$;
Poster, Symposium on New Nuclear Structure Phenomena in the Vicinity of Closed Shells, Stockholm-Uppsala, 1994

Rotter, I.:
Description of an open quantum mechanical system;
Preprint FZR-42 (1994)

Rotter, I.:
Selforganization and chaos in the nuclear system;
Proc. of the Int. Conf. on Dynamical Systems and Chaos, Tokyo, Japan, May 1994

Rotter, I.:
Selforganization and quantum chaos in an open quantum system;
Applications of Chaos in Many-Body Quantum Physics, Seattle, USA, Jun. 1994

Schleif, M. and R. Wünsch:
Pushing and cranking corrections to the meson fields of the bosonized Nambu & Jona-Lasinio model;
Preprint FZR-55 (1994)

Schneider, Chr., H. Müller, L. von Horn, H. Ohm, V. Kruglov:
Anforderungen an die Detektoren zur Spurrekonstruktion an der 0°-Facility von COSY;
Verhandlungen der DPG 6 (1994) 1818

Schülke, A., P. Michel, K. Möller, A. Schamlott und COSY-TOF-Kollaboration:
Methodische Untersuchungen zur zweiseitigen Auslese langer Szintillatorstreifen;
Verhandlungen der DPG 6 (1994) 1794

Schubart, R., H. Grawe, J. Heese, M.K. Kabadiyski, L. Käubler, H. Kluge, K.P. Lieb, K.H. Maier, J. Nyberg, D. Rudolph, D. Seweryniak and M. Schramm:
Experimental and shell model approach to ^{100}Sn - a status report;
Verhandlungen der DPG 6 (1994) 1881

Schult, O.W.B., K. Sistemich, V. Koptev, H. Müller, W. Cassing, L. Larczyk, V.I. Komarov, A. Sibirtsev, J. Ernst, R. Santo, M. Nioradze, N.S. Amaglobeli, M. Büscher, U. Bechstedt, W. Borgs, B. Chiladze, T. Dembski, S. Dienel, H. Dombrowski, S.V. Dshemuchadse, R. Eßer, A. Franzen, L. Glonti, D. Gotta, D. Grzonka, A. Hardt, F. Hinterberger, M. Ivanov, A. Kacharava, B. Kamys, W. Klein, W. Klimala, H.R. Koch, M. Köhler, D. Kopyto, S. Kopyto, A. Kozela, A.V. Kulikov, K. W. Leege, G. Macharashvili, Z. Menteshashvili, G. Müller, W. Oehme, W. Oelert, H. Ohm, B. Prietzschk, A. Puzynin, A. Petrus, B. Rimarzig, Chr. Schneider, Chr. Schneidereit, H. Seyfarth, U. Sieling, J. Smyrski, H. Stechemesser, A. Strzalkowski, W. Tenten, S.V. Trusov, V. Chernyshev, K.-H. Watzlawik, B.Zh. Zalykhanov, N.I. Zhuravlev, P. Zolmierczuk and K. Zwoll:
Plans for investigations of subthreshold K^+ production in p + A collisions;
5. Int. Conf. on Nucleus-Nucleus Collisions, Taormina, May/Jun. 1994

Schult, O.W.B., J. Bisplinghoff, H. Müller, R. Bilger, V. Koptev, B. Kamys, W. Cassing, V. Komarov, W. Scobel, R. Santo, A. Sibirtsev, M. Nioradze, A. Kulikov, W. Eyrich, H. Brand, H. Freiesleben, N.S. Amaglobeli, S. Belostotski, S. Brand, M. Büscher, V. Chernyshev, H.A. Clement, M. Dahmen, T. Demski, J. Ernst, R. Eßer, A. Franzen, D. Grzonka, Th. Hermes, F. Hinterberger, L. v. Horn, R. Jahn, L. Jarzcyk, K. Kilian, M. Kirsch, St. Kistryn, H.R. Koch, E. Kuhlmann, S. Lange, H. Machner, P. Michel, K. Möller, Chr. Nake, B. Naumann, L. Naumann, W. Oelert, H. Ohm, K. Pysz, V. Renken, P. Ringe, E. Roderburg, M. Rogge, A. Schamlott, Chr. Schneidereit, A.Schülke, H. Seyfarth, K. Sistemich, M. Steinke, R. Stratmann, A. Strzalkowski, P. Turek, G.J. Wagner, S. Wirth:
Experiments at COSY;
Proc. of the 7th International Conference on Nuclear Reactions Mechanismus, Varenna, Jun. 1994

Schwengner, R., G. Winter, J. Reif, H. Prade, L. Käubler, R. Wirowski, N. Nicolay, S. Albers, S. Esser, P. von Brentano and W. Andrejtscheff:
Shell-model states and collectivity in ^{83}Br and ^{85}Rb;
Symposium on New Nuclear Structure Phenomena in the Vicinity of Closed Shells, Stockholm-Uppsala, 1994

Seidel, W., M. Andrassy, K. Heidel, H.-G. Ortlepp, A.A. Aleksandrov, I.A. Aleksandrova, C. -M. Herbach, A. Matthies, K D. Schilling, H. Sodan:
Double-grid avalanche counters with large dynamic range;
im Buch der Firma ALTIUM (USA) "P-CAD Productivity Across the Board"

Siwek, A., A. Budzanowski, H. Fuchs, H. Homeyer, G. Pausch, W. Kantor, G. Röschert, A. Sourell, C. Schwarz, W. Terlau and A. Tutay:
Verdampfung, Spaltung und Multifragmentation im System ^{32}S (960 MeV) + Ni;
Verhandlungen der DPG 6 (1994) 1944

Siwek, A., A. Sourell, A. Budzanowski, H. Fuchs, H. Homeyer, G. Pausch, W. Kantor, G. Röschert, C. Schwarz, W. Terlau and A. Tutay:
Multifragmentation study on 30 AMeV ^{32}S + ^{58}Ni;
Preprint HMI/FK-Fucl, Hahn-Meitner-Institut Berlin, 1994

Sobeslavsky, E., W. Cassing, F.M. Dittes, W. Iskra und I. Rotter:
Strukturen in Wirkungsquerschnitten - Widerspiegelung des Trappings?
Verhandlungen der DPG 6 (1994) 1814

Sobeslavsky, E., F.M. Dittes and I. Rotter:
Resonance phenomena at high level density;
Preprint FZR-60 (1994)

Titov, A.I., B. Kämpfer, E.L. Baratkovskaya:
Dielectron production in pp and pd collisions at 1 - 5 GeV;
FZR-34 (1994)

Winter, G., R. Schwengner, J. Reif, H. Prade, R. Wirowski, N. Nicolay, P. von Brentano, H. Grawe and R. Schubart:
Particle and collective excitations in nuclei with 48, 49 or 50 neutrons;
Verhandlungen der DPG 6 (1994) 1792

Wünsch, R.:
Zero-point energy corrected solitonic configurations of the semi-bosonized Nambu&Jona-Lasinio model;
Int. Conf. on Mesons and Nuclei at Intermediate Energy, Dubna, Rußland, May 1994, World Scientific, Signapore, in print

3 Lectures and Seminars

Barz, H.W.:
Anisotropic flow and multifragmentation;
XXII. Int. Workshop on Gross Properties of Nuclei and Nuclear Excitations, Hirschegg, Austria, Jan. 1994

Barz, H.W.:
Pioneninterferometrie eines expandierenden Mesonengases;
Frühjahrstagung "Physik der Hadronen und Kerne", München, Mar. 1994

Barz, H.W.:
Flow in heavy ion collisions at intermediate energies;
FOBOS Workshop '94, Cracow, Poland, Jun. 1994

Barz, H.W.:
Flow and multifragmentation;
Seminar, Nuclear Physics Group, NBI Copenhagen, Danmark, Dec. 1994

Biegansky, J.:
Auswertung der Messungen von Au + Au bei 1 AGeV mit dem 4π-Spektrometer FOPI;
Seminar, IKH/FZ Rossendorf, Apr. 1994

Dittes, F.M.:
Zerfall chaotischer Quantensysteme;
Seminar, TU Dresden, FB Physik, Jan. 1994

Dittes, F.M.:
Neue Ergebnisse zur semiklassischen Bäcker-Abbildung;
Tagung der DPG, Hamburg, Mar. 1994

Dittes, F.M.:
MATLAB - ein Werkzeug zur Behandlung numerischer Probleme mit hohem Datenaufkommen:
Computer-Nutzerseminar, FZ Rossendorf, Apr. 1994

Dittes, F.M.:
Parametrische Röntgenstrahlung;
Seminar, FZ Rossendorf, LINAC-Studiengruppe, May 1994

Dittes, F.M.:
Fraktale Strukturen in der Bäcker-Abbildung;
Seminar, TU Dresden, FB Mathematik, May 1994

Dittes, F.M.:
Semiklassische Quantisierung chaotischer Abbildungen;
Universität Hamburg, Jul. 1994

Dittes, F.M.:
QCD-Strahlungskorrekturen zum Pionen-Formfaktor;
Universität / GHS Wuppertal, Nov. 1994

Dönau, F.:
Rotationsbanden mit geneigter Spinorientierung in geraden Xe- und Ba-Kernen;
Frühjahrstagung "Physik der Hadronen und Kerne", München, Mar. 1994

Dönau, F.:
Tilted cranking;
Universität Gießen, Nov. 1994

Enghardt, W.:
Die Nutzung der Projektilfragmentierung zur Kontrolle der Schwerionentherapie mit PET;
Seminar am Universitätsklinikum der TU Dresden, Klinik für Strahlentherapie, Feb. 1994

Enghardt, W.:
Das PET-Zentrum im FZ Rossendorf;
Seminar am Universitätsklinikum der TU Dresden, Klinik für Radiologie, Mar. 1994

Enghardt, W.:
PET for treatment plan verification and beam monitoring in light ion tumour therapy;
Int. Conf. on Heavy Ions Research: Space, Radiation Protection and Therapy, Sophia-Antipolis, Frankreich, Mar. 1994

Enghardt, W.:
Heavy ion therapy monitoring - a special application of PET;
CTI PET Systems Inc., Knoxville, TN, USA, Jul. 1994

Enghardt, W.:
Biomedizinische Untersuchungen an einem Elektronenbeschleuniger;
Seminar, FZ Rossendorf, LINAC-Studiengruppe, May 1994

Frauendorf, S.:
Die Form von Quantentröpfchen: Alkalicluster und Kerne;
P-Colloquium am Hahn-Meitner-Institut Berlin, Jan. 1994

Frauendorf, S.:
Spinorientationshopping - Eine Interpretation des anomalen Zerfalls von K-Isomeren;
Frühjahrstagung "Physik der Hadronen und Kerne", München, Mar. 1994

Frauendorf, S.:
Photonenquellen mit einem Elektronenstrahl;
Seminar, FZ Rossendorf, LINAC-Studiengruppe, Mar. 1994

Frauendorf, S.:
Shape and abundances of molten sodium clusters;
Niels-Bohr Institute Copenhagen, Danmark, Apr. 1994

Frauendorf, S.:
Magnetic rotation;
Circus, Niels-Bohr Institute Copenhagen, Danmark, Apr. 1994

Frauendorf, S.:
Shears bands;
Department of Physics, Vanderbilt University, Nashville, USA, Jul. 1994

Frauendorf, S.:
C_4-Symmetry in superdeformed nuclei;
Nuclear Physics Division Seminar, Oak Ridge National Laboratory, USA, Jul. 1994

Frauendorf, S.:
Nuclei and clusters - a prolific union;
Department of Physics and Astronomy, University of Tennessee, Knoxville, USA, Jul. 1994

Frauendorf, S.:
Shears bands and C_4-symmetry;
2 Lectures at the Lawrence Berkeley Laboratory, Berkeley, USA, Jul. 1994

Frauendorf, S.:
Tilted cranking;
Conf. on Physics on Large γ-Ray Detectors, Berkeley, USA, Aug. 1994

Frauendorf, S.:
Magnetism and rotation of sodium clusters;
Department of Physics, Kyoto University, Japan, Sep. 1994

Frauendorf, S.:
Clusters and nuclei - a prolific union;
Yukawa Institute for Advanced Studies, Kyoto, Japan, Sep. 1994

Frauendorf, S.:
Probing the spin orientation;
EUROBALL Users Meeting, Strasbourg, Frankreich, Sep. 1994

Frauendorf, S.:
Bericht zur DPG-Schule über mesoskopische Systeme;
Seminar, IKH/FZ Rossendorf, Nov. 1994

Frauendorf, S.:
Tilted Cranking - das Abkippen der Rotationsachse bei hohem Drehimpuls;
Kernphysikalisches Kolloquium der LMU und der TU München, Dec. 1994

Hasch, B.G.:
Positronen-Emissions-Tomographie zur Kontrolle der Schwerionen-Tumortherapie;
Seminar, IKH/FZ Rossendorf, Jun. 1994

Heide, B.:
Mittelenergetische Schwerionenstöße im Rahmen eines Hybrid-Modells;
Seminar, TU Dresden, Feb. 1994

Heide, B.:
Verbindung des BUU-Modells und des Kopenhagener Multifragmentationsmodells zur Beschreibung von Schwerionenstößen;
Seminar, IKH/FZ Rossendorf, Feb. 1994

Heide, B.:
Flußeffekte bei mittelschweren Fragmenten;
GIS - Theorie-Treffen in Fischbachau, Jul. 1994

Herbach, C.-M.:
Analyse von leichten, intermediären und Spaltfragmenten in der Reaktion ^{7}Li (43 AMeV) + ^{232}Th mit dem Multidetektorsystem FOBOS;
Frühjahrstagung "Physik der Hadronen und Kerne", München, Mar. 1994

Herbach, C.-M.:
IMFs emitted before and during fission induced by 43 AMeV ^{7}Li on ^{232}Th studied at FOBOS;
FOBOS Workshop '94, Cracow, Poland, Jun. 1994

Kämpfer, B.:
IMF correlation in central Au + Au collisions;
XXII Int. Workshop on Cross Properties of Nuclei and Nuclear Excitations, Hirschegg, Österreich, Jan. 1994

Kämpfer, B.:
IMF-Korrelationen und Fragment-Fluß in zentralen Stößen Au + Au;
Frühjahrstagung "Physik der Hadronen und Kerne", München, Mar. 1994

Kämpfer, B.:
Excitation and decay of nuclear matter in heavy-ion collisions;
Spring Meeting, Holzhau, Apr. 1994

Kämpfer, B.:
Excitation and decay of nuclear matter in intermediate heavy-ion collisions;
Kolloquium, Uni Clermont-Ferrand, France, Jun. 1994

Kämpfer, B.:
Partonenkinetik in ultrarelativistischen Schwerionenstößen;
Kernphysikalisches Kolloquium, Uni Gießen, Oct. 1994

Kämpfer, B.:
Kinetik von Partonen in ultrarelativistischen Schwerionenstößen;
Theorieseminar, Uni Regensburg, Nov. 1994

Kämpfer, B.:
Quantenelektrodynamik;
Lecture course, TU Dresden, WS 1993/94

Kämpfer, B.:
Kosmologie und Elementarteilchenphysik;
Lecture course, TU Dresden, SS 1994

Kämpfer, B.:
Quantenchromodynamik;
Lecture course, TU Dresden, WS 1994/95

Käubler, L.:
In-Beam Investigation of ^{109}Sn;
Frühjahrstagung "Physik der Hadronen und Kerne", München, Mar. 1994

Käubler, L.:
Kernstrukturphysik bei hohen Drehimpulsen - Detektoren für EUROBALL;
Seminar, Institut für Kern- und Teilchenphysik, TU Dresden, Apr. 1994

Kolomeitsev, E.:
Kaonen-Polarisation in Kernmaterie;
GSI - Theorie-Treffen in Fischbachau, Jul. 1994

Kolomeitsev, E.:
Kaonen-Polarisation in Kernmaterie;
Arbeitstreffen "Kern- und Teilchenphysik 1994", Pirna, Oct. 1994

Krüger, J.:
Untersuchung der Projektilfragmentation und IMF-Emission im System ^{32}S (960 MeV) + ^{197}Au am erweiterten ARGUS-Detektor;
Frühjahrstagung "Physik der Hadronen und Kerne", München, Mar. 1994

Krüger, J.:
Projektilfragmentation und IMF-Emission im System ^{32}S (960 MeV) + ^{197}Au;
Seminar, IKH/FZ Rossendorf, May 1994

Krüger, J.:
Projectile fragmentation and fission in ^{32}S + ^{197}Au at 30 AMeV studied at VICKSI;
FOBOS Workshop '94, Cracow, Poland, Jun. 1994

Matthies, A.:
The FOBOS ionization chambers;
FOBOS Workshop '94, Cracow, Poland, Jun. 1994

Meng, J.:
On the quality of tilted axis cranking;
Seminar, IKH/FZ Rossendorf, May 1994

Michel, P.:
Erzeugung von getaggten Photonenstrahlen;
Seminar, FZ Rossendorf, LINAC-Studiengruppe, Jun. 1994

Michel, P.:
Entwicklung eines schnellen TDC mit Konvertierungszeiten im Bereich weniger Nanosekunden;
Arbeitstreffen "Kern- und Teilchenphysik 1994", Pirna, Oct. 1994

Möhlenkamp, Th.:
Der TP-MUSIC III Detector am ALADIN-Spektrometer:
Frühjahrstagung "Physik der Hadronen und Kerne", München, Mar. 1994

Möhlenkamp, Th.:
Isotope ratios of light fragments in heavy ion collisions;
ALADIN Workshop 1994, Rathen, Sep. 1994

Möhlenkamp, Th.:
Auswertung von ALADIN-Experimenten zur Bestimmung der Isotopenverhältnisse leichter Fragmente in Schwerionenstößen;
Seminar, IKH/FZ Rossendorf, Nov. 1994

Möller, K.:
Einführung in die Mittelenergiephysik;
Lecture course, TU Dresden, WS 1994/95

Möller, K.:
Eine Übersicht über Experimente am MAMI A;
Seminar, FZ Rossendorf, LINAC-Studiengruppe, Apr. 1994

Mösner, J.:
HELITRON status report;
FOPI-Meeting, GSI Darmstadt, Feb. 1994

Müller, H.:
Statistical description of hadronic and nuclear interactions at medium energies;
Int. Conf. on Physics with GeV - Particle Beams, Jülich, Aug. 1994

Müller, M.;
Untersuchungen eines offenen Quantensystems;
Seminar, IKH/FZ Rossendorf, Mar. 1994

Müller, M.:
Sättigung der Riesenresonanzstärke im Bereich sehr hoher Niveaudichte;
Frühjahrstagung "Physik der Hadronen und Kerne", München, Mar. 1994

Müller, M.:
Untersuchung eines offenen Quantensystems am Beispiel des Kontinuum-Schalenmodells;
Seminar, TU Dresden, Institut für Theoretische Physik, May 1994

Müller, M.:
Dynamik offener Quantensysteme;
Universität Bonn, Institut für Strahlen- und Kernphysik, Nov. 1994

Müller, M.:
Dynamik offener Quantensysteme;
Forschungszentrum Jülich, Institut für Kernphysik, Nov. 1994

Naumann, B.:
Simulationsrechnungen zum ppγ und ppπ^0 Nachweis;
TOF-Meeting, KFA Jülich, Dec. 1994

Naumann, L.:
Die Vakuumkonzeption des COSY-TOF-Spektrometers;
TOF-Meeting, KFA Jülich, Mar. 1994

Ortlepp, H.-G.:
Investigation of IMF emission and fission at the FOBOS detector;
Flerov Laboratory of Nuclear Reactions Dubna, Russia, Mar. 1994

Ortlepp, H.-G.:
First experimental results of the FOBOS detector system;
Spring Meeting, Holzhau, Apr. 1994

Ortlepp, H.-G.:
Present status of the FOBOS array;
FOBOS Workshop '94, Cracow, Poland, Jun. 1994

Ortlepp, H.-G.:
First results at FOBOS and the research program for 1995;
Flerov Laboratory of Nuclear Reactions Meeting, Ratmino near Dubna, Russia, Oct. 1994

Ortlepp, H.-G.:
Neueste Ergebnisse vom Spektrometer FOBOS;
Seminar, IKH/FZ Rossendorf, Nov. 1994

Ortlepp, H.-G.:
Study of cluster emission in nuclear reactions near the Fermi energy;
Flerov Laboratory of Nuclear Reactions, Session of the Program Advisory Committee for Heavy-Ion Physics, Dubna, Russia, Nov. 1994

Ortlepp, H.-G.:
Upgrade of the FOBOS data acquisition system;
FOBOS Workshop '94, Cracow, Poland, Jun. 1994

Ortlepp, H.-G.:
Recent results obtained at FOBOS for the reaction $^{14}N + {}^{197}A$ at 34 AMeV;
FOBOS Workshop '94, Cracow, Poland, Jun. 1994

Pausch, G.:
Identifikation geladener Teilchen in Siliziumdetektoren anhand der Impulsform;
Arbeitstreffen für Kernphysik, Schleching, Mar. 1994

Pausch, G.:
Pulse shape analysis with Si detectors;
EUROBALL LCP Detectors Meeting, C.E.N.B.G. Bordeaux-Gradignan, May 1994

Pausch, G.:
Weiterentwicklung der Impulsform-Methode zur Identifikation schwerer Ionen in Halbleiterdetektoren;
Frühjahrstagung "Physik der Hadronen und Kerne", München, Mar. 1994

Pausch, G.:
Activities at the detector lab Rossendorf for FOBOS;
FOBOS Workshop '94, Cracow, Poland, Jun. 1994

Pausch, G.:
Experimente zur $\bar{p}$-Annihilation an Kernen am LEAR/CERN;
Seminar, IKH/FZ Rossendorf, Sep. 1994

Pausch, G.:
A 4π charged-particle silicon ball utilizing pulse-shape information for particle identification;
EUROBALL Users Meeting/Ancillary Detectors Group, Strasbourg, France, Sep. 1994

Pausch, G.:
New Pulse Shape Results;
SATURNE E243 / LEAR PS208 Collaboration Meeting, Hahn-Meitner-Institut Berlin, Nov. 1994

Pawelke, J.:
In-beam PET imaging with different detectors;
Int. Conf. on Heavy Ions Research: Space, Radiation Protection and Therapy, Sophia-Antipolis, Frankreich, Mar. 1994

Pawelke, J.:
A positron camera for heavy ion therapy control;
Int. Workshop of the EORTC Heavy Particle Therapy Group, Heidelberg, Oct. 1994

Pfitzner, A.:
Consistent treatment of short- and long-range correlations in nuclear dynamics;
Int. Workshop on Fluctuations in Nuclear Dynamics, European Center for Theoretical Nuclear Physics, Trento, Italy, Jan./ Feb. 1994

Pfitzner, A.:
Dynamics of two-body correlations: a toy model for light nuclei;
Gemeinsames Seminar der TU/LMU München, May 1994

Pfitzner, A., W. Cassing, A. Peter:
Competition of short- and long-range correlations in nuclear damping;
7th Internat. Conference on Nuclear Reaction Mechanisms, Varenna, Italy, Jun. 1994

Reif, J.:
Neutron-core excitations in the N=50 nuclei ^{86}Kr and ^{89}Y;
Frühjahrstagung "Physik der Hadronen und Kerne", München, Mar. 1994

Renz, G.:
The evacuation and gas-supply system of FOBOS;
FOBOS Workshop '94, Cracow, Poland, Jun. 1994

Rotter, H.:
Zwischen Gunst und Gewalt: Russische Physiker unter Stalin;
Seminar, IKH/FZ Rossendorf, Dec. 1994

Rotter, I.:
Selforganization in the nuclear system;
Workshop "Fluctuations in Nuclear Dynamics", European Centre for Theoretical Studies in Nuclear Physics and Related Areas, Trento, Italy, Jan./ Feb. 1994

Rotter, I.:
Zeitskalen in Kernreaktionen;
Gruppenbericht, Frühjahrstagung "Physik der Hadronen und Kerne", München, Mar. 1994

Rotter, I.:
The interplay of different time scales at high excitation energy;
2nd Int. Seminar on Interaction of Neutrons with Nuclei, Dubna, Russia, Apr. 1994

Rotter, I.:
Selforganization and chaos in the nuclear system;
Int. Conference on Dynamical Systems and Chaos, Tokyo, Japan, May 1994

Rotter, I.:
Selforganization and quantum chaos in an open quantum system;
Applications of Chaos in Many-Body Quantum Physics, Seattle, USA, Jun. 1994

Schleif, M.:
Beschreibung von Nukleonen im Nambu & Jona-Lasinio Modell;
Seminar, TU Dresden, May 1994

Schneider, Chr.:
Anforderungen an die Detektoren zur Spurrekonstruktion an der 0°-Facility von COSY;
Frühjahrstagung "Physik der Hadronen und Kerne", München, Mar. 1994

Schneider, Chr.:
Drahtkammerbau für ein Experiment zur K^+-Produktion an der 0°-Facility bei COSY;
Seminar, IKH/FZ Rossendorf, Jun. 1994

Schülke, A.:
Aufbau eines Experiments zur Untersuchung der Proton-Proton-Bremsstrahlung;
Seminar, IKH/FZ Rossendorf, May 1994

Schwengner, R.:
Particle and Collective Excitations in Nuclei with 48,49 or 50 Neutrons;
Frühjahrstagung "Physik der Hadronen und Kerne", München, Mar. 1994

Schwengner, R.:
Shell-model states and collectivity in ^{83}Br and ^{85}Rb;
Symposium on New Nuclear Structure Phenomena in the Vicinity of Closed Shells, Stockholm-Uppsala, Aug./ Sep.1994

Sobeslavsky, E.:
Strukturen in Wirkungsquerschnitten - Widerspiegelung des Trappings?;
Frühjahrstagung "Physik der Hadronen und Kerne", München, Mar. 1994

Wagner, W.:
The FOBOS CsI scintillator shell and the phoswich forward array;
FOBOS Workshop '94, Cracow, Poland, Jun. 1994

Wagner, W.:
Alpha particles from ^{244}Cm ternary spontaneous fission measured at FOBOS;
FOBOS Workshop '94, Cracow, Poland, Jun. 1994

Wagner, W.:
Conclusions for the research program at FOBOS from the FOBOS Workshop '94 in Cracow (Poland);
Flerov Laboratory of Nuclear Reactions, Session of the Scientific and Technical Council, Dubna, Russia, Jul. 1994

Wünsch, R.:
Nukleon und Delta-Resonanz als selbstkonsistente Feldkonfiguration eines bosonisierten Nambu & Jona-Lasinio Modells mit Spin-Isospin und Schwerpunktskorrekturen;
Frühjahrstagung "Physik der Hadronen und Kerne", München, Mar. 1994

Wünsch, R.:
Zero-point energy corrected solitonic configurations of the semi-bosonized Nambu & Jona-Lasinio model;
Int. Conf. on Mesons and Nuclei at Intermediate Energy, Dubna, Russia, May 1994

4 Talks of Visitors

Y. Leifels, Bochum:
Squeéze-out von Neutronen in mitelenergetischen Schwerionenreaktionen (Bericht über Messungen mit dem LAND-Detektor):
Jan. 24, 1994

B. Gebauer, Berlin:
Die Spektrometer für binäre Reaktionen an OSIRIS und EUROGAM II;
Jan. 26, 1994

H.S. Taylor, Los Angeles:
A new Hamiltonian method for solving resonance and non-resonance scattering problems;
Mar. 10, 1994

S. Fayancs, Moskau:
Self-consistent theory of finite Fermi systems: from magicity to exotics;
Apr. 8, 1994

P. Doll, Karlsruhe:
Ladungsaustauschreaktion in der Nähe der Δ-Schwelle;
Apr. 20, 1994

A. Botvina, Berlin:
Fragment and multifragment production in proton- and nucleus-nucleus reactions at intermediate energies;
May 2, 1994

J. Dietrich, Jülich:
Strahldiagnose am COSY-Beschleuniger;
May 26, 1994

D. Fossan, Stony Brook:
New collective features near the Z = 50 closed shell. Gamma sphere studies;
Jun. 6, 1994

P. von Neumann-Cosel, Darmstadt:
(e,e'X)-Reaktionen an mittelschweren Kernen bei s-Dalinac-Energien;
Jun. 8, 1994

L. Sihver, Darmstadt:
Calculation of reaction and partial cross sections, momentum loss and depth-dose distributions when using heavy-ion beams;
Jun. 10, 1994

V. Kruglov, Dubna:
$\pi^+\pi^-$-Atome;
Jul. 4, 1994

W. Cassing, Gießen:
Was lernen wir aus der Kernphysik über QCD?
Aug. 5, 1994

L. Moretto, Berkeley:
Complex fragment emission, from compound nucleus decay to multifragmentation;
Sep. 23, 1994

Yu.V. Pyatkov, Dubna:
Untersuchungen zur kalten spontanen Spaltung von ^{244}Cm am FOBOS-Spektrometer;
Sep. 30, 1994

D. Pelte, Heidelberg:
Zentrale Schwerionenstöße: Neue Resultate vom FOPI-Spektrometer an der GSI;
Oct. 10, 1994

R. Nojarov, Tübingen:
Magnetische Dipolanregungen in Kernen;
Nov. 14, 1994

A. I. Titov, Dubna:
Photo- and electro-production of Φ mesons at protons as probe of the strangeness content of nucleons;
Dec. 5, 1994

U. Keyser, Tübingen:
Stand des PIAFFE-Projektes;
Dec. 7, 1994

R. Rossmanith, Hamburg:
Neuere Projekte für Freie-Elektronen-Laser;
Dec. 8, 1994

Th. Meißner, South-Carolina:
Isospin-verletzende Mesonenmischung in QCD-Summenregeln;
Dec. 12, 1994

A. Pelster, Stuttgart:
Nichtintegrable Raum-Zeit-Transformationen in der klassischen Mechanik und in der Quantenmechanik;
Dec. 14, 1994

J. Zhang, Tennessee:
High spin physics: Identical and non-identical bands at normal deformation;
Dec. 19, 1994

III Personnel

Acting Director: Dr. H. Prade

Scientific Staff

Dr. Barz, H.W. [1]
Dietterle, L. [2,4]
Dr. Dittes, F.M.
Dr. Dönau, F.
Dr. Dshemuchadse, S. [2]
Dr. Enghardt, W. [1]
Dr. Frauendorf, S.
Dr. Gippner, P. [4]
Dr. Herbach, C.-M.
Dr. Kämpfer, B. [1]
Dr. Käubler, L. [1]
Dr. Kirchner, Th. [2]
Dr. Kleinwächter, P. [2]
Dr. Kotte, R.
Dr. Matthies, A. [2,4]
May, D. [2,4]
Dr. Michel, P.
Dr. Möller, K. [1]
Dr. Mösner, J.
Dr. Müller, H.
Dr. Naumann, B. [2]
Dr. Naumann, L.
Dr. Neubert, W.
Dr. Ortlepp, H.-G. [4]
Dr. Pausch, G.
Dr. Pfitzner, A. [3]
Dr. Pilz, W. [3]
Dr. Reif, J. [2]
Renz, G. [2,4]
Richter, H. [3]
Dr. Rotter, H. [3]
Prof. Rotter, I. [1]
Schamlott, A. [2]
Dr. Schilling, K.D.
Dr. Schlett, M.
Dr. Schwengner, R.
Dr. Seidel, W.
Dr. Sobeslavsky, E. [2]
Dr. Wagner, W. [4]
Dr. Winter, G.
Wohlfarth, D.
Dr. Wünsch, R.

Technical Staff

Altus, M.
Angermann, H.
Baumann, U.
Berlin, J.U.
Boeck, M.
Böse, M.
Fiedler, J.
Förster, R.
Freitag, M.
Göbel, L.
Heidel, K.
Hermann, K.H.
Hutsch, J.
Kerber, J.
Kluge, E.
Langer, M.
Meier, B.
Prietzschk, B.
Probst, I.
Rimarzig, B.
Römer, H.
Scheinpflug, M.
Schneidereit, Chr.
Schulze, W.
Sobiella, M.
Uhlmann, A.
Umlauf, C. [2,4]

Postgraduate Students

Biegansky, J. [2]
Hasch, B.-G. [2]
Heide, B. [2]
Hofmann, C.-H.
Kamanin, D. [2]
Kolomeizew, J.
Krüger, J.
Lauckner, K.
Möhlenkamp, T.
Müller, M. [2]
Pawelke, J.
Peshier, A.
Schleif, M. [2]
Schneider, Chr.
Schülke, A. [2]
Servene, Th. [2]

Post Docs

Dr. Meng, J.
Dr. Mylaeus, Th.
Dr. Skoda, S. [2]

[1] WIP/TU Dresden
[2] Project
[3] ABM/Free coworker
[4] at present JINR Dubna